

ACS SYMPOSIUM SERIES **822**

Group 13 Chemistry

From Fundamentals to Applications

Pamela J. Shapiro, Editor
University of Idaho

David A. Atwood, Editor
University of Kentucky



American Chemical Society, Washington, DC

QD 466 .G67 2002 c. 1



**Group 13 chemistry : from
fundamentals to applications**

Library of Congress Cataloging-in-Publication Data

Group 13 chemistry : from fundamentals to applications / Pamela J. Shapiro, editor,
David A. Atwood, editor.

p. cm.—(ACS symposium series ; 822)

Includes bibliographical references and index.

ISBN 0-8412-3785-9

1. Group 13 elements.

I. Title: Group thirteen elements. II. Shapiro, Pamela J. III. Atwood, David A., 1965- IV. American Chemical Society. Division of Inorganic Chemistry. V. American Chemical Society. Meeting (221st : 2001 : San Diego, Calif.) VI. Pacificchem 2000 (2000 : Honolulu, Hawaii) VII. Series.

QD466 .G67 2002
546'.67—dc21

2002016466

The paper used in this publication meets the minimum requirements of American National Standard for Information Sciences—Permanence of Paper for Printed Library Materials, ANSI Z39.48-1984.

Copyright © 2002 American Chemical Society

Distributed by Oxford University Press

All Rights Reserved. Reprographic copying beyond that permitted by Sections 107 or 108 of the U.S. Copyright Act is allowed for internal use only, provided that a per-chapter fee of \$22.50 plus \$0.75 per page is paid to the Copyright Clearance Center, Inc., 222 Rosewood Drive, Danvers, MA 01923, USA. Republication or reproduction for sale of pages in this book is permitted only under license from ACS. Direct these and other permission requests to ACS Copyright Office, Publications Division, 1155 16th St., N.W., Washington, DC 20036.

The citation of trade names and/or names of manufacturers in this publication is not to be construed as an endorsement or as approval by ACS of the commercial products or services referenced herein; nor should the mere reference herein to any drawing, specification, chemical process, or other data be regarded as a license or as a conveyance of any right or permission to the holder, reader, or any other person or corporation, to manufacture, reproduce, use, or sell any patented invention or copyrighted work that may in any way be related thereto. Registered names, trademarks, etc., used in this publication, even without specific indication thereof, are not to be considered unprotected by law.

PRINTED IN THE UNITED STATES OF AMERICA

**American Chemical Society
Library**

1155 16th St., N.W.

ACS Symposium Series 822, Shapiro, P., et al.;
Washington, D.C.: American Chemical Society; Washington, DC, 2002.

Foreword

The ACS Symposium Series was first published in 1974 to provide a mechanism for publishing symposia quickly in book form. The purpose of the series is to publish timely, comprehensive books developed from ACS sponsored symposia based on current scientific research. Occasionally, books are developed from symposia sponsored by other organizations when the topic is of keen interest to the chemistry audience.

Before agreeing to publish a book, the proposed table of contents is reviewed for appropriate and comprehensive coverage and for interest to the audience. Some papers may be excluded to better focus the book; others may be added to provide comprehensiveness. When appropriate, overview or introductory chapters are added. Drafts of chapters are peer-reviewed prior to final acceptance or rejection, and manuscripts are prepared in camera-ready format.

As a rule, only original research papers and original review papers are included in the volumes. Verbatim reproductions of previously published papers are not accepted.

ACS Books Department

Preface

This volume is based on two symposia sponsored by the American Chemical Society (ACS) Division of Inorganic Chemistry, one at Pacificchem 2000 and the other at the 221st National ACS Meeting. The volume is different from traditional conference proceedings in that contributions were not limited to conference participants. Rather, a general invitation was sent out to chemists specializing in group 13 chemistry, and this collection of chapters represents the response to that invitation. As such, the content of this volume does not reflect any preconceived outline orchestrated by the editors.

We had two objectives in organizing this volume. One was to offer a perspective on the present and future impact of group 13 chemistry on research in the 21st century. The other was to provide a resource for presenting modern main group chemistry to students at the college and graduate levels. Therefore, besides bringing the reader up to date on recent developments, some chapters offer in-depth reviews of their topic.

The headings under which the chapters are organized (i.e., fundamentals of structures, bonding, and reactivity; organic synthesis and catalysis, new materials and clusters; and aluminum compounds: biological and environmental aspects) are a rough guide to help the reader navigate through the multitude of topics involving group 13 chemistry. Due to the increasing interdisciplinary nature of research, the different headings are not mutually exclusive and many of the chapters could have easily been listed under more than one heading.

Because concepts of structure and bonding are the foundation upon which we build our understanding of chemistry, chapters dealing with these topics are presented first. In Chapters 1 and 2, Power and Jutzi describe the syntheses and properties of group 13 compounds in the +1 oxidation state, which is an unstable and rare oxidation state for the lighter group 13 elements B–Ga. These two chapters illustrate the synthetic ingenuity chemists use to prepare highly reactive species to uncover new modes of reactivity and bonding. Even compounds with B–Ga in the more prevalent +3 oxidation state exhibit unusual and

interesting bonding modes, particularly when they are complexed by cyclopentadienyl ligands, as described by Shapiro in Chapter 3. Theories of bonding in electron-deficient molecules are the hallmark of group 13 compounds. These theories continue to evolve as new structures are discovered and as computational methods become more sophisticated. In Chapter 4, Fehlner develops a conceptual framework for explaining the structures of earlier transition metal-containing metalloboranes that are not easily accommodated by general electron-counting rules.

The next section examines modern applications of group 13 compounds to organic synthesis and catalysis. In Chapter 5, Carter et al. describe their use of diboranes for the stereoselective coupling of diarylaldimines and the selective deoxygenation of non-metal oxides and organic carbonyl compounds. The Lewis-acidity of group 13 compounds is key to the acceleration of various organic reactions and the activation of transition metals for catalysis. Efforts to “juice-up” the Lewis acidity of these compounds by having multiple Lewis-acidic group 13 centers act in concert is a recent focus of several research groups. The number of contributions about multidentate Lewis acids, from Eisch, Jäkle, and Gabbaï, demonstrates the growing importance of this relatively new field. In Chapter 9, Harvey and Atwood review chelated aluminum anions, which are finding application as counter anions in catalysis. Recent reports of ethylene polymerization by aluminum compounds have caused a flurry of prospecting for aluminum compounds that could be the next generation of alkene polymerization catalysts. Is ethylene polymerization at aluminum centers too good to be true? Budzelaar and Talarico take a theoretical approach to examining this question in Chapter 10.

Group 13 elements are components of many technologically important materials, such as heat-resistant ceramics, zeolites, and the semiconductors used in transistors and light-emitting devices. Current efforts in this area are at the molecular and materials interface—developing molecular precursors and methods for the controlled growth of nanostructural materials and materials with well-defined structures and compositions. In Chapters 11–13, Schnöckel, Sneddon, and Mason describe new types of fundamentally interesting and technologically relevant clusters, networks, and materials. In Chapter 14, Chivers reveals the unique oligomeric structures that result when trisamido derivatives of the group 13 elements are made anionic. In Chapter 15, King et al. use

density functional theory to understand the distorted structures of hypoelectronic six-atom clusters of B, In, and Tl.

The final section of this volume takes a look at the biological and environmental properties of aluminum compounds. Despite its relative abundance, aluminum does not appear to play a supportive role in biological systems. On the contrary, as discussed in Chapter 16 by Anitha et al., aluminum appears to be involved in the etiology Alzheimer's Disease and other neurological disorders in humans. Understanding the role of aluminum in these age-related diseases becomes that much more important as the age-expectancy of the human population increases. For this reason, it is also important to understand the complex aqueous chemistry of aluminum and how it is released into aquatic environments, and this is the topic of Chapter 17 by Wang et al. The potential benefits of aluminum to biology in the form of AlF_4^- are presented in Chapters 18 and 19. Conley et al. outline the fundamental chemistry of AlF_4^- whereas Strunecka reveals how this anion behaves in biological systems.

We are grateful to the contributing authors for the time and care they have given to this project. The diversity of topics reveals how widespread the influence of group 13 element chemistry is in science and technology.

We also thank the Petroleum Research Fund, administered by the ACS, and the ACS Division of Inorganic Chemistry for their generous support of the two symposia from which this volume issued as well as the ACS Books Department for recognizing the timeliness of such a volume.

Pamela J. Shapiro

Department of Chemistry
University of Idaho
Moscow, ID 83844-2343
Email: Shapiro@uidaho.edu
Telephone: 208-885-5785
Fax; 208-885-6173

David A. Atwood

Department of Chemistry
The University of Kentucky
Lexington, KY 40506-0055
Email: datwood@uky.edu

Chapter 1

Bonding and Reactivity of a β -Diketiminate, Gallium(I), Carbene Analogue

Ned J. Hardman, Andrew D. Phillips, and Philip P. Power*

Department of Chemistry, University of California at Davis,
One Shields Avenue, Davis, CA 95616

The gallium(I) diketiminate, $:\text{Ga}[\{\text{N}(\text{Dipp})\text{C}(\text{Me})\}_2\text{CH}]$ (Dipp = $\text{C}_6\text{H}_3\text{-2,6-}i\text{-Pr}_2$), is a carbene analogue featuring a planar GaN_2C_3 ring structure in which the gallium valence shell contains two bond pairs, a lone pair and an empty orbital perpendicular to the ring plane. Computational studies for the model species $:\text{Ga}[\{\text{N}(\text{H})\text{C}(\text{H})\}_2\text{CH}]$ showed that, although the HOMO corresponds to the gallium lone pair, the LUMO does not involve the gallium p-orbital. The latter is represented by the LUMO+1 level, and this is separated from the HOMO by *ca.* 110 kcal mol⁻¹. The low energy of the HOMO and its large energy separation from the acceptor orbital point to good σ -donor but poor π -acceptor characteristics for the $:\text{Ga}[\{\text{N}(\text{Dipp})\text{C}(\text{Me})\}_2\text{CH}]$ ligand. Calculations on the aluminum analogue showed that the HOMO-LUMO+1 separation is *ca.* 12 kcal mol⁻¹ less than the gallium species which is due primarily to the higher energy of the aluminum lone pair. The reaction of $:\text{Ga}[\{\text{N}(\text{Dipp})\text{C}(\text{Me})\}_2\text{CH}]$ with N_2O or S_8 produced the novel μ -chalcogenides $(\text{E}\text{Ga}[\{\text{N}(\text{Dipp})\text{C}(\text{Me})\}_2\text{CH}])_2$ (E = O or S). However, the reaction with N_3SiMe_3 afforded the isomeric tetrazole $[\text{HC}\{\text{C}(\text{Me})\text{N}(\text{Dipp})\}_2]\overline{\text{GaN}(\text{SiMe}_3)\text{N}_2\text{N}(\text{SiMe}_3)}$

and amide/azide $[\text{HC}\{\text{C}(\text{Me})\text{N}(\text{Dipp})\}_2]\text{Ga}(\text{N}_3)\text{N}(\text{SiMe}_3)_2$. In contrast, the reaction with the bulkier azide N_3Ar^* ($\text{Ar}^* = \text{C}_6\text{H}_3\text{-2,6-Trip}_2$, $\text{Trip} = \text{C}_6\text{H}_2\text{-2,4,6-}i\text{-Pr}_3$) yielded the first monomeric gallium imide $[\text{H}\{\text{C}(\text{Me})\text{N}(\text{Dipp})\}_2]\text{Ga}=\text{NAr}^*$. Computational data on model complexes for the latter showed that the π -bonding component in the Ga–N imide bond is 48.6 kJ mol^{-1} which is similar to the value calculated for H_2GaNH_2 . The relative weakness of the Ga–N π -bonding is consistent with the strong σ -donor/weak π -acceptor bonding character expected from the large HOMO-LUMO+1 gap in the model gallium(I) diketiminate precursor.

Introduction

The sterically crowded Al(I) and Ga(I) β -diketimines $:\text{M}(\text{Dipp}_2\text{nacnac})$, ie. $:\text{M}[\{\text{N}(\text{Dipp})\text{C}(\text{Me})\}_2\text{CH}]$, ($\text{M} = \text{Al}$, (1), or Ga , (2), $\text{Dipp} = \text{C}_6\text{H}_3\text{-2,6-}i\text{-Pr}_2$), possess monomeric structures (see Figure 1) in which the metal valence shells contain two bond pairs, a lone pair and an empty p-orbital. Stable, neutral, monomers of this general type, ie. $:\text{MR}$ ($\text{R} = \text{organic or related ligand}$, $\text{M} = \text{Al}$, Ga , In or Tl), are rare in the solid state, particularly in the case of Al and Ga. Structurally characterized examples include $:\text{M}(\text{Tp}^{\text{Bu}^t_2})$ ($\text{M} = \text{Ga}$, (3), or In , (4); $\text{Tp}^{\text{Bu}^t_2} = \text{tris}(3,5\text{-di-tert-butylpyrazolyl})\text{hydroborato}$), $:\text{In}(\text{Tp}^{\text{Ph}})$, (5), $:\text{In}(\text{Tp}^{\text{Bu}^t})$, (4), $:\text{In}(\text{Tp}(\text{CF}_3)_2)$, (6), several Tl derivatives of the Tp ligands, (7), some Tl derivatives of bis(pyrazolyl)hydroborato (Bp) ligands, in which Tl is bound to two nitrogens and the B–H hydrogen of the Bp ligand, (8), as well as the one-coordinate terphenyl derivatives $:\text{MC}_6\text{H}_3\text{-2,6-Trip}_2$ ($\text{M} = \text{In}$, (10), or Tl , (11); $\text{Trip} = \text{-C}_6\text{H}_2\text{-2,4,6-}i\text{-Pr}_3$). In addition the anionic gallium carbene analogue $[\text{Ga}\{\text{N}(\text{Bu}^t)\text{CH}\}_2]^-$ has been isolated although its chemistry has not been explored (9). The presence of a pair of electrons and formally unoccupied p-orbital(s) in low (1 or 2) coordinate $:\text{MR}$ species suggest that they may behave as both electron donors and acceptors. However, the acceptor capacity of the metal in the Tp derivatives is to some extent compromised by the fact that the Tp ligand, being tridentate, occupies three coordination sites and potentially engages three of the four available metal valence orbitals in bonding. Even for the formally two-coordinate Bp derivatives, the hydrogen of the B–H moiety occupies a site in the metal coordination sphere (8,9). The $:\text{M}(\text{Dipp}_2\text{nacnac})$ ($\text{M} = \text{Al}$ or Ga) and $\text{MC}_6\text{H}_3\text{-2,6-Trip}_2$ ($\text{M} = \text{In}$ or Tl) species differ in that they contain only bi or monodentate ligands, in which case either one or two metal p-orbitals are formally available for bonding. They resemble singlet carbenes (12,13), both electronically and structurally, and are expected to have some

similarity in their reactivity patterns. However, important differences can also be anticipated which may arise from several factors. For example, the properties of the central aluminum or gallium and carbon atoms differ markedly in terms of their electronegativities and sizes. In addition, the energy difference between lone pair and empty p-orbital(s) of the Al or Ga derivatives is expected to be larger than that in carbenes, and this difference should exert a strong influence on the bonding characteristics of these ligands. In this article, we focus on the structure, physical properties and some reaction chemistry of the two coordinate gallium species :Ga(Dipp₂nacnac) (2) and show that it possesses some unique and unexpected bonding and chemical characteristics.

Structure and Bonding

The structure of the :Ga(Dipp₂nacnac) is shown in Figure 1. The GaN₂C₃ ring has planar geometry with an approximate C₂ symmetry axis along the

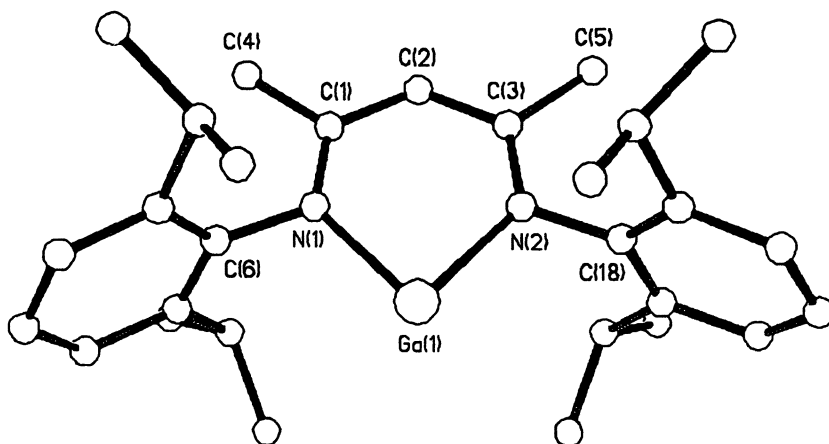


Figure 1. Drawing of :Ga(Dipp₂nacnac) illustrating the planar structure of the β -diketiminato ring.

Ga(1)--C(2) vector which indicates delocalization of the C–C and C–N double bonds over the N₂C₃ ring array. Some important structural parameters for this compound are compared with those of its aluminum analogue in Table I. Calculated structural parameters for the unsubstituted model species :M(nacnac) (M = Al or Ga) are also provided in parenthesis (14). These were calculated using a hybrid method (15) of Hartree-Fock and density functional theories (DFT) with Becke's exchange functional (B3), (16), and the Lee-Yang-Parr non-local correlation functional (LYP), (17). A basis set of 6-31G was employed for all atoms. Calculations were carried out using the Gaussian 98 suite of programs (18). Both molecules represent energy minima and were optimized as

having C_{2v} symmetry. It is obvious from the data in Table I that there is good agreement between the calculated and experimental results. The major

Table I. Comparison of Experimental and Calculated Structural Data for :M(Dipp₂nacnac)₂ and :M(nacnac) (M = Al or Ga)

	:Al(Dipp ₂ nacnac) ^a		:Ga(Dipp ₂ nacnac) ^b	
M–N(Å)	1.957(2)	(1.992) ^c	2.055(2)	(2.063) ^c
N–C(Å) ^d	1.341(3)	(1.329)	1.338(2)	(1.326)
C–C(Å) ^d	1.391(3)	(1.396)	1.400(3)	(1.397)
N–M–N ^o	89.86(8)	(86.3)	87.53(5)	(85.2)

^aRef. 1, ^bRef. 2, ^cCalculated values for :M(nacnac), Ref. 14, ^dMN₂C₃ ring.

difference between the two compounds involves the M–N bond lengths which were experimentally found to be *ca.* 0.1 Å longer for the gallium compound. In low coordinate Al–N and Ga–N compounds, longer distances are usually observed in the case of gallium (19). However, in these compounds the difference is twice that normally observed. Both the Al–N and Ga–N distances are considerably longer (*ca.* 0.1 Å) than those reported (20) for Al(III) and Ga(III), β-diketiminates and this is consistent with the larger effective ionic radii expected for the M(I) ions. The computational data provide further insight into the bonding through the ordering of various energy levels. These levels and their energies are listed in Table II. An illustration of the electron density surfaces for the :Ga(nacnac) species is given in Figure 2. It can be seen from Table II that the order and energies of the MO's are similar for the Al and Ga derivatives. In each compound, the HOMO is the lone pair orbital, and it is primarily s in character. However, the LUMO is not the Al or Ga valence p-orbital but a π* orbital localized at the C–N moieties. The LUMO+1 level corresponds to the metal p-orbital with a small component localized on the organic ring. The HOMO-LUMO and HOMO-LUMO+1 energy differences are significantly larger in gallium where the HOMO-LUMO+1 gap is calculated to be 109.81 kcal mol⁻¹ (*ca.* 4.76 eV). It is notable that the HOMO also has σ*-antibonding character with respect to the M–N bond. The HOMO-1 has M–N π-bonding as well as some C–C π-bonding character. The HOMO-2 orbital involves M–N σ-bonding as well as C–C and C–H σ-bonding while the HOMO-4 is a ring π-orbital with slight delocalization onto the metal. In sum the HOMO-1(π) and HOMO-2(σ) are the orbitals that are mainly

Table II. Molecular Orbital Energies (kcal mol⁻¹) for the Model Species :M(nacnac) (M = Al or Ga) at 6-31G Level^a

Orbital	Al	Ga	Orbital Character	
LUMO+1	-8.16	-10.43	Ga(4p)	NB, C-C π^*
LUMO	-29.73	-24.00	π^*	C-N
HOMO	-105.49	-120.24	Ga(4s-p)	LP, Ga-N σ^*
HOMO-1	-142.57	-136.57	π	Ga-N, C-N
HOMO-2	-200.58	-190.94	σ^*	Ga-N, C-N, CH
HOMO-3	-208.38	-203.80	π	C-N
HOMO-4	-242.85	-237.34	π	Ga-N, C-N, C-C
HOMO-5	-255.93	-254.07	σ	C-H, C-N, C-C
Δ HOMO-LUMO	75.76	96.24		
Δ HOMO-LUMO+1	97.33	109.81		

^aPhillips, A. D., Power, P. P. Unpublished results.

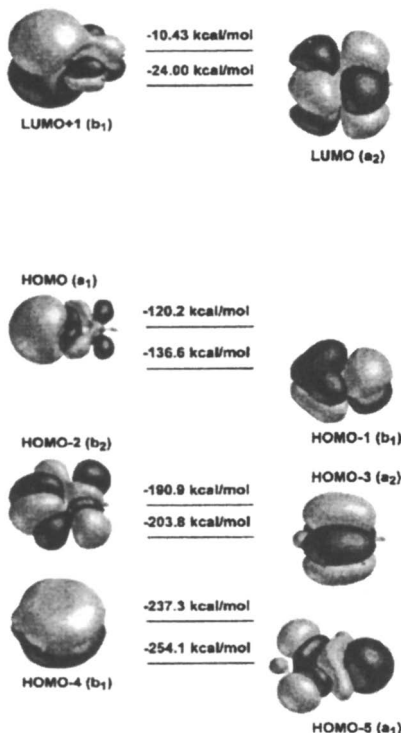


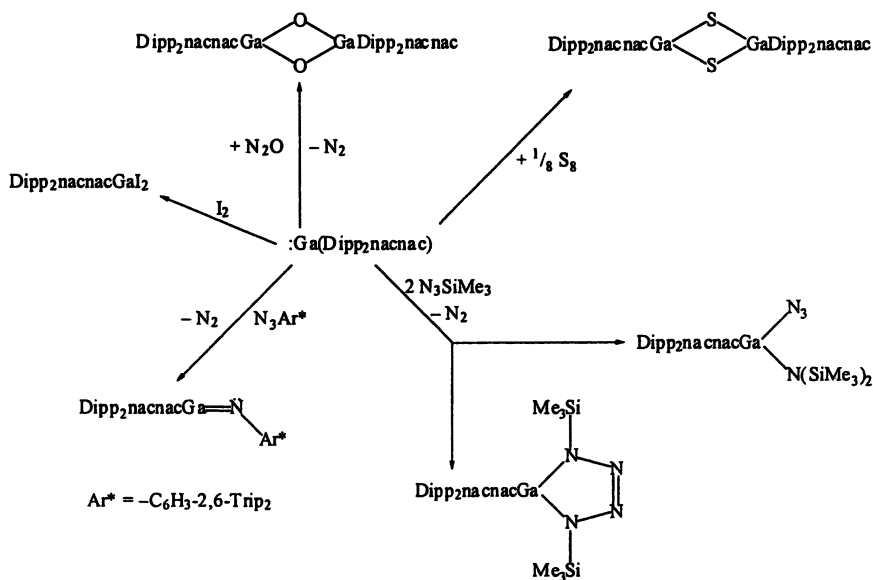
Figure 2. Electron density surfaces and MO energies of :Ga(nacnac).

associated with M–N bonding. Also, there is some M–N σ -antibonding character associated with the HOMO and some M–N π -bonding character from HOMO-4, but, to a first approximation, these effects cancel each other so that M–N bonding corresponds to the delocalized HOMO-1 and HOMO-2 orbitals. Even though HOMO-1 is a π -orbital which also extends to the carbon atoms of the ring, it does not give rise to short M–N bonds since it does not confer multiple character on the M–N interaction. In addition we note that the σ M–N bonding HOMO-2 orbital involves a considerable component localized on other atoms. Thus, the computational data suggest weakened Ga–N bonding which is in agreement with the relatively long Ga–N bonds seen in the crystal structure. Both the computational and structural data are also in harmony with Haaland's analysis (21) of related Al–N bonded compounds which regards the M–N bonds as having equal components of normal and dative character. The low energy and high s-character of the HOMO, and the large energy difference between the HOMO and the rather diffuse acceptor 4p-orbital (LUMO+1) suggest that :Ga(Dipp₂nacnac) should be a good σ -donor but a poor π -acceptor. The π^* -LUMO orbital, which is *ca.* 14 kcal mol⁻¹ more stable than the LUMO+1 level,

could behave as a δ -type acceptor orbital (e.g., a face-on interaction with a d-orbital) but it would be non-bonding with respect to any interactions with s or p-orbitals.

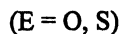
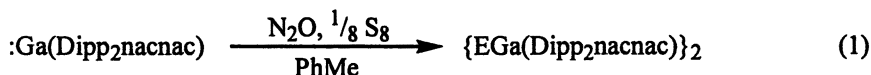
Reaction Chemistry

The initial investigations of the reaction chemistry of $:\text{Ga}(\text{Dipp}_2\text{nacnac})$ are summarized in Scheme 1. The work has focused mainly on reactions with the electronically related unsaturated molecules N_2O , N_3SiMe_3 and N_3Ar^* ($\text{Ar}^* = \text{C}_6\text{H}_3\text{-2,6-Trip}_2$, $\text{Trip} = \text{C}_6\text{H}_3\text{-2,4,6-}i\text{-Pr}_3$) with the objective of synthesizing compounds with multiple bonds to gallium. A similar intention was planned



Scheme 1. Reaction of $:\text{Ga}(\text{Dipp}_2\text{nacnac})$ with N_2O , S_8 , N_3SiMe_3 , N_3Ar^*

for the reaction with sulfur. However, for the reaction with iodine, a simple oxidative addition reaction was expected. The reaction of $:\text{Ga}(\text{Dipp}_2\text{nacnac})$ with N_2O or S_8 (22) in the appropriate stoichiometries led to the oxo or sulfido bridged dimers $\{\text{EGa}(\text{Dipp}_2\text{nacnac})\}_2$ ($\text{E} = \text{O}$ or S) in accordance with Eqn. (1).



It was hoped that these reactions would lead to monomeric species having GaO or GaS multiple bonds. However, a dimeric species (Figure 3) was isolated in

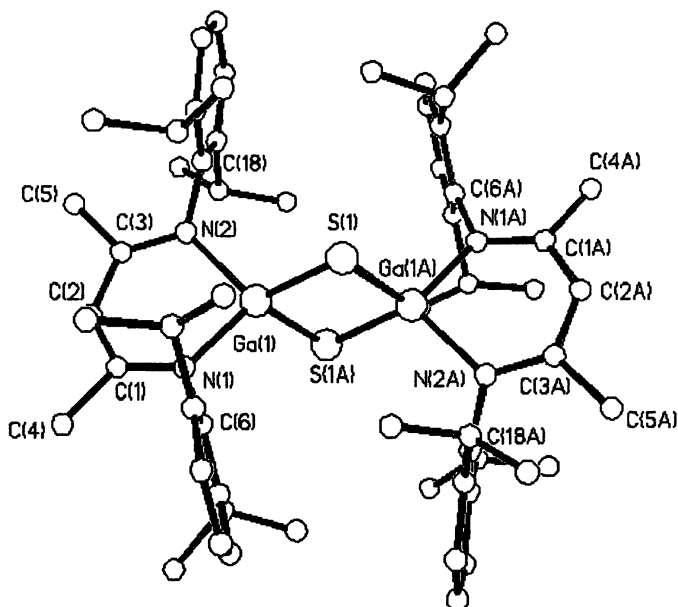
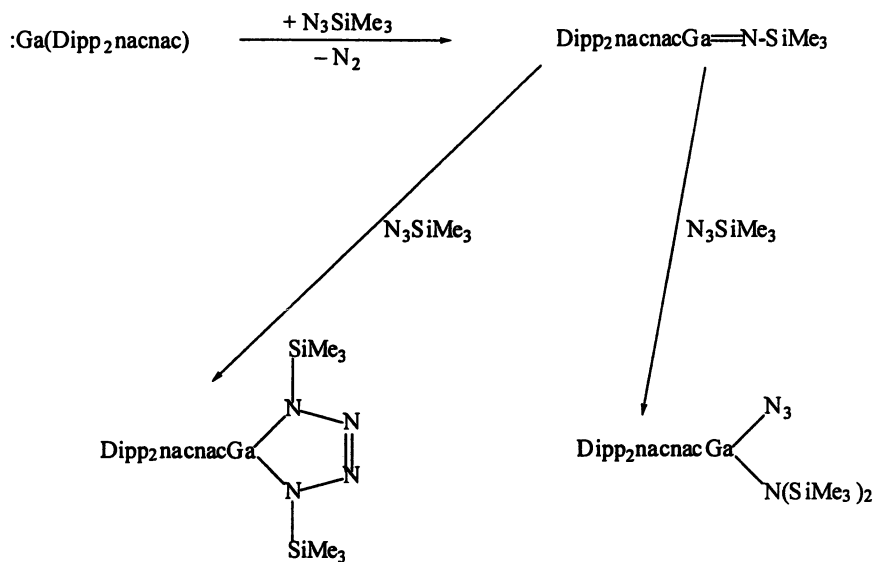


Figure 3. Drawing of the structure of $\{\text{SGa}(\text{Dipp}_2\text{nacnac})\}_2$.

each case. This is probably due to the ionic character of the GaE bonds which results in high energy of association for these units. The structures consist of centrosymmetric, dimeric molecules with planar Ga_2E_2 cores in which each metal is four coordinate as a result of bonding to the $\text{Dipp}_2\text{nacnac}$ ligand. The Ga–O and Ga–S distances average 1.851(3) and 2.26(1)Å. The Ga_2O_2 core is almost perfectly square with Ga–O–Ga and O–Ga–O angles of 88.18(4) and 90.82(4)°. The Ga–S–Ga and S–Ga–S angles of 83.49(2) and 96.51(2)° show a much greater difference. The Ga–N distances in the oxo compound are marginally shorter than those in the sulfur species; 1.970(1) and 1.978(1)Å versus 1.983(2) and 1.986(2)Å, probably as a result of the greater electronegativity difference between Ga and O which further reduces the effective ionic radius of the Ga^{3+} ion. Both pairs of Ga–N distances are much shorter than the 2.054(3)Å average observed for $\text{Ga}(\text{Dipp}_2\text{nacnac})$, probably as a result of the oxidation of the metal from Ga^{+1} to Ga^{+3} . The $\text{Dipp}_2\text{nacnac}$ rings are also folded along the N–N

vectors (160.3° for the oxo and 158.5° for the sulfido species) in contrast the essentially planar structure of $:\text{Ga}(\text{Dipp}_2\text{nacnac})$. Both molecules show evidence of steric congestion which is apparent in the orientation of the Dipp substituents. In effect these groups are displaced so as to avoid steric interference across the Ga_2E_2 core. In the oxo species the C(ipso)–C(para) vectors deviate by 7.1° from the line of the N–C(ipso) bond. In addition, the Ga–N–C(ipso) angles; avg. 123.1° (oxo), avg. 121.9° (sulfido) are significantly wider than the avg. of 111.7° in $:\text{Ga}(\text{Dipp}_2\text{nacnac})$. In view of these data, it seems likely that the use of bulkier substituents on the aryl or β -diketiminato rings will eventually result in the stabilization of a monomeric species featuring GaE species with multiple bond character (23).

Treatment of $:\text{Ga}(\text{Dipp}_2\text{nacnac})$ with N_3SiMe_3 results in two products which are probably generated via a monomeric gallium imide intermediate in accordance with Scheme 2 (24). Apparently, the multipolar cumulene N_3SiMe_3 can react by more than one pathway with the $\text{Dipp}_2\text{nacnacGa}=\text{NSiMe}_3$ intermediate to yield the isomeric gallium tetrazole and amide/azide compounds in a 2:5 ratio. The tetrazole is much less soluble than the



Scheme 2. Reaction of $:\text{Ga}(\text{Dipp}_2\text{nacnac})$ with N_3SiMe_3

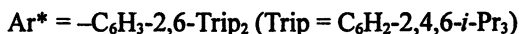
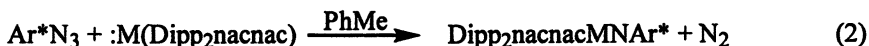
azide/amide so that separation of the products is a relatively straightforward matter. Both compounds decompose at *ca.* 230°C to give a red solid whose composition is currently unknown. The ^1H NMR spectra of both compounds display two signals for the $-\text{SiMe}_3$ groups which do not coalesce up to a

temperature of 95°C in d^8 -PhMe. The distinct magnetic environments of the $-\text{SiMe}_3$ groups are believed to arise from the crowded nature of the compounds in which they are locked into a specific conformation. The Dipp₂nacnac rings display strong folding along the N(1)–N(2) vector which is a feature common to many bulky β -diketiminate derivatives (20). For the tetrazole species the fold angle is a relatively sharp 138.7° and in the amide/azide it is 154.5°. The Ga–N(β -diketiminate) bonds, avg. 1.947(2)Å in the tetrazole and 1.952(7)Å in the amide/azide derivative are very similar in each compound, and compare closely to those in the previously discussed oxo and sulfido bridged species (22). However, the Ga–N bonds to the tetrazole nitrogens (avg. 1.875(16)Å) and the amide (1.884(1)Å) nitrogen in the amide/azide isomer are notably shorter than these owing to their 'normal' character (19,21). They are also similar to the 1.872(2)Å observed in $\text{Cp}^*\{(\text{Me}_3\text{Si})_2\text{N}\}\text{Ga}(\mu\text{-N}_3)\}_2$ (25). The Ga–N (azide) bond length, 1.918(3)Å is almost the same as the 1.921(4)Å observed in $2,6\text{-}(\text{Me}_2\text{NCH}_2)_2\text{C}_6\text{H}_3\text{Ga}(\text{N}_3)_2$ (26). Within the N_3 ligand the N–N distances are similar to those previously reported.

The observation of tetrazole-amide/azide isomers in the same reaction mixture appears to be unique although both types of structures have been observed in various other systems (22). Their isolation appears to depend on the unique properties of the Dipp₂nacnac ligand which is large enough to prevent dimerization of the Dipp₂nacnacGaNSiMe₃ imide but small enough to allow reaction with a further equivalent of N_3SiMe_3 .

The postulated existence of the gallium imide intermediate prompted us to attempt the isolation of a stable example of such a species with use of a larger nitrogen-substituent. Monomeric gallium imides had been previously unknown as stable molecules. The lowest degree of aggregation known to occur for aluminum and gallium imides had been in the dimers (25,27-29) of the general formula $(\text{RMNR}')_2$ ($\text{M} = \text{Al}$ or Ga). In addition, synthetic approaches to these compounds had involved the elimination of alkanes, alkenes or dihydrogen from metal amides (or related species) at elevated ($> 100^\circ\text{C}$) temperatures (28-30). Unfortunately, this synthetic approach has frequently led to activation of C–H bonds within the molecule rather than an imide product (30). This route also has the disadvantage that it involves the elimination of atoms or groups from both the group 13 metal and the nitrogen, so that the coordination number of the metal and nitrogen are lowered. In effect, the imide product is less crowded than the precursor so that the probability of an associated product is increased. In contrast, the reaction of an $\text{M}(\text{I})$ species with an azide to afford an imide with elimination of N_2 usually proceeds at or below room temperature which minimizes the probability of side reactions. The reaction also results in an increase of the metal coordination number, while the coordination of the imide nitrogen remains unchanged from that in the azide precursor. The net result is that the steric crowding of the imide product is increased in comparison to that in the precursors. This diminishes the association tendency in the product.

Nonetheless, previous attempts (25,27) to use this approach with precursors such as $:\text{M}(\eta^5\text{-C}_5\text{Me}_5)$ ($\text{M} = \text{Al}$ or Ga) in reactions with the azides RN_3 ($\text{R} = \text{Si}(i\text{-Pr})_3$, $\text{Si}(t\text{-Bu})_3$, SiPh_3 or $2,6\text{-Me}_2\text{C}_6\text{H}_3$) have always led to associated products. Apparently, the substituents were insufficiently large in these cases. We therefore turned to the recently synthesized (31), very crowded azide Ar^*N_3 ($\text{Ar}^* = -\text{C}_6\text{H}_3\text{-}2,6\text{-Trip}_2$, $\text{Trip} = \text{C}_6\text{H}_2\text{-}2,4,6\text{-}i\text{-Pr}_3$) to stabilize a monomeric structure. Reaction of Ar^*N_3 with $:\text{M}(\text{Dipp}_2\text{nacnac})$ ($\text{M} = \text{Al}$ or Ga) in toluene solution in accordance with Eqn. (2) afforded the monomeric



imide products $\text{Dipp}_2\text{nacnacMNAr}^*$ ($\text{M} = \text{Al}$ or Ga) in moderate yield (32). Only the gallium species $\text{Dipp}_2\text{nacnacGaNAr}^*$ has been structurally characterized to date, and this molecule is illustrated in Figure 4. The *i*-Pr substituents are not shown for clarity. The gallium is bonded to two β -diketiminate nitrogens with an average bond length of $1.925(5)\text{\AA}$, and to an imide nitrogen which has a much shorter Ga–N distance of $1.742(3)\text{\AA}$. The latter is the shortest known GaN bond length in a molecular species (19) and suggests the existence of multiple character in the GaN bond. The Ga–N (β -diketiminate) distances are marginally shorter than those discussed earlier for the oxo, sulfido, tetrazole and amide/azide derivatives and this shortening is consistent with the lower coordination number (ie, 3 versus 4) of gallium. There is a rather large fold angle (151.4°) at the N(1)–N(2) vector. Furthermore, the coordination at gallium deviates slightly from planarity ($\Sigma^\circ\text{Ga} = 351.69$). The imide nitrogen (N(3)) has a bent coordination geometry with a Ga(1)–N(3)–C(30) angle of $134.6(3)^\circ$ which is in harmony with the presence of a stereochemically active lone pair of electrons. Formally, the gallium and nitrogen each provide a pair of electrons to create the GaN double bond. For maximum overlap the double bond requires the alignment of coordination planes at gallium and nitrogen. However, there is a torsion angle of 26.4° between these planes in the crystal structure. This angle probably represents a compromise between orbital overlap efficiency and steric interference between the Dipp rings of the $\text{Dipp}_2\text{nacnac}$ ligand and the Ar^* substituent at the imide nitrogen. The steric effects of the Ar^* substituent are also seen in the very unequal N(1)–Ga(1)–N(3) and N(2)–Ga(1)–N(3) angles which differ by 26.22° . Thus, it appears that the quasi planar N_2GaNC array is maintained at the expense of considerable steric congestion. The solution ^1H NMR spectrum also displays

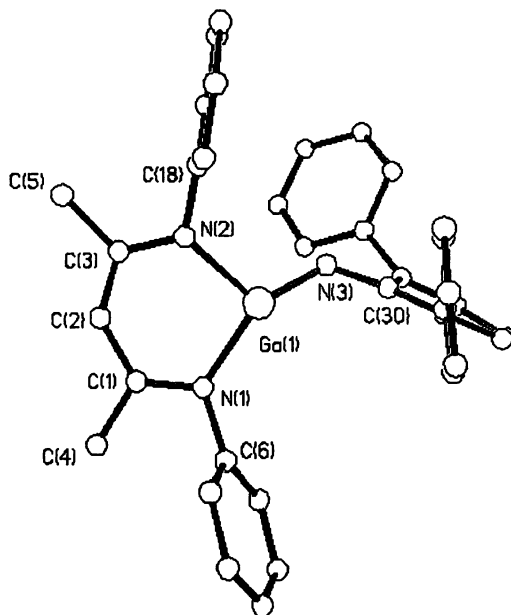


Figure 4. Drawing of $\text{Dipp}_2\text{nacnacGa=N-Ar}^*$ without *i*-Pr groups.

inequivalent Dipp-*i*-Pr signals at room temperature consistent with restricted rotation around the Ga–N bond and the presence of a Ga–N π bond involving overlap of gallium and nitrogen p-orbitals.

The nature of the Ga–N (imide) bond was investigated (32) by restricted Hartree-Fock calculations on the hypothetical molecule nacnacGa=NH using the Gaussian 98 program employing a 6-311G(d) basis set. It was found that the planar configuration, with the imido hydrogen atom coplanar to the GaN_2C_3 β -diketiminato ring skeleton, is a minimum on the potential energy surface. The calculated Ga–N (β -diketiminato) and Ga–N (imide) distances of 1.940 and 1.726 Å bear a close resemblance to the experimentally determined values. The configuration in which the imido hydrogen is oriented perpendicular to the plane of the remainder of the molecule was optimized to a transition state and it displayed one imaginary frequency. The calculated energy difference between the ground and transition state configurations is 48.6 kJ mol^{-1} . This value is very similar to the 53.8 kJ mol^{-1} calculated for the aminogallane H_2GaNH_2 (33). Clearly, there exists some Ga–N p-p π -bonding in the imide but the extent of this bonding is relatively small compared to the π -bonding seen in the lighter boron imides. The weakness of the π -bonding in Ga–N species may be attributed to the polar nature of the bonding and the disparity in sizes between gallium and nitrogen. The short Ga–N (imide) distance is probably due to the

polar character of the $\text{Ga}^{\delta+}-\text{N}^{\delta-}$ bonding. The strong donor character and relatively weak acceptor character of the $:\text{Ga}(\text{Dipp})_2\text{nacnac}$ species predicted from the energies of the frontier molecular orbitals are consistent with this view.

Acknowledgements

We are grateful to the National Science Foundation and the Alexander von Humboldt Stiftung for financial support and to P. J. Brothers, C. Raston, D. A. Atwood, and P. Shapiro who organized the main group chemistry symposia at Honolulu and San Diego. We also thank the National Computational Science Alliance for Grant No. 10047 using the SGI Origin 2000.

References

1. Cui, C.; Roesky, H. W.; Schmidt, H.-G.; Noltemeyer, M.; Hao, H.; Cimpoesu, F. *Angew. Chem. Int. Ed.* **2000**, *39*, 6274.
2. Hardman, N. J.; Eichler, B. E.; Power, P. P. *Chem. Commun.* **2000**, 1491.
3. Kuchta, M. C.; Bonanno, J.; Parkin, G. *J. Am. Chem. Soc.* **1996**, *118*, 10914.
4. Kuchta, M. C.; Dias, H. V. R.; Bott, S. G.; Parkin, G. *Inorg. Chem.* **1996**, *35*, 943.
5. Frazer, A.; Piggott, B.; Hursthouse, M. B.; Mazid, M. *J. Am. Chem. Soc.* **1994**, *116*, 4127.
6. Dias, H. V. R.; Jin, W. *Inorg. Chem.* **2000**, *39*, 815.
7. Janiak, C. *Coord. Chem. Rev.* **1997**, *163*, 107.
8. Dowling, C.; Ghosh, P.; Parkin, G. *Polyhedron* **1997**, *16*, 3469; Ghosh, P.; Hascall, T.; Dowling, C.; Parkin, G. *J. Chem. Soc. Dalton Trans.* **1998**, 3355.
9. Schmidt, E. S.; Jockisch, A.; Schmidbaur, H. *J. Am. Chem. Soc.* **1999**, *121*, 9758.
10. Haubrich, S. T.; Power, P. P. *J. Am. Chem. Soc.* **1998**, *120*, 2202.
11. Niemeyer, M.; Power, P. P. *Angew. Chem. Int. Ed. Engl.* **1998**, *37*, 1277.
12. Arduengo, A. J. *Acc. Chem. Res.* **1999**, *32*, 913.
13. Bourissou, D.; Guerret, O.; Gabbai, F. P.; Bertrand, G. *Chem. Rev.* **2000**, *100*, 39.
14. Phillips, A. D.; Power, P. P. Unpublished work.
15. Becke, A. D. *Phys. Rev.* **1988**, *A38*, 3098.
16. Becke, A. D. *Chem. Phys.* **1993**, *98*, 5648.
17. Lee, C.; Wang, Y.; Parr, R. G. *Phys. Rev.* **1988**, *B37*, 785.
18. Frisch, M. J.; Trucks, G. W.; Schlegel, H. B.; Scuseria, G. E.; Robb, M. A.; Cheeseman, J. R.; Zakrzewski, V. G.; Montgomery, Jr., J. A.; Stratmann, R. E.; Burant, J. C.; Dapprich, S.; Millam, J. M.; Daniels, A. D.; Kudin, K. N.;

- Strain, M. C.; Farkas, O.; Tomasi, J.; Barone, V.; Cossi, M.; Cammi, R.; Mennucci, B.; Pomelli, C.; Adamo, C.; Clifford, S.; Ochterski, J.; Petersson, G. A.; Ayala, P. Y.; Cui, Q.; Morokuma, K.; Malick, D. K.; Rabuck, A. D.; Raghavachari, K.; Foresman, J. B.; Cioslowski, J.; Ortiz, J. V.; Stefanov, B. B.; Liu, G.; Liashenko, A.; Piskorz, P.; Komaromi, I.; Gomperts, R.; Martin, R. L.; Fox, D. J.; Keith, T.; Al-Laham, M.; Peng, C. Y.; Nanayakkara, A.; Gonzalez, C.; Challacombe, M.; Gill, P. M. W.; Johnson, B.; Chen, W.; Wong, M. W.; Andres, J. L.; Gonzalez, C.; Head-Gordon, M.; Replogle, E. S.; Pople, J. A. Gaussian 98, Revision A.3. Gaussian, Inc., Pittsburgh, PA, 1998.
19. Brothers, P. J.; Power, P. P. *Adv. Organomet. Chem.* **1996**, *39*, 1.
 20. Stender, M.; Eichler, B. E.; Hardman, N. J.; Power, P. P.; Prust, J.; Noltemeyer, M.; Roesky, H. W. *Inorg. Chem.* **2001**, *40*, XXXX and references therein.
 21. Haaland, A. *Coordination Chemistry of Aluminum*; Robinson, G. H., Ed.; VCH: New York, NY, 1993, p 1-56.
 22. Hardman, N. J.; Power, P. P. *Inorg. Chem.* **2001**, *40*, 2474.
 23. Kuchta, M. C.; Parkin G. *Coord. Chem. Rev.* **1998**, *176*, 323.
 24. Hardman, N. J.; Power, P. P. *Chem. Commun.* **2001**, 1174.
 25. Jutzi, P.; Newmann, B.; Reumann, G.; Stammeler, H.-G. *Organometallics* **1999**, *18*, 2037.
 26. Cowley, A. H.; Gabbai, F.; Olbrich, F.; Corbelin, S.; Lagow, R. J. *J. Organomet. Chem.* **1995**, *487*, C5.
 27. Schulz, S.; Häming, L.; Herbst-Irmer, R.; Roesky, H. W.; Sheldrick, G. M. *Angew. Chem. Int. Ed. Engl.* **1994**, *33*, 969.
 28. Fischer, J. D.; Shapiro, P. J.; Yap, G. P. A.; Rheingold, A. L. *Inorg. Chem.* **1996**, *35*, 21.
 29. Wehmschulte, R. J.; Power, P. P. *J. Am. Chem. Soc.* **1996**, *118*, 791.
 30. Waggoner, K. M.; Power, P. P. *J. Am. Chem. Soc.* **1991**, *113*, 3385.
 31. Twamley, B.; Hwang, C.-S.; Hardman, N. J.; Power, P. P. *J. Organomet. Chem.* **2000**, *609*, 152.
 32. Hardman, N. J.; Cui, C.; Roesky, H. W.; Fink W. H.; Power, P. P. *Angew. Chem. Int. Ed.*, in press.
 33. Fink, W. H.; Power, P. P.; Allen, T. L. *Inorg. Chem.* **1997**, *36*, 1431.

Chapter 2

Pentamethylcyclopentadienyl Complexes of the Monovalent Group 13 Elements

L. O. Schebaum and P. Jutzi*

Faculty of Chemistry, University of Bielefeld, 33615 Bielefeld, Germany

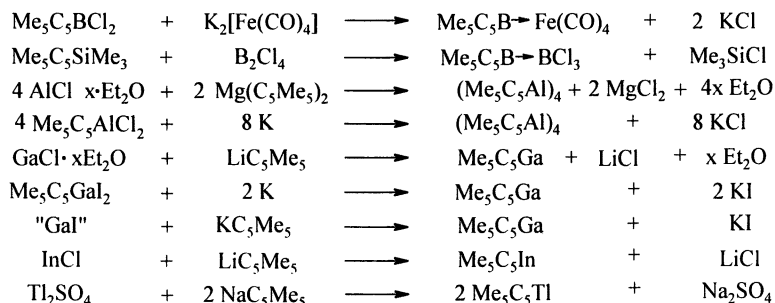
The group 13 elements can be stabilized in their formal +1 oxidation state by means of the π -bonded pentamethylcyclopentadienyl (Me_5C_5 , Cp^*) ligand. Synthesis, structure, bonding, and chemistry of Cp^*El (El = B, Al, Ga, In, Tl) compounds are described. The chemistry is dominated by I) homolytic and heterolytic $\text{Cp}^*\text{-El}$ bond cleavage, II) the donor function of the El centered lone-pair, and III) by a carbene-like bonding situation.

Introduction

The cyclopentadienyl (Cp) chemistry of the Group 13 elements has experienced great progress during the last decade. A prerequisite for this development was the knowledge of the fundamental properties of Cp substituents. Their versatile application is based on the rather flexible bonding mode ($\eta^1\text{-}\eta^5$; ionic-covalent), on the steric demand of ring-substituted species (kinetic stabilization), and on the leaving group character (homolytic and heterolytic El-C(Cp) bond cleavage) (1,2). A fascinating aspect of Group 13 element Cp chemistry concerns the possibility to stabilize the elements boron, aluminium and gallium in their +1 oxidation state with the help of the π -bonded pentamethylcyclopentadienyl (Cp^*) ligand. In this article, these compounds together with their indium and thallium analogues are described with respect to their synthesis, structure, bonding and reactivity and with a special emphasis on the effects exerted by the Cp^* ligand.

Synthesis

Synthetic routes to Cp*El compounds with El = B, Al, Ga, In, Tl are described in Scheme 1. The synthesis of Cp*Tl (3,4) and Cp*In (5,6) was performed by metathesis reactions starting from stable inorganic precursors and following strategies already known for the preparation of other cyclopentadienyl thallium and indium species. Both compounds are extremely sensitive to decomposition in the presence of air, moisture, and even light. Cp*Tl is soluble in ethereal and aromatic solvents and even in hydrocarbons. Cp*In has limited thermal stability in ethereal and aromatic solvents, in which decomposition to elemental In is observed. It dissolves in cyclohexane without decomposition.



*Scheme 1. Synthetic routes to Cp*El compounds [Cp* = Me₅C₅; El = B, Al, Ga, In, Tl; in case of boron only adducts with Lewis acids have been isolated].*

A real breakthrough in this field was the first preparation of Cp*Al in the group of Schnöckel. This compound was obtained as a tetrameric species by the reaction of a metastable Al(I)Cl solution in toluene/ether with Cp*₂Mg as Cp* transfer agent (7). Later on, the compound could be prepared by a more convenient route, namely by reduction of the trivalent aluminum compound Cp*AlCl₂ with potassium metal (8). (Cp*Al)₄ is only a little air- and moisture-sensitive and is sparingly soluble in aromatic solvents. The compound decomposes at temperatures above 100°C. Interestingly, longer thermal treatment in boiling toluene led to the formation of the Cp*₂Al⁺ cation (9).

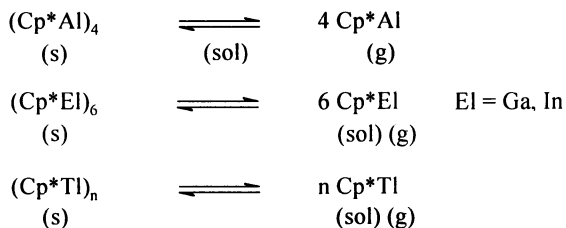
Similarly, the gallium compound Cp*Ga was first prepared in the group of Schnöckel by a metathesis reaction using a metastable Ga(I)Cl solution (10). More convenient synthetic routes were described some years later. The trivalent gallium compound Cp*GaI₂ was reduced with potassium (11), and the easy to

prepare gallium compound „Gal“ (12) reacted with Cp*K to give Cp*Ga in good yields (13). The compound is very sensitive to air and moisture and is soluble in all aprotic and halogen free organic solvents. No decomposition was observed under irradiation or in boiling toluene. Purification can be performed by distillation in vacuo without any decomposition.

So far it has not been possible to synthesize the boron compound of composition (Cp*B)_n, but there is access to stable adducts of monomeric Cp*B with Lewis aids. Thus, the Fe(CO)₄ stabilized complex Cp*B-Fe(CO)₄ was obtained by a metathesis reaction of Cp*BCl₂ with the ferrate complex K₂[Fe(CO)₄] (14), and the BCl₃ stabilized complex Cp*B-BCl₃ was formed in the reaction of Cp*SiMe₃ with B₂Cl₄ under elimination of Me₃SiCl (15). These compounds will be discussed in context with comparable adducts of the other Cp*El species.

Structure and Bonding

Scheme 2 specifies the structures of the Cp*El compounds (El = Al, Ga, In, Tl) in the solid state, in solution, and in the gas phase. In the gas phase, all compounds exist as monomers possessing a C_{5v}-halfsandwich structure (16,17,5,18). As an example, the structure of Cp*Ga determined by GED (17) is presented in Figure 1. Experimental parameters for these compounds are collected in Table I together with calculated parameters for Cp*B (19).



*Scheme 2. Solid state (s), solution (sol), and gas phase (g) structures of Cp*El compounds.*

In the solid state, oligomeric or polymeric structures are observed for the Cp*El compounds. A tetrameric structure with a tetrahedral Al₄ core and with

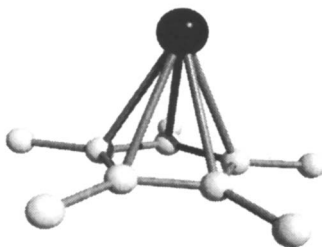


Figure 1. Drawing of the gas phase structure of Cp^*Ga .

Table I: Calculated (El = B) and experimental (El = Al, Ga, In, Tl) parameters for $\eta^5\text{-Cp}^*\text{El}$ compounds in the gas phase.^{a)}

Cp^*El	B ⁽¹⁹⁾	Al ⁽¹⁶⁾	Ga ⁽¹⁷⁾	In ⁽⁵⁾	Tl ⁽¹⁸⁾
El-C (Å)	1.925	2.388(7)	2.405(4)	2.592(4)	2.663(5)
C-C (Å)	1.434	1.414(5)	1.420(3)	1.432(4)	1.422(6)
C-C(Me) (Å)	1.504	1.529(6)	1.522(3)	1.505(5)	1.520(7)
$\angle \text{C}_3\text{C/C-C}$ (°) ^{b)}	+ 5.46	+ 5(2)	+0.2(3)	-4.1(3)	-6.4(6)
$\text{Cp}_{\text{centroid}}\text{-El}$	-	2.063(9)	2.081(5)	2.288(4)	2.372(5)

a) measured by GED

b) defined as positive when the methyl groups are bent towards the metal atom

Al-Al distances of 2.77 Å is found for $(\text{Cp}^*\text{Al})_4$; each Al atom is η^5 -bonded to a terminal Cp^* ring in such a manner that the ring plane is parallel to the opposite Al_3 face of the tetrahedron (7). According to quantum chemical calculations (20,21), the Al_4 cluster with four cluster-binding electron pairs is held together by four $2e3c$ bonds on the four faces of the tetrahedron. The relative weakness of the Al-Al bonding is inferred from the Al-Al distance, which is considerably longer than a typical single bond distance (2.66 Å), and is caused by π -back-bonding from the Cp^* ligand to the Al center. In contrast to the tetrameric structure of $(\text{Cp}^*\text{Al})_4$, hexameric aggregates with distorted octahedral El_6 cores are found in the solid state structures of the isomorphous $(\text{Cp}^*\text{Ga})_6$ (22) and $(\text{Cp}^*\text{In})_6$ (5,6). Interestingly, the Cp^*El vectors do not point towards the center of the octahedron and El-El distances are nearly identical and rather long (~4.10

Å). It was proposed that both clusters are held together by van der Waals interactions between the Cp* ligands (21) and by only rather weak donor-acceptor interactions between the metals (23,24). Finally, Cp*Tl crystallizes in a polymeric chain-like structure with alternating Tl atoms and $\mu_2\eta^5$ bonded Cp* rings (13). This type of structure is found also for some alkali metal Cp* compounds (2) and is indicative of predominantly ionic bonding interactions. Representations of the solid state structures of (Cp*Al)₄, (Cp*El)₆ (El = Ga, In), and (Cp*Tl)_x are presented in Figure 2.

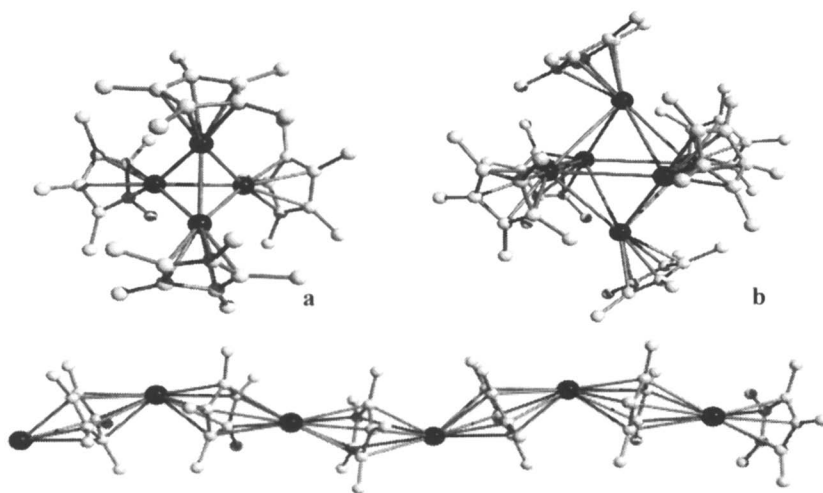


Figure 2. Drawings of the structures of (Cp*Al)₄, (Cp*El)₆ (El = Ga, In), and of (Cp*Tl)_x. (a: Reproduction from reference 7. Copyright 1991; b: Reproduction from reference 22. Copyright 1997)

In solution, facile degradation to monomeric structures of the half-sandwich type takes place for the Cp* compounds of gallium, indium, and thallium (see Scheme 2). On the other hand, the aluminum compound still exists as a tetramer, at least at room temperature. At higher temperatures, dissociation into monomeric half-sandwich species is observed. Quite different chemical shifts in ²⁷Al NMR spectroscopy are found for (Cp*Al)₄ ($\delta = -80.7$ ppm) and for Cp*Al ($\delta = -149$ ppm) (16). The energy for the tetramerisation of Cp*Al was calculated to be $-150 (\pm 20)$ kJ mol⁻¹.

Cp*El (El = B, Al, Ga, In) compounds have been examined by DFT calculations to establish their ground states and their frontier orbitals (19). Each species possesses a singlet ground state, and the singlet-triplet energy gap is rather large (~ 60 kcal mol⁻¹). In general, there is excellent agreement between

the DFT calculations and the gas phase electron diffraction data obtained for Cp*Al, Cp*Ga and Cp*In. As expected, the El-C and Cp(centroid)-El distances increase with the atomic number of El, and the Al-C and Ga-C bond distances are almost identical. With the exception of Cp*Ga, the methyl groups are bent out of the plane of the Cp* ring; they are oriented toward the group 13 element in the case of Cp*B and Cp*Al and away from the element in the case of Cp*In and Cp*Tl. These orientations are consistent with the view that covalent interactions dominate and determine the final structures (25). The relative amount of electron transfer between the Cp* ligand and the group 13 element (viewing Cp* as anion and El⁺ as cation) can be estimated from the NBO charges on the elements (19), which are collected in Table II. The positive charge on boron turns out to be much lower than that of any other group 13 element.

Table II. NBO charge (q) of El in Cp*El compounds.

El	B	Al	Ga	In
q	+ 0.07726	+ 0.61591	+ 0.5844	+ 0.6599

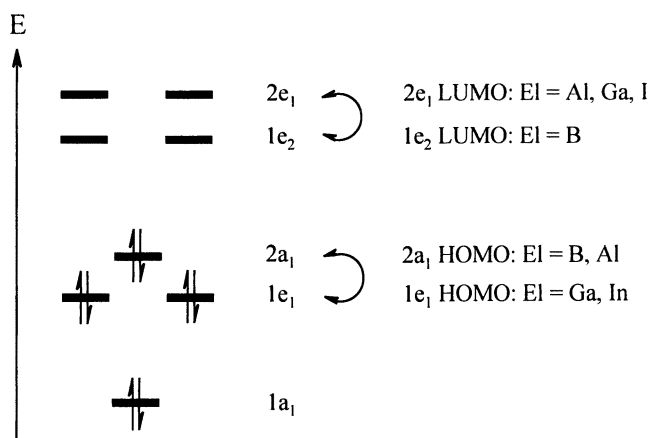


*Figure 3. Qualitative MO scheme for η^5 -Cp*El compounds (El = B, Al, Ga, In).*

A qualitative MO description for the Cp*El compounds (El = B, Al, Ga, In) is presented in Figure 3. According to the DFT calculations (19), the HOMO of

Cp*B and Cp*Al exhibits a distinctly lone pair (σ -type) character, whereas the HOMO of Cp*Ga and Cp*In is degenerate and corresponds to π -bonding between the Cp* fragment and the group 13 element. The magnitude of π -overlap is reflected in the energy gap of the respective orbitals ($1e_1$ and $2e_1$). As a result, the symmetry of the LUMO for Cp*B is different from that for the other Cp*E1 compounds. In Cp*B, the stronger π -interaction renders the antibonding $2e_1$ orbitals higher in energy than the $1e_2$ orbitals which have no contribution from E1 and are localized on the Cp* ligand. For the heavier group 13 elements, the relatively weaker π -overlap leaves the $2e_1$ orbitals as the LUMO's.

Reaction Chemistry

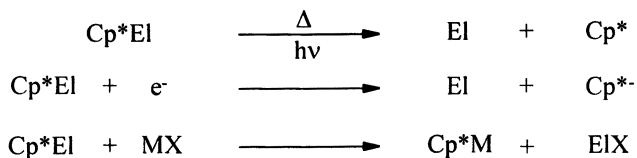
The chemistry of the pentamethylcyclopentadienyl complexes of the monovalent group 13 elements is dominated by

- I) homolytic and heterolytic Cp*-E1 bond cleavage,
- II) the donor function of the E1 centered lone-pair, and
- III) the carbene-like bonding situation at the E1 center

On the basis of these phenomena, the reactions performed with Cp*E1 compounds will be classified and briefly described.

Homolytic and Heterolytic Cp*-E1 Bond Cleavage

It is well known in the cyclopentadienyl chemistry of the p-block elements that the Cp-E1 bond can be split thermally, photo-chemically, or by attack of nucleophiles, electrophiles, oxidizing agents and reducing agents (1). In the chemistry of the Cp*E1 compounds, homolytic and heterolytic bond cleavage as depicted in Scheme 3 have been used in synthetic procedures.



Scheme 3. Homolytic and heterolytic Cp-E1 bond cleavage.*

The deposition of indium metal in a low-temperature MOCVD process was performed with the help of Cp*In (25); similarly, the deposition of elemental gallium from the precursor Cp*Ga was reported to occur, but only at higher temperatures (~ 600°C) (11). The formation of elemental indium and thallium was observed during irradiation of the corresponding Cp*El compounds in solution and in the solid state (3,4,5,6). Cp*Tl is known to be a synthetically useful reagent for transferring Cp* ligands in a nucleophilic substitution process, for example to d-block element centers (26). Nucleophilic substitution and reduction processes have been observed in the reaction of Cp*In with supersilyl sodium (^tBu₃SiNa), whereby the novel cluster hexasupersilyl octaindane [(^tBu₃Si)₆In₈] was formed (27).

Cp*El Compounds as Donors in Donor-Acceptor Complexes

The exposed lone-pair at the group 13 element in Cp*El compounds allows the formation of donor-acceptor complexes of the type Cp*El-Acceptor and several of such complexes with trivalent group 13-element compounds and with transition-metal complex fragments as acceptors have already been described; they are collected in Table III and IV. Figure 4 shows the molecular structures of Cp*B-BCl₃ and of Cp*Ga-B(C₆F₅)₃, and Figure 5 shows the molecular structures of Cp*Ga-Cr(CO)₅, (Cp*Ga)₄Ni, (CO)₃Fe(μ₂-Cp*Ga)₃Fe(CO)₃, and (Cp*Ga)Pt(μ₂-Cp*Ga)₃Pt(Cp*Ga). Only a couple of these complexes have been synthesized by routes other than direct combination of Cp*El and the corresponding Lewis-acidic component. Thus, the compound Cp*Al-Fe(CO)₄ was prepared by reaction of Cp*AlCl₂ with K₂[Fe(CO)₄] (32); the synthesis of the Cp*B complex has already been described (see Synthesis).

Table III. Donor-acceptor complexes with group 13-element acceptors.

Cp*B→BCl ₃ (28)	Cp*B→B(SiCl ₃)Cl ₂ (28)
Cp*Al→B(C ₆ F ₅) ₃ (29)	Cp*Al→Al(C ₆ F ₅) ₃ (30)
Cp*Ga→B(C ₆ F ₅) ₃ (31)	Cp*Ga→Ga ^t Bu ₃ (31)
Cp*Ga→Ga(Cp*)Cl ₂ (31)	Cp*Ga→Ga(Cp*)I ₂ (31)

Table IV. Transition-metal complexes with Cp*El ligands.

Cp*B-Fe(CO) ₄ (14)		
Cp*Al-Fe(CO) ₄ (32)	Cp*Al-Cr(CO) ₅ (33)	cis(Cp*Al) ₂ Pt(dcpe)(34)
(CpNi) ₂ (μ ₂ -AlCp*) ₂ (35)	(CO) ₆ Co ₂ (μ ₂ -AlCp*) ₂ (36)	
Cp*Ga-Fe(CO) ₄ (37)	Cp*Ga-Cr(CO) ₅ (37)	cis(Cp*Ga) ₂ Mo(CO) ₄ (38)
cis(Cp*Ga) ₂ Pt(dcpe)(34)	(Cp*Ga) ₄ Ni(38)	(CO) ₆ Co ₂ (μ ₂ -GaCp*) ₂ (37)
(CO) ₆ Fe ₂ (μ ₂ -GaCp*) ₃ (37)	(CO) ₆ Ni(μ _x -GaCp*) ₄ (37)	
(Cp*Ga) ₂ Pt ₂ (μ ₂ -GaCp*) ₃ (39)	(Cp*Ga) ₂ Fe(Cp*)GaCl ₂ ·THF(40)	
Cp*In-Cr(CO) ₅ (41)		
Cp* = Me ₅ C ₅		
dcpe = bis(dicyclohexylphosphino)ethane		

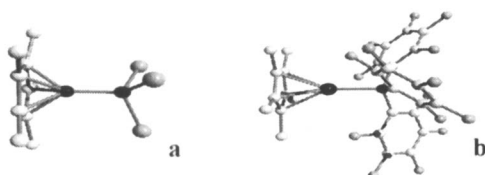


Figure 4. Drawings of the molecular structure of Cp*BBCl₃ and of Cp*GaB(C₆F₅)₃. (a: Reproduction from reference 28. Copyright 2000; b: Reproduction from reference 31. Copyright 2001)

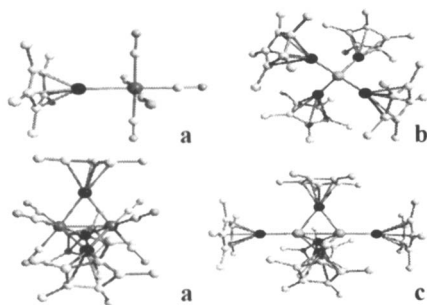


Figure 5. Drawings of the molecular structures of Cp*Ga-Cr(CO)₅, (Cp*Ga)₄Ni, (CO)₃Fe(μ₂-Cp*Ga)₃Fe(CO)₃, and (Cp*Ga)₃Pt(μ₂-Cp*Ga)₃Pt(Cp*Ga). (a: Reproduction from reference 37. Copyright 1998; b: Reproduction from reference 38. Copyright 1999; c: Reproduction from reference 39. Copyright 2000)

Structure and bonding in these complexes with special emphasis on the donor-acceptor bond have been discussed in detail on the basis of experimental findings and theoretical calculations (32,33,34,36,39). The results can be summarized as follows: I) The non-directional *s*-orbital character of the lone-pair on Cp*E1 allows unusual geometries with Cp*(centroid)-E1-acceptor arrangements deviating from linearity; II) The positive charge on the group 13 element is reduced by a stronger π -bond within the Cp*E1 unit, as concluded from the observed shorter Cp*(centroid)-E1 distance; III) In transition-metal complexes, the Cp*E1 ligand is a strong σ -donor and a weak π -acceptor; the Cp*(centroid)-E1 distance reflects the donor capability of the Cp*E1 unit and can adjust to the electronic requirements on the complexed metal or metalloid (see Table V); IV) The Cp*E1 ligands are found in terminal (μ_1) and in bridging (μ_2 , μ_3) positions.

In Table V, the Cp*(centroid)-Ga distances of some representative Cp*Ga donor-acceptor complexes are presented.

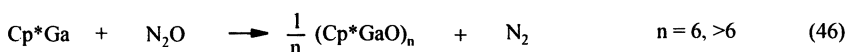
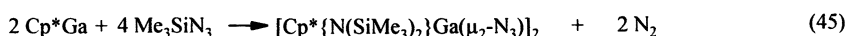
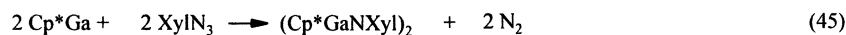
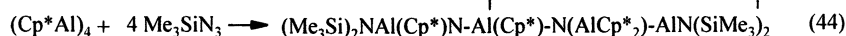
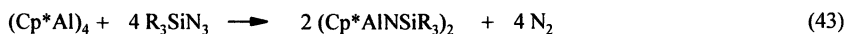
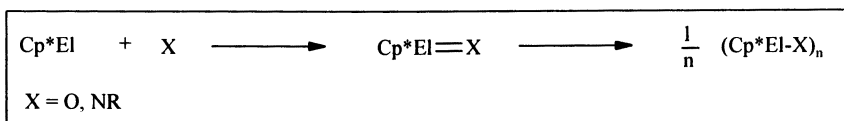
Table V. Cp*(centroid)-Ga distances (d [Å]) in donor-acceptor complexes.

Cp*Ga-B(C ₆ F ₅) ₃	Cp*Ga-Fe(CO) ₄	Cp*Ga-Cr(CO) ₅
1.906(5)	1.863(4)	1.910(4)
cis(Cp*Ga) ₂ Mo(CO) ₄	(Cp*Ga) ₄ Ni	(Cp*Ga) ₂ Pt ₂ (μ^2 -GaCp*) ₃
1.930(6)	2.003(4)	1.969(4)/2.013(4)

A surprising result was observed in the reaction of Cp*In with the Lewis-acid B(C₆F₅)₃ and with H₂O·B(C₆F₅)₃ in toluene solution, whereby the compound [(η^5 -C₇H₈)In(μ - η^5 -Cp*)In(η^6 -C₇H₈)]⁺[(F₅C₆)₃BO(H)B(C₆F₅)₃]⁻ was obtained. The central core of the triple-decker cation features an η^5 -bonded In atom on each face the μ -Cp* group (42).

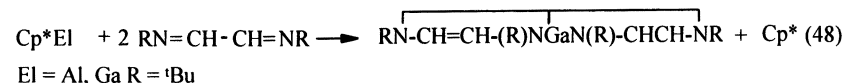
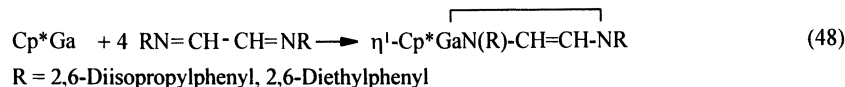
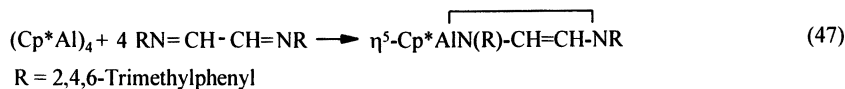
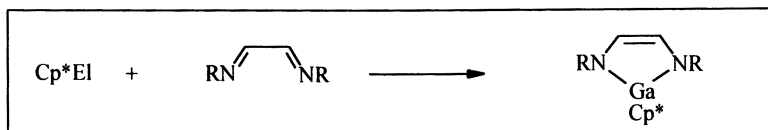
Oxidative Addition, Cycloaddition, and Insertion Reactions

A carbene-like bonding situation in Cp*E1 compounds is the necessary prerequisite for the oxidative addition, cycloaddition and insertion reactions, which have been observed mainly for the aluminium and gallium compounds. Such a constellation is created by haptotropic shifts of the η^5 -Cp* ligand. Oxidative addition reactions are collected in Scheme 4, cycloaddition reactions in Scheme 5, and insertions reactions in Scheme 6.

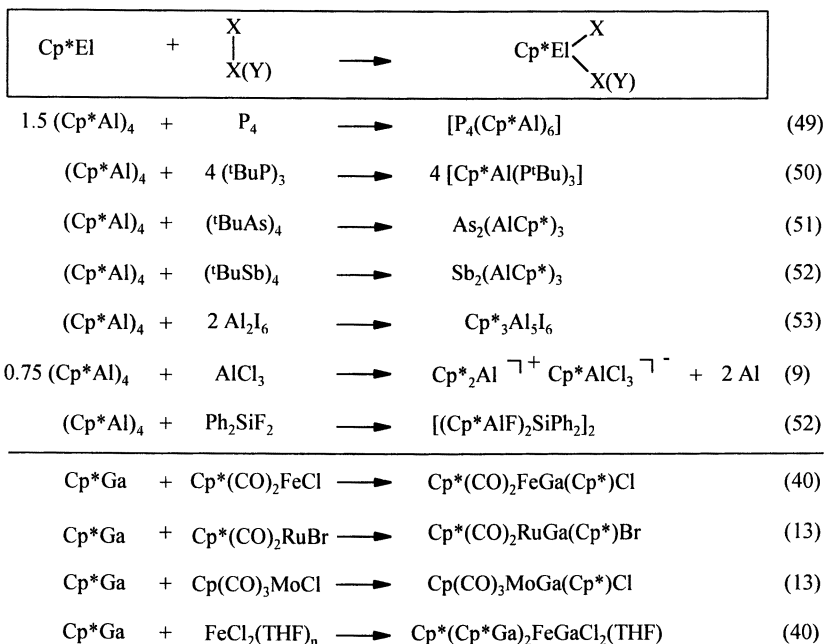


Mes = 2,4,6-Trimethylphenyl; Xyl = 2,6-Dimethylphenyl; R = ⁱPr, ^tBu, Ph

Scheme 4. Oxidative Addition.



Scheme 5. Cycloaddition.



Scheme 6. Insertion Reactions.

Several organic azides have been used as sources for nitrene fragments (NR) in oxidative addition reactions with (Cp*Al)₄ or with Cp*Ga (45-47). The experiments clearly show that oxidative addition products of the type Cp*E=NR cannot be stabilized under ordinary conditions. They dimerize to give [2+2] cycloaddition products or they undergo further insertion and rearrangement reactions to give structurally more complicated products. Only oligomeric products have been observed in the reaction of Cp*Ga with N₂O (46).

[4+1] Cycloaddition products are obtained in the reaction of (Cp*Al)₄ or of Cp*Ga with differently substituted diazabutadienes (47,48). The leaving-group character of the Cp* substituents is the reason for a further reaction with a second equivalent of t-butylazabutadiene. There exist several examples for the insertion of (Cp*Al)₄ or of Cp*Ga into homo- and heteropolar bonds. Thus insertions into P-P, As-As, Al-I, Al-Cl, Si-F, Fe-Cl, Ru-Br, and into Mo-Cl bonds have been described, which lead to quite novel types of compounds.

Given the leaving group character of the Cp* substituent, the novel compounds prepared by oxidative addition, cycloaddition and insertion

reactions possess the potential for a further interesting reaction chemistry. This has already been demonstrated in a few cases (44,48).

Acknowledgements

We thank Prof. P. Shapiro for improving the English. The experimental work reported from our group was accomplished by G. Reumann and T. Pott. The dedication and expertise of these co-workers is gratefully acknowledged. Funding was kindly provided by the Deutsche Forschungsgemeinschaft, by the Fond der Chemischen Industrie and by the University of Bielefeld.

References

1. Jutzi, P.; Reumann, G. *J. Chem. Soc., Dalton Trans.* **2000**, 2237.
2. Jutzi, P.; Burford, N. *Chem. Rev.* **1999**, 99, 969.
3. Rupprecht, G. A.; Mersele, L. W.; Fellmann, J. D.; Schrock, R. R. *J. Am. Chem. Soc.* **1980**, 102, 6236.
4. Werner, H.; Otto, H.; Kraus, H. *J. Organomet. Chem.* **1986**, 315, C57.
5. Beachley Jr. O. T.; Churchill, M. R.; Fettingner, J. C.; Pazik, J. C.; Victoriano, L. *J. Am. Chem. Soc.* **1986**, 108, 346.
6. Beachley, Jr. O. T.; Blom, R.; Churchill, M. R.; Faigri Jr. K.; Fettingner, J. C.; Pazik, J. C.; Victoriano, L. *Organometallics* **1989**, 8, 346.
7. Dohmeier, C.; Robl, C.; Tacke, M.; Schnöckel, H. *Angew. Chem.* **1991**, 103, 594; *Angew. Chem. Int. Ed. Engl.* **1991**, 30, 564.
8. Schulz, S.; Roesky, H. W.; Koch, H. J.; Sheldrick, G. M.; Stalke, D.; Kuhn, A. *Angew. Chem.* **1993**, 105, 1828; *Angew. Chem. Int. Ed. Engl.* **1993**, 32, 1729.
9. Dohmeier, C.; Schnöckel, H.; Robl, C.; Schneider, U.; Ahlrichs, R. *Angew. Chem.* **1993**, 105, 1714; *Angew. Chem. Int. Ed. Engl.* **1993**, 32, 1655.
10. Loos, D.; Schnöckel, H. *J. Organomet. Chem.* **1993**, 463, 37.
11. Jutzi, P.; Neumann, B.; Reumann, G.; Stammler, H.-G. *Organometallics* **1998**, 17, 1305.
12. Green, M. L. H.; Mountford, P.; Smout, G. J.; Speel, S. R. *Polyhedron* **1990**, 9, 2763.
13. Jutzi, P.; Schebaum, L. O. Unpublished results.
14. Cowley, A. H.; Lomeli, V.; Voigt, A. *J. Am. Chem. Soc.* **1998**, 120, 6401.
15. Greiwe, P.; Bethäuser, A.; Pritzkow, H.; Kühler, T.; Jutzi, P.; Siebert, W. *Eur. J. Inorg. Chem.* **2000**, 1927.

16. Haaland, A.; Martinsen, K.-G.; Shlykov, S. A.; Volden, H. V.; Dohmeier, C.; Schnöckel, H. *Organometallics* **1995**, *14*, 3116.
17. Haaland, A.; Martinsen, K.-G.; Volden, H. V.; Loos, D.; Schnöckel, H. *Acta Chem. Scand.* **1994**, *48*, 172.
18. Blom, R.; Werner, H.; Wolf, J. J. *Organomet. Chem.* **1988**, *354*, 293.
19. Macdonald, C. L. B.; Cowley, A. H. *J. Am. Chem. Soc.* **1999**, *121*, 12113.
20. Ahlrichs, R.; Ehrig, M.; Horn, H. *Chem. Phys. Lett.* **1991**, *183*, 227.
21. Dohmeier, C.; Loos, D.; Schnöckel, H. *Angew. Chem.* **1996**, *108*, 141; *Angew. Chem. Int. Ed. Engl.* **1996**, *35*, 129.
22. Loos, D.; Baum, E.; Ecker, A.; Schnöckel, H.; Downs, A. J. *Angew. Chem.* **1997**, *109*, 894; *Angew. Chem. Int. Ed. Engl.* **1997**, *36*, 860.
23. Budzelaar, P. H. M.; Boersma, J. *Recl. Trav. Chim. Pays-Bas* **1990**, *109*, 187.
24. Janiak, C.; Hoffmann, R. *J. Am. Chem. Soc.* **1990**, *112*, 5924.
25. Jang, H. J. *Diss. Abstr. Int. B.* **1995**, *56*(7), 3829. In this context it is interesting to note that the parent compound CpIn has been used for the preparation of monodisperse indium nanoparticles: Soulantica, K.; Maisonnat, A.; Fromen, M.-C.; Casanove, M.-J.; Lecante, P.; Chaudret, B. *Angew. Chem.* **2001**, *113*, 462; *Angew. Chem. Int. Ed. Engl.* **2001**, *40*, 448.
26. a) Salzer, A.; Schmale, H.; Stauber, R.; Streiff, S. *J. Organomet. Chem.* **1991**, *408*, 403; b) Kölle, U.; Ding, T.-Z.; Keller, H.; Ramakrishna, B. L.; Raabe, E.; Krüger, C.; Raabe, G.; Fleischhauer, J. *Chem. Ber.* **1990**, *123*, 227; c) Andell, O.; Goddard, R.; Holle, S.; Jolly, P. W.; Krüger, C.; Tsay, Y. H. *Polyhedron* **1989**, *8*, 203; d) Herrmann, W. A.; Thiel, W. R.; Herdtweck, E. *J. Organomet. Chem.* **1988**, *353*, 323; e) Hachgenei, J. W.; Angelici, R. J. *J. Organomet. Chem.* **1988**, *355*, 359; f) Kraus, H.-J.; Werner, H.; Krüger, C. *Z. Naturforsch. B* **1983**, *38B*(6), 733.
27. Wiberg, N.; Blank, T.; Purath, A.; Stößer, G.; Schnöckel, H. *Angew. Chem.* **1999**, *111*, 2745; *Angew. Chem. Int. Ed. Engl.* **1999**, *38*, 2563.
28. Greiwe, P.; Bethäuser, A.; Pritzkow, H.; Kühler, T.; Jutzi, P.; Siebert, W. *Eur. J. Inorg. Chem.* **2000**, 1927.
29. Gordon, J. D.; Voigt, A.; Macdonald, C. L. B.; Silverman, J. S.; Cowley, A. H. *J. Am. Chem. Soc.* **2000**, *122*, 950.
30. Gordon, J. D.; Macdonald, C. L. B.; Cowley, A. H. *Chem. Commun.* **2001**, 75.
31. Jutzi, P.; Neumann, B.; Reumann, G.; Schebaum, L. O.; Stammli, H.-G. *Organometallics* **2001**, *20*, 2854.
32. Weiss, J.; Stetzkamp, D.; Nuber, B.; Fischer, R. A.; Boehme, C.; Frenking, G. *Angew. Chem.* **1997**, *109*, 95; *Angew. Chem. Int. Ed. Engl.* **1997**, *36*, 70.
33. Yu, Q.; Purath, A.; Donchev, A.; Schnöckel, H. *J. Organomet. Chem.* **1999**, *584*, 94.

34. Weiss, D.; Steinke, T.; Winter, M.; Fischer, R. A.; Fröhlich, N.; Uddin, J.; Frenking, G. *Organometallics* **2000**, *19*, 4583.
35. Dohmeier, C.; Krautscheid, H.; Schnöckel, H. *Angew. Chem.* **1994**, *106*, 2570; *Angew. Chem. Int. Ed. Engl.* **1994**, *33*, 2482.
36. Üffing, C.; Ecker, A.; Köppe, R.; Schnöckel, H. *Organometallics* **1998**, *17*, 2373.
37. Jutzi, P.; Neumann, B.; Reumann, G.; Stammler, H.-G. *Organometallics* **1998**, *17*, 1305.
38. Jutzi, P.; Neumann, B.; Schebaum, L. O.; Stammler, A.; Stammler, H.-G. *Organometallics*, **1999**, *18*, 4462.
39. Weiß, D.; Winter, M.; Fischer, R. A.; Yu, C.; Wichmann, K.; Frenking, G. *Chem. Commun.* **2000**, 2495.
40. Jutzi, P.; Neumann, B.; Schebaum, L. O.; Stammler, A.; Stammler, H.-G. *Organometallics* **2000**, *19*, 1445.
41. Jutzi, P.; Neumann, B.; Reumann, G.; Schebaum, L. O.; Stammler, H.-G. *Organometallics* **1999**, *18*, 2550.
42. Cowley, A. H.; Macdonald, C. L. B.; Silverman, J. S.; Gordon, J. D.; Voigt, A. *Chem. Commun.* **2001**, 175.
43. Schulz, S.; Voigt, A.; Roesky, H. W.; Häming, L.; Herbst-Irmer, R. *Organometallics* **1996**, *15*, 5252.
44. Schulz, S.; Häming, L.; Herbst-Irmer, R.; Roesky, H. W.; Sheldrick, G. M. *Angew. Chem.* **1994**, *106*, 1052; *Angew. Chem. Int. Ed. Engl.* **1994**, *33*, 969.
45. Jutzi, P.; Neumann, B.; Reumann, G.; Stammler, H.-G. *Organometallics* **1999**, *18*, 2037.
46. Reumann, G. Ph.D. thesis, University of Bielefeld, Bielefeld, Ge, **1999**.
47. Cowley, A. H.; Gordon, J. D.; Abernethy, C. D.; Clyburne, J. A. C.; McBurnett, B. G. *J. Chem. Soc., Dalton Trans.* **1998**, 1937.
48. Pott, T.; Jutzi, P.; Neumann, B.; Stammler, H.-G. *Organometallics* **2001**, *20*, 1965.
49. Dohmeier, C.; Schnöckel, H.; Robl, C.; Schneider, U.; Ahlrichs, R. *Angew. Chem.* **1994**, *106*, 225; *Angew. Chem. Int. Ed. Engl.* **1994**, *33*, 199.
50. Üffing, C.; von Hänisch, C.; Schnöckel, H. *Z. Anorg. Allg. Chem.* **2000**, *626*, 1557.
51. von Hänisch, C. K. F.; Üffing, C.; Junker, M. A.; Ecker, A.; Kneisel, B. O.; Schnöckel, H. *Angew. Chem.* **1996**, *108*, 3003; *Angew. Chem. Int. Ed. Engl.* **1996**, *35*, 2875.
52. Schulz, S.; Schoop, T.; Roesky, H. W.; Häming, L.; Steiner, A.; Herbst-Irmer, R. *Angew. Chem.* **1995**, *107*, 1015; *Angew. Chem. Int. Ed. Engl.* **1995**, *34*, 919.
53. Üffing, C.; Baum, E.; Köppe, R.; Schnöckel, H. *Angew. Chem.* **1998**, *110*, 2488; *Angew. Chem. Int. Ed. Engl.* **1998**, *37*, 2397.

Chapter 3

A Comparison of the Structural and Chemical Properties of Cyclopentadienyl Compounds of B(III), Al(III), Ga(III), In(III), and Tl(III)

Pamela J. Shapiro

Department of Chemistry, University of Idaho, Moscow, ID 83844-2343

This chapter reviews the chemistry of trivalent cyclopentadienyl compounds of the group 13 elements B, Al, Ga, In, and Tl. The syntheses, structures, fluxionalities and reactivities of these compounds are compared with an emphasis on how variations in the electronic properties of these elements affect their bonding to cyclopentadienyl ligands.

Introduction

It has been written that group 13 is "considered to be the worst group in the periodic table for trends since....they often seem to be rather irregular" (1). Irregular though they may be, variations in the the electronic properties of the group 13 elements are quite sharply reflected in the chemistry of their cyclopentadienyl compounds. This is due to the cyclopentadienyl ring's ability to vary its bonding characteristics from primarily ionic to π -covalent and σ -covalent depending on the size and electronic requirements of the element to which it is attached.

This chapter reviews the chemistry of cyclopentadienyl group 13 compounds with an emphasis on how variations in cyclopentadienyl-element bonding, as a result of electronic trends, are manifested in the syntheses,

structures, fluxionalities, and reactivities of these compounds. Some review articles were particularly helpful guides to the literature on cyclopentadienyl group 13 compounds (2,3). There are only a few communications on the synthesis of cyclopentadienyl compounds of Tl(III) (4-6). ^1H NMR spectra and elemental analyses are consistent with the assigned formulae; however, no further reports on these compounds have appeared. Given the interesting properties of the lighter congeners and the utility of the NMR active I=1/2 nuclei ^{205}Tl (70%) and ^{203}Tl (30%) for characterizing bonding (7), further investigation of the thallium compounds is worthwhile.

Univalent cyclopentadienyl-gallium and -aluminum compounds are considerably less stable and therefore less common than the In(I) and Tl(I) compounds. Nevertheless, access to their chemistry has been gained through the pioneering work of Schnöckel and coworkers (8-11) and subsequent synthetic improvements introduced by Roesky (12) and Jutzi (13). Since this chemistry is discussed in another chapter in this volume, limited reference to it is made here.

The term cyclopentadienyl ligand, as used herein, refers to a broad class of ligands which includes substituted cyclopentadienyl rings, indenyl rings, and fluorenyl rings.

Syntheses of Cyclopentadienyl Compounds of El(III); El = In, Ga, Al, and B

The most common synthetic approach to these compounds involves metathetical reactions between alkali metal cyclopentadienide salts, cyclopentadienyl-Grignard reagents, magnesocenes, dicyclopentadienylmercury, and even cyclopentadienylthallium with halide derivatives of group 13. A variety of mono-, di-, and tricyclopentadienyl compounds of In(III) (14-18), Ga(III) (14, 18-23), Al(III) (14, 23-36), and B(III) (18, 24, 37-44) have been prepared in this manner. In the case of indium, the outcome of the reaction can be sensitive to the reducing nature of the alkali metal cyclopentadienide salt. For example, yields of In(III) compounds vs. In(I) compounds improve when cyclopentadienyllithium is used instead of sodium cyclopentadienide (16,45). Sometimes, only partial exchange of the halide ligands with cyclopentadienyl ligands is achieved, particularly when the cyclopentadienyl rings are sterically hindered. Although Cp_2Mg ($\text{Cp} = \text{C}_5\text{H}_5$) replaces two chlorides on $\text{Cl}_2\text{Al}(\text{O}-i\text{-Pr})$ to form $[\text{Cp}_2\text{Al}(\mu\text{-O}-i\text{-Pr})_2]$, $\text{Cp}'_2\text{Mg}$ ($\text{Cp}' = \text{C}_5\text{Me}_4\text{H}$), replaces only one chloride on $\text{Cl}_2\text{Al}(\text{O}-i\text{-Pr})$ to form $[\text{Cp}'\text{AlCl}(\text{O}-i\text{-Pr})_2]$ and $\text{Cp}'\text{MgCl}$ (36). Also, AlCl_3 reacts with only two out of three equivalents of Cp^*M ($\text{Cp}^* = \text{C}_5\text{Me}_5$; $\text{M} = \text{Na}, \text{K}$) to form Cp^*_2AlCl (35) even though it reacts with 1.5 equivalents of $\text{Cp}'_2\text{Mg}$ to form $\text{Cp}'_3\text{Al}$ (46).

Metathesis of cyclopentadienyl-silanes, -germanes, and -stannanes with group 13 element halides offers a salt-free route to their synthesis. This chemistry has been demonstrated in only a few cases for Ga(III) (13) and Al(III) (47) but has been used extensively for the synthesis of cyclopentadienyl- (48-54) and indenyl- (43,55) boranes. Silyl-substituted cyclopentadienes react only with

highly Lewis acidic haloboranes such as BCl_3 , BBr_3 , and BI_3 . A cyclopentadienylstannane is required for reactions involving the less electrophilic alkyl-, alkoxy-, and amido-boron halides.

Although these reactions, as well as salt metathesis reactions, initially place the boryl group in the allylic position of the cyclopentadiene ring, a subsequent, irreversible 1,5-H shift leaves the boron in a vinylic position (38, 49), where its vacant p orbital can interact with the π -system of the ring. It is possible to introduce a second boryl group onto the ring by replacing an additional trimethylsilyl or trimethylstannyl substituent to form a 1,4-diborylcyclopentadiene (56). Such double metalation of a cyclopentadienyl ring has not been achieved with any of the other 13 elements.

A less common synthetic approach to cyclopentadienyl group 13 compounds has been the deprotonation of the cyclopentadiene ring by a basic amide or alkyl anion on the metal. This approach appears to work best for compounds of the heavier group 13 elements Tl and In, in which the metal amide and alkyl bonds are more ionic. A communication in 1969 by Lee and Sheldrick reports the synthesis of CpTl via an acid-base reaction between Me_3Tl and cyclopentadiene (6). Similarly, Krommes and Lorberth prepared Me_2InCp by reacting cyclopentadiene with either Me_3In or $[\text{Me}_2\text{InNMe}_2]_2$ (57). The efforts of these authors to metalate cyclopentadiene with either GaMe_3 or $\text{Me}_2\text{GaNMe}_2$ in the same manner were unsuccessful, however. Al-C bonds are more polar and therefore more reactive than Ga-C bonds. Trialkylaluminum compounds do undergo alkane elimination reactions with cyclopentadiene, albeit under forcing conditions (28). Kroll and Hudson were able to metalate cyclopentadiene with triisobutylaluminum by introducing a nitrogen stream of gaseous cyclopentadiene to neat triisobutylaluminum at 170°C ; however, the yield of CpAl^iBu_2 was only 11%, and side products arising from the insertion of the C=C bonds of CpH into the Al-H bond of $(i\text{-C}_4\text{H}_9)_2\text{AlH}$ were also found (58). Alkane elimination has been employed in the preparation CpAlMe_2 from AlMe_3 and an excess of CpH, again, under somewhat forcing conditions; the reagents were heated at 130°C in a sealed tube (59).

Trivalent cyclopentadienyl-group 13 compounds have also been prepared by oxidation of the monovalent species Cp^*In (60), Cp^*Ga (61,62), and Cp^*Al (12, 63-67).

Molecular Structures and Fluxionality

In contrast to transition metals, which typically form strong, covalent, symmetric η^5 bonds to cyclopentadienyl groups, main group elements, the group 13 elements in particular, exhibit a variety of cyclopentadienyl bonding modes ranging from η^5 through various ring-slipped structures all the way to pure σ -bound. The wide variety of structures observed is caused by the rather different metal-ring σ - and π -bonding capabilities of the metal ns and np orbitals and the varying degrees of ionicity in the cyclopentadienyl-element bonds.

Boron

Boron is distinct from the other members of group 13 in that its bonding with cyclopentadienyl rings is almost purely covalent. Therefore, in general, the boron prefers η^1 ring coordination. The metathetical reactions used to prepare cyclopentadienylboranes attach the boron initially to the allylic carbon on the ring, from where it can undergo 1,5-sigmatropic shifts about the ring (Figure 1) (24,38,48,49). The fluxionality of these allylic isomers depends on the Lewis acidity of the boron atom (68). Whereas dihaloboryl groups migrate rapidly about the cyclopentadienyl ring, even below -80°C , temperatures above 150°C are required for migration of the less Lewis-acidic diaminoboryl group, and complexation of the boron by a Lewis base shuts down the migration of the boryl group altogether. Usually, raising the temperature of the cyclopentadienylborane above -10°C during synthetic work-up results in an irreversible 1,5-hydrogen shift, producing a more stable vinyl isomer which is no longer fluxional. Exceptions to this are pentamethylcyclopentadienylboranes (69), in which the boron must remain bound to the allylic position of the ring due to the high barrier for 1,5 methyl migration and fluorenylboranes (40), in which only the allylic isomer is possible. Indenylboranes, on the other hand, form a mixture of 1-allylic and 3-vinyl isomers. Lewis bases such as triethylamine (70) and tri-isopropylphosphine (42) have been used to catalyze the isomerization of the allylic isomers of indenylboranes to their vinyl isomers.

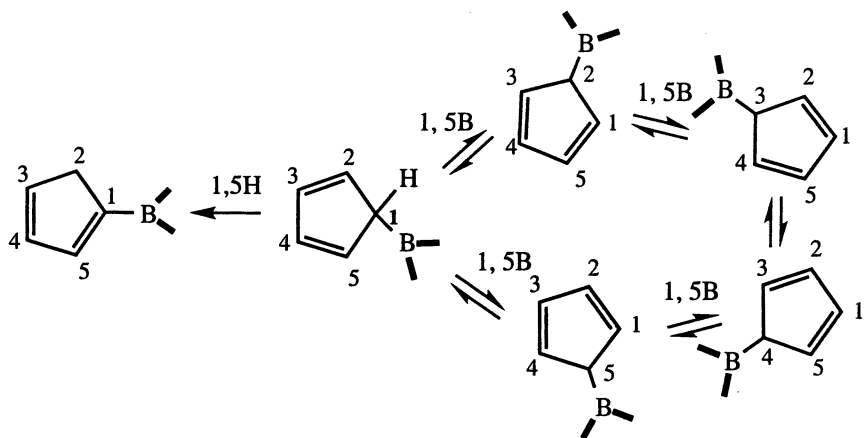


Figure 1. Sigmatropic rearrangements of cyclopentadienylborane compounds

Pentahapto coordination of the cyclopentadienyl ring to the boron has been characterized only in cationic mono- and bis-(pentamethylcyclopentadienyl)boranes (71-73). The cationic nature of these

compounds allows additional π interactions between the two vacant p orbitals on the boron and the filled e orbitals of the cyclopentadienyl ring (Figure 2).

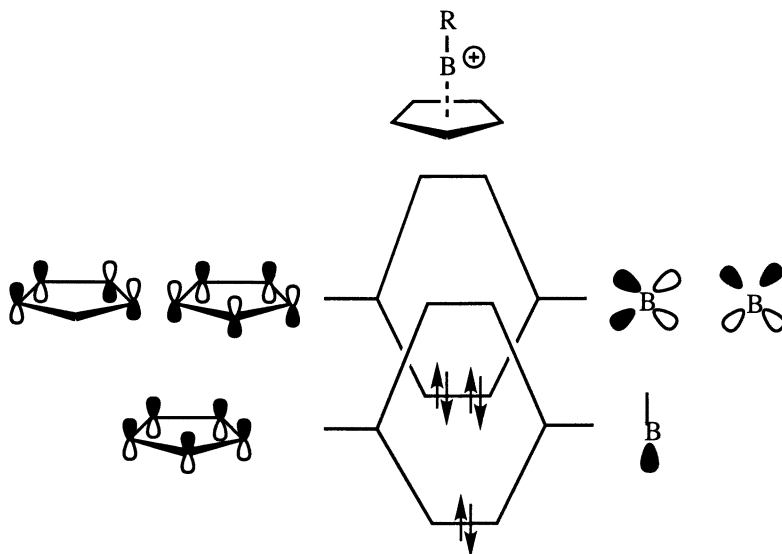


Figure 2. Qualitative MO diagram for cationic cyclopentadienylborane compound (Adapted with permission from ref 71. Copyright 1979 WILEY-VCH)

The decamethylborocenium cation has been crystallographically characterized by Cowley and coworkers (Figure 3) (73). It exhibits mixed η^1/η^5 ring coordination. The room temperature ^1H NMR spectrum of the cation in solution is consistent with this geometry.

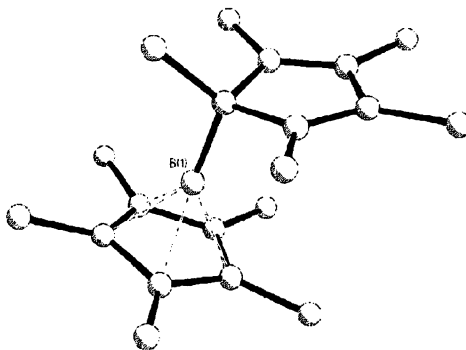


Figure 3. Molecular structure of $[\text{Cp}^*_2\text{B}]^+$ without its counteranion. (Adapted from ref 73 by permission of the Royal Society of Chemistry)

Dynamic behavior was observed when a sample of $[\text{BCp}^*_2][\text{BCl}_4]$ was warmed above room temperature (72). First, a broadening of the signals for the methyl groups on the η^1 ring was observed due to 1,5-migration of the boron about the ring. Ultimately, at 160°C, all of the methyl groups in the complex became equivalent due to an exchange in coordination between the η^1 and the η^5 rings. DFT calculations by Cowley and coworkers indicate that an η^1/η^5 arrangement of cyclopentadienyl rings is the global minimum for both $[\text{Cp}^*_2\text{B}]^+$ and $[\text{Cp}_2\text{B}]^+$ and that the bis- η^5 structures are higher in energy by 49 kcal/mole and 45 kcal/mole, respectively (79). These calculations also indicate that $[\text{Cp}_2\text{Ga}]^+$ prefers an η^1/η^5 geometry, but with a more shallow potential for deformation and only a 8.81kcal barrier to the bis- η^5 structure. The aluminumocenium cation, $[\text{Cp}_2\text{Al}]^+$, by contrast, exhibits no minimum for an η^1/η^5 geometry, preferring a bis- η^5 structure instead.

Aluminum

Dramatic changes in the bonding between the cyclopentadienyl ring and the group 13 element occur upon progressing down one row from boron to aluminum. Interestingly, the differences between boron and aluminum appear to be even greater than those between boron and gallium. This can be attributed to the fact that gallium is actually more electronegative than aluminum (Pauling electronegativities are 1.81(Ga) vs. 1.61(Al)) (1) due to the increased effective nuclear charge of the 4*p* element resulting from incomplete shielding by its filled 3*d* shell. Thus, both B(III) and Ga(III) exhibit a high propensity for the σ type η^1 cyclopentadienyl ring geometry, whereas Al(III) tends to favor a more π type η^2 interaction with its cyclopentadienyl rings. This η^2 geometry was first identified in the gas phase electron diffraction structure of CpAlMe_2 (74) and has been more recently identified in the X-ray crystal structures of (η^2 -Cp) $_2\text{AlMe}$ (32,33), (η^2 -Cp*) $_2\text{AlMe}$ (35), and Cp_3Al (34) (Figure 4).

Restricted Hartree-Fock calculations (RHF/3-21G(*)) establish a general preference for η^2 -Cp coordination by neutral, cyclopentadienylaluminum species (34). This preference is weak, however, and is easily tilted toward other geometries (η^1 , η^3 , η^5) by steric and electronic influences from other ligands on aluminum due to a very flat potential energy surface for ring slippage. Due to this flexibility in ring coordination, cyclopentadienylaluminum compounds are highly fluxional and only averaged structures are observable in solution on the NMR time scale, even when the aluminum is electronically saturated, as in (η^1 -Cp) $_3\text{Al-L}$ (L = *t*-BuCN, *t*-BuNC) (32) and $[(\eta^1\text{-Cp})_2\text{Al}(\mu\text{-O-}i\text{-Pr})_2]$ (36). Furthermore, all possible ring coordination geometries (η^1 , η^2 , η^3 , η^5), with the exception of η^4 , have been characterized among cyclopentadienylaluminum compounds in the solid state (75).

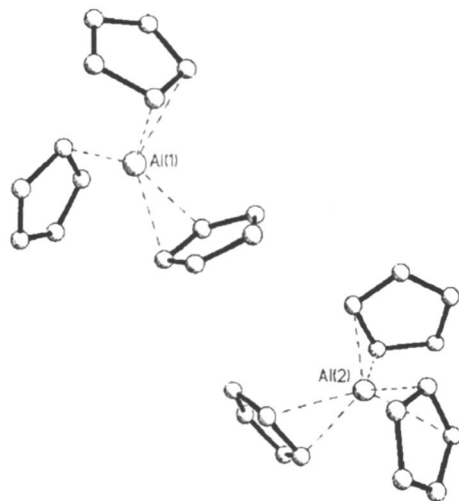


Figure 4. Molecular structure of Cp_3Al with two unique molecules in the unit cell, one with η^1, η^2, η^2 and the other with η^2, η^2, η^2 coordination geometries.. (Adapted with permission from reference 34. Copyright1997 American Chemical Society)

The aluminocenium cations $[Cp_2Al]^+$ (46) and $[Cp^*_2Al]^+$ (35, 77, 78) are the only cationic cyclopentadienylaluminum species that have been reported to date. Consistent with DFT calculations on $[Cp_2Al]^+$ (79), all $[Cp^*_2Al]^+$ salts exhibit a bis- η^5 ring coordination geometry (Figure 5).

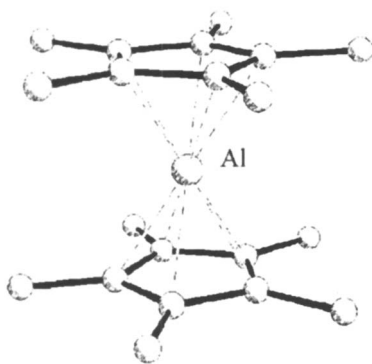


Figure 5. Molecular structure of $[Cp^*_2Al]^+$ without its counteranion. (Adapted with permission from ref 77. Copyright1993 WILEY-VCH)

Gallium

As mentioned earlier, cyclopentadienylgallium compounds prefer η^1 cyclopentadienyl ring coordination more often than cyclopentadienylaluminum compounds. For example, whereas Cp_2AlMe is monomeric in the solid state, with its two Cp rings η^2 to the aluminum, Cp_2GaMe is polymeric (79). The aluminum compensates for its electron deficiency through increased intramolecular π -bonding to its cyclopentadienyl rings. Gallium, on the other hand, gains additional electron density by forming Ga–Cp–Ga bridges in which the Cp is coordinated η^1 to each gallium. Another example of these differences in Cp-coordination is seen among the crystallographically characterized series of group 13 element compounds with the formula $(\text{C}_5\text{Me}_4\text{CH}_2\text{CH}_2\text{NMe}_2)\text{MCl}_2$ (M=Al, Ga, In) (18). Only the aluminum species exhibits η^2 ring coordination in the solid state; the gallium and indium compounds both have η^1 -coordinated cyclopentadienyl rings.

Gallium's preference for η^1 ring coordination as compared with aluminum is also exhibited in structures of the diazabutadiene complexes $\text{Cp}^*\text{AlN}(\text{Mes})\text{CH}=\text{CHN}(\text{Mes})$] (63) and $\text{Cp}^*\text{GaN}(\text{Dipp})\text{CH}=\text{CHN}(\text{Dipp})$] (Dipp = 2,6-diisopropylphenyl) (61). The ligand make-ups of the two complexes are very similar, and yet the aluminum prefers η^5 coordination to its Cp^* ring while the gallium exhibits a purely σ , η^1 mode of bonding.

The preference of the gallium for η^1 over π coordination can perhaps be attributed to gallium's slightly greater electronegativity (relative to aluminum) as well as to the poorer overlap between the empty Ga 4p orbital and the filled π orbitals of the cyclopentadienyl ring. This could also explain why Cp^*_3Ga is preparable by standard salt metathesis routes (21) and Cp^*_3Al is not (35). Whereas gallium is able to accommodate all three Cp^* rings because of their monohapto coordination, aluminum's preference for higher hapticities makes incorporation of the third Cp^* ring less favorable both sterically and thermodynamically. With the exception of the compounds $[(\eta^1\text{-C}_5\text{Me}_5)(\eta^3\text{-C}_5\text{Me}_5)\text{Ga}(\text{BF}_4)]$ and $(\eta^1\text{-C}_5\text{Me}_5)(\eta^2\text{-C}_5\text{Me}_5)\text{Ga}(\text{C}_6\text{F}_5)$ (80) (Figure 6), all other crystallographically characterized cyclopentadienylgallium(III) compounds have η^1 cyclopentadienyl rings. This list includes the structures of $[\text{CpGa}(\text{CH}_3)_2]_\infty$ (79), $[\text{CpGaEt}_2]_\infty$ (81), Cp^*_3Ga (21), $[\text{Cp}^*_2\text{GaCl}]_2$ (19), $[\text{Cp}^*\text{GaCl}_2]_2$ (19), $\text{Cp}^*_2\text{Ga-As}(\text{SiMe}_3)_2$ (82), $[\text{CpGa}(\mu\text{-OEt})]_2$ (83), $[\text{Cp}^*\text{GaNXyl}]_2$ (62), and $[\text{Cp}^*\text{Ga}(\mu_2\text{-N}_3)\{\text{N}(\text{SiMe}_3)_3\}]_2$ (68).

The solid state structures of $[\text{CpAl}(\text{CH}_3)_2]_\infty$ (59), $[\text{CpGa}(\text{CH}_3)_2]_\infty$ (79), and $[\text{CpIn}(\text{CH}_3)_2]_\infty$ (17), are actually isomorphous. The M–Cp–M bridges contain η^1 -coordinated metals at 1,3 positions on opposites of the ring. Like cyclopentadienylaluminum compounds, cyclopentadienylgallium and cyclopentadienylindium compounds are highly fluxional in solution, exhibiting averaged ^1H and ^{13}C NMR spectra.

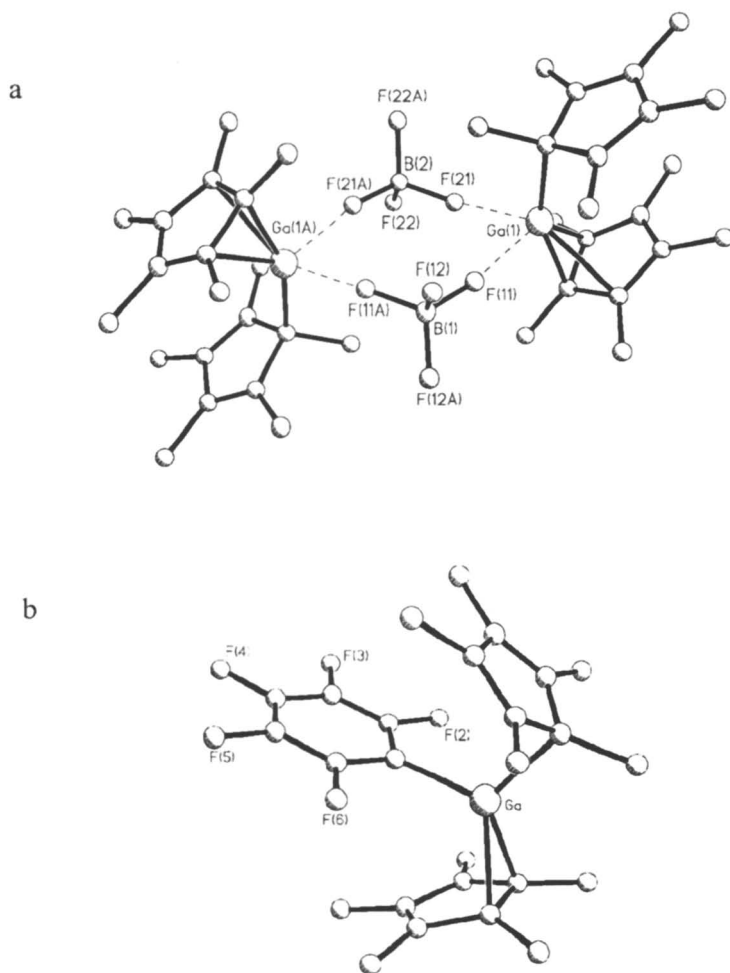


Figure 6. Molecular structures of a) $[(\eta^1\text{-C}_5\text{Me}_5)(\eta^3\text{-C}_5\text{Me}_5)\text{Ga}(\text{BF}_4)]$ and b) $(\eta^1\text{-C}_5\text{Me}_5)(\eta^2\text{-C}_5\text{Me}_5)\text{Ga}(\text{C}_6\text{F}_5)$ (Adapted with permission from ref 81. Copyright 2000 American Chemical Society)

Indium

Only four crystallographically characterized cyclopentadienyl compounds of In(III) have been reported to date. In all of these the cyclopentadienyl ring exhibits η^1 coordination. In the absence of heteroatom donors such as N and P to stabilize the electron-deficient Indium center as a dimer in $[\text{Cp}^*(\text{Cl})\text{In}(\mu\text{-P}(\text{SiMe}_3)_2)]_2$ (84) or a monomer in $(\text{C}_5\text{Me}_4\text{CH}_2\text{CH}_2\text{NMe}_2)\text{InCl}_2$ (18), the compounds CpInMe_2 (17) and Cp_3In (45) adopt polymeric structures in the solid state through the formation of M–Cp–M bridges similar to those formed in the polymeric structures of CpAlMe_2 , CpGaMe_2 , and CpGaEt_2 , and Cp_2GaEt .

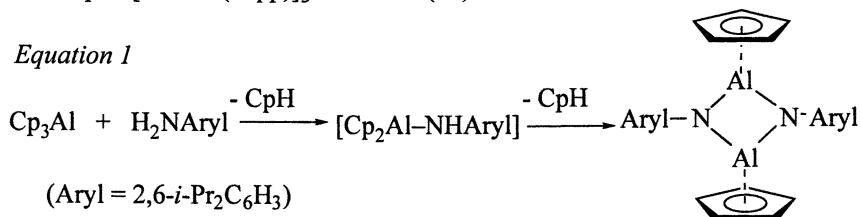
Reactivity and Chemical Applications

As with other group 13 compounds, the cyclopentadienyl compounds are susceptible to ligand redistribution reactions. To date these reactions have been noted in only the aluminum and gallium compounds. Ligand redistribution can be exploited as a synthetic tool; however, it can also interfere with the preparation of a compound or undermine a compound's compositional integrity in solution. For example, although CpGaR_2 ($\text{R} = \text{Me}, \text{Et}$) and CpGaCl_2 can be isolated by combining three molar equivalents of tricyclopentadienylgallium with either GaR_3 or GaCl_3 (20,82,85,86), the CpGaR_2 species are unstable in solution, forming equilibrium mixtures of $\text{Cp}_x\text{GaR}_{3-x}$. Cp_2AlMe and CpAlMe also decompose to a mixture of $\text{Cp}_x\text{AlMe}_{3-x}$ species in solution when exposed to coordinating solvents such as THF and Et_2O (32,87). In fact, $\text{Cp}_3\text{Al}(\text{L})$ ($\text{L} = \text{is CN-}t\text{Bu}$ and $t\text{-BuCN}$) precipitates selectively from an alkane solution of Cp_2AlMe treated with L (32, 33). Although compositionally related to Cp_2AlMe and Cp^*_2AlMe , $\text{Cp}'\text{AlMe}_2$ cannot be isolated unless it is stabilized by a molecule of THF. Otherwise, $\text{Cp}'_3\text{Al}$ crystallizes selectively from the reaction of MeAl_2Cl and two equivalents of NaCp' in toluene (88).

We have observed that Al-cyclopentadienyl bonds are more labile than Al–Me bonds, and this is probably also true for the other group 13 elements. For example, protonolysis of the Cp–Al bond in Cp_2AlMe occurs in preference to protonolysis of the Al–Me bond. A comparison of the reactivity of Cp_3Al vs. Me_3Al with substituted anilines also reveals this trend. Whereas Cp_3Al readily eliminates cyclopentadiene upon reaction with $\text{H}_2\text{N}(\text{Dipp})$ ($\text{Dipp} = 2,6\text{-}i\text{Pr}_2\text{C}_6\text{H}_3$) to form $[\text{Cp}_2\text{Al-NH}(\text{Dipp})]_x$ at room temperature (89), thermolysis of a mixture of AlMe_3 and $\text{H}_2\text{N}(\text{Dipp})$ in refluxing toluene is necessary for methane elimination to occur to form $[\text{Me}_2\text{Al-NH}(\text{Dipp})]_2$ (90). Furthermore, $[\text{Cp}_2\text{Al-NH}(\text{Dipp})]_x$ eliminates a second molecule of cyclopentadiene, even upon standing at room temperature in the solid state, to form the dimeric iminoalane $[\text{CpAlN}(\text{Dipp})]_2$ (Equation 1). $[\text{Me}_2\text{Al-NH}(\text{Dipp})]_2$, by contrast,

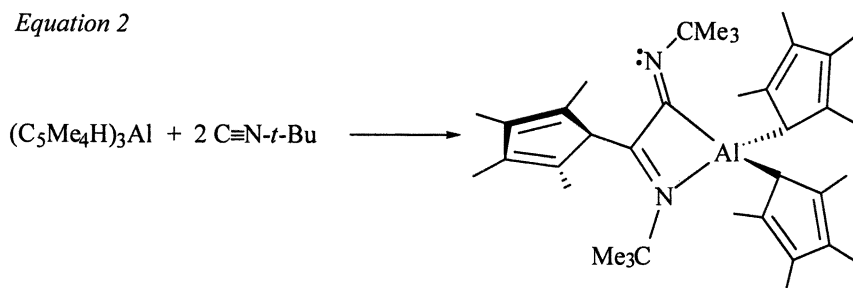
must be heated to 170°C for the second molecule of methane to be eliminated, whereupon $[\text{MeAl}(\text{Dipp})_3]$ is formed (91).

Equation 1



Besides undergoing Al-C bond cleavage more readily than Al-Me bonds, cyclopentadienyl-aluminum bonds also have a higher propensity for small molecule insertion. A single case in point is the insertion of *t*-butyl isocyanide by Cp₃Al and by (Me₃C₅H₂)₃Al. Whereas trimethylaluminum forms an adduct with methyl isocyanide which is stable even upon sublimation of the complex at 40°C, these bulkier tri-cyclopentadienylaluminum complexes insert two molecules of *t*-butyl isocyanide between the aluminum and one of its cyclopentadienyl rings. The double insertion product (η^1 -C₅Me₄H)₂Al{C(=N*t*Bu)-C(=N*t*Bu)(C₅Me₄H)} (Equation 2) was characterized crystallographically (46). Other isocyanides and unsaturated small molecules also react with (Me₄C₅H)₃Al, presumably by insertion, but the products are not clean and efforts to characterize them were unsuccessful. It should be noted that, like AlMe₃, AlCp₃ coordinates *t*-butyl isocyanide and does not react further, even with heating. Thus, the steric bulk of the cyclopentadienyl rings plays a role in this insertion chemistry.

Equation 2



Cyclopentadienylboranes are less vulnerable to ring loss than their heavier congeners, although they can undergo Diels-Alder dimerization (24) and polymerization (49) if they are not sterically stabilized. Ring deborylation is sometimes an undesired outcome of efforts to deprotonate or metalate the ring of the cyclopentadienylborane (24,92,53). Protonation and further metalation of the ring has been accomplished successfully in several instances, however. Herberich and Fischer have deprotonated a variety of cyclopentadienylboranes of formula (C₅H₄)BR₂ (R₂ = (NMe₂)₂, (*i*-Pr)₂, (Me)₂, (-O(Me₂)C-C(Me₂)O-) (39,93). The choice of base depends on the nature of R in terms of its effect on

the accessibility of the boron center and the Brønsted acidity of the cyclopentadienyl ring since the deprotonation must compete kinetically with quarternization of the boron. The sterically hindered bases LiTMP and LDA were suitable for a number of cyclopentadienylborane substrates. In a few cases, deprotonation with LiNMe₂, LiCp, and NaCp was also accomplished, as was direct metalation with Na under hydrogen evolution. Other researchers have successfully deprotonated cyclopentadienyl- and indenyl-boranes as a means of attaching these molecules to transition metals (42,43,70,94,95). Cyclopentadienyl-borate monoanions have also been successfully deprotonated at the ring to form dianions which are attached to transition metals by salt metathesis to form borate-derivatized metallocenes (96,97). An alternative, base-free approach to introducing boryl-cyclopentadienyl rings onto a transition metal was introduced by Jutzi and Seufert in 1979 (98). Reaction of the trimethylsilyl-cyclopentadienylborane with TiCl₄ produces the half sandwich boryl-cyclopentadienyltitanium trichloride via the elimination of Me₃SiCl. This approach has since been used to attach cyclopentadienylboranes to zirconium. (53-55). Zirconation of trimethylstannyl-substituted cyclopentadienylboranes has also been described (43,55) as has metalation of cyclopentadienylboranes with Ti(NMe₂)₄ (95,99).

Further metalation of cyclopentadienyl rings bonded to aluminum, gallium, and indium are complicated by the tendency of the cyclopentadienyl rings on these elements to transmetalate. An alternate approach to alane-derivatized cyclopentadienyl complexes of early transition metals is the electrophilic addition of alanes to rings that are already attached to a metal. This chemistry has been demonstrated in a few cases for aluminum (100-102). Electrophilic addition of boranes to the rings of metallocenes is even more common (103-106).

The lability of the cyclopentadienyl-metal bond in Al, Ga, and In compounds makes these compounds attractive precursors to III-V semiconductors and thin metal films. Theopold and coworkers have demonstrated that alcoholysis of Cp*Ga-As(SiMe₃)₂ (82) and Cp*InR(Cl) (84) compounds (R = Me₃SiCH₂ or Me₃CCH₂) produces nanoparticles of the III-V semiconductor materials GaAs and InP. Jutzi and coworkers have shown that compounds of the type [(Me₂NCH₂CH₂)C₅R₄]MR'₂ with M = Al, Ga, R=H, Me and R'=H, *i*-Bu are useful precursors to thin metal films using MOCVD methods (22,23). The dihydride compounds [(Me₂NCH₂CH₂)C₅H₄]MH₂ (M=Al, Ga) fragment cleanly to elemental metal, free ligand, and half an equivalent of H₂ upon thermolysis. Whereas deposition of an aluminum film required substrate temperatures between 580- 620°C at a reduced pressure of 1x10⁻³ mbar, gallium films were obtained at lower substrate temperatures (240-260°) at this pressure, indicating that the gallium compounds are more labile. Irradiation of C₆D₆ solutions of these compounds in a quartz NMR tube with a Hg lamp causes similar fragmentation, producing either a highly reflective metallic film of elementary gallium or gray aluminum powder.

Although electrophilic boron and aluminum compounds are commonly used as Lewis acid catalysts for a variety of organic reactions, the only reported catalytic application of cyclopentadienyl-group 13 compounds to date has been the use of the aluminocenium cations $[\text{Cp}_2\text{Al}]^+$ (81) and $[\text{Cp}^*_2\text{Al}]^+$ (35) to initiate the polymerization of isobutene, isoprene, and styrene, presumably by a cationic mechanism. Although the Cp^* species is the more stable of the two aluminocenium cations, the Cp species initiates these polymerizations at a much lower temperature. The potential to control the stability, reactivity, and selectivity of these compounds by varying the substituents on the cyclopentadienyl rings could prove useful for other catalytic applications.

Summary

Because the cyclopentadienyl ligand is able to adopt such a wide range of bonding motifs, it is a sensitive probe of the differences in the electronic properties of the group 13 elements. It is also sensitive to subtle electronic differences between different cyclopentadienyl compounds of the same element.

Boron, the most electronegative group 13 element, exhibits the strongest covalent interaction with its cyclopentadienyl rings. As a result, the cyclopentadienyl–boron bonds are less susceptible to cleavage by transmetalation and protonolysis. The more ionic cyclopentadienyl compounds of Al, Ga, and In are more fluxional and more inclined toward ligand redistribution reactions. Because the composition of these compounds is more difficult to control, their reaction chemistry is less predictable than that of cyclopentadienylboranes. Aluminum(III) exhibits π -covalent interactions (η^2 , η^3 , and η^5) with its cyclopentadienyl rings more often than either gallium(III) or indium(III), again illustrating how slight differences in the electronic properties of these elements are manifested in the structures of their cyclopentadienyl compounds.

Interestingly, the relative number of examples of trivalent group 13 cyclopentadienyl compounds follows the trend $\text{B} > \text{Al} > \text{Ga} > \text{In} > \text{Tl}$. While this may be partly a reflection of scientific interest in these compounds, it is probably also a reflection of their relative stability. There are, conversely, numerous examples of cyclopentadienyl-indium(I) and -thallium(I) compounds, very few monovalent cyclopentadienyl-aluminum and -gallium species and no examples for boron, except for the transition metal-stabilized form in $\text{Cp}^*\text{B}-\text{Fe}(\text{CO})_4$ (107). As for cyclopentadienyl–M(II) compounds, the diboranes (Indenyl)(Me_2N)B–B(Me_2N)(Indenyl) (108) and (Fluorenyl)(Me_2N)B–B(Me_2N)(Fluorenyl) (109) are the only examples in the literature so far.

Acknowledgment

I am grateful to Brendan Twamley for providing the figures of the molecular structures and to Peter Budzelaar, David Atwood, and Peter Jutzi for their helpful comments.

References

1. Norman, N. C. *Periodicity and the p-Block Elements*; Oxford Science Publications: Oxford, 1994.
2. Jutzi, P. *Adv. Organomet. Chem.* **1986**, *26*, 217-295.
3. Jutzi, P.; Burford, N. *Chem. Rev.* **1999**, *99*, 969-990.
4. Hari, S. C. A., R. S.; Bhalla, M. S.; Multani, R. K. *J. Chinese Chem. Soc.* **1978**, *25*, 161-162.
5. Kumar, N.; Kalostra, B. L.; Multani, R. K. *Curr. Sci.* **1973**, *42*, 58-59.
6. Lee, A. G.; Sheldrick, G. M. *J. Chem. Soc., Chem. Commun.* **1969**, 441-442.
7. Lee, A. G.; Sheldrick, G.M. *Trans. Faraday. Soc.* **1971**, *67*, 7-11.
8. Dohmeier, C.; Robl, C.; Tacke, M.; Schnöckel, H. *Angew. Chem. Int. Ed. Engl.* **1991**, *30*, 564-565.
9. Dohmeier, C.; Loos, D.; Schnöckel, H. *Angew. Chem., Int. Ed. Engl.* **1996**, *35*, 129-149.
10. Sitzmann, H.; Lappert, M. F.; Dohmeier, C.; Uffing, C.; Schnöckel, H. *J. Organomet. Chem.* **1998**, *561(1-2)*, 203-208.
11. Loos, D.; Baum, E.; Ecker, A.; Schnöckel, H.; Downs, A. J. *Angew. Chem., Int. Ed. Engl.* **1997**, *36*, 860-862.
12. Schulz, S.; Roesky, H. W.; Koch, H. J.; Sheldrick, G. M.; Stalke, D.; Kuhn, A. *Angew. Chem., Int. Ed. Engl.* **1993**, *32*, 1729-1731.
13. Jutzi, P.; Neumann, B.; Reumann, G.; Stammler, H.-G. *Organometallics* **1998**, *17*, 1305-1314.
14. Stadelhofer, J.; Weidlein, J.; Haaland, A. *J. Organomet. Chem.* **1975**, *84*, C1-C4.
15. Beachley, O. T., Jr.; Blom, R.; Churchill, M. R.; Faegri, K.; Fettinger, J. C.; Pazik, J. C.; Victoriano, L. *Organometallics* **1989**, *8*, 346-356.
16. Poland, J. S.; Tuck, D. G. *J. Organomet. Chem.* **1972**, *42*, 307-314.
17. Beachley, O. T.; Robirds, E. S.; Atwood, D. A.; Wei, P. *Organometallics* **1999**, *18*, 2561-2564.
18. Jutzi, P.; Dahlhaus, J.; Neumann, B.; Stammler, H.-G. *Organometallics* **1996**, *15*, 747-752.
19. Beachley, O. T., Jr.; Getman, T. D.; Kirss, R. U.; Hallock, R. B.; Hunter, W. E.; Atwood, J. L. *Organometallics* **1985**, *4*, 751-754.
20. Beachley, O. T.; Moss crop, M. T. *Organometallics* **2000**, *19*, 4550-4556.

21. Schumann, H.; Nickel, S.; Weimann, R. *J. Organomet. Chem.* **1994**, *468*, 43-47.
22. Jutzi, P.; Bangel, M.; Neumann, B.; Stammler, H.-G. *Organometallics* **1996**, *15*, 4559-4564.
23. Bensiak, S.; Bangel, M.; Neumann, B.; Stammler, H.-G.; Jutzi, P. *Organometallics* **2000**, *19*, 1292-1298.
24. Grundke, H.; Paetzold, P. I. *Chem. Ber.* **1971**, *104*, 1136-1146.
25. Schonberg, P. R.; Paine, R. T.; Campana, C. F. *J. Am. Chem. Soc.* **1979**, *101*, 7725-7728.
26. Schonberg, P. R.; Paine, R. T.; Campana, C. F.; Duesler, E. N. *Organometallics* **1982**, *1*, 799-807.
27. Thiyagarajan, B.; Jordan, R. F.; Young, V. G. *Organometallics* **1999**, *18*, 5347-5359.
28. Kroll, W. R.; McDivitt, J. R.; Naegele, W. *Inorg. Nucl. Chem. Letters* **1969**, *5*, 973-976.
29. Giannini, U.; Cesca, S. *Gazz. Chim. Ital.* **1961**, *91*, 597-604.
30. Scherer, M.; Kruck, T. *J. Organomet. Chem.* **1996**, *513*, 135-138.
31. Kunicki, A.; Sadowski, R.; Zachara, J. *J. Organomet. Chem.* **1996**, *508*, 249-250.
32. Fisher, J. D.; Wei, M.-Y.; Willett, R.; Shapiro, P. J. *Organometallics* **1994**, *13*, 3324-3329.
33. Fisher, J. D.; Wei, M.-Y.; Willett, R.; Shapiro, P. J. *Organometallics* **1995**, *14*, 4030.
34. Fisher, J. D.; Budzelaar, P. H. M.; Shapiro, P. J.; Staples, R. J.; Yap, G. P. A.; Rheingold, A. L. *Organometallics* **1997**, *16*, 871-879.
35. Burns, C. T.; Shapiro, P. J.; Budzelaar, P. H. M.; Willett, R.; Vij, A. *Organometallics* **2000**, *19*, 3361-3367.
36. Fisher, J. D.; Golden, J. T.; Shapiro, P. J.; Yap, G. P. A.; Rheingold, A. L. *Main Group Met. Chem.* **1996**, *19*, 521-530.
37. Prokhorova, A.; Paushkin, Y. M. *Dokl. Akad. Nauk. S.S.S.R.* **1960**, *135*, 84-86.
38. Johnson, H. D.; Hartford, T. W.; Spangler, C. W. *J. Chem. Soc., Chem. Commun.* **1978**, 242.
39. Herberich, G. E.; Fischer, A. *Organometallics* **1996**, *15*, 58-67.
40. Duchateau, R.; Lancaster, S. J.; Thornton-Pett, M.; Bochmann, M. *Organometallics* **1997**, *16*, 4995-5005.
41. Lockman, B.; Onak, T. *J. Org. Chem.* **1973**, *38*, 2552-2553.
42. Reetz, M. T.; Willuhn, M.; Psiorz, C.; Goddard, R. *Chem. Commun.* **1999**, 1105-1106.
43. Rufanov, K.; Avtomonov, E.; Kaennova, N.; Kotov, V.; Khvorost, A.; Lemenovskii, D.; Lorberth, J. *J. Organomet. Chem.* **1997**, *536-537*, 361-373.
44. Ashe, A. J.; Fang, X.; Kampf, J. W. *Organometallics* **1999**, *18*, 2288-2290.

45. Einstein, F. W. B.; Gilbert, M. M.; Tuck, D. G. *Inorg. Chem.* **1972**, *11*, 2832-2836.
46. Shapiro, P. J.; Vij, A.; Yap, G. P. A.; Rheingold, A. L. *Polyhedron* **1995**, *14*, 203-209.
47. Koch, H.-J.; Schulz, S.; Roesky, H. W.; Noltemeyer, M.; Schmidt, H.-G.; Heine, A.; Herbst-Irmer, R.; Stalke, D.; Sheldrick, G. M. *Chem. Ber.* **1992**, *125*, 1107-1109.
48. Jutzi, P.; Seufert, A. *Angew. Chem., Int. Ed. Engl.* **1976**, *15*, 295-296.
49. Jutzi, P.; Seufert, A. *J. Organomet. Chem* **1979**, *169*, 327-355.
50. Jutzi, P.; Seufert, A. *Angew. Chem., Int. Ed. Engl.* **1977**, *16*, 330-331.
51. Jutzi, P.; Seufert, A. *Chem. Ber.* **1979**, *112*, 2481-2487.
52. Larkin, S. A.; Golden, J. T.; Shapiro, P. J.; Yap, G. P. A.; Foo, D. M. J.; Rheingold, A. L. *Organometallics* **1996**, *15*, 2393-2398.
53. Stelck, D. S.; Shapiro, P. J.; Basicckes, N. *Organometallics* **1997**, *16*, 4546-4550.
54. Reetz, M. T.; Brümmer, H.; Kessler, M.; Kuhnigk, J. *Chimia* **1995**, *49*, 501-503.
55. Rufanov, K. A.; Kotov, V. V.; Kazennova, N. B.; Lemenovskii, D. A.; Avtomonov, E. V.; Lorberth, J. *J. Organomet. Chem.* **1996**, *525*, 287-289.
56. Jutzi, P.; Seufert, A. *J. Organomet. Chem.* **1979**, *169*, 357-371.
57. Krommes, P.; Lorberth, J. *J. Organomet. Chem.* **1975**, *88*, 329-336.
58. Kroll, W.R.; Hudson, B. E. *J. Organomet. Chem.* **1971**, 205-210.
59. Teclé, B.; Corfield, P. W. R.; Oliver, J. P. *Inorg. Chem.* **1982**, *21*, 458.
60. Contreras, J. G.; Tuck, D. G. *J. Organomet. Chem.* **1974**, *66*, 405-412.
61. Pott, T.; Jutzi, P.; Neumann, B.; Stammeler, H.-G. *Organometallics* **2001**, *20*, 1965-1967.
62. Jutzi, P. *Organometallics* **1999**, *18*, 2037-2039.
63. Cowley, A. H.; Gorden, J. D.; Abernethyl, C. D.; Clyburne, J. A. C.; McBurnett, B. G. *J. Chem. Soc., Dalton Trans.* **1998**, 1937-1938.
64. Schulz, S.; Häming, L.; Herbst-Irmer, R.; Roesky, H. W.; Sheldrick, G. M. *Angew. Chem., Int. Ed. Engl.* **1994**, *33*, 969.
65. von Hänisch, C. K. F. *Angew. Chem. Int. Ed. Engl.* **1996**, *35*, 2875-2877.
66. Dohmeier, C.; Schnöckel, H.; Robl, C.; Schneider, U.; Ahlrichs, R. *Angew. Chem., Int. Ed. Engl.* **1994**, *33*, 199-200.
67. Üffing, C.; Baum, E.; Köppe, R.; Schnöckel, H. *Angew. Chem. Int. Ed.* **1998**, *37*, 2397-2399.
68. Schoeller, W. W. *J. Chem. Soc., Dalton Trans.* **1984**, 2233-2236.
69. Jutzi, P.; Seufert, A. *Angew. Chem., Int. Ed. Engl.* **1977**, *16*, 41-42.

70. Barday, E.; Frange, B.; Hanquet, B.; Herberich, G. E. *J. Organomet. Chem.* **1999**, *572*, 225-232.
71. Jutzi, P.; Seufert, A.; Buchner, W. *Chem. Ber.* **1979**, *112*, 2488-2493.
72. Jutzi, P.; Seufert, A. *J. Organomet. Chem.* **1978**, *161*, C5-C7.
73. Cowley, A. H.; Voigt, A.; Filipponi, S.; Macdonald, C. L. B.; Gorden, J. D. *Chem. Commun.* **2000**, 911-912.
74. Drew, D. A.; Haaland, A. *Acta Chem. Scand.* **1973**, *27*, 3735-3745.
75. Shapiro, P. J. *Coord. Chem. Rev.* **1999**, *189*, 1-17, and references therein.
76. Bochmann, M.; Dawson, D. M. *Angew. Chem., Int. Ed. Engl.* **1996**, *35*, 2226-2228.
77. Dohmeier, C.; Schnöckel, H.; Robl, C.; Schneider, U.; Ahlrichs, R. *Angew. Chem., Int. Ed. Engl.* **1993**, *32*, 1655-1657.
78. Burns, C. T.; Stelck, D. S.; Shapiro, P. J.; Vij, A. *Organometallics* **1999**, *18*, 5432-5434.
79. Mertz, K.; Zettler, F.; Hausen, H. D.; Weidlein, J. *J. Organomet. Chem.* **1976**, *122*, 159-170.
80. MacDonald, C. I. R.; Gorden, J. D.; Voigt, A.; Cowley, A. H. *J. Am. Chem. Soc.* **2000**, *122*, 11725-11726.
81. Beachley, O. T.; Rosenblum, D. B.; Churchill, M. R.; Lake, C. H.; Krajkowski, L. M. *Organometallics* **1995**, *14*, 4402-4408.
82. Byrne, E. K.; Parkanyi, L.; Theopold, K. H. *Science* **1988**, *241*, 332-334.
83. Cowley, A. H.; Mehrotra, S. K.; Atwood, J. L.; Hunter, W. E. *Organometallics* **1985**, *4*, 1115-1116.
84. Trevor, D.; Theopold, K. H. *Inorg. Chem.* **1991**, *30*, 594-596.
85. Beachley, O. T., Jr.; Royster, T. L., Jr.; Arhar, J. R. *J. Organomet. Chem.* **1992**, *434*, 11-17.
86. Beachley, O. T.; Hallock, R. B.; Zhang, H. M.; Atwood, J. L. *Organometallics* **1985**, *4*, 1675-1680.
87. Kroll, W. R. *Chem. Commun.* **1969**, 844-845.
88. C. Burns, University of Idaho, unreported results.
89. Fisher, J. D.; Shapiro, P. J.; Yap, G. P. A.; Rheingold, A. L. *Inorg. Chem.* **1996**, *35*, 271-272.
90. Waggoner, K. M.; Power, P. P. *J. Am. Chem. Soc.* **1991**, *113*, 3385-3393.
91. Waggoner, K. M.; Hope, H.; Power, P. P. *Angew. Chem., Int. Ed. Engl.* **1988**, *27*, 1699-1670.
92. Shafiq, F. A.; Abboud, K. A.; Richardson, D. E.; Boncella, J. M. *Organometallics* **1998**, *17*, 982-.
93. Herberich, G. E.; Fischer, A.; Wiebelhaus, D. *Organometallics* **1996**, *15*, 3106-3108.
94. Aleksander, K.; Starzewski, O.; Kelly, W. M.; Stumpf, A.; Freitag, D. *Angew. Chem., Int. Ed.* **1999**, *38*, 2439-2442.

**American Chemical Society
Library**

1155 16th St., N.W.

Washington, D.C. 20036

95. Braunschweig, H.; von Koblinski, C.; Wang, R. *Eur. J. Inorg. Chem.* **1999**, 69-73.
96. Kleigrewe, N.; Brackemeyer, T.; Kehr, G.; Fröhlich, R.; Erker, G. *Organometallics* **2001**, *20*, 1952-1955.
97. Bochmann, M.; Lancaster, S. J.; Robinson, O. B. *Chem. Commun.* **1995**, 2081-2082.
98. Jutzi, P.; Seufert, A. *J. Organomet. Chem.* **1979**, *169*, 373-380.
99. Braunschweig, H.; von Koblinski, C.; Engert, U. *Chem. Commun.* **2000**, 1049-1050.
100. Green, M. L. H.; MacKenzie, R. E.; Poland, J. S. *J. Chem. Soc., Dalton Trans.* **1976**, 1993-1994.
101. Corradini, P.; Sirigu, A. *Inorg. Chem.* **1967**, *6*, 601-605.
102. Nakamura, H.; Nakayama, Y.; Yasuda, H.; Maruo, T.; Kanehisa, N.; Kai, Y. *Organometallics* **2000**, *19*, 5392-5399.
103. Ruwwe, J.; Erker, G.; Fröhlich, R. *Angew. Chem. Int. Ed. Engl.* **1996**, *35*, 80-82.
104. Braunschweig, H.; Wagner, T. *Chem. Ber.* **1994**, *127*, 1613-1614.
105. Burlakov, V. V.; Troyanov, S. I.; Letov, A. V.; Strunkina, L. I.; Minachev, M. K.; Furin, G. G.; Rosenthal, U.; Shur, V. V. *J. Organomet. Chem.* **2000**, *598*, 243-247.
106. Doerrer, L. H.; Graham, A. J.; Haussinger, D.; Green, M. L. H. *J. Chem. Soc., Dalton Trans.* **2000**, 813-820.
107. Cowley, A. H.; Lomelf, V.; Voigt, A. *J. Am. Chem. Soc.* **1998**, *120*, 6401-6402.
108. Knizek, J.; Krossing, I.; Nöth, H.; Pnikwar, W. *Eur. J. Inorg. Chem.* **1998**, 505-509.
109. Littger, R.; Metzler, N.; Nöth, H.; Wagner, M. *Chem. Ber.* **1994**, *127*, 1901-1908.
110. Note added in proof: Prior to the final printing of this chapter, the abstraction of a methanide ion from the complex $[\text{Me}_2\text{Si}(\eta^1\text{-C}_5\text{Me}_4)(\text{N-}t\text{-Bu})]\text{AlMe}\cdot\text{THF}$ was reported although the resulting cyclopentadienylaluminum cation has not yet been described. Ref: Pietryga, J. M.; Gorden, J. D.; Macdonald, C. L. B.; Voigt, A.; Wiacek, R. J.; Cowley, A. H. *J. Am. Chem. Soc.* **2001**, *123*, 7713-7714.

Chapter 4

Metallaboranes of the Earlier Transition Metals: Relevance to the Cluster Electron Counting Rules

Thomas P. Fehlner

Department of Chemistry and Biochemistry, University of Notre Dame,
Notre Dame, IN 46556

Structures of the known hypoelectronic metallaboranes of tungsten and rhenium are used to explore the applicability of the electron counting rules to metallaborane clusters containing earlier transition metal fragments. It is demonstrated that for metallaboranes with formal skeletal electron pairs (sep) less than the $p + 1$ closo count, p = the number of vertices, the cluster shapes adopted are intermediate between the most spherical deltahedral shapes found in the closed borane anions (canonical structures) and the multi-capped skeletons found in metal systems. For a given cluster size the total connectivity, or number of bonded edges, is a constant and independent of the skeletal electron count. What varies is the distribution of vertex connectivities with the hypoelectronic skeletons exhibiting a greater number of high (occupied by the metal atoms) and low (occupied by the boron atoms) connectivity vertices. Consequently, as the number of sep falls below the $p + 1$ count, the average coordination number of the metals increases and the average coordination number of the boron atoms decreases. For each missing sep, the observed shape is related to the canonical form by one, in some cases more than one, diamond-square-diamond

rearrangement or a cross cage metal-metal bond. In the specific case of the rhenia- and tungstaboranes, it is shown that two of the missing sep are delocalized over the cluster bonding network and one is localized on the metal centers in the form of a Re-Re bond.

Metallaborane chemistry has been reviewed a number of times and the area is well defined in terms of structural chemistry.(1-7) With a few notable exceptions, these compounds can be described using the skeletal electron counting rules developed for the polyhedral boranes along with the isolobal relationships between transition metal fragments and main group fragments.(8-13) Recently, a more general electron counting rule that interrelates boranes, heteroboranes, organometallic complexes and various condensed structures has been described.(14) However, despite the large number of structurally characterized compounds and the predictive capabilities of the counting rules combined with the isolobal analogy, significant challenges still exist. First, the earlier synthetic routes utilized lacked generality and, in many cases, selectivity. A consequence of the former is that the majority of metallaboranes characterized in the earlier work contain almost exclusively late transition metal fragments (group 8-10). A consequence of the latter is that the known reaction chemistry of metallaboranes is extremely limited.

As we have described elsewhere, the large number of known monocyclopentadienyl metal halides constitute a potential source of metallaboranes of all the transition metals.(15,16) In fact, the utilization of LiBH_4 and BH_3THF as both activating agents and sources of polyborane fragments permits the formation of metallaboranes containing metals from groups 5 - 9 from the first to the third row of the transition metals. The reactions are generally selective giving good yields without complex separation steps. Thus, both structures of metallaboranes of the earlier transition metals and reaction chemistry can be investigated in a systematic fashion for the first time.

The series of compounds $\text{Cp}^*_2\text{M}_2\text{B}_4\text{H}_8$, $\text{M} = \text{Cr},(17) \text{Re},(18) \text{Ru},(19) \text{Ir},(20)$ in which the metal ancillary ligand and the number of "extra" hydrogen atoms are constant is particularly interesting. Equally interesting, although incomplete, is the monometallic series $\text{Cp}^*\text{MXB}_4\text{H}_8$, $\text{MX} = \text{TaCl}_2,(21) \text{WH}_3,(22,23) \text{Co}.(24,25)$ In a third series, $\text{Cp}^*_2\text{M}_2\text{B}_5\text{H}_9$, $\text{M} = \text{Cr},(26) \text{Mo},(22) \text{W},(27)$ the three compounds have the same geometric structure as well as similar ^{11}B NMR spectra(28) confirming that geometry and gross electronic structures depend primarily on metal electron count.

The structures of these compounds are shown schematically in Figure 1. For the $\text{Cp}^*_2\text{M}_2\text{B}_4\text{H}_8$ series, suffice it to say that those of Ir, Ru, and Re obey

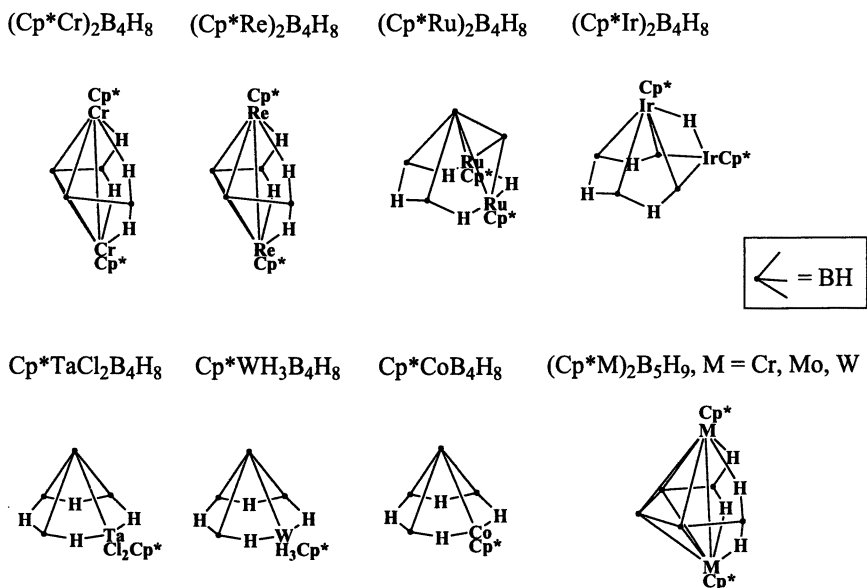


Figure 1. Structurally characterized metallaboranes with M_2B_4 , MB_4 and M_2B_5 skeletons containing early through late transition metals.

the electron counting rules, exhibiting pentagonal pyramidal, capped square pyramidal, and bicapped tetrahedral geometries appropriate for $\text{sep} = 8, 7, 6$, respectively ($\text{sep} = \text{skeletal electron pairs}$). Note that the BH capping groups are associated with M-M bonded edges. The Cr compound has a bicapped tetrahedral geometry but only 5 sep and is formally unsaturated. As discussed elsewhere, this unsaturation is not expressed in a localized multiple bond but rather is delocalized over the cluster bonding network.⁽²⁹⁾ The distortions in geometry thereby generated are fully consistent with the bonding and antibonding properties of the frontier orbitals of the hypothetical $\text{Cp}^*\text{Mn}_2\text{B}_4\text{H}_8$ saturated cluster.⁽¹⁸⁾ For the $\text{Cp}^*\text{MXB}_4\text{H}_8$ series, all adopt a square pyramidal geometry appropriate for 7 sep. Those with $\text{MX} = \text{WH}_3$ and Co do possess 7 sep; however, that with $\text{MX} = \text{TaCl}_2$ has 6 sep. As shown elsewhere, the missing pair of electrons is localized at the Ta center.⁽¹⁵⁾ The contrast between the chromium and tantalum systems is striking and unambiguous--delocalized vs localized electronic unsaturation. On the other hand, the organometallic compound $\text{Cp}_2\text{Cr}_2(\text{CO})\text{C}_4\text{R}_4$ exhibits a pentagonal pyramidal structure and a localized Cr-Cr triple bond.⁽¹⁷⁾ Clearly, more than a single mechanism is available for accommodating electronic unsaturation in a metal-main group atom cluster.

Some aspects of the comparative chemistry of the $\text{Cp}^*\text{M}_2\text{B}_4\text{H}_8$ series in terms of thermolysis, reactions with Lewis bases, Lewis acids, sources of metal fragments, and small organic molecules have been discussed earlier.(16) For the $\text{Cp}^*\text{MXB}_4\text{H}_8$ series the Co compounds have been extensively studied by Grimes(2) but only the thermolysis of the W compounds has been examined.(23) The principal interest in these studies lies in the effects of the metal on the observed chemistry. In essence, the work demonstrates how one can control the chemistry of metallaboranes by varying the transition metal. In the process, new structural problems are presented. Indeed, as will be seen, some of the clusters of the earlier transition metals present significant difficulties for the present models of cluster structure. Hence, the development of a conceptual framework for the resolution of these difficulties constitutes the focus of the present article.

Chemistry of Metallaboranes Containing Metals from Groups 6 and 7

Thermal elimination of some or all of the extra hydrogens required to meet the sep requirements for an observed cluster shape can be facile for ruthenium(30) as well as tungsten.(23) Thus, simply heating $\text{Cp}^*\text{W}(\text{H})_3\text{B}_4\text{H}_8$ results in the formation of a mixture of products containing $\text{Cp}^*\text{W}_2\text{B}_5\text{H}_9$, $\text{Cp}^*\text{W}_2\text{H}_2\text{B}_7\text{H}_7$, and $\text{Cp}^*\text{W}_3\text{HB}_8\text{H}_8$. The first can be prepared more easily by another route(27); however, there is presently no better route to the last two. These two are of considerable interest as they are distinctly electron poor. Formally, the Cp^*W fragment is a -1 electron donor and thus each possesses only 7 sep despite the need to accommodate 9 and 11 cluster fragments, respectively.

The addition of borane to $\text{Cp}^*\text{Re}_2\text{B}_4\text{H}_8$ concomitant with hydrogen elimination also leads to related electron poor compounds. The process is distinctly metal dependent. Addition of borane to formally unsaturated $\text{Cp}^*\text{Cr}_2\text{B}_4\text{H}_8$ with hydrogen elimination leads to the formation of saturated $\text{Cp}^*\text{Cr}_2\text{B}_5\text{H}_9$.(26) Similar addition of a single borane fragment is found with metallaboranes containing Ru, Rh and Ir.(19,20) The extra hydrogens on these skeletons are not readily lost. However, addition of borane to formally saturated $\text{Cp}^*\text{Re}_2\text{B}_4\text{H}_8$ leads to the sequential formation of $\text{Cp}^*\text{Re}_2\text{B}_7\text{H}_7$.(31) $\text{Cp}^*\text{Re}_2\text{B}_8\text{H}_8$, $\text{Cp}^*\text{Re}_2\text{B}_9\text{H}_9$, $\text{Cp}^*\text{Re}_2\text{B}_{10}\text{H}_{10}$ at which point cluster growth stops.(32) The four extra hydrogens present in the starting cluster are lost. Taking the Cp^*Re fragment as a three-orbital, 0 electron fragment means that the $\text{Cp}^*\text{Re}_2\text{B}_n\text{H}_n$, $n = 7 - 10$, clusters have $p - 2$ sep, $p = 9 - 12$. Further, modest variation in reaction conditions permits $\text{Cp}^*\text{Re}_2\text{H}_2\text{B}_7\text{H}_9$ with 9 sep to be isolated.(33)

Geometric Structures of Hypoelectronic Metallaboranes of Tungsten and Rhenium

The geometric structures of $\text{Cp}^*\text{Re}_2\text{B}_n\text{H}_n$, $n = 7 - 10$ are illustrated in Figure 2 in two ways. By elimination of all the lines corresponding to M-B bonded edges, one can see that each contains a ring-like borane fragment

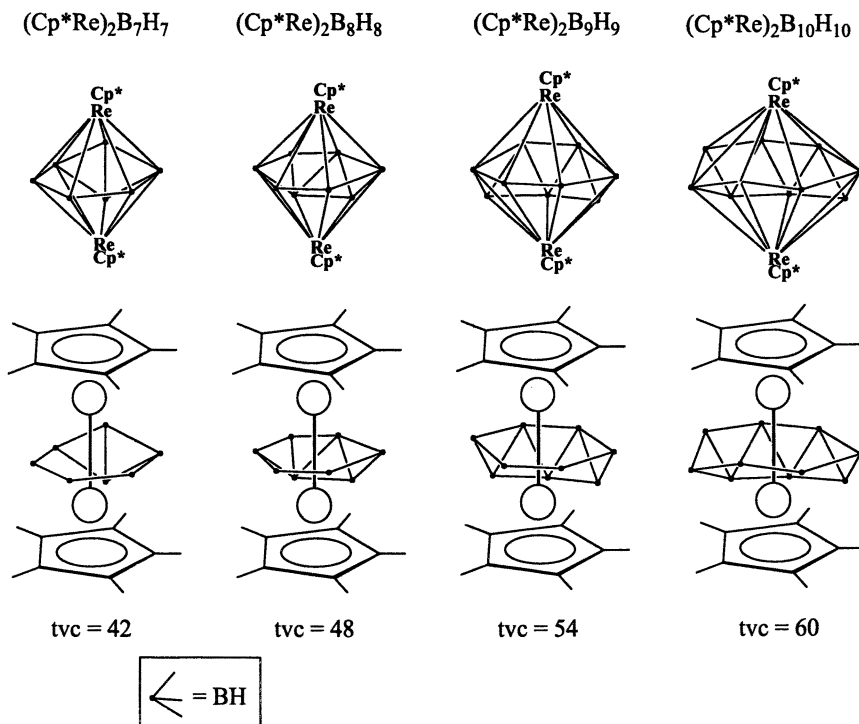
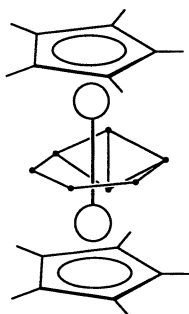
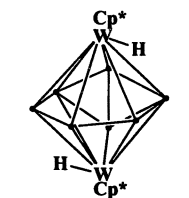


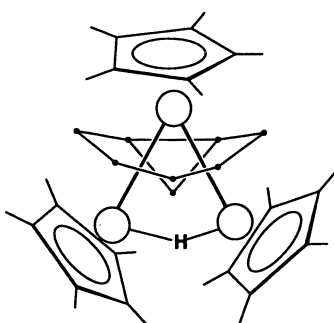
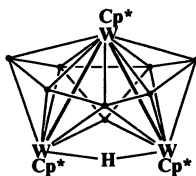
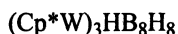
Figure 2. Structures of hypoelectronic closed rhenaboranes shown with and without the lines corresponding to the metal-boron bonding interactions.

pierced by a metal-metal bonded dirhenium fragment. These geometries do not correspond to the most spherical deltahedra that characterize the structures of the closo boranes and carboranes (canonical structures(34,35)) nor do they correspond to the capped structures that are prevalent for metal clusters when the total sep falls below $p + 1$ where p is the number of metal fragments. (12) In fact the rhenium centers occupy vertices with connectivities of either 6 or 7 and

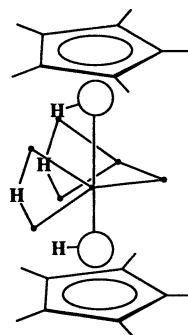
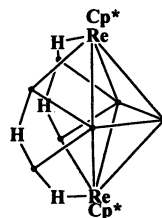
the cluster adopts a much less spherical shape than the corresponding closo borane. Further, in each case there is a cross cage metal-metal bond with a bond distance corresponding to that of a single bond. $\text{Cp}^*_2\text{Re}_2\text{H}_2\text{B}_7\text{H}_9$ (Figure 3) is unique in that it exhibits an open framework despite having a cross-cage metal-metal bond.



tvc = 42



tvc = 54



tvc = 36

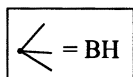


Figure 3. Structures of hypoelectronic closed tungstaboranes and a hypoelectronic open rhenaborane shown with and without lines corresponding to the metal-boron bonding interactions.

$\text{Cp}^*_2\text{W}_2\text{H}_2\text{B}_7\text{H}_7$ (Figure 3)(31) is isoelectronic and nearly isostructural with $\text{Cp}^*_2\text{Re}_2\text{B}_7\text{H}_7$, the structural distortions being associated with the two extra hydrogen atoms. This pair of compounds shows that whatever the number of electrons the metal fragment contributes to cluster bonding, it must be one less for W than Re. $\text{Cp}^*_3\text{W}_3\text{HB}_8\text{H}_8$ (Figure 3) possesses a related structure but now there are two cross-cage metal-metal bonds. Previously, we have related its structure to that of a Ru_{11} cluster which exhibits a hexagonal close-packed metal

core.(36) Again there are significant differences when compared to the canonical 11 vertex closo structure. (23)

Hypercloso vs Isocloso Metallaboranes

Cluster structural anomalies related to those displayed by the hypoelectronic tungsta- and rhenaboranes described above have been known for some time. Although the first example involved a metallacarborane,(37) the majority involve metallaboranes.(38,39) Two views of these cluster types emerged and were later compared and contrasted by others. Both focused on geometric structure and viewed the differences relative to the canonical geometry as due to (a) an isomeric form of the canonical shape possessing the same number of filled cluster bonding orbitals; hence isocloso and isonido,(38,40) and (b) a new shape reflecting a number of filled cluster bonding orbitals less than the $p + 1$ required for the canonical closo geometry; hence, hypercloso.(41) The drawback of approach (a) is that it treats the contribution of a metal center as an additional variable. The drawback of approach (b) is that it cannot account for open structures with closo counts. As was pointed out later in a molecular orbital analysis, the former view requires localization of the missing electrons at the metal center whereas the latter requires delocalization of the missing electrons over the cluster bonding network.(39,42) The analysis of the electronic structure calculations generally supported the hypercloso view; however, one system was best understood in terms of metal localized unsaturation.(39) In this analysis, the variable sep count permitted for clusters with structures of C_{mv} symmetry (polar deltahedra) was used to account for many of the shapes observed for closo systems with a formal sep = p .

In the totally different experimental venue of Zintl phases containing homonuclear, group 13, bare cluster anions, noncanonical shapes observed were explained as a response to the large electron-electron repulsive energies involved in generating the $p + 1$ sep required for a canonical closo structure.(43,44) Compounds of this type were described as hypoelectronic and, as these compounds are homonuclear, it is unlikely the missing electrons will be localized at a selected sites. We adopted this nomenclature to describe the tungsta- and rhenaboranes simply because it avoids the necessity of specifically describing where the electrons are, i.e., compounds with formal sep less than the $p + 1$ count for the geometric cluster type (closo, nido, arachno) are designated hypoelectronic.

A complicating factor is that, as one moves to the earlier transition metals, the number of orbitals and electrons contributed really can be a variable.(45) Formally, Cp^*Co is a three orbital, 2 electron fragment like BH, $CpFe$ is 1 electron, $CpMn$ is 0, and $CpCr$ is -1 electron. However, this assumes that each metal has 6 filled d functions that do not participate in bonding. Although

reasonable for late transition metals, the earlier transition metals can use these "extra" orbitals in bonding. Thus, $[\text{CpFe}(\text{CO})_2]_2$ contains a Fe-Fe single bond (the 17 electron $\text{CpFe}(\text{CO})_2$ fragment is a one orbital, 1 electron fragment with 3 filled nonbonding metal orbitals and isolobal with CH_3) whereas $[\text{CpCr}(\text{CO})_2]_2$ contains a Cr-Cr triple bond (the 15 electron $\text{CpCr}(\text{CO})_2$ fragment is a three orbital, 3 electron fragment with 1 filled nonbonding orbital on the metal and isolobal with CH). In the dimer, the $\text{CpCr}(\text{CO})_2$ fragment does not behave like a one orbital, -1 electron fragment. So one might reasonably call Cp^*Re a 0 or a 2 electron donor, i.e., the electron count of a transition metal is more variable than a main group fragment. For compounds with localized bonding, e.g. metal dimers, bond distances reveal the behavior of the metal fragment. Unfortunately, for clusters with delocalized bonding the role of the metal in generating a cluster count is less apparent in the structural parameters alone.

Analysis of Hypoelectronic Metallaboranes of Tungsten and Rhenium

The earlier ideas of isocloso and hypercloso clusters can be applied to the new compounds of tungsten and rhenium; however, they are inadequate in several aspects. These closed compounds have formal $\text{sep} = p - 2$ and $p - 3$ rather than $p + 1$ (isocloso) or p (hypercloso). Neither capped structures nor the canonical structures are observed. The former is unlikely as three-connected BH fragments are not observed unless two or three metal atoms are involved. The symmetry of the structures is low (C_s generally with one example of C_2 symmetry) thereby limiting arguments based on polar deltahedra. Cross cage metal-metal bonding is observed suggesting some localization of the missing electrons at the metal centers. The systematic variation in structure with the size of the borane fragment as well as the existence of an open structure with $\text{sep} = p$ (classified as arachno) suggests the existence of a systematic structural principle.

Multiple bonds between the metal atoms are ruled out by the structural parameters. As already explained, the Cp^*Re fragment could be counted as a three orbital-two electron fragment(45) giving sep counts of p for $\text{Cp}^*_2\text{Re}_2\text{B}_n\text{H}_n$ and $p + 2$ for $\text{Cp}^*_2\text{Re}_2\text{H}_2\text{B}_7\text{H}_9$. With the cross cage Re-Re bonds the electron counting rules would be satisfied and one would conclude that the missing electrons were metal localized. This would make $\text{Cp}^*_2\text{Re}_2\text{B}_4\text{H}_8$ an 8 sep nido cluster based on a pentagonal bipyramidal cage with one equatorial vertex unoccupied rather than a 6 sep bicapped tetrahedron. Unfortunately, this does not account for the Re-Re bond. Treating Cp^*Cr as a 1 electron fragment yields 6 sep for $\text{Cp}^*_2\text{Cr}_2\text{B}_4\text{H}_8$ and a bicapped tetrahedron does describe the qualitative structure but now fails to explain the very long Cr-Cr distance. This approach also backfires when applied to $\text{Cp}^*_2\text{M}_2\text{B}_5\text{H}_9$, $\text{M} = \text{Cr}, \text{Mo}, \text{W}$, as now the 8 sep

requires a closo structure which is not consistent with the open five-member borane ring, the M-M bond, or the presence of four extra B-M bridging hydrogens. A treatment that requires adjusting the metal fragment count for small variation in metal properties while ignoring obviously important structural features is a rationalization of little utility. Thus, metal localization alone is insufficient to rationalize the observed geometries in a consistent manner.

What is needed is a parameter of the cluster that carries over from canonical structures to those observed for the capped and hypoelectronic clusters. One that does is the total vertex connectivity (tvc) of the cluster (number of bonded edges). Thus, a tricapped trigonal prism (canonical, $p + 1$ sep), a monocapped dodecahedron (p sep), bicapped pentagonal bipyramid ($p - 1$ sep), and a tricapped octahedron ($p - 2$ sep) all have $tvc = 42$. Likewise, $Cp^*_2Re_2B_nH_n$ have connectivities identical to those of the canonical closo shapes with 9 through 12 vertices (42, 48, 54, 60); $Cp^*_2Re_2H_2B_7H_9$ the same as an arachno nine-vertex canonical geometry (36); $Cp^*_3W_3HB_8H_8$ the same as a closo eleven vertex canonical geometry (54); $Cp^*_2W_2H_2B_7H_7$ the same as a closo nine vertex canonical geometry (42); and $Cp^*_2M_2B_5H_9$ the same as a closo seven vertex canonical geometry (30). The reason the tvc is constant is that all of these structures are related by diamond-square-diamond (dsd) rearrangements.(46) An example of a dsd rearrangement is given in Figure 4 where it is seen that such a rearrangement leads to a less spherical cluster shape (greater number of higher and lower vertex connectivities). A set of dsd

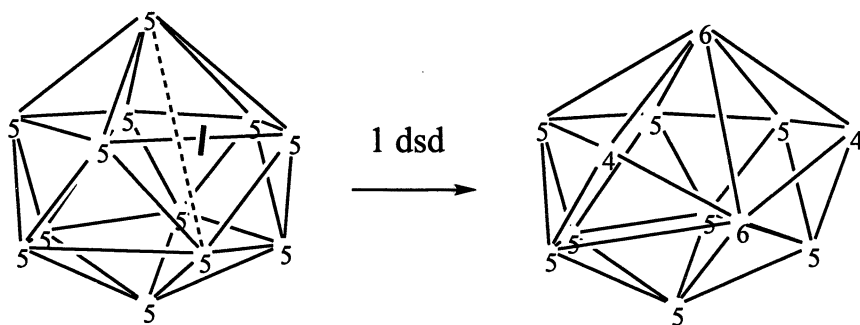


Figure 4. Representation of a diamond-square-diamond (dsd) rearrangement for an icosahedron (canonical shape for $p = 12$) leading to a change in the distribution of vertex connectivities at constant total vertex connectivity (tvc).

rearrangements also provides a mechanism for cluster rearrangement--one originally suggested by Lipscomb.(47)

This relationship by itself does not provide any information on the structure adopted for any given composition. It does, however, limit the number of

cluster shapes possible for a given number of vertices, p . It is instructive to first analyze the effect of applying the capping principle to a couple of canonical shapes. Consider the pentagonal bipyramid which is appropriate for seven cluster fragments and a $\text{sep} = 8$ (Figure 5). If only 7 sep are available one

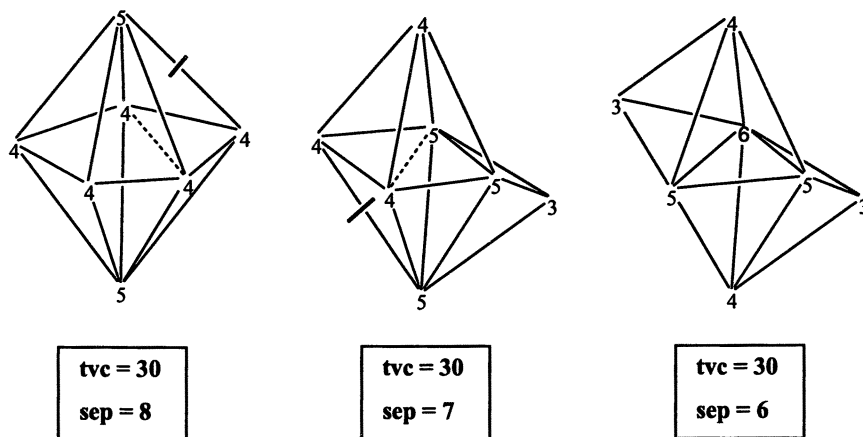


Figure 5. The generation of capped deltahedra via dsd rearrangements thereby accommodating $p + 1$, p , and $p - 1$ sep, $p = 7$. The cross bar indicates the connection ruptured and the dotted line the connection formed.

expects a monocapped octahedral shape to be adopted. This can be achieved via a single dsd rearrangement in which the connectivity of a four-connected vertex increases by one and the connectivity of another decreases by one. If only 6 sep are available the shape appropriate is a bicapped trigonal bipyramid. This requires another dsd rearrangement with similar changes in vertex connectivities. On this basis, one would predict that 7 sep $\text{Cp}^*_2\text{Re}_2\text{B}_7\text{H}_7$ should adopt the shape of a tricapped octahedron derived from a canonical tricapped trigonal prism via three dsd rearrangement that require three vertex connectivities to increase by one and three to decrease by one (Figure 6). The observed shape can be derived from the canonical tricapped trigonal prism via two dsd rearrangement that require two vertex connectivities to increase by one and two to decrease by one plus the addition of a cross-cage Re-Re bond. This suggests that $\text{Cp}^*_2\text{Re}_2\text{B}_7\text{H}_7$ adopts a shape that avoids three-connected vertices (with the limited number of metal atoms one BH would be required to cap a MB_2 triangle and another B atom would occupy a 6-connected vertex). Rather it adopts one in which two of the missing sep are delocalized over the cluster framework via a mechanism analogous to that operative in the capping

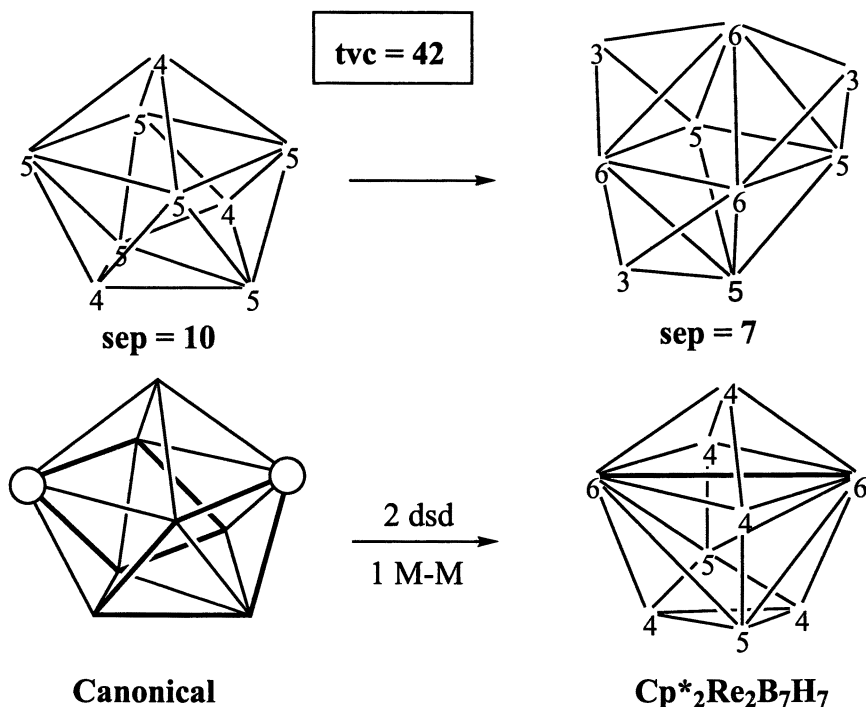


Figure 6. (top) The generation of a capped shape to accommodate the 7 sep of $\text{Cp}^*_2\text{Re}_2\text{B}_7\text{H}_7$ in a bicapped octahedron. (bottom) The generation of the observed deltahedron for $\text{Cp}^*_2\text{Re}_2\text{B}_7\text{H}_7$ from the canonical deltahedron for $p = 9$. The bold lines outline the diamond that undergoes rearrangement.

principle and the third generates a cross-cage metal-metal bond. The same considerations apply to $\text{Cp}^*_2\text{W}_2\text{H}_2\text{B}_7\text{H}_7$.

As shown in Figure 7, an identical structural mechanism connects the observed structures of $\text{Cp}^*_2\text{Re}_2\text{B}_8\text{H}_8$, and $\text{Cp}^*_2\text{Re}_2\text{B}_9\text{H}_9$ to the canonical structure thereby justifying the $p - 2$ sep count obtained by treating Cp^*W and Cp^*Re as -1 and 0 electron fragments, respectively. The shape observed for $\text{Cp}^*_3\text{W}_3\text{HB}_8\text{H}_8$ is generated by two non-degenerate dsd rearrangements along

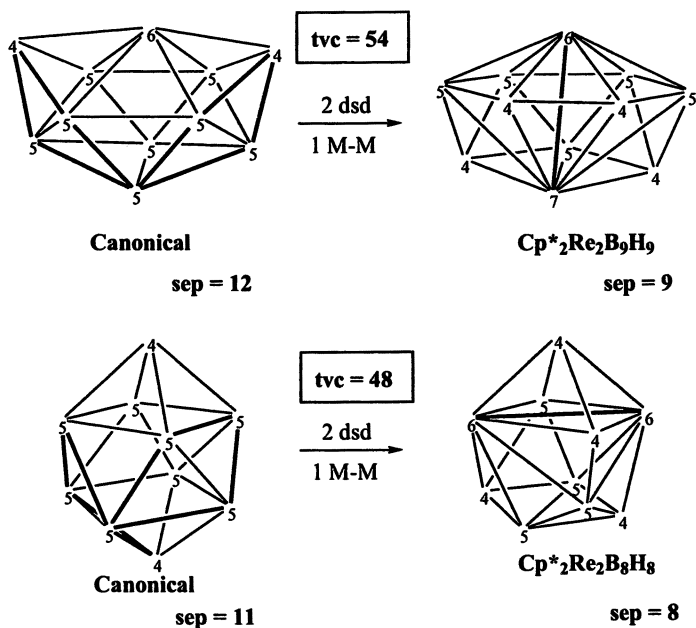


Figure 7. The generation of the observed deltahedron for $\text{Cp}^*_2\text{Re}_2\text{B}_8\text{H}_8$ and $\text{Cp}^*_2\text{Re}_2\text{B}_9\text{H}_9$ from the canonical deltahedra for $p = 10$ and 11 . The bold lines outline the diamond that undergoes rearrangement as well as the Re-Re bond.

with two cross-cage W-W bonds thereby accounting for its $p - 3$ sep count. Likewise the series $[(\eta^6\text{-C}_6\text{Me}_6)\text{RuB}_9\text{H}_9]^{2-}$, (48) $(\eta^6\text{-C}_6\text{Me}_6)\text{RuB}_9\text{H}_9$, (49) and $\{\text{Cp}^*\text{Ru}\}_2(\eta^6\text{-C}_6\text{H}_6)\text{Ru}\text{B}_7\text{H}_7\}$ with $p + 1$, p , and $p - 1$ sep, respectively, fit the paradigm (Figure 8). If one includes $\text{Cp}^*_2\text{Re}_2\text{B}_8\text{H}_8$, hypoelectronic metallaboranes with sep from $p + 1$ to $p - 2$ are accommodated. It is important to note that the clusters containing ruthenium do not suffer from the same ambiguity in electron count as do the earlier metals.

Unfortunately, $\text{Cp}^*_2\text{Re}_2\text{B}_{10}\text{H}_{10}$ appears to be an exception. As shown in Figure 9 four dsd rearrangements are required taking two vertices up two in connectivity and four down one. In addition there is a Re-Re bond. The icosahedron is highly spherical and two dsd are insufficient to generate a shape that permits a cross-cage metal-metal bond. The two additional dsd

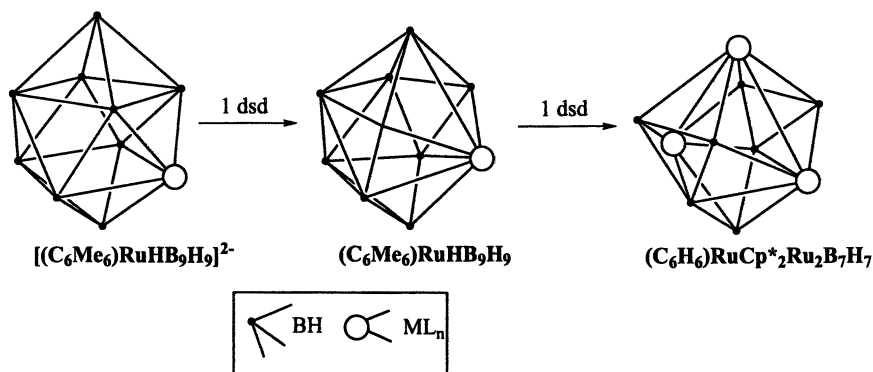


Figure 8. The connections between the observed deltahedra for $[(\eta^6-C_6Me_6)RuB_9H_9]^{2-}$, $(\eta^6-C_6Me_6)RuB_9H_9$ and $\{Cp^*Ru\}_2(\eta^6-C_6H_6)Ru\}B_7H_7$ in which the first compound displays the canonical deltahedron for $p = 10$.

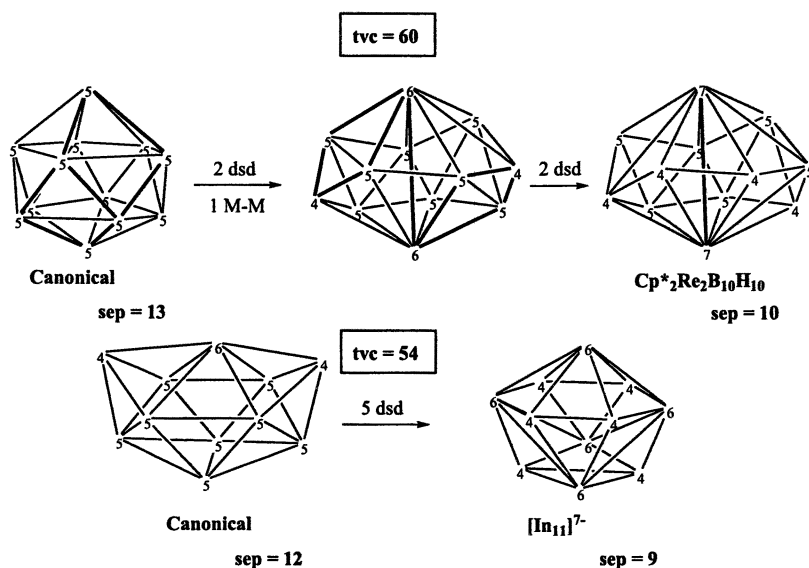


Figure 9. The generation of the observed deltahedra for $Cp^*_2Re_2B_{10}H_{10}$ and $[In_{11}]^{7-}$ from the canonical deltahedra for $p = 12$ and 11 . The bold lines outline the diamond that undergoes rearrangement in the first case.

rearrangements generate two vertices of connectivity seven thereby flattening out the cluster sufficiently such that a Re-Re bond is possible. Likewise, in the hypoelectronic naked clusters of group 13 elements, the connection between the number of dsd rearrangements required and the electron count is not straightforward, e.g., In_{11}^{7-} with $p - 2$ sep requires five dsd rearrangements taking four vertices up one in connectivity and four down one to generate the observed structure from the canonical 11 vertex deltahedron.(44) Note that this is not the rearrangement described in the original work albeit equivalent to it. Unfortunately, these exceptions limit the usefulness of the analysis described even though in all cases the qualitative change in distribution of vertex connectivities is the same.

Implicit in the capping principle is the existence of capped nido and arachno structures. In fact these are often observed in metal systems.(11,50) Thus, a capped square pyramidal cluster, $\text{sep} = 7$, is an alternative structure to an octahedron. Further a bicapped butterfly (edge-fused tetrahedra), $\text{sep} = 7$, is an additional alternative. Likewise, Kennedy has described both isonido and isoarachno metallaboranes with $p + 1$, and $p + 2$, sep respectively.(51,52) Therefore, in principle, open analogs of the rhenia- and tungstaboranes should also exist with $p - 1$ (nido analog) and p (arachno analog). We have recently characterized $\text{Cp}^*_2\text{Re}_2\text{H}_2\text{B}_7\text{H}_9$ as an arachno analog of $\text{Cp}^*_2\text{Re}_2\text{B}_7\text{H}_7$ with 9 sep by the expedient of demonstrating that its $\text{tvc} = 36$ is the same as the preferred structure for an arachno 9 vertex canonical structure.(53) It is important to note that the additional four hydrogen atoms on the $\text{Cp}^*_2\text{Re}_2\text{B}_7\text{H}_7$ framework do not simply convert it into an isocloso (hypercloso) structure but rather into an open structure that retains features favored by the metal fragment. Although the requirement of a Re-Re bond is important, the demands of the bridging hydrogen atoms must play a role—one analogous to the role they play in the octahedral structure of $[\text{Os}_6(\text{CO})_{18}]^{2-}$ vs the capped square pyramidal structure of $\text{H}_2\text{Os}_6(\text{CO})_{18}$.(54)

Molecular Orbital Model of Hypoelectronic Metallaboranes of Tungsten and Rhenium

Finally, the question why two cluster geometries with equal tvc 's can have differing numbers of cluster bonding orbitals must be addressed. The origin of the capping principle has already been discussed in detail by Mingos as have the variation in number of cluster bonding orbitals in polar deltahedra, high nuclearity clusters with more than one shell, and clusters with metals associated with π -donor ancillary ligands.(12,55,56) All these ideas are clearly related to the present problem but either not sufficiently flexible or detailed enough to accommodate the series of compounds under discussion.

In their exploration of physical factorization of the secular equation for various deltahedra, Hoffmann and Lipscomb considered a ring-polar separation in which the equatorial ring is capped by two polar fragments to form the complete cage. (57) Used effectively recently by others, (58,59) this fragmentation connects cage structures to those of so-called triple-decker complexes where the polar fragments are now metal fragments such as CpM. We have already presented an analysis of the 24 electron $\{\text{Cp}^*\text{Cr}\}_2\{\mu\text{-}\eta^6\text{:}\eta^6\text{-C}_3\text{H}_6\text{C}_2\text{B}_4\text{H}_4\}$ triple-decker (60) in which we showed that formation of the Cr-Cr bond destabilizes and empties two in-plane ring orbitals that are metal-ring antibonding while concurrently stabilizing a cross cage MM bonding orbital and destabilizing (and emptying) its antibonding partner. This constitutes one example of a triple-decker sandwich complex, many of which have been characterized for a range of transition metals. (61) The variation in the structures of these compounds with d electron count is well understood. (62)

The parent compound of the $\text{Cp}^*_2\text{Re}_2\text{B}_n\text{H}_n$ series is the unknown $\text{Cp}^*_2\text{Re}_2\text{B}_6\text{H}_6$, which we have recently characterized as the dichloro-derivative. (63) However, $\{\text{Cp}^*\text{Re}\}_2\{\mu\text{-}\eta^6\text{:}\eta^6\text{-B}_4\text{H}_4\text{Co}_2(\text{CO})_5\}$ is known and constitutes an isolobal analog of $\text{Cp}^*_2\text{Re}_2\text{B}_6\text{H}_6$ (Figure 10). (64) Comparing 9 sep $[\{\text{Cp}^*\text{Rh}\}_2\{\mu\text{-}\eta^6\text{:}\eta^6\text{-C}_4\text{H}_4\text{B}_2\text{Me}_2\}]^{2+}$ (65) with 6 sep $\text{Cp}^*_2\text{Re}_2\text{B}_6\text{H}_6$ shows that as the Cp^*M fragments are moved within bonding distance three orbitals, which are filled in the 9 sep compound, are emptied and a substantial HOMO-LUMO gap is produced for 6 sep. (57,62) These MO's consist of a M-M antibonding orbital and two M-B orbitals that are boron ring-metal δ

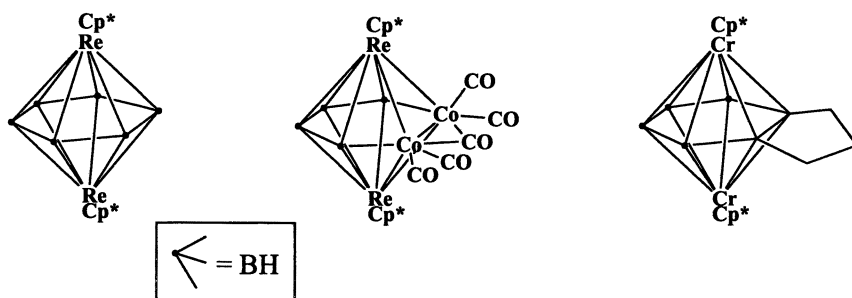
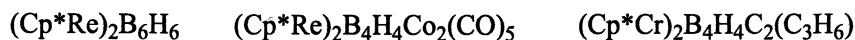


Figure 10. Comparison of $\text{Cp}^*_2\text{Re}_2\text{B}_6\text{H}_6$ as a triple-decker complex with known $\text{Cp}^*_2\text{Re}_2\text{B}_4\text{H}_4\text{Co}_2(\text{CO})_5$ and $\text{Cp}^*_2\text{Cr}_2\text{B}_4\text{H}_4\text{C}_2\text{C}_3\text{H}_6$.

antibonding (Figure 11). Now the view of $\text{Cp}^*_2\text{Re}_2\text{B}_n\text{H}_n$ as pseudo triple-decker complexes (Figure 2) begins to make even more sense. That is, the generation of the observed structure of $(\text{Cp}^*\text{Re})_2\text{B}_7\text{H}_7$ from the canonical tricapped trigonal prismatic geometry causes three orbitals to rise sufficiently high in energy to become unoccupied. (31,66) As with $\text{Cp}^*_2\text{Re}_2\text{B}_6\text{H}_6$, one is Re-Re antibonding, and two are Re-boron ring antibonding. Thus, there is an increase in Re-Re and Re-B bonding at the expense of B-B bonding. Application of the same mechanism to the rest of the $\text{Cp}^*_2\text{Re}_2\text{B}_n\text{H}_n$ series accounts for the electron count of $p - 2$.

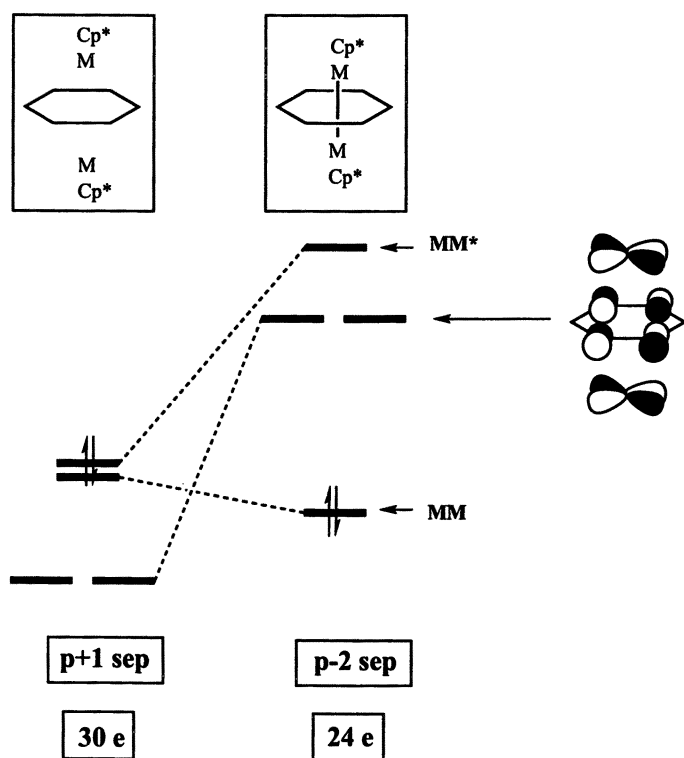


Figure 11. Schematic molecular orbital diagram showing the destabilization of two cluster orbitals and one metal centered orbital on reducing the metal-metal distance. The same mechanism is postulated to account for the more complex "triple-decker" structures of the hypoelectronic rhenia- and tungstaboranes.

Summary

The number of skeletal electron pairs required for fully closed cluster geometries is variable, however the total vertex connectivity is not. Thus, polar and capped deltahedra are not the only cluster types in which a number of sep less than $p + 1$, where p corresponds to the number of cluster fragments, can be accommodated. Diamond-square-diamond rearrangements of canonical geometries leading to vertices of increased and decreased connectivities can also lower the number of filled cluster bonding orbitals. The resulting oblate shape permits the introduction of cross-cage metal-metal bonds which can further reduce the number of filled orbitals. The overall result is increased metal-metal and metal-boron bonding and decreased boron-boron bonding as one moves from later to earlier transition metals. This is not unlike the effects found in the metal borides of intermediate composition.(67,68)

References

1. Greenwood, N. N.; Ward, I. M. *Chem. Soc. Rev.* **1974**, 3, 231.
2. Grimes, R. N. *Accts. Chem. Research* **1978**, 11, 420.
3. Grimes, R. N. In *Metal Interactions with Boron Clusters*; R. N. Grimes, Ed.; Plenum: New York, 1982; pp 269.
4. Housecroft, C. E.; Fehlner, T. P. *Adv. Organomet. Chem.* **1982**, 21, 57.
5. Housecroft, C. E. *Boranes and Metalloboranes*; Ellis Horwood: Chichester, 1990.
6. Kennedy, J. D. *Prog. Inorg. Chem.* **1984**, 32, 519.
7. Kennedy, J. D. *Prog. in Inorg. Chem.* **1986**, 34, 211.
8. Wade, K. *Inorg. Nucl. Chem. Lett.* **1972**, 8, 559.
9. Wade, K. *Adv. Inorg. Chem. & Radiochem.* **1976**, 18, 1.
10. Mingos, D. M. P. *Nature (London) Phys. Sci.* **1972**, 236, 99.
11. Mingos, D. M. P.; Johnston, R. L. *Structure and Bonding* **1987**, 68, 29.
12. Mingos, D. M. P.; Wales, D. J. *Introduction to Cluster Chemistry*; Prentice Hall: New York, 1990.
13. *Structural and Electronic Paradigms in Cluster Chemistry*; Mingos, D. M. P., Ed.; Springer: 1997; Vol. 87.
14. Jemmis, E. D.; Balakrishnarajan, M. M.; Pancharatna, P. D. *J. Am. Chem. Soc.* **2001**, 123, 4313.
15. Fehlner, T. P. *J. Chem. Soc., Dalton Trans.* **1998**, 1525.
16. Fehlner, T. P. *Organometallics* **2000**, 19, 2643.
17. Deck, K. J.; Nishihara, Y.; Shang, M.; Fehlner, T. P. *J. Am. Chem. Soc.* **1994**, 116, 8408.
18. Ghosh, S.; Shang, M.; Fehlner, T. P. *J. Organomet. Chem.* **2000**, 614-15, 92.

19. Lei, X.; Shang, M.; Fehlner, T. P. *J. Am. Chem. Soc.* **1999**, *121*, 1275.
20. Lei, X.; Shang, M.; Fehlner, T. P. *Chemistry. A European Journal* **2000**, *6*, 2653.
21. Aldridge, S.; Hashimoto, H.; Shang, M.; Fehlner, T. P. *Chem. Comm.* **1998**, 207.
22. Bullick, H. J.; Grebenik, P. D.; Green, M. L. H.; Hughes, A. K.; Leach, J. B.; McGowan, P. C. *J. Chem. Soc. Dalton Trans* **1995**, 67.
23. Weller, A. S.; Shang, M.; Fehlner, T. P. *J. Am. Chem. Soc.* **1998**, *120*, 8283.
24. Miller, V. R.; Weiss, R.; Grimes, R. N. *J. Am. Chem. Soc.* **1977**, *99*, 5646.
25. Venable, T. L.; Sinn, E.; Grimes, R. N. *J. Chem. Soc., Dalton Trans.* **1984**, 2275.
26. Aldridge, S.; Hashimoto, H.; Kawamura, K.; Shang, M.; Fehlner, T. P. *Inorg. Chem.* **1998**, *37*, 928.
27. Weller, A. S.; Shang, M.; Fehlner, T. P. *Organometallics* **1999**, *18*, 53.
28. Weller, A. S.; Fehlner, T. P. *Organometallics* **1999**, *18*, 447.
29. Fehlner, T. P. *J. Organomet. Chem.* **1998**, *550*, 21.
30. Lei, X.; Shang, M.; Fehlner, T. P. *Organometallics* **2001**, *20*, 1479.
31. Weller, A. S.; Shang, M.; Fehlner, T. P. *Chem. Commun.* **1998**, 1787.
32. Ghosh, S.; Shang, M.; Li, Y.; Fehlner, T. P. *Angew. Chem. Int. Ed.* **2001**, *40*, 1125.
33. Ghosh, S.; Rheingold, A. L.; Fehlner, T. P. *Chem. Commun.* **2001**, 895.
34. Williams, R. E. *Inorg. Chem.* **1971**, *10*, 210.
35. Williams, R. E. *Adv. Inorg. Chem. & Radiochem.* **1976**, *18*, 67.
36. Bailey, P. J.; Beswick, M. A.; Johnson, B. F. G.; Lewis, J.; Raithby, P. R.; Ramirez de Arellano, M. C. *J. Chem. Soc., Dalton Trans.* **1992**, 3159.
37. Callahan, K. P.; Evans, W. J.; Lo, F. Y.; Strouse, C. E.; Hawthorne, M. F. *J. Am. Chem. Soc.* **1975**, *97*, 296.
38. Kennedy, J. D. In *The Borane, Carborane, Carbocation Continuum*; J. Casanova, Ed.; Wiley: New York, 1998; pp 85.
39. Johnston, R. L.; Mingos, D. M. P.; Sherwood, P. *New J. Chem.* **1991**, *15*, 831.
40. Kennedy, J. D. *Inorg. Chem.* **1986**, *25*, 111.
41. Baker, R. T. *Inorg. Chem.* **1986**, *25*, 109.
42. Johnston, R. L.; Mingos, D. M. P. *Inorg. Chem.* **1986**, *25*, 3321.
43. Sevov, S. C.; Corbett, J. D. *Inorg. Chem.* **1991**, *30*, 4875.
44. Corbett, J. D. *Structure and Bonding* **1997**, *87*, 157.
45. Hoffmann, R. *Science* **1981**, *211*, 995.
46. King, R. B. *Inorg. Chem.* **1999**, *38*, 5151.
47. Lipscomb, W. N. *Science* **1966**, *153*, 373.
48. Littger, R.; English, U.; Ruhlandt-Senge, K.; Spencer, J. T. *Angew Chem. Int. Ed.* **2000**, *39*, 1472.
49. Ditzel, E. J.; Fontaine, X. L. R.; Greenwood, N. N.; Kennedy, J. D.; Thornton-Pett, M. Z. *Anorg. Allg. Chem.* **1992**, *616*, 79.

50. *The Chemistry of Metal Cluster Complexes*; Shriver, D. F.; Kaesz, H. D.; Adams, R. D., Ed.; VCH: New York, 1990.
51. Bould, J.; Clegg, W.; Teat, S. J.; Barton, L.; Rath, N. P.; Thornton-Pett, M.; Kennedy, J. D. *Inorg. Chim. Acta* **1999**, 289, 95.
52. Bould, J.; Cooke, P. A.; Dorfler, U.; Kennedy, J. D.; Barton, L.; Rath, N. P.; Thornton-Pett, M. *Inorg. Chim. Acta* **1999**, 285, 290.
53. Williams, R. E. In *The Borane, Carborane, Carbocation Continuum*; J. Casanova, Ed.; Wiley-Interscience: New York, 1997; pp 3.
54. Cavanaugh, M. A.; Fehlner, T. P.; Stramel, R.; O'Neill, M. E.; Wade, K. *Polyhedron* **1985**, 4, 687.
55. Kahlal, S.; Halet, J.-F.; Saillard, J.-Y. *Inorg. Chem.* **1991**, 30, 2567.
56. Kahlal, S.; Halet, J.-F.; Saillard, J.-Y. *Inorg. Chem.* **1991**, 30, 2567.
57. Hoffmann, R.; Lipscomb, W. N. *J. Chem. Phys.* **1962**, 36, 2179.
58. Jemmis, E. D. *J. Am. Chem. Soc.* **1982**, 104, 7017.
59. Jemmis, E. D.; Schleyer, P. v. R. *J. Am. Chem. Soc.* **1982**, 104, 4781.
60. Kawamura, K.; Shang, M.; Wiest, O.; Fehlner, T. P. *Inorg. Chem.* **1998**, 37, 608.
61. Herberich, G. E. In *Comprehensive Organometallic Chemistry II*; E. Abel, F. G. A. Stone and G. Wilkinson, Ed.; Pergamon Press: Oxford, 1995; Vol. 1; pp 197.
62. Jemmis, E. D.; Reddy, A. C. *Organometallics* **1988**, 7, 1561.
63. Ghosh, S.; Beatty, A. M.; Fehlner, T. P. *J. Am. Chem. Soc.* **2001**, in press.
64. Ghosh, S.; Shang, M.; Fehlner, T. P. *J. Am. Chem. Soc.* **1999**, 121, 7451.
65. Herberich, G. E.; Hessner, B.; Huttner, G.; Zsolnai, L. *Angew. Chem. Int. Ed.* **1981**, 20, 472.
66. Weller, A. S.; Shang, M.; Fehlner, T. P. *Organometallics* **1999**, 18, 853.
67. Burdett, J. K.; Canadell, E. *Inorg. Chem.* **1988**, 27, 4437.
68. Fehlner, T. P. *J. Solid State Chem.* **2000**, 154, 110.

Chapter 5

Bifunctional Lewis Acid Reactivity of Diol-Derived Diboron Reagents

Charles A. G. Carter¹, Kevin D. John¹, Grace Mann¹, Richard L. Martin¹,
Thomas M. Cameron¹, R. Tom Baker^{1,*}, Karyn L. Bishop²,
Richard D. Broene^{2,*}, and Stephen A. Westcott^{3,*}

¹Los Alamos Catalysis Initiative, Chemistry and Theory Divisions,
Los Alamos National Laboratory, Los Alamos, NM 87545

²Department of Chemistry, Bowdoin College, Brunswick, ME 04011

³Department of Chemistry, Mount Allison University, Sackville,
NB E411G8, Canada

Divalent, diol-derived diboron reagents such as B₂cat₂ (cat = catecholato, 1,2-O₂C₆H₄) have been used recently for metal-catalyzed diboration and borylation reactions of unsaturated organic substrates. In this report we describe two new reactions of these reagents that take advantage of their bifunctional Lewis acidity. Stereoselective coupling of diarylaldimines, ArN=CHAr', using B₂cat₂ affords *rac-N*-boryldiamines. The efficiency of this reaction depends on both the Lewis acidity of the boron centers (to bind the imine substrates) and the reducing potential of the B-B bond. The large driving force for B-O bond formation also allows the diboron compounds to serve as selective deoxygenation reagents for amine oxides, sulfoxides, phosphine oxides, and even organic carbonyl compounds. Some of these deoxygenation reactions require transition metal catalysis and possible reaction pathways are discussed. Density Functional Theory is used to probe the relative Lewis acidities of the divalent diboron compounds and their trivalent B-O-B analogs. The increased acidity of the latter is attributed to increased bond polarity and reduction of B-O π -bonding effects in the base adducts.

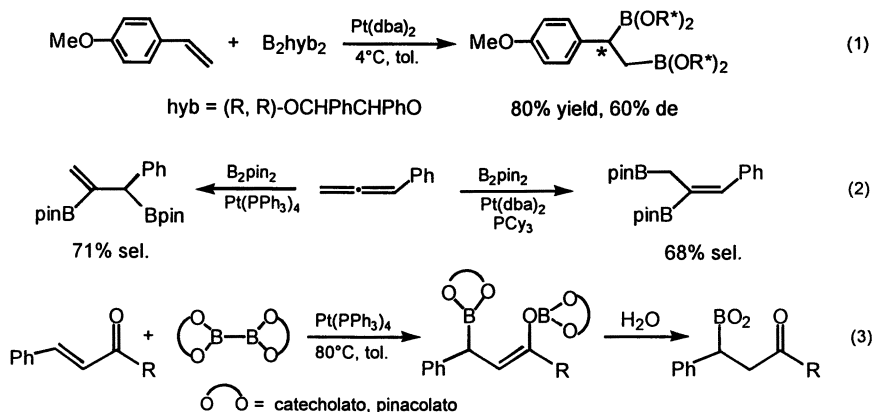
Introduction

Divalent diboron reagents such as B_2Cl_4 were prepared over 75 years ago (1) and B_2X_4 compounds ($X = F, Cl, Br$) were subsequently shown to add to alkenes and alkynes (2-4). Due to their difficult synthesis and handling and tendency to disproportionate, it was only with the advent of amino- and diol-derived diboron reagents (5-8) such as $B_2(NMe_2)_4$, B_2cat_2 (1a) and B_2pin_2 (1b) that more detailed development and catalysis of these addition reactions became possible (cat = catecholato, 1,2- $O_2C_6H_4$ and pin = pinacolato, $OCMe_2CMe_2O$). In particular, the isolation of a trivalent bis(boryl)rhodium complex (9) and subsequent observation of its reductive elimination of B_2cat_2 (10) initiated a number of studies of the 'dihydrogen-like' reactivity of these B_2 reagents including oxidative addition to metals (11-13), insertion of unsaturated organics into M-B bonds (10) and subsequent diboration and borylation of a variety of unsaturated hydrocarbons (14-20).

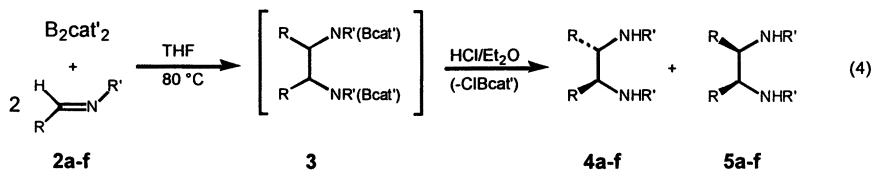
The versatility of the diboration reaction is demonstrated in equations 1-3 in which diastereoselective additions can be effected with diboron reagents derived from chiral diols (21), diene diboration products can be controlled by changing phosphine ligands on the metal catalyst (22), and 1,4-addition to α,β -enones affords β -borylketones (23). More recently, diboration reactions have been extended to other heteroatom-containing alkenes such as enamines (24) and alkenylsulfides (25), and even to $C=X$ multiple bonds ($X = N, S, O$) (24-27). While much remains to be done in catalyst development (28) for these potentially valuable addition reactions (particularly for asymmetric variants), considerable progress has been made in the preparation and characterization of the diboron reagents. Divergent synthesis from $B_2(NMe_2)_4$ allows for facile synthesis of many derivatives from diols, dithiols and potentially diamines and aminoalcohols, although the latter have not yet been applied widely to addition reactions (29). Norman, Marder, and co-workers prepared a number of these derivatives and studied their molecular and electronic structures as well as their propensity to coordinate one or two Lewis bases (30-32). In this report we describe two new reactions of these reagents that take advantage of their bifunctional Lewis acidity.

Diboron Reagents as Two-electron Reductants: Stereoselective Aldimine Coupling

In the course of investigating the Pt-catalyzed addition of diol-derived diboron compounds to aldimines (26), we found that a different reaction occurred in the absence of the catalyst and under more forcing conditions; namely the reductive coupling of aldimines to C_2 -symmetric, *rac*-*N*-boryldiamines (Equation 4). A number of examples of aldimine reductive coupling to diamines have been reported previously using both main group and



transition metal compounds (33-41), but this approach suffers from poor diastereoselectivity, competitive reduction of the imine to the amine, and no reaction with electron-poor or bulky imines. In spite of these limitations, a few recent reports show the potential of this approach. Shimizu and co-workers reported an enantioselective method for the preparation of chiral diamines (60% yield, 88% ee) by reductive coupling of benzaldimines using a Zn-Cu couple in the presence of (+)-camphorsulfonic acid (42). It has been demonstrated recently that only *meso*-diamines are observed during the samarium diiodide-mediated coupling of enantiopure tricarbonyl(benzaldimine) chromium complexes. More recent studies with uncoordinated aldimines show similarly high *meso*-diastereoselectivity of diamines using either $\text{Cp}_2\text{VCl}_2/\text{PhMe}_2\text{SiCl}/\text{Zn}$ or $\text{Cp}_2\text{VCl}_2/\text{PhMe}_2\text{SiCl}/\text{imidazole}/\text{Al}$ as the catalytic system (36,37). Recently, it was reported that C_2 -symmetric vicinal diamines were prepared in high yields by alkylation of chiral α -diimines (43-45).



Heating a THF solution of bis(4-*tert*-butylcatecholato)-diboron ($\text{B}_2\text{cat}'_2$, $\text{cat}' = 4\text{-tert-butylcatecholato}$) **1c** and two equivalents of aldimine **2** for several days afforded the vicinal *N*-boryldiamines as pale yellow foamy solids. Protonolysis of the resulting product afforded the corresponding C_2 -symmetric vicinal diamines **4a-f**. We subjected a variety of aldimines to our reductive coupling protocol with some variation of the diboron reagent and reaction

solvent. As shown in Table I, the reaction is fairly sluggish, even with B_2cat_2 in THF. Aldimine reduction is not observed and only *rac-N*-boryldiamines are observed from diarylaldimines. Aldimines with bulky or electron-withdrawing substituents, however, are still poor substrates for this reductive coupling. The important electronic factors for the diboron reagent are the Lewis acidity and the oxidation potential of the B-B bond. The diboron reagent derived from thiocatechol, for example, is a stronger Lewis acid than B_2cat_2 , but it is also more difficult to oxidize and as a result, aldimine coupling is not observed with this compound.

The imine coupling reaction is presumed to occur by initial coordination of two aldimine molecules to the diboron compound (30, 31) followed by a pseudo-[3,3]-sigmatropic rearrangement (Figure 1). The two-center-two-electron (2c/2e) boron-boron bond of **1** acts as a 2-electron reductant in this reaction in which each boron atom is oxidized to the +3 oxidation state. Conformational analysis of the putative 2:1 adduct provides a simple rationale to explain the effect of bulky and electron-poor substituents on the rate and stereoselectivity of the reaction. A pseudo-chair transition state is favored on steric grounds (Figure 1, TS_A) over the corresponding pseudo-boat conformer (Figure 1, TS_B) during product formation. The former will lead to the *rac* diastereomer while the latter leads to the *meso* isomer. This transition state geometry that favors product formation also accounts for the low tolerance for bulky groups on both the imines and diboron compounds since these groups will be placed in the axial orientation (Figure 1A). Electron-withdrawing groups on the imines are expected to destabilize the transition state structure, which presumably has a partial positive charge on the imine carbon. This will result in decreased or no reactivity for electron-poor imines towards coupling.

Subtle steric effects appear to significantly affect the stereochemical outcome of this coupling reaction. This is illustrated by the significantly higher regioselectivity observed in reactions with *N*-aryl imines compared with the *N*-alkyl analogues. Apparently, the *N*-aryl group on the imine disfavors TS_B to a greater extent than the smaller *N*-alkyl groups to afford excellent selectivity (99:1) for the *rac* isomer. With the *N*-alkyl imines, TS_B can be accessed and hence lower selectivities are observed with these imines. It is thus not surprising that no chiral induction was observed in coupling reactions of imines using chiral diboron compounds. The chiral moiety on boron is farther from the reaction center than the substituents on the imine nitrogen and hence is not expected to induce chirality in the products.

Table I. B₂cat'₂-Mediated Coupling of Aldimines in THF

Entry	Imine	R	R'	Time (days)	Yield (%) ^a	de ^b (4:5)
1	2a	Ph	Me	6 h	75	78:22 <i>c</i>
2	2b	Ph	CH ₂ Ph	2	33	45:55 <i>d</i>
3	2c	Ph	ⁱ Bu	2	30	67:33 <i>d</i>
4	2d	Ph	Ph	7	20	>99:1 ^e
5	2e	Ph	4-MeO-Ph	7	10	>99:1 ^e
6	2f	4-MeO-Ph	Ph	7	44	>99:1 ^e
7	2g	Ph	2-MeO-Ph	7	0	-
8	2h	Ph	4-CF ₃ -Ph	9	0	-
9	2i	4-CF ₃ -Ph	Ph	9	0	-
10	2j	4-MeO-Ph	4-CF ₃ -Ph	7	0	-

^a Isolated yield. ^b Determined by ¹H NMR. ^c Lower de's (70:30) are obtained in Bu₂O, ClCH₂CH₂Cl and toluene. ^d Similar de's are obtained in the other solvents. ^e Identical de's are also obtained in Bu₂O, ClCH₂CH₂Cl and toluene.

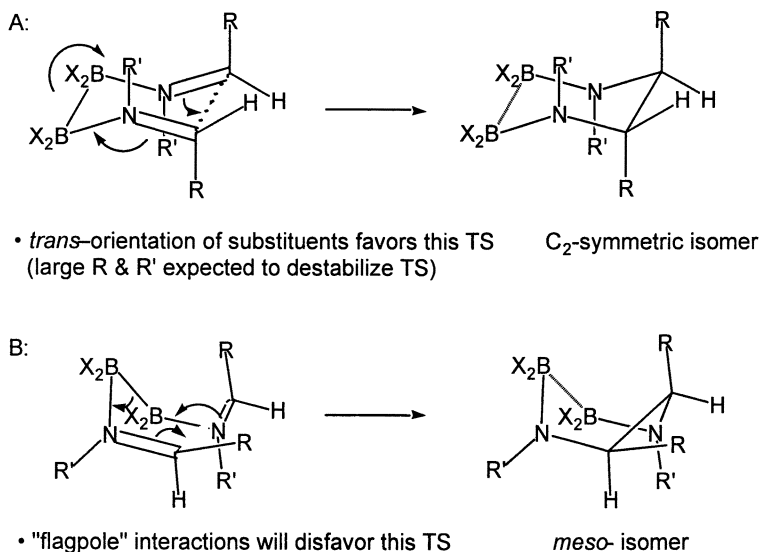
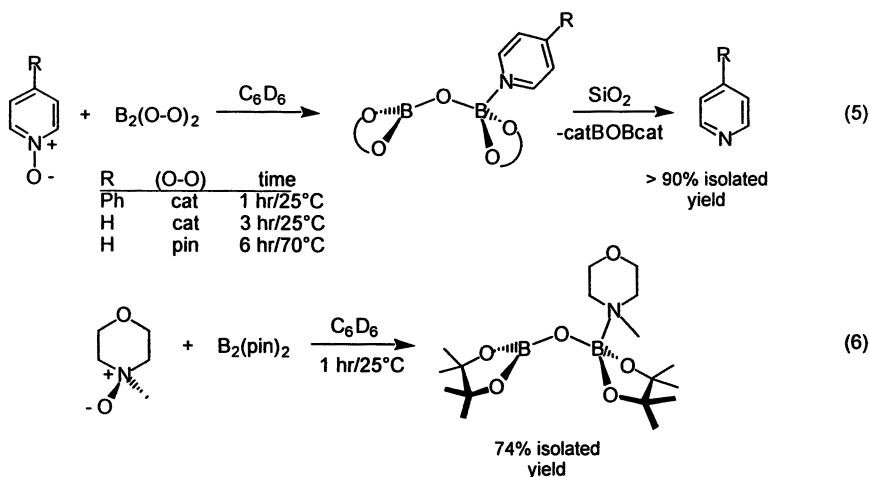


Figure 1. Transition state model for stereoselective imine coupling

Deoxygenation of Main Group Element Oxides

Deoxygenation of organic carbonyl compounds by boron reagents takes advantage of the large thermodynamic driving force for B-O bond formation. Trialkylboranes, for example, reduce triphenylphosphine oxide to the phosphine at 150°C (46). For the diol-derived diboron reagents, formation of two B-O bonds provides an enormous enthalpic driving force ($\Delta H \sim 180$ kcal/mol) and their lack of reactivity with most functional groups offers prospects for selective deoxygenations. This concept is well illustrated by the facile reactions with amine *N*-oxides. As shown in Equation 5, pyridine *N*-oxide is deoxygenated at 25°C by B₂cat₂ over several hours to give the monopyridine adduct of catBOBcat. The pinacol-derived diboron compound requires heating at 65°C for several hours to deoxygenate pyridine *N*-oxide, while reaction with morpholine *N*-oxide (Eq. 6) proceeds at 25°C. The convenient synthesis of a wide variety of diol-derived diboron reagents thus offers the possibility of selective deprotection of polyamine *N*-oxide compounds under conditions that tolerate many functional groups.



The deoxygenation reaction pathway likely takes advantage of the Lewis acidity of the diboron compound to interact with the oxygen of the amine *N*-oxide. The increased acidity of the BOB product (*vide supra*) then provides an efficient intramolecular trap for the amine product (Figure 2).

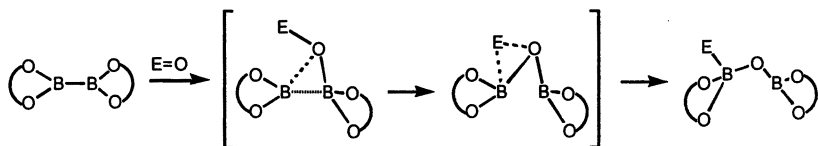
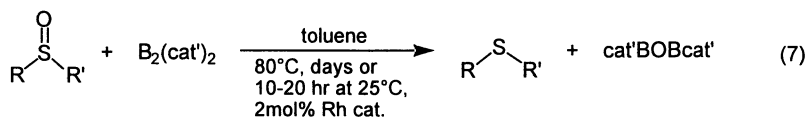


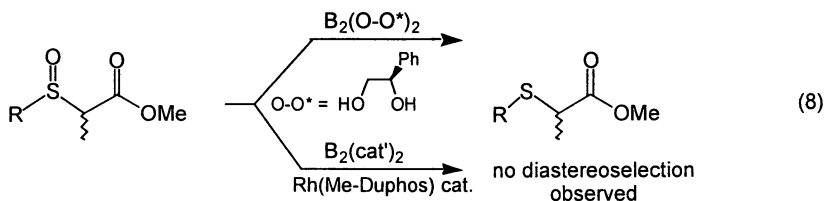
Figure 2. Proposed deoxygenation reaction pathway

Aryl- and alkylsulfoxides are slowly deoxygenated by B_2cat_2 at 80°C, but the reaction is effectively catalyzed at 25°C by Rh complexes such as Wilkinson's catalyst, $RhCl(PPh_3)_3$ (Eq. 7). While bis(phosphine) Rh catalysts are also effective, we were unable to obtain any diastereoselection in the deoxygenation of the two diastereomers of sulfoxide **6** by employing either a chiral bis(phosphine) ligand on Rh or a chiral diol auxiliary on the diboron reagent (Eq. 8). The sulfoxide deoxygenation rate increases for electron-rich sulfoxides, consistent with the diboron reagent's role as an electrophilic reductant (47). Transition metal carbonyl complex-catalyzed deoxygenation of main group element oxides using carbon monoxide likely follows a similar mechanism, but is only effective for weaker E-O bonds such as N and Se (47). In contrast, rhenium-catalyzed sulfoxide reductions are faster with electron poor sulfoxides, consistent with the proposed metal oxo-mediated mechanism (48).



R = Ph; R' = Me, CH₂CO₂Me, CH=CH₂

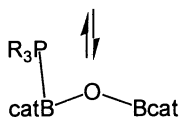
R = R' = Me, *p*-tolyl, benzyl



Although no reaction is observed between B₂cat₂ and tertiary phosphine oxides such as O=PPh₃ and O=PCy₃, addition of 2 mol% Wilkinson's catalyst gives the corresponding phosphines over several hours at 25°C (Eq. 9). With Wilkinson's catalyst, only bulky phosphine oxides give high conversions, as smaller phosphines rapidly form Rh complexes that no longer catalyze the deoxygenation reaction.



relative rates: R = Cy > *p*-tol > Ph



The proposed reaction pathway for these rhodium-catalyzed deoxygenations involves initial oxidative addition of the diboron reagent, followed by interaction of the oxygen atom with the boron atom of the metal boryl linkage (Figure 3). Formation of such 'base-stabilized' metal boryls are rare, however (49), and we can not yet rule out element oxide coordination to the Rh center through oxygen or even through sulfur in the case of the sulfoxides.

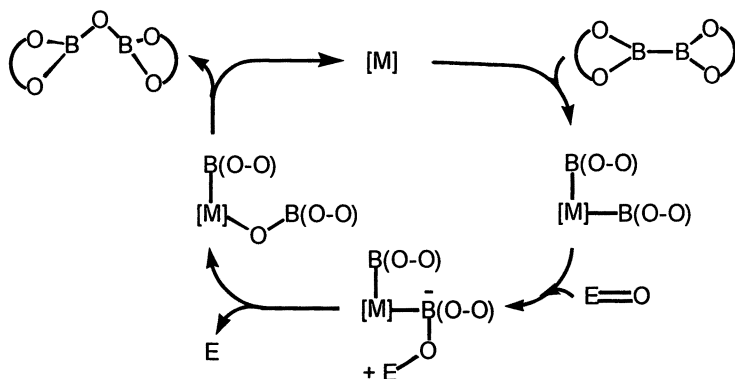
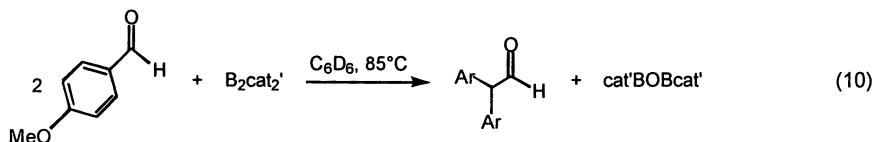


Figure 3. Proposed metal-catalyzed deoxygenation reaction pathway

With the enormous driving force for conversion of the diboron reagents to their BOB analogs, we turned to organic carbonyl compounds. We were surprised initially to find that treatment of benzaldehyde with B_2cat_2 at $85^\circ C$ over several hours leads to high yields of diphenylacetaldehyde at about 50% conversion (Equation 10). In light of the imine coupling chemistry, however,



one can easily account for this product by a reductive coupling to form a cyclic intermediate, followed by a pinacolone-type rearrangement and elimination of $cat'BOBcat'$ (Figure 4). In the presence of 2 mol% of Wilkinson's catalyst at $25^\circ C$, however, the reaction takes a different course, with predominant formation of *cis*- and *trans*-stilbene (Equation 11). While an analogous deoxygenation pathway to that in Figure 3 would generate a Rh carbene intermediate that could subsequently couple to form the alkene, attempted trapping experiments have been inconclusive and further work is required to substantiate such a pathway.

Attempts to extend this deoxygenation reaction to a host of aldehyde and ketone substrates met with limited success. In substrates with enolizable

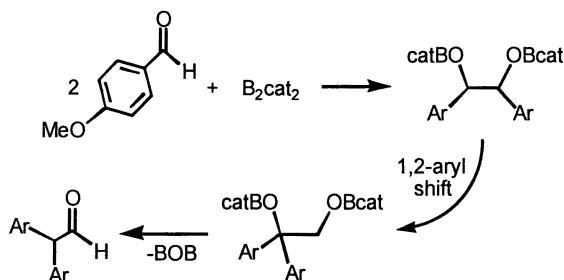
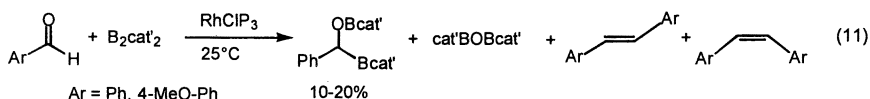
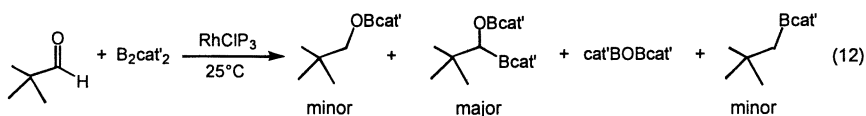


Figure 4. Proposed reaction pathway for diphenylacetaldehyde formation



hydrogens, competing diboration and hydroboration reactions gave rise to a mixture of products, including aldol products generated from boron enolate intermediates (50). Even a seemingly innocent substrate such as pivaldehyde showed that several competing reaction pathways are operating (Equation 12) and additional studies are needed to fully elucidate them.



Lewis Acidity of Divalent B₂ and Trivalent BOB Compounds

Returning now to the relative Lewis acidities of the divalent diol-derived diboron reagents and their trivalent BOB counterparts, previous solution and MAS NMR studies estimated the inter- and intramolecular relative rates of 4-picoline binding to B₂cat₂; structures of mono- and bis(adducts) were structurally characterized. In contrast, no adduct formation of PMe₃ with B₂cat₂ or of 4-picoline with B₂pin₂ could be observed (30). In our investigations, trivalent pinBOBpin forms strong adducts with pyridine and slow binding of

PMe_2Ph to catBOBcat affords an adduct which undergoes rapid intramolecular phosphine exchange on the NMR time scale (Figure 5). Thus, the BOB compounds are clearly more potent Lewis acids than their B_2 counterparts. In order to better understand these acidity differences, we investigated their electronic structures using Density Functional Theory (DFT) (51).

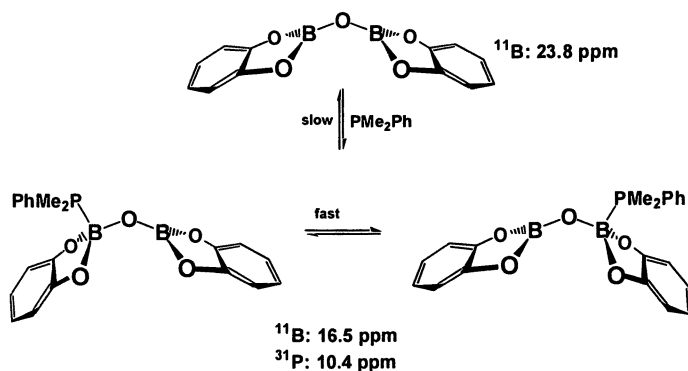
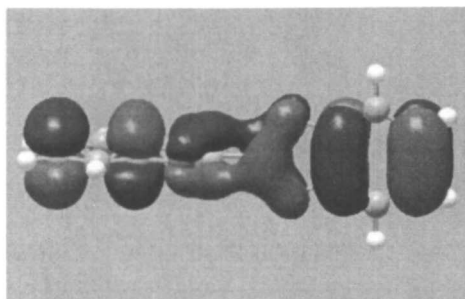


Figure 5. Phosphine adduct formation with B_2cat_2

Our initial calculations on B_2cat_2 showed reasonable agreement with metrical details from the solid-state structure (52). The global minimum has a staggered geometry as found previously for $\text{B}_2(\text{OH})_2$; the planar structure was only 0.6 kcal less stable for the latter (53). The HOMO and HOMO-1 for B_2cat_2 are a degenerate pair of orbitals that contain the B-O π -bonds to the catecholate oxygens, while the orbital that contains the $2c/2e^-$ B-B bond lies 2.72 eV below the HOMO (Figure 6). For catBOBcat , on the other hand, the HOMO is mostly B-O π -bonding to the catecholate rings with the B-O-B π -bonding orbitals lying well below the HOMO in energy (Figure 7). We then optimized the structures of the monopyridine adducts for B_2cat_2 , B_2pin_2 , and their BOB counterparts (Figure 8); B-N distances and pyridine binding energies are presented in Table II. The best Lewis acid is clearly catBOBcat with the pinacolate analog binding pyridine about 8.5 kcal/mol less strongly. An examination of the metrical details of the pyridine adduct clearly shows the significant lengthening of the B-O bonds to both the bridge and catecholate oxygens as the π -bonding is effectively reduced (or eliminated) at the sp^3 -hybridized boron center. Similar effects were observed in the structure of the 4-picoline adduct of B_2cat_2 (30) and it is likely that the increased acidity of the BOB compounds stems from electronegativity factors, i.e. three polar B-O bonds in the BOB base adduct vs. two in the B_2 adduct.

B_2cat_2 HOMO



2.72 eV below HOMO

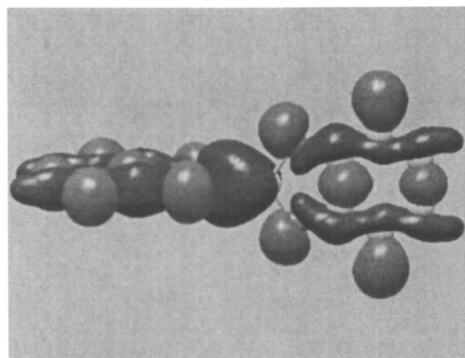
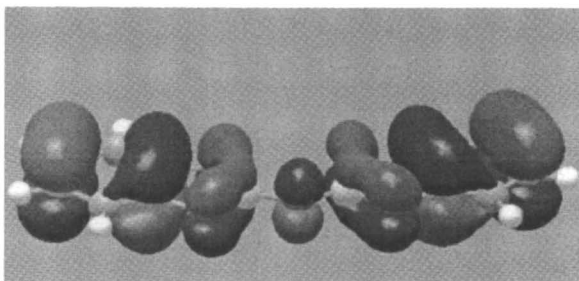
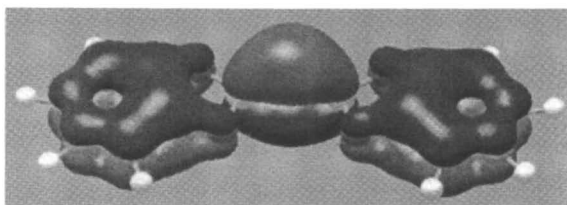


Figure 6. HOMO and B-B bonding MOs of B_2cat_2

CatBOBcat HOMO



4.64 eV below HOMO



6.67 eV below HOMO

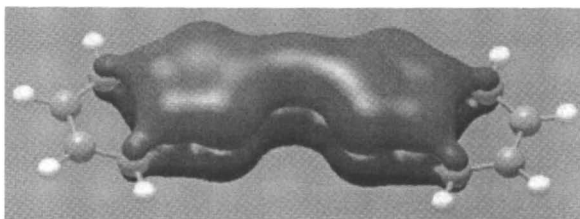
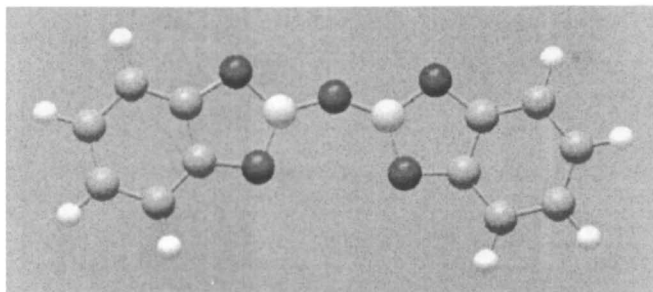


Figure 7. HOMO and B-O-B π -bonding MOs of catBOBcat

CatBOBcat

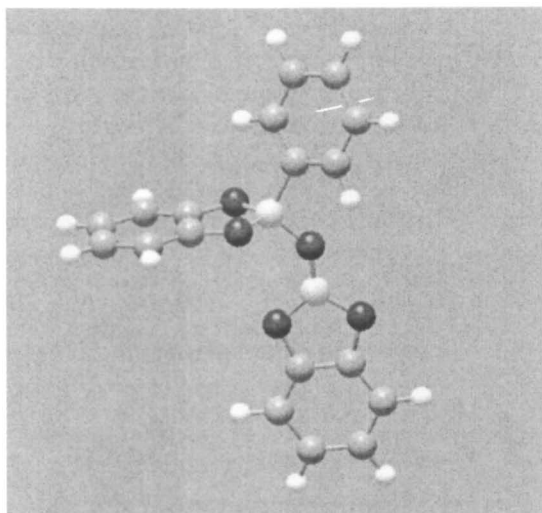


$$\text{B-O}_{\text{term}} = 1.414 \text{ \AA} \text{ [cf. } 1.390(3) \text{ \AA} \text{ from X-ray (54)]}$$

$$\text{B-O}_{\text{bridge}} = 1.354 [1.356(3)] \text{ \AA}$$

$$\text{B-O-B} = 145.2 [135.9(2)]^\circ$$

Pyridine Adduct



$$\text{B-O}_{\text{term}} = 1.426, 1.490 \text{ \AA}$$

$$\text{B-O}_{\text{bridge}} = 1.340, 1.446 \text{ \AA}$$

$$\text{B-O-B} = 134.7^\circ$$

Figure 8. Optimized structures of catBOBcat and its pyridine adduct

Table II. Computational Results for Pyridine Adducts

<i>Compound</i>	<i>B-N (Å)</i>	<i>E_b</i> <i>(kcal/mol)</i>
catBOBcat(pyr)	1.628Å	22.4
pinBOBpin(pyr)	1.668Å	13.8
B ₂ cat ₂ (pyr)	1.669Å	16.4
B ₂ pin ₂ (pyr)	1.681Å	10.6

Conclusions and Future Prospects

The diol-derived diboron reagents described herein appear to be excellent examples of electrophilic reductants and useful sources of even more potent and versatile metal boryl complexes. The metal boryl moiety has recently been employed for the selective functionalization of arenes and even linear alkanes (55-61). While the general utility of diboron reagents for the stereoselective reductive coupling and cross-coupling of imines and carbonyl compounds has not yet been demonstrated, the ease of preparation of a wide variety of diol-, diamine-, and aminoalcohol-derived reagents may allow for the development of improved reaction rates and selectivities. Although the deoxygenation of main group element oxides is stoichiometric in boron, their prospects for selective deprotection may have applications in natural product synthesis and materials chemistry. In addition, the stability of the BOB compounds may warrant further investigation of these compounds as Lewis acid catalysts for organic transformations.

Acknowledgements

RTB thanks the US Department of Energy's Laboratory-Directed Research and Development program for research support and partial support for RDB's sabbatical leave and SAW thanks the Natural Science and Engineering Research Council of Canada.

References

1. Stock, A.; Brandt, A.; Fischer, H. *Chem. Ber.* **1925**, *58*, 641.
2. Ceron, P.; Finch, A.; Frey, J.; Kerrigan, J.; Parsons, T.; Urry, G.; Schlesinger, H. I. *J. Am. Chem. Soc.* **1959**, *81*, 6368.
3. Morrison, J. A. *Chem. Rev.* **1991**, *91*, 35.
4. Ahmed, L.; Castillo, J.; Saulys, D. A.; Morrison, J. A. *Inorg. Chem.* **1992**, *31*, 706.
5. McCloskey, A.L.; Brotherton, R. J.; Boone, J. L.; Manasevit, H. M. *J. Am. Chem. Soc.* **1960**, *82*, 6245.
6. Welch, C. N.; Shore, S. G. *Inorg. Chem.* **1968**, *7*, 451.
7. Massey, A. G.; *Adv. Inorg. Chem. Radiochem.* **1967**, *10*, 1.
8. Noth, H.; *Z. Naturforsch.* **1984**, *39b*, 1463.
9. Burgess, K.; van der Donk, W. A.; Westcott, S. A.; Marder, T. B.; Baker, R. T.; Calabrese, J. C. *J. Am. Chem. Soc.* **1992**, *114*, 9350.
10. Baker, R. T.; Calabrese, J. C.; Westcott, S. A.; Nguyen, P.; Marder, T. B. *J. Am. Chem. Soc.* **1993**, *115*, 4367.
11. Nguyen, P.; Lesley, G.; Taylor, N. J.; Marder, T. B.; Pickett, N. L.; Clegg, W.; Elsegood, M. R. J.; Norman, N. C. *Inorg. Chem.* **1995**, *34*, 1336.
12. Irvine, G. J.; Lesley, M. J. G.; Marder, T. B.; Norman, N. C.; Rice, C. R.; Robins, E. G.; Roper, W. R.; Whitell, G. R.; Wright, L. J. *Chem. Rev.* **1998**, *98*, 2685.
13. Smith, M. R. III *Prog. Inorg. Chem.* **2000**, *48*, 505.
14. Marder, T. B.; Norman, N. C. *Top. Catal.* **1998**, *5*, 63.
15. Ishiyama, T.; Miyaura, N. *J. Organomet. Chem.* **2000**, *611*, 392.
16. Anderson, K. M.; Lesley, M. J. G.; Norman, N. C.; Orpen, A. G.; Starbuck, J. *New J. Chem.* **1999**, *23*, 1053.
17. Ito, H.; Yamanaka, H.; Tateiwa, J.-I.; Hosomi, A. *Tetrahedron Lett.* **2000**, *41*, 6821.
18. Thomas, R. L.; Souza, F. E. S.; Marder, T. B. *J. Chem. Soc., Dalton Trans.* **2001**, 1650.
19. Yang, F.-Y.; Cheng, C.-H. *J. Am. Chem. Soc.* **2001**, *115*, 761.
20. Takahashi, K.; Ishiyama, T.; Miyaura, N. *J. Organomet. Chem.* **2001**, *625*, 47.
21. Marder, T. B.; Norman, N. C.; Rice, C. R. *Tetrahedron Lett.* **1998**, *39*, 155.
22. Ishiyama, T.; Kitano, T.; Miyaura, N. *Tetrahedron Lett.* **1998**, *39*, 2357.
23. Lawson, Y. G.; Lesley, M. J. G.; Marder, T. B.; Norman, N. C.; Rice, C. R. *Chem. Commun.* **1997**, 2051.

24. Cameron, T. M.; R. T. Baker, R. T.; Westcott, S. A. *Chem. Commun.* **1998**, 2395.
25. Carter, C. A. G.; Vogels, C. M.; Harrison, D. J.; Gagnon, M. K. J.; Norman, D. W.; Langler, R. F.; Baker, R. T.; Westcott, S. A. *Organometallics*, **2001**,
26. Mann, G.; John, K. D.; Baker, R. T. *Org. Lett.* **2000**,
27. Broene, R. D.; Baker, R. T., manuscript in preparation.
28. Dai, C.; Robins, E. G.; Scott, A. J.; Clegg, W.; Yufit, D. S.; Howard, J. A. K.; Marder, T. B. *Chem. Commun.* **1998**, 1983.
29. Marcuccio, S. M.; Rodopoulos, M.; Weigold, H. European patents WO9912940, WO9933845, 1999.
30. Nguyen, P.; Dai, C.; Taylor, N. J.; Power, W. P.; Marder, T. B.; Pickett, N. L.; Norman, N. C. *Inorg. Chem.* **1995**, *34*, 4290.
31. Dai, C.; Johnson, S. M.; Lawlor, F. J.; Lightfoot, P.; Marder, T. B.; Norman, N. C.; Orpen, A. G.; Pickett, N. L.; Quayle, M. J.; Rice, C. R. *Polyhedron* **1998**, *17*, 4139.
32. Lawlor, F. J.; Norman, N. C.; Pickett, N. L.; Robins, E. G.; Nguyen, P.; Lesley, G.; Marder, T. B.; Ashmore, J. A.; Green, J. C. *Inorg. Chem.* **1998**, *37*, 5282.
33. Lucet, D.; Le Gall, T.; Mioskowski, C. *Angew. Chem. Int. Ed. Engl.* **1998**, *37*, 2580.
34. Periasamy, M.; Srinivas, G.; Karunakar, G. V.; Bharathi, P. *Tetrahedron Lett.* **1999**, *40*, 7577-7580.
35. Taniguchi, N.; Uemura, M. *Synlett* **1997**, 51.
36. Hatano, B.; Ogawa, A.; Hirao, T. *J. Org. Chem.* **1998**, *63*, 9421.
37. Hirao, T.; Hatano, B.; Imamoto, Y.; Ogawa, A. *J. Org. Chem.* **1999**, *64*, 7665.
38. Rieke, R. D.; Kim, S.-H. *J. Org. Chem.* **1998**, *63*, 5235.
39. Yanada, R.; Negoro, N.; Okaniwa, M.; Miwa, Y.; Taga, T.; Yanada, K.; Fujita, T. *Synlett* **1999**, 537-540.
40. Machrouhi, F.; Namy, J. L. *Tetrahedron Lett.* **1999**, *40*, 1315-1318.
41. Collin, J.; Giuseppone, N.; Machrouhi, F.; Namy, J. L.; Nief, F. *Tetrahedron Lett.* **1999**, *40*, 3161-3164.
42. Shimizu, M.; Iida, T.; Fujisawa, T. *Chem. Lett.* **1995**, 609.
43. Neumann, W. L.; Rogic, M. M.; Dunn, T. J. *Tetrahedron Lett.* **1991**, *32*, 5865.
44. Bambridge, K.; Begley, M. J.; Simpkins, N. S. *Tetrahedron Lett.* **1994**, *35*, 3391.
45. Alvaro, G.; Grepioni, F.; Savoia, D. *J. Org. Chem.* **1997**, *62*, 4180.
46. Koster, R.; Morita, Y. *Angew. Chem.* **1965**, *77*, 589.
47. Kelly, A. M.; Rosini, G. P.; Goldman, A. S. *J. Am. Chem. Soc.* **1997**, *119*, 6115.

48. Arterburn, J. B.; Perry, M. C. *Tetrahedron Lett.* **1996**, *44*, 7941.
49. Braunschweig, H. *Angew. Chem., Int. Ed. Engl.* **1998**, *37*, 1786.
50. Duffy, J. L.; Yoon, T. P.; Evans, D. A. *Tetrahedron Lett.* **1995**, *36*, 9245.
51. Calculations employed the B3LYP hybrid DFT approximation with double zeta basis sets (6-31G).
52. B-B = 1.670Å [vs. 1.679(3)Å from X-ray] and B-O = 1.415Å [1.388(2)Å]: Clegg, W. Elsegood, M. R. J.; Lawlor, F. J.; Norman, N. C.; Pickett, N. L.; Robins, E. G.; Scott, A. J.; Nguyen, P.; Taylor, N. J.; Marder, T. B. *Inorg. Chem.* **1998**, *37*, 5289.
53. Cui, Q.; Musaev, D. G.; Morokuma, K.; *Organometallics* **1997**, *16*, 1355.
54. Noth, H. Z. *Anorg. Allgm. Chem.* **1997**, *623*, 901.
55. Waltz, K. M.; Hartwig, J. F. *Science* **1997**, *277*, 211.
56. Chen, H.; Hartwig, J. F. *Angew. Chem., Int. Ed. Engl.* **1998**, *38*, 3391.
57. Chen, H.; Schlecht, S.; Semple, T. C.; Hartwig, J. F. *Science* **2000**, *287*, 1995.
58. Iverson, C. N.; Smith, M. R., III *J. Am. Chem. Soc.* **1999**, *121*, 7696.
59. Cho, J.-Y.; Iverson, C. N.; Smith, M. R., III *J. Am. Chem. Soc.* **2000**, *122*, 12868.
60. Tse, M. K.; Cho, J.-Y.; Smith, M. R., III *Organic Lett.* **2001**, *3*, 2831.
61. Shinada, S.; Batsanov, A. S.; Howard, J. A. K.; Marder, T. B. *Angew. Chem. Int. Ed. Engl.* **2001**, *407*, 2168.

Chapter 6

Electronic and Steric Design of Novel Group 13 Lewis Acids and Their Synthesis via Metal–Tin Exchange Reactions (1): Toward the Ideal Olefin Polymerization Catalyst

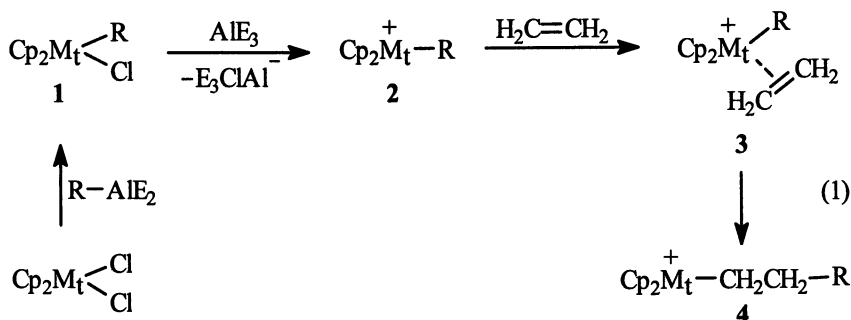
John J. Eisch, Peter O. Otieno, Katrin Mackenzie,
and Boguslaw W. Kotowicz

Department of Chemistry, The State University of New York at Binghamton,
Binghamton, NY 13902–6016

Group 13 Lewis acids have long played a leading role as catalysts in organic synthesis, extending from the discovery of AlCl_3 -catalysis by Friedel and Crafts in 1877 through the *Aufbau*-synthesis of unsolvated aluminum alkyls from ethylene by Ziegler in 1952 and culminating in the discovery of poly(methylaluminoxane) (MAO) cocatalysis of olefin polymerization by Sinn and Kaminsky in 1976. In our current work we present how electronic and steric contributions of the ligands attached to the particular Group 13 metal can modulate the resultant Lewis acidity. The inherent Lewis acidity of the Group 13 metal center itself is further dependent upon the extent that its available np_z -orbital might interact with adjacent

unshared or *pi*-electrons of the ligand system. In order to evaluate the effect of such electronic factors on their Lewis acidity, both a series of bidentate Group 13 organoboron and organoaluminum candidate acids, as well as their antiaromatic metallole analogs, have been synthesized by exchange reactions between the corresponding organotin compound and the appropriate metal halide. Their Lewis acidity has been evaluated based upon their efficacy as a cocatalyst with titanocene(IV) methyl chloride or titanocene(IV) dichloride in effecting the polymerization of ethylene.

The extraordinary importance of aluminum(III) chloride as a catalyst for the alkylation or acylation of aromatic derivatives, first published by Friedel and Crafts in 1877 (2), antedated by almost 50 years the proposal by Lewis of the electronic basis for such catalysis (3). Just 50 years ago Ziegler and coworkers discovered that combinations of zirconium(IV) or titanium(IV) salts and aluminum alkyls could effect the astonishing polymerization of ethylene at room temperature and atmospheric pressure (4). Although the cocatalytic action of the aluminum component was initially attributed solely to its generating the requisite carbon-transition metal bond, C-M_t, in 1 (5), subsequent research with soluble metallocene procatalysts uncovered yet another function for such aluminum alkyls or their by-products; namely that of Lewis acids that turn the alkyl derivative (1) into a more electrophilic cation (2) capable of rapid carbometallation of coordinated ethylene (3 → 4) (eq. 1) (6, 7). With this insight

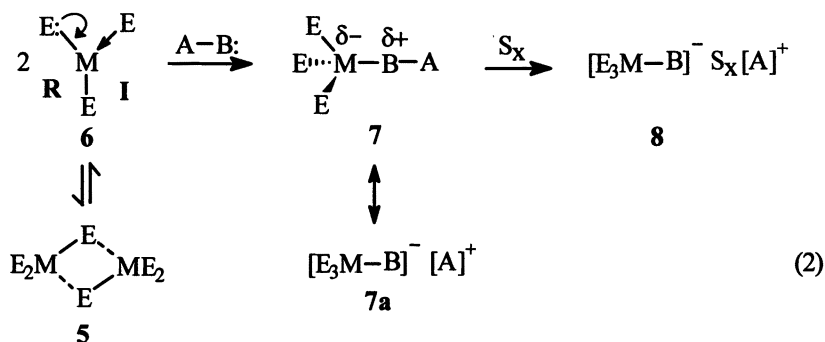


came the realization that the Lewis acidity of the main group Ziegler cocatalyst is an essential feature in olefin polymerization. The dual prerequisite of alkylating ability and Lewis acidity were found also to be valid for the heterogeneous stereoregular polymerization of alpha-olefins initially discovered by Natta and coworkers in 1953 (8). As applied to the homogeneous polymerization of olefins

by metallocenes, both roles have been shown by Sinn and Kaminsky to be fulfilled preeminently by poly(methylaluminumoxane) (9, 10, 11). The present study was undertaken, in order to learn if highly effective cocatalysts could be rationally designed for transition metal procatalysts of olefin polymerizations, heterogeneous or homogeneous, that we here term inclusively Ziegler-Natta processes (12).

Lewis Acidity of Group 13 Derivatives

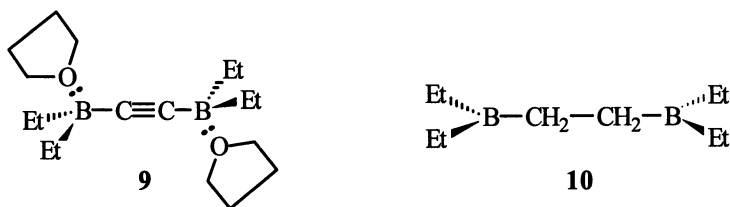
Because of the available np -orbital on the metal atom of the tricoordinate, coplanar derivatives of Group 13 metal, ME_3 (6), all such derivatives are capable of accepting an unshared electron pair from a Lewis base, $A-B:$ with the formation of the tetrahedral complex 7 (eq. 2) (13 (explanatory footnote), 14). If



electronegativity effects on nuclear charge of M alone were operative, Lewis acidity of 6 would decrease in the series, $B > Al > Ga > In > Tl$. However, because of the small covalent radius of boron (81 pm) versus that of aluminum and gallium (125 pm), steric factors weaken the acidity of boron derivatives. The Lewis acidity can also be decreased by several factors that make the np -orbital on M less available: 1) autodimerization of 6 to 5; 2) π -bonding with unshared electron pairs on E: $\ddot{E}-M \leftrightarrow E=M$ (resonance effect, R), 3) σ -bond donation by E: $E \rightarrow M$, in order of $E = NR_2 > OR > X$ (inductive effect, I), 4) F(front)-steric hindrance between groups E and A in 7 and B(back)-steric hindrance among groups E in 7. As an illustration of F-steric hindrance, note that triphenylborane does not form a complex with diethyl ether, while triphenylaluminum does. The lessening of any of the foregoing factors will conversely enhance the Lewis acidity of 6. The interplay of such inductive, resonance and steric factors on Lewis acidity is now well understood and has been lucidly discussed elsewhere (13, 14, 15).

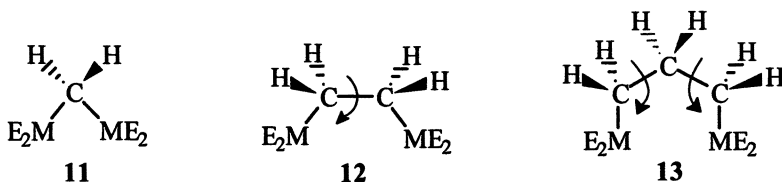
The particular case of the enhanced acidity of fluoro-substituted organoboranes and bifunctional organoboranes has been explored by various research groups, such as those of Marks, Bochmann, Gabbai and Piers, and has also been authoritatively reviewed most recently (16). Despite the superior Lewis acidity of such derivatives in Ziegler-Natta catalysis the present authors deem it necessary to state a grave caveat against their use: the boron and aluminum derivatives are generally thermodynamically highly unstable to explosive decomposition and their main group precursors (R_FLi , R_FMgX) are demonstrably kinetically unstable as well. Safety and prudence should accordingly deter their widespread use and spur efforts to identify safe substitutes. Possibly cyano-substituted triarylboranes would possess enhanced Lewis acidities even more than fluoro- or trifluoromethyl-derivatives, as might be predicted from their Hammett *sigma-para* values: CN, 0.66; CF_3 , 0.54; F, 0.06. The single drawback may be that the cyano group can itself act as a Lewis base towards the strongest Lewis acids (cf. *infra*) (17).

A less obvious factor in enhancing Lewis acidity is the hybridization of the atom in E attached directly to the metal in 6. In rationalizing the C-H Brønsted acidity of protons in the series, $H-C\equiv C-H > H_2C=CH_2 > H_3C-CH_3$, organic chemists invoke the greater effective electronegativity of the sp-hybridized acetylenic carbon (whose nuclear charge is less screened by a smaller proportion of *sigma*-electrons) in explaining anion stability of this gradation: $H-C\equiv C > H_2C=CH > H_3C-CH_2$. Such inductive electron-withdrawal should make 1-alkynylboranes stronger Lewis acids and that is exactly what we have recently observed: compound 9 forms from bis(diethylboryl)acetylene in THF solution at 25°C, as shown by NMR spectroscopy, while compound 10 forms no such mono- or di-complex (18). Similarly, bis(phenylethynyl)phenylborane forms a complex with THF but triphenylborane does not (19).



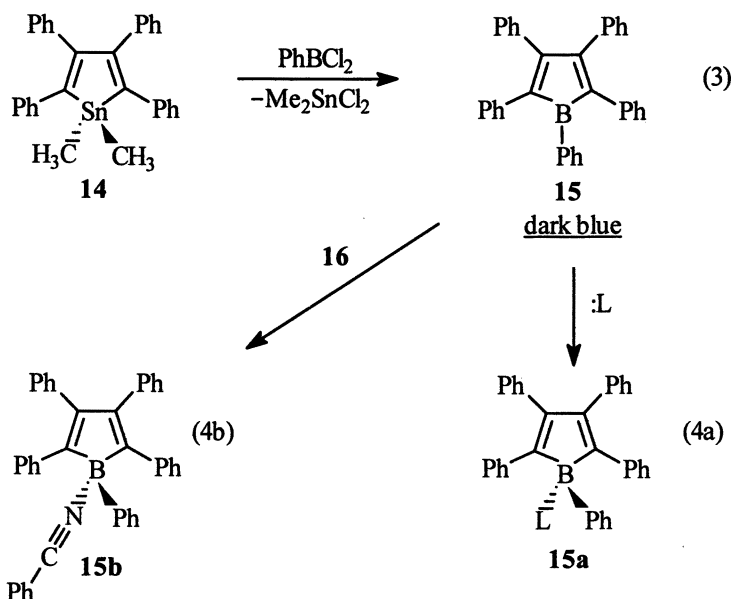
Returning to eq. 2 and structure 7, we can further note that although F-steric hindrance destabilizes the M-B bond and decreases the stability of 7, the same effect weakens the B-A bond and promotes its heterolysis. In this regard, 7 can be viewed in its extreme as the tight ion pair 7a, which when solvent molecules (S_x) intervene becomes the solvent-separated ion pair 8. This complete separation of B^- as the anion $[E_3MB]^-$ from A-B: is an integral part of the Lewis acidity role of Group 13 catalysts in generating ion pairs both in the Friedel-Crafts and the Ziegler-Natta catalytic processes.

In addition to the general electronic and steric roles of substituents in Lewis acidity, two further structural factors, the one, chelation, is general in applicability and the other, antiaromaticity, is specific for certain metallacyclopolyenes. Although chelating and multidentate Lewis bases have been recognized and used to advantage in coordination chemistry by Werner over a century ago (20), interest and research in the corresponding Lewis acids stems from the early 1980s (21, 22). With 1,*n*-dimetalloalkanes (11-13), it is clear that the "bite" or aperture and the conformational mobility can greatly affect the acidity. Thus although 11 has little unfavorable mobility, its "bite" is too large to chelate an anion effectively. On the other hand, 12 and 13 are well-disposed to form stable 5- and 6-membered anionic chelate rings, but their great conformational mobility will weaken their Lewis acidity.



As will be seen (28 and 29), strong Lewis acids can result from 1,2- and 1,3-dimetalloorganics when a rigid carbon backbone for the chelate ring is employed.

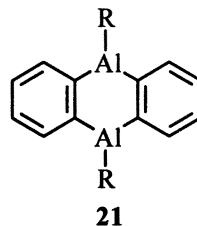
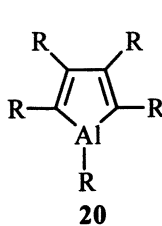
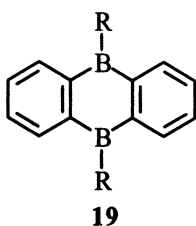
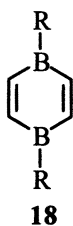
The use of certain metallacyclopolyenes as strong Lewis acids is based upon the Hückel theory of aromaticity (23). In this electronic interpretation a monocyclic array of sp^2 -hybridized carbon or first period elements will form a number of bonding molecular orbitals, which can just be filled by $4n + 2$ π -electrons ($n = 0, 1, 2, 3, \dots$). Such a completely filled array of orbitals confers exceptional stability or aromaticity on the ring. If the ring would have two more or fewer electrons than $4n + 2$, the system would be antiaromatic and thus destabilized, tending to gain or lose two π -electrons or to add a Lewis base (A-B:), so as to remove that p -orbital from destabilizing overlap. Such an antiaromatic nucleus is pentaphenylborole (15), which was synthesized from 14 according to eq. 3 (24). Note from eq. 4a that either a Lewis base, such as pyridine or THF, or two electrons from potassium metal add readily to 15 to relieve the antiaromatic instability of this 4- π -electron ring. Even the extremely weakly basic benzonitrile (16) forms a complex 15b that permits an estimate of the Lewis acidity of borole 15. Pasykiewicz has proposed that the high-frequency shift of the IR $C\equiv N$ stretch of a Lewis acid complex of 16 be approximately proportional to the polar character of the complex, 17a – 17b, and hence the Lewis acidity of A-B (17). In this light, borole 15 is a stronger Lewis acid than aluminum(III) chloride.



<u>Complex of 16</u>	<u>IR</u> (cm ⁻¹)	<u>:L</u>	<u>11B</u> (ppm)	<u>λ_{max}</u> (nm)
-	2300	-	55	567
AlCl ₃	2359	pyridine	5	332
Ph ₅ borole	2370	THF	-	335
		2K(2e ⁻)	26	-



This insight inspired the hope that boroles might serve both as alkylating agent and as strong Lewis acid in Ziegler-Natta olefin polymerizations. On analogous grounds, the antiaromatic 1,4-diborocyclohexadiene (**18**) or its dibenzo derivative (**19**) became attractive candidates for novel Ziegler-Natta cocatalysts. For the event that the boron derivatives **15** and **18** proved to be too weak as alkylating agents of the transition metal salts (formation of **1**, eq. 1) or as too sterically hindered as Lewis acids (**1** → **2**, eq. 1), recourse to the corresponding aluminum antiaromatic rings (**20**, **21**) gave promise of succeeding.

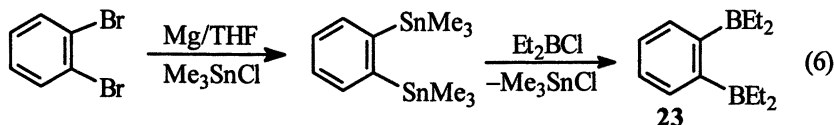
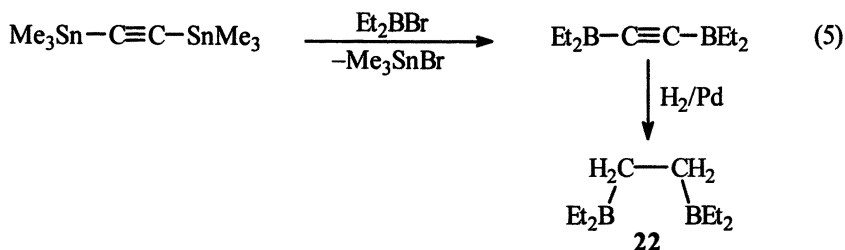


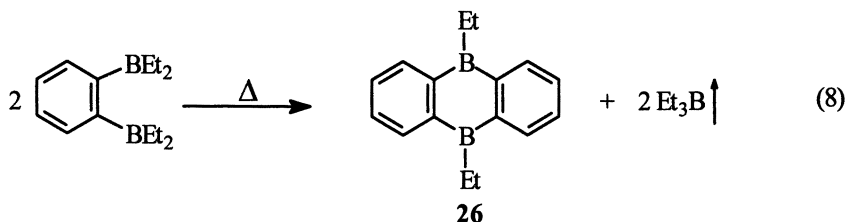
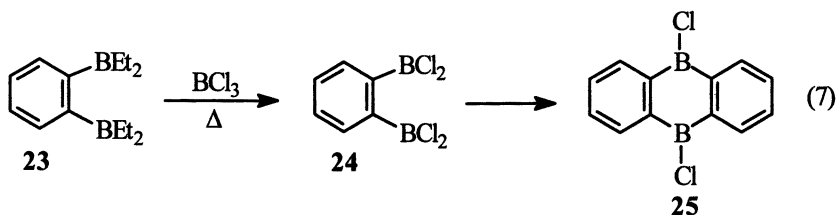
In the following section we report our efforts on the synthesis of both chelating (e.g. 11 – 13) and antiaromatic organoboron and organoaluminum derivatives having great potential of being superior olefin polymerization cocatalysts.

Synthesis of Group 13 Organometallics by Tin-Metal Exchange

Organoboranes

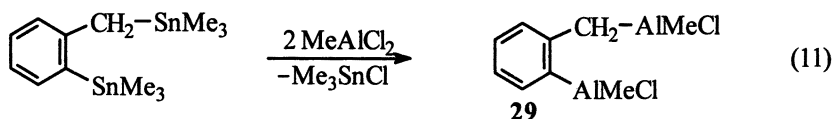
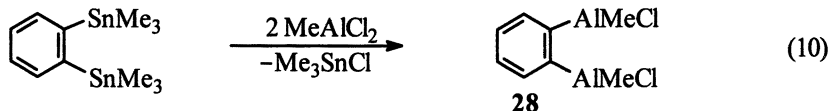
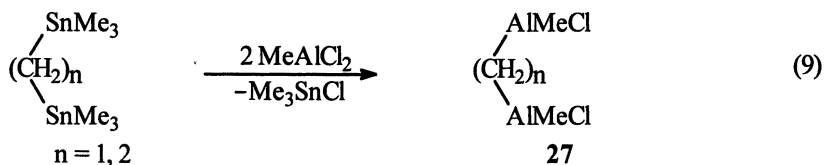
The requisite chelating and antiaromatic organoboranes were prepared from organotin precursors by tin-boron exchange (eqs. 3, 5, 6) or by thermal boron-boron interchange processes (eqs. 7, 8) (18). The tin-boron exchanges proceeded cleanly and completely because the tin by-product, R_2SnX_2 or R_3SnX , complexed only weakly with the boron Lewis acid, 15 or 23, possibly for steric reasons (cf. *infra* for aluminum analogs).



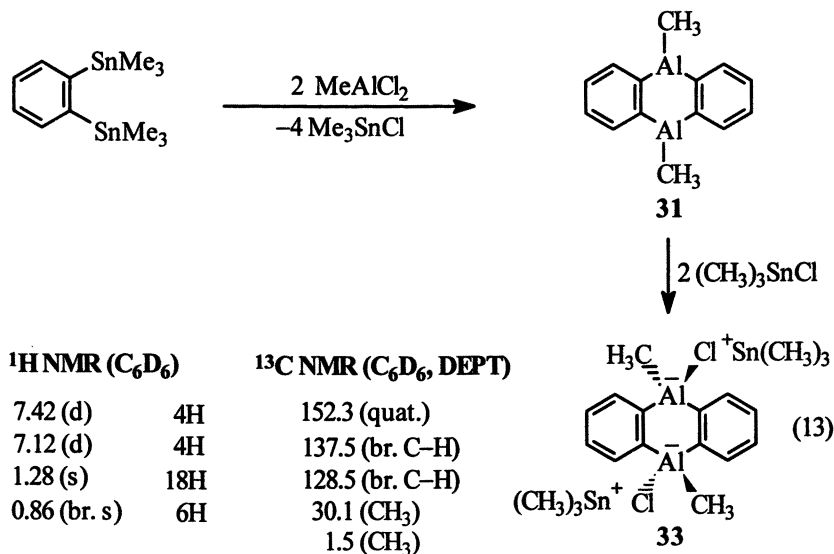
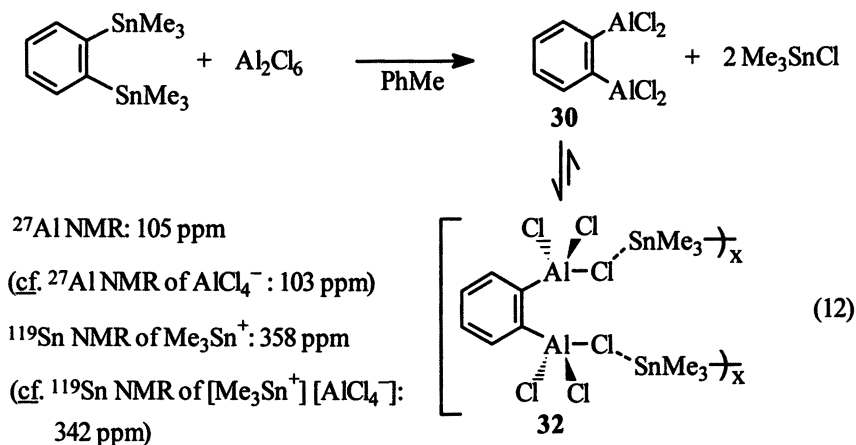


Organoaluminum analogs

All of these chelating and potentially antiaromatic organoaluminum Lewis acids proved to be accessible from the corresponding tin precursors by the tin-aluminum exchange process (25). Illustrative preparations are given in eqs. 9, 10 and 11. The preparation of aluminole **34** will be treated separately (cf. *infra* and eq. 14). In all such reactions, the by-product Me_3SnCl complexed more or less strongly with **27**, **28** or **29** and could only be removed by heating and “chasing off” with toluene or mesitylene under reduced pressure (25).

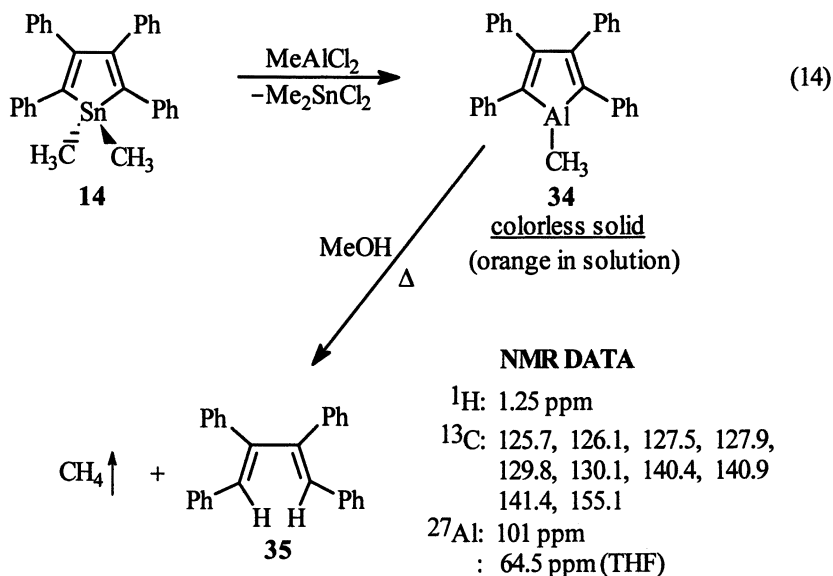


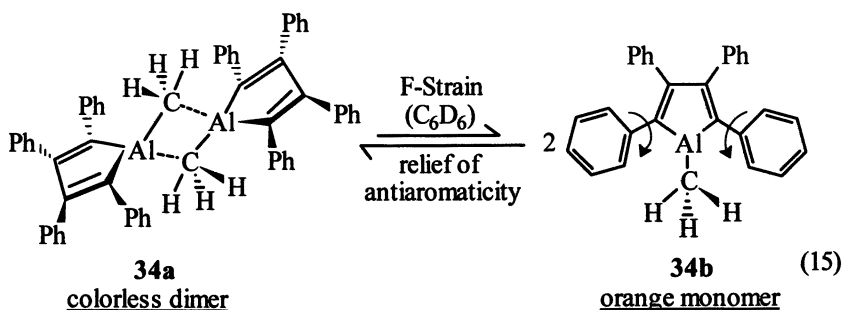
In fact, in attempts to prepare either 1,2-bis(dichloroalumino)benzene (**30**) (eq. 12) or 9,10-dimethyl-9,10-dialuminoanthracene (**31**) (eq. 13), free of Me_3SnCl , complexes resulted (**32** and **33**) that were stable up to 100°C *in vacuo* (19). This attests to the heightened acidity of chelating **30** and antiaromatic **31**. Efforts continue to isolate uncomplexed **30** and **31**.



Synthesis of 1-Methyl-2,3,4,5-tetraphenylaluminole (34).

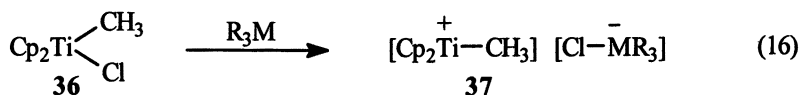
This compound was readily synthesized from **14** and a tin-aluminum exchange reaction with MeAlCl_2 (eq. 14). Noteworthy here is the ease with which the by-product Me_2SnCl_2 could be removed, in sharp contrast to the attempted isolations of pure **30** and **31** in eqs. 12 and 13. The aluminole **34** readily evolves methane with methanol and forms the expected amount of (E,E)-1,2,3,4-tetraphenylbutadiene (**35**). Although the XRD determination of the structure for **34** has yet to be carried out, ^1H , ^{13}C and especially ^{27}Al NMR data are consistent with the existence of a dimer of **34** in the solid state and largely in solution: ^{27}Al values for monomeric Bu_3^iAl at 286 ppm, anionic AlCl_4^- at 103 ppm and dimeric Me_3Al at 155 ppm are strongly indicative of tetracoordinate Al in **34** (**34a** in eq. 15). The orange color of **34** in solution can be ascribed to small amounts of monomer **34b**, which as an antiaromatic π -system may be expected to exhibit π - π^* transitions in the visible spectrum (cf. **15**). Dissolution in benzene should foster dissociation of dimeric **34a** as should the F-strain generated in the likely bridged structure of **34a**. On the other hand, association of monomeric **34b** to **34a** would remove the destabilizing 3p-orbital on aluminum from conjugation and thereby offer relief from antiaromaticity (19).





Cocatalytic Activity of Bidentate Group 13 Organometallics in the Polymerization of Ethylene with Titanocene(IV) Methyl Chloride(36)

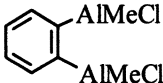
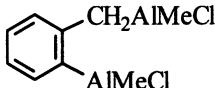
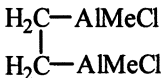
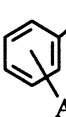
As considered above, the Group 13 organometallic cocatalyst generally has two roles to play, alkylation of the transition metal to form the C–M_t bond and extraction of an anion to form the cationic C–M_t⁺ site (cf. eq. 1). To evaluate the latter function separately, namely the Lewis acidity of the Group 13 cocatalyst, the various bidentate Lewis acids synthesized in this study were admixed with titanocene(IV) methyl chloride (36) in toluene in an 8:1 (R₃M equiv.:Ti) ratio to learn if the individual system could polymerize ethylene, via the formation of 37 (eq. 16) (6). With all of the bidentate organoboron Lewis acids tried, 22, 23, 24 and 25, none produced any polyethylene whatsoever, leading to the conclusion that even with vicinal tricoordinate borons on a hydrocarbon chain such R₃B could not extract the chloride from 36. A parallel examination of both



monodentate and bidentate organoaluminum Lewis acids in such polymerizations (Table I) showed, on the other hand, that all such compounds were active as cocatalysts. Noteworthy, however, are the generally higher productivity numbers (PN, an approximate measure of activity) of those cocatalysts able to form 5- and 6-membered chelate rings with the extracted chloride (38) (n = 1, 2): entries 1, 2 and 4, where the PN can be tenfold that of entries 6 and 7 where only monodentate Lewis acidity is possible. That such Lewis acidity of entries of 1 and 2 can even surpass that of an equivalent amount of MAO (entry 3) is instructive. Since MAO has rings or chains that could readily form a 6-membered

chelate ring with chloride (**39**), one would have to explain the lower activity of MAO at this Ti:Al ratio by electronic factors other than chelation. The lesser stability of a 4-membered chelate ring **38** ($n = 0$) is reflected in the low PN value of entry 5.

Table I. Polymerizations with $\text{Cp}_2\text{Ti}(\text{Me})\text{Cl}$ and Organoaluminum Cocatalysts^a

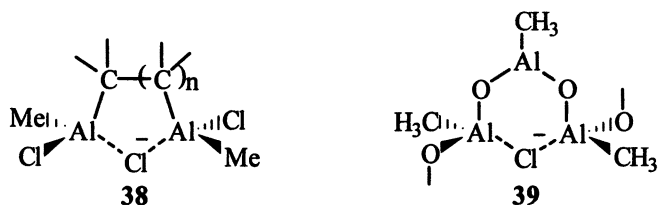
<i>Entry</i>	<i>Cocatalyst</i> ^b	<i>PN</i> ^{c,d}
1		2,300
2		1,900
3	MAO	810
4		550
5	$\text{H}_2\text{C}(\text{AlMeCl})_2$	250
6	MeAlCl_2	200
7	 (<i>meta- or para</i>)	~ 200

^a Eisch, J.J.; Uzick, W.; Mackenzie, K.; Gürtzgen, S. and Rieger, R., U.S. Patent 5,726,332, March 10, 1998, with Witco GmbH and Research Foundation-SUNY as assignees.

^b Conditions: start at ambient temperature in toluene with Ti:Al equivalents ratio of 1:8

^c Productivity numbers: grams PE/gram Ti • h • atm

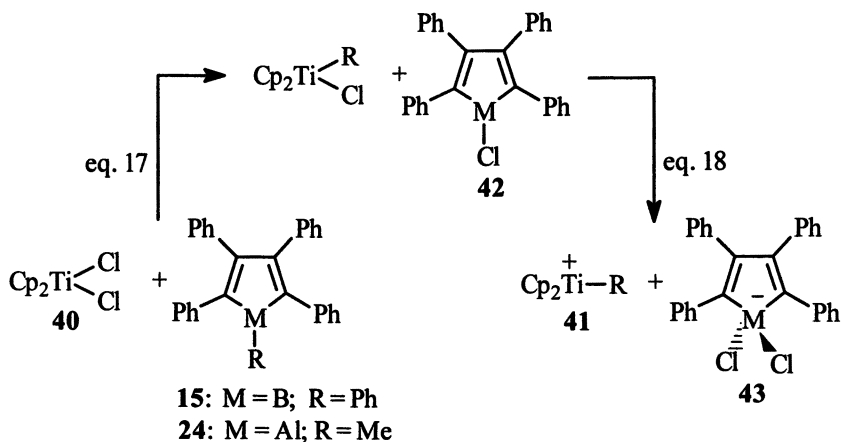
^d Under the same conditions with $\text{Cp}_2\text{Ti}(\text{Me})\text{Cl}$ the candidate organoboron cocatalysts, **22**, **23**, **24** or **25**, gave no polymer.



Since boron is more electronegative than aluminum (2.0 vs. 1.5 on the Allred-Rochow scale), absent steric effects and the *pi*-bonding resonance effect ($\ddot{E}-B \leftrightarrow E=B$), the boron Lewis acid, BE_3 , should be a stronger Lewis acid than the analogous AlE_3 . The failure of the bidentate boron Lewis acids, **22** - **25**, as cocatalysts in the foregoing polymerization trials can confidently be ascribed to overwhelming F-strain in the transition state of the chloride ion removal (**36** \rightarrow **37**, eq. 16).

Cocatalytic Activity of Group 13 Metalloles with Titanocene(IV) Dichloride (**40**) in the Polymerization of Ethylene

In order to evaluate Group 13 metalloles as cocatalysts in their dual roles as alkylating agents for transition metal salts (formation of **1** in eq. 1), titanocene(IV) dichloride (**40**) was individually admixed with borole **15** and with aluminole **34**, in order to learn whether titanocenium(IV) cation (**41**) would result and hence ethylene polymerization would ensue, via eqs. 17-18:



In studies with pentaphenylborole (**15**) and titanocene **40**, admixing the components in toluene at 25°C or even heating the mixture at 50°C did not give a catalyst capable of polymerizing ethylene. The failure of this system to initiate ethylene polymerization can be attributed to the inability to generate the active site, **41**, (R = phenyl). At this time, such inactivity could be attributed to the slowness of chlorine-phenyl exchange (eq. 17) or to the large activation energy for ion-pair formation (eq. 18). Whichever is the retarded step, the root-cause is undoubtedly steric hindrance of such reactions at the boron center. The contrasting behavior of the aluminole **24** in parallel reactions corroborates this mechanistic interpretation.

Admixing aluminole **24** and titanocene **40** in toluene at 25°C in a 1:1 ratio resulted immediately in an active system for the polymerization of ethylene. The moderate activity of this system was gauged by comparison with a 1:1 ratio of **40** and MeAlCl₂ under identical conditions, which gave a PN of 100 ± 2. The homogeneous mixture resulting from simply combining **24** and titanocene **40** at 25°C showed a PN of 10, but heating such a mixture at 50°C for 1h caused the PN to rise to 60. This result clearly shows that the reaction of aluminole **24** with titanocene **40** (eqs. 17, 18) is not rapid at 25°C and requires thermal promotion to produce an optimal amount of **41**. With such thermal pretreatment aluminole **24** proves comparable to MeAlCl₂ as a cocatalyst with titanocene **40** in polymerizing ethylene. This observation thus means that the roles of methylating **40** and by Lewis acidity forming cation **41** are played similarly well by aluminole **24** and by MeAlCl₂. Thus the Lewis acids involved, chloroaluminole **42** and AlCl₃, must be of comparably high acidity, which for **42** is in keeping with its antiaromatic character.

Conclusions and Prospects

The foregoing investigation has demonstrated the crucial importance of the Lewis acidity of the cocatalyst in activating the alkylated metallocene procatalyst for olefin polymerization. Such requisite Lewis acidity can be enhanced not only by well-recognized inductive, resonance and steric effects but by the special factors of ligand hybridization, antiaromaticity, and chelate ring formation with bidentate Lewis acids.

However, despite all that has by now been learned about the effects of metallocene structure on the procatalyst and the influence of cocatalysts on the overall reactivity of such homogeneous Ziegler-Natta systems, the principal remaining factor requiring more elucidation in the search for the "ideal" or optimal catalyst is that of ion-pairing. Studies have shown that even with reactive metallocene procatalysts and effective cocatalysts such as MAO, the fostering of solvent-separated ion pairs over contact ion pairs (cf. **7a** and **8** in eq.

2) by experimental conditions can strongly influence the polymerization activity (26, 27). An understanding and control of such ion-pairing are of great fundamental and industrial importance.

Acknowledgments

For the financial support of our Ziegler-Natta research over the last two decades, the authors are indebted to a number of governmental agencies and industrial firms, prominent among which are the U.S. National Science Foundation and the Alexander von Humboldt Stiftung of Germany, as well as the firms, Solvay, S.A. of Belgium, Akzo-Nobel of The Netherlands and Witco (formerly Schering) of Germany.

References

1. Part 56 of the series, Organometallic Compounds of Group 13. Part 55: Eisch, J.J.; Mackenzie, K.; Windisch; Krüger, C. *Eur. J. Inorg. Chem.* **1999**, 153.
2. Friedel, C.; Crafts, J.M. *Compt. Rend.* **1877**, *84*, 1392, 1450.
3. Lewis, G.N. *Valence and the Structure of Molecules*, Chemical Catalogue, New York, NY 1923.
4. Ziegler, K.; Holzkamp, E.; Breil, H.; Martin, H. *Angew. Chem.* **1955**, *67*, 541.
5. Boor, Jr., J. *Ziegler-Natta Catalysts and Polymerizations*, Academic Press, New York, NY, 1979, Chap. 11.
6. Eisch, J.J.; Piotrowski, A.M.; Brownstein, S.K.; Gabe, E.J.; Lee, F.L. *J. Am. Chem. Soc.* **1985**, *107*, 7219.
7. Eisch, J.J.; Caldwell, K.R.; Werner, S.; Krüger, C. *Organometallics* **1991**, *10*, 3417.
8. Natta, G.; Pino, P.; Mazzanti, G.; Lanzo, R. *Chem. Ind. (Milan)* **1957**, *39*, 1032.
9. Andresen, A.; Cordes, H.; Herwig, J.; Kaminsky, W.; Merck, A.; Mottweiler, R.; Pein, J.; Sinn, H.; Vollmer, H. *Angew. Chem. Int. Ed. Engl.* **1976**, *15*, 629.
10. Ewen, J.A. *J. Am. Chem. Soc.* **1984**, *106*, 6355.
11. Kaminsky, W.; Külper, K.; Brintzinger, H.H.; Wild, F.R.W.P. *Angew. Chem. Int. Ed. Engl.* **1985**, *24*, 507.
12. Some researchers adhere to the precise distinctions of terming the heterogeneous polymerizations of ethylene derived from titanium(IV) or zirconium(IV) salts with aluminum alkyls as the Ziegler process, the

heterogeneous, stereoregular polymerization of olefins obtained from titanium(III) and similar subvalent salts and aluminum alkyls as the Natta process and the homogeneous polymerizations derived from metallocene or soluble procatalysts with aluminum derivatives as yet a third, distinct process. At present, however, there is every reason to conclude that the key mechanistic steps depicted in eq. 1 are operative in each process. Thus, all such processes may generally be considered as the essential aspects of Ziegler's and Natta's discoveries.

13. Coates, G.E.; Wade, K. *Organometallic Compounds*, 3rd ed., Methuen, London, 1967, Vol. 2, pp. 304-319. The partial negative charge on M and the partial positive charge on B in structure 7 merely represent the relative changes in the electron density about ME₃ and about A-B; respectively, upon complexation. Such charges do not indicate the actual polarity of the M-B bond in 7.
14. Brown, H.C.; Davidson, N. *J. Am. Chem. Soc.* **1942**, *64*, 316.
15. Eisch, J.J. In *Comprehensive Organometallic Chemistry*; Wilkinson, G.; Stone, F.G.A.; Abel, E.W., Eds., Pergamon Press, Oxford, 1982, Vol. 1, pp. 595-598; pp. 614-616.
16. (a) Piers, W.E.; Irvine, G.J.; Williams, V.C. *Eur. J. Inorg. Chem.* **2000**, 2131. (b) Chen, E.Y.X.; Marks, T.J. *Chem. Rev.* **2000**, *100*, 1391.
17. Starowieyski, S.; Pasykiewicz, S. *Rocz. Chem.* **1964**, *38*, 331.
18. Eisch, J.J.; Kotowicz, B.W. *Eur. J. Inorg. Chem.* **1998**, 761.
19. P.O. Otieno, unpublished studies of this Laboratory, 1999.
20. Werner, A.; King, V.L. *Chem. Ber.* **1911**, *44*, 1887.
21. Hyde, J.R.; Karol, T.J.; Hutchinson, J.P.; Kuivila, H.G.; Zubieta, J. *Organometallics* **1982**, *1*, 404.
22. Katz, H.E. *J. Am. Chem. Soc.* **1985**, *107*, 1420.
23. Streitwieser, J.A. *Molecular Orbital Theory for Organic Chemistry*, Wiley, New York, NY, 1961, pp. 256-304.
24. Eisch, J.J.; Galle, J.E.; Kozima, S. *J. Am. Chem. Soc.* **1986**, *108*, 379.
25. Eisch, J.J.; Mackenzie, K.; Windisch, H.; Krüger, C. *Eur. J. Inorg. Chem.* **1999**, 153.
26. Eisch, J.J.; Pombrik, S.I.; Zheng, G.X. *Organometallics* **1993**, *12*, 3856.
27. Eisch, J.J.; Pombrik, S.I.; Gürtzgen, S.; Rieger, R.; Uzick, W. In *Catalyst Design for Tailor-Made Polyolefins*; Soga, K.; Terano, M., Ed., Studies in Surface Science and Catalysis, Vol. 89; Kodansha, Tokyo, 1994, pp. 221-235.

Chapter 7

Metallocene-Based Bidentate Lewis Acids

Frieder Jäkle

Department of Chemistry, Rutgers University, Newark, NJ 07102

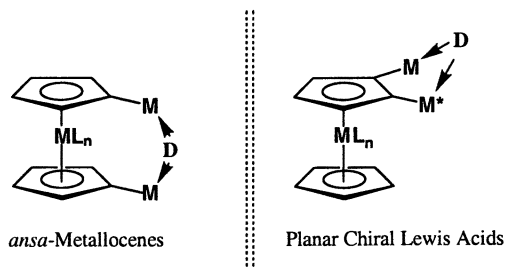
This chapter reviews the synthesis and properties of bidentate metallocene-based Lewis acids. In general, the Lewis acidic centers may be attached to the cyclopentadienyl (Cp) rings of a metallocene either in the 1,1'- or the 1,2-positions. Examples of both types of bifunctional Lewis acids are discussed. Although the latter may be potentially very interesting for the design of planar-chiral Lewis acid catalysts, efforts have been scarce, and their synthesis quite challenging. Herein we describe a straightforward route to bidentate Lewis acids consisting of a three-dimensional ferrocene backbone, to which a boryl and a stannyl group are attached at the same Cp-ring. A 1-stannyl-2-borylferrocene was obtained with high selectivity through treatment of 1,1'-bis(trimethylstannyl)-ferrocene with one equivalent of boron trichloride in hexanes at low temperature. We propose a mechanism for this unusual rearrangement reaction involving initial *exo*-attack of the electrophile at the position *ortho* to the stannyl group, and subsequent proton transfer to the other Cp-ring followed by destannylation.

Introduction

Bi- and multidentate Lewis acids have attracted attention for many years as a result of their potential as selective receptors for anions and neutral Lewis bases (1-6). Coordination of the inorganic or organic nucleophile to multiple Lewis acid centers has been supported by X-ray crystallography (7-15), by investigations on thermodynamic and kinetic effects associated with the binding process in solution (12,16), and by theoretical calculations (17,18). As catalysts in organic syntheses, bidentate species have been shown to display superior reactivity and stereoselectivity in comparison to their monofunctional counterparts (19-22). Indeed, several examples of the use of chiral derivatives in stereoselective synthesis have also been reported (21-24). Moreover, highly electron-deficient bidentate organoboron and organoaluminum species have proven to be superior cocatalysts in Ziegler Natta polymerization (25,26).

A common feature for most of the above mentioned bidentate Lewis acids is the attachment of the Lewis acidic centers to a flat two-dimensional aromatic backbone. Metallocenes such as ferrocene possess a unique, fairly rigid three-dimensional backbone. As a result of the metallocene framework, planar and central chirality provide a rather unique possibility for the design of stereoselective catalysts (27). Another favorable aspect is that most ferrocene derivatives can be reversibly oxidized. This feature may allow for control of the Lewis acidity of the bifunctional Lewis acids via (electro)chemical oxidation/reduction of the central iron atom.

There are two options for the design of a bifunctional metallocene-based Lewis acid, either the attachment of one substituent to each Cp-ring leading to a 1,1'-disubstituted species, or attachment of both substituents at the same Cp-ring.



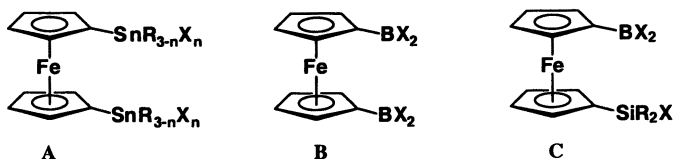
Several 1,1'-dielement-substituted metallocenes are known and their syntheses and applications will be briefly summarized in the following section. On the other hand very few examples of 1,2-dimetallated metallocenes have been reported in the literature. In these systems the Lewis acidic centers would not be part of a mirror plane, but rather attached to the "edge" of a cylindrical molecule providing a unique geometric environment. The discovery of a selective high-yield access to 1-stannyl-2-borylferrocenes, and our recent findings on the

properties and chemical reactivity of such hetero-bidentate Lewis acids will be described.

1,1'-Bifunctional Metallocene-Based Lewis Acids

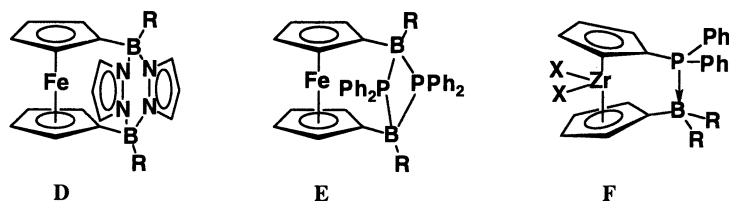
Ferrocene-Based Systems

Dimercurated ferrocenes such as 1,1'-bis(chloromercury)ferrocene and related species have been known for many years and proven invaluable as synthetic intermediates to other metallated and halogenated ferrocenes (27). However, as the ferrocene bridging unit is highly electron rich, they have not been applied to binding of anions and Lewis bases, as have the related phenylene and naphthalenediyl species. Similarly, examples for silylated (28,29) and stannylated (30-34) ferrocenes such as **A** ($X = \text{Cl}, \text{I}; n = 0-3$) are known, but detailed binding studies have not been performed. However, in an interesting related study, Jurkschat and coworkers have used macrocycles containing two ferrocenylsilane units and two Lewis acidic tin centers for binding of anions (35).



Diborylated ferrocenes (**B**; $X = \text{F}, \text{Cl}, \text{Br}, \text{Me}, \text{Ph}, \text{C}_6\text{F}_5, \text{Mes}$) are probably the most thoroughly studied class of bidentate metallocene-based Lewis acids. Their synthesis via direct borylation of ferrocene was developed by Siebert and coworkers in 1976 (36-39) and has since been further investigated (40-43). Interestingly, they also serve as precursors to dibora[2]ferrocenophanes (44). The influence of the electron-rich iron atom on the Lewis acidic centers has received much attention, such that a relationship between the number of Lewis acidic boryl groups attached to the Cp-rings versus the degree of iron-boron interaction has been established. The degree of the individual iron-boron interactions has been shown to decrease with increasing number of boryl groups as established via X-ray crystallography (41,43), Mößbauer spectroscopy (45), and theoretical calculations (46). On the other hand, very few examples of the higher homologues, the aluminum (47) and gallium (48) substituted ferrocenes have been reported. Potentially interesting hetero-bidentate Lewis acids (**C**; $R = \text{Me}, \text{Ph}; X = \text{Cl}$) have recently been obtained through highly selective ring-opening addition reactions of strained silicon- and tin-bridged [1]ferrocenophanes with boron halides (49).

Ferrocene-based bidentate Lewis acids have been studied for a variety of different applications. For example, Wagner and coworkers have used diborylated ferrocenes for the synthesis of so-called switchable *ansa*-metallocenes **D** and **E**, in which the *ansa*-bridge is formed and reopened via reversible formation of donor-acceptor bonds (50-54). This type of molecular switch is especially interesting for the development of smart Ziegler Natta-type catalysts such as the boron-phosphorous bridged zirconocene species **F** (55).



Very recently, Piers and coworkers have investigated pentafluorophenyl-substituted ferrocenylboranes (**C**; X= C₆F₅) as cocatalysts in Ziegler-Natta polymerization (56). The bidentate species was found to be significantly more Lewis acidic than the monoborylated analog effecting methide abstraction from Cp₂ZrMe₂ under mild conditions. The diminished Lewis acidity of the monoborylated species was rationalized by a strong degree of interaction with the electron-rich iron center.

The cyclopentadienyl rings in 1,1'-disubstituted ferrocenes can freely rotate as long as an *ansa*-bridge does not prevent this motion, and bulky substituents are not present. Accordingly, 1,1'-dielement-substituted ferrocenes can also serve as building blocks for the generation of coordination polymers, in which the two Lewis acidic sites are at opposite sites of the individual ferrocene molecules (Fig. 1). Treatment of diborylated ferrocenes with bifunctional aromatic amines has been shown to lead to spontaneous and reversible formation of ferrocene-containing coordination polymers (57-59).

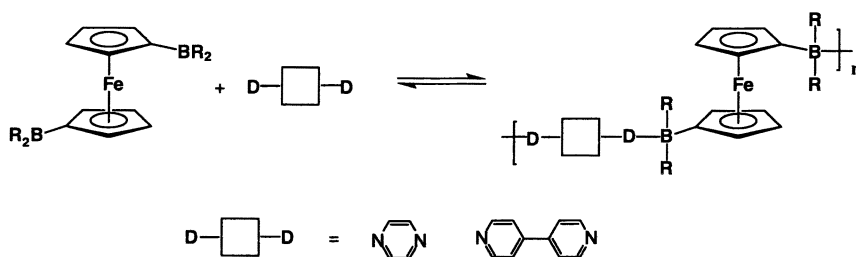
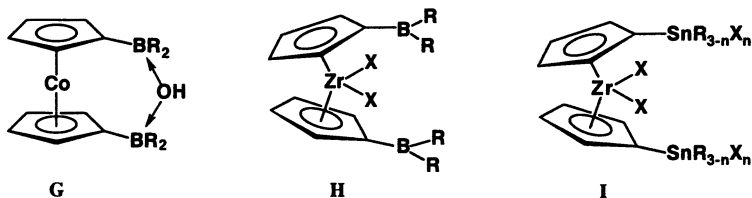


Fig. 1. Coordination polymers from ferrocene-based bifunctional Lewis acids.

Other Metallocenes

Although the higher homologues of the ferrocenes, the diborylated ruthenocenes and osmocenes have been synthesized, they have not been further studied (41,43). However, the related isoelectronic diborylated cobaltocenium species have been made from alkali metal borylcyclopentadienides, and a series of anion binding studies have been performed with these systems by Herberich and coworkers (60,61). With hydroxy counterions, an oxygen-bridged complex (G) formed in both, the solid state and in solution ($R = i\text{-Pr}$, F). The binding mode (salt-like structure vs. zwitterionic 1:1 complex vs. inverse chelate structure) depends on both, the substituents at boron and the counteranion.

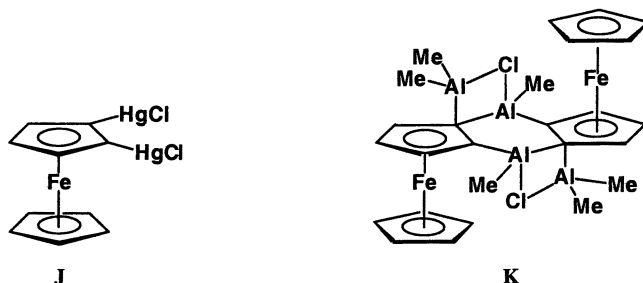


A few examples of titanocene and zirconocene complexes with multiple pendant boryl groups (H) have been synthesized and shown to be efficient Ziegler-Natta catalysts (62,63). However, the main focus in this area has been on the synthesis of ansa-bridged structures (64). In an effort to synthesize electrophile-substituted zirconocenes, Deck and coworkers have studied the treatment of silylated and trimethylstannylated zirconocene dichloride with boron halides and iodine. These reactions resulted in cleavage of the Si-Me or Sn-Me bonds to give zirconocenes such as I (65).

1,2-Bifunctional Metallocene-Based Lewis Acids

Very few reports have appeared in the literature on 1,2-dimetallated ferrocenes. Rausch and coworkers discovered the formation of 1,2-bis(chloromercury)ferrocene (J) as a byproduct in the mercuriation of ferrocene using mercuric acetate with a yield of about 0.4% relative to ferrocene (Fig. 3) (66). Isolation of this species in pure form involves extensive purification procedures including Soxhlet extraction, column chromatography and recrystallization steps. Atwood and coworkers reported the crystal structure of a 1,2-dialuminated compound (K), which was obtained from reaction of bis(chloromercury)ferrocene and trimethylaluminum (67). However, they reported a "low yield" and did not further characterize the product. Since 1,2-bis(chloromercury)ferrocene forms as a byproduct in the mercuriation of ferrocene, it is not clear whether the aluminum species in ref. 67 results from a metal exchange with the 1,2-bis(chloromercury)ferrocene byproduct, or whether it is indeed a rearranged product originating from the 1,1'-disubstituted species.

Recently, Butler and coworkers have developed a synthetic route to 1,2-dibromoferrocene, which serves as a precursor to 1,2-dilithioferrocene (68).

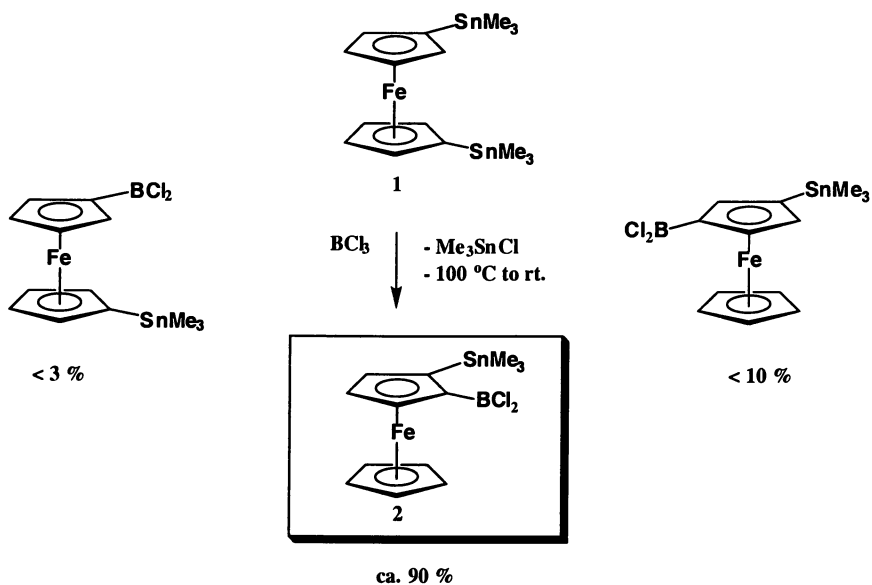


The formation of 1,2-disubstituted ferrocenes through reaction of silylated and stannylated ferrocenes with organic electrophiles has been observed by Cunningham. He reported that Friedel-Crafts acetylation of bis(trimethylsilyl)- or bis(trimethylstannyl)ferrocene gives three different products, mostly the 1,3-disubstituted species, about 30% of the 1,1'-disubstituted compound and about 16 to 17% of the 1,2-isomer (69). He also proposed a mechanism for the formation of these products which involves initial exo-attack of the acetyl cation at the 2,5- and 3,4-positions and subsequent iron-mediated rearrangement to give the observed acetylated products.

Boron-Tin Exchange as a Route to 1,2-Dimetallated Ferrocenes

Encouraged by Cunningham's results, we decided to investigate the reactivity of silylated and stannylated ferrocenes towards inorganic electrophiles. Bis(trimethylstannyl)ferrocene (**1**) can be made easily and in large quantities from dilithioferrocene and trimethyltin chloride (70,71). We treated compound **1** with boron trichloride at low temperature (72), let the reaction mixture slowly warm to room temperature and examined the crude product by multinuclear NMR spectroscopy. Surprisingly, we found formation of ca. 90% of the 1,2-isomer (**2**) with less than 10% of the 1,3-species and less than 3% of the 1,1'-isomer (Scheme 1) (73).

The different isomers can easily be distinguished in the proton NMR spectrum (see Figure 2). For the 1,3-isomer a pseudo-triplet with a coupling constant of 1.2 Hertz is observed, whereas the 1,2 isomer gives rise to a much wider pseudo-triplet with a splitting of 2.4 Hz. This feature has been consistently observed for a variety of ferrocenes with organic substituents as well as the previously mentioned 1,2-dimercurated species (66). The discovery of this high yield access to 1,2-difunctionalized ferrocenes involving an unusually selective electrophilic substitution followed by a rearrangement reaction invoked questions regarding the mechanism of this process and the potential of such dimetallated species to act as precursors to bidentate Lewis acids.



Scheme 1. Reaction of 1 with boron trichloride.

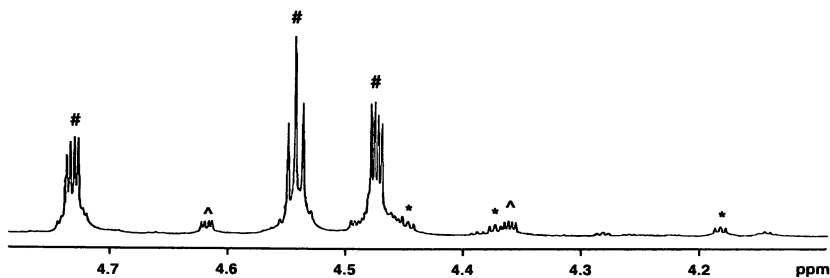


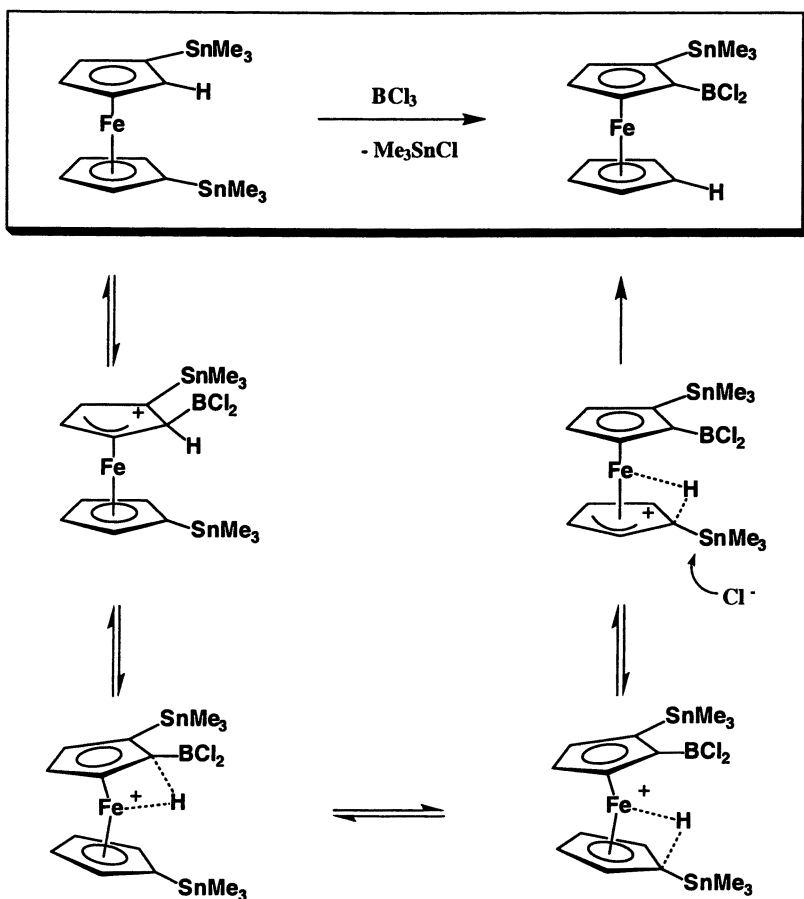
*Figure 2. Region of substituted Cp-rings in the ^1H NMR spectrum of crude 2; 1,2-isomer: # ; 1,3-isomer: ^ ; 1,1'-isomer: *.*

Mechanism of the Boron-Tin Exchange Reaction

Recent experimental and theoretical studies give a concise picture of the mechanism of electrophilic aromatic substitution at ferrocene although some issues are still not fully understood. In the acetylation of ferrocene, the hard electrophile attacks exclusively at the exo-position of the Cp ring (69,74). Mercuric acetate, a soft electrophile, on the other hand attacks at the metal center and subsequently at the endo side of the Cp-ring (75). The situation is less clear in the case of the protonation of ferrocene, the mechanism of which has been an issue of continued dispute. Recent investigations by Mueller-Westerhoff (76) and Cunningham (75) based on a series of labeling experiments point to an initial exo-attack and subsequent transfer of the endo-proton to the iron center. Direct protonation of the iron center does not appear to be favorable. A recent DFT study by Weber (77) is in agreement with the experimental results and suggests the existence of both, a metal-protonated and a ring protonated species, in which the proton shows some interaction with the iron center.

Borylation of stannylferrocenes may occur either from the endo- or the exo-side. An intermediate forms, in which the positive charge is resonance-stabilized by the electron-rich trimethylstannyl group favoring the 2,5-position over the 3,4-attack. Exo-attack would be followed by proton transfer to the iron center and then to the more electron-rich Cp-ring. Back-transfer of the proton to the original Cp-ring would be strongly disfavored by the electron-withdrawing boryl group. This may explain that we observed only trace amounts of the 1,1'-disubstituted species. If endo attack occurred, the exo proton would have to be transferred intermolecularly to another molecule. Two observations clearly speak against this possibility: We did not find any trisubstituted product, and we only found trace amounts of a mono-substituted species. A free proton would be expected to react much faster (or at least with a comparable rate) with our starting material, the 1,1'-distannylferrocene leading to considerable amounts of mono- and trisubstituted species (69). We further confirmed the intramolecular pathway through a labeling experiment. When a mixture of non-deuterated and perdeuterated starting material was treated with boron trichloride no scrambling occurred. The only products were the non-deuterated and the perdeuterated species **2** as observed by mass spectrometry.

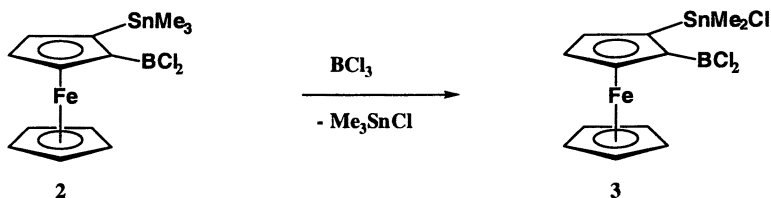
Based on these observations, we propose a mechanism as shown in Scheme 2. The boron trichloride attacks from the exo-side and preferentially in the 2,5-position, then the endo-proton is transferred to the other Cp-ring mediated by the iron atom. Finally, formation of the very stable Sn-Cl bond in the last step drives the reaction to completion.



Scheme 2. Proposed mechanism for the reaction of **1** with boron trichloride.

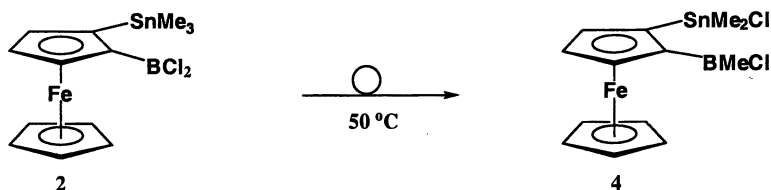
Reactivity of 1-Stannyl-2-borylferrocene (2)

In order to gain access to bidentate Lewis acids it was necessary to find suitable methods to increase the Lewis acidity of the tin center. This was achieved by simply reacting **2** with a further equivalent of boron trichloride leading to the chlorostannylated ferrocene **3** (Scheme 3).



Scheme 3. Cleavage of a Sn-Me bond in 2.

Alternatively, when compound **2** was heated to 50 °C under vacuum for a period of two to three hours, a selective rearrangement reaction occurred, in which a methyl group was transferred from tin to boron and the chlorine substituent migrated to the tin center (**4**, Scheme 4).



Scheme 4. Thermal rearrangement of 2.

This rearrangement reaction was conveniently monitored by ^{11}B , ^{119}Sn , and ^1H NMR spectroscopy. The ^{11}B NMR spectrum of **4** shows a broad signal at 61.5 ppm indicative of methyl transfer to boron (2: 51.1 ppm). More strikingly, the ^{119}Sn NMR signal for **4** (+89.8 ppm) is strongly downfield shifted in comparison to **2** (-5.1 ppm), thereby providing evidence for the increased Lewis acidity of the tin center. Interestingly, the remaining two methyl groups on tin give rise to two signals in the ^1H NMR spectrum (0.65, 0.82 ppm), as is expected for the diastereotopic protons of this planar chiral bidentate Lewis acid.

Conclusions

We have found a simple high yield access to 1,2-dimetallated ferrocenes starting from readily available 1,1'-distannylderrocene. This molecule is attacked by boron trichloride preferentially in the 2,5-position, a proton is subsequently transferred to the other Cp ring mediated by the central iron atom and trimethyltinchloride is released in the final step. The tin-methyl bonds in the resulting 1-stannyl-2-borylderrocenes are intramolecularly activated leading to facile rearrangement reactions. The described reaction sequence gives planar-chiral heterobidentate Lewis acids and we are currently investigating potential applications of these species.

Acknowledgements: I would like to thank my students, in particular Juan A. Gamboa, for their hard work. Acknowledgement is made to the donors of the Petroleum Research Fund, administered by the ACS, and to the Rutgers University Research Council for partial support of this research. I am indebted to Prof. Ian Manners (University of Toronto) for his generous support.

References

1. Katz, H. E. *Inclusion Compd.* **1991**, *4*, 391-405.
2. Kaufmann, D. E.; Otten, A. *Angew. Chem.* **1994**, *106*, 1917-1918.
3. Schmidtchen, F. P.; Berger, M. *Chem. Rev.* **1997**, *97*, 1609-1646.
4. Antonisse, M. M. G.; Reinhoudt, D. N. *Chem. Commun.* **1998**, 443-448.
5. Wuest, J. D. *Acc. Chem. Res.* **1999**, *32*, 81-89.
6. Beer, P. D.; Gale, P. A. *Angew. Chem., Int. Ed.* **2001**, *40*, 486-516.
7. Katz, H. E. *J. Am. Chem. Soc.* **1985**, *107*, 1420-1421.
8. Wuest, J. D.; Zacharie, B. *Organometallics* **1985**, *4*, 410-411.
9. Newcomb, M.; Horner, J. H.; Blanda, M. T.; Squattrito, P. J. *J. Am. Chem. Soc.* **1989**, *111*, 6294-6301.
10. Sharma, V.; Simard, M.; Wuest, J. D. *J. Am. Chem. Soc.* **1992**, *114*, 7931-7933.
11. Altmann, R.; Jurkschat, K.; Schurmann, M.; Dakternieks, D.; Duthie, A. *Organometallics* **1998**, *17*, 5858-5866.
12. Tschinkl, M.; Schier, A.; Riede, J.; Gabbai, F. P. *Organometallics* **1999**, *18*, 1747-1753.
13. Lopez, P.; Oh, T. *Tetrahedron Lett.* **2000**, *41*, 2313-2317.
14. Tikhonova, I. A.; Dolgushin, F. M.; Yanovsky, A. I.; Starikova, Z. A.; Petrovskii, P. V.; Furin, G. G.; Shur, V. B. *J. Organomet. Chem.* **2000**, *613*, 60-67.
15. Cottone III, A.; Scott, M. J. *Organometallics* **2000**, *19*, 5254-5256.

16. Vaugeois, J.; Wuest, J. D. *J. Am. Chem. Soc.* **1998**, *120*, 13016-13022.
17. Jacobson, S.; Pizer, R. *J. Am. Chem. Soc.* **1993**, *115*, 11216-11221.
18. Aldridge, S.; Fallis, I. A.; Howard, S. T. *Chem. Commun.* **2001**, 231-232.
19. Wuest, J. D.; Zacharie, B. *J. Am. Chem. Soc.* **1985**, *107*, 6121-6123.
20. Lee, H.; Diaz, M.; Hawthorne, M. F. *Tetrahedron Letters* **1999**, *40*, 7651-7655.
21. Reilly, M.; Oh, T. *Tetrahedron Lett.* **1995**, *36*, 221-224.
22. Ooi, T.; Miura, T.; Maruoka, K. *Angew. Chem. Int. Ed. Engl.* **1998**, *37*, 2347-2349.
23. Kaufmann, D.; Boese, R. *Angew. Chem.* **1990**, *102*, 568-569.
24. Kii, S.; Maruoka, K. *Tetrahedron Letters* **2001**, *42*, 1935-1939.
25. Chen, E. Y.-X.; Marks, T. J. *Chem. Rev.* **2000**, *100*, 1391-1434.
26. Piers, W. E.; Irvine, G. J.; Williams, V. C. *Eur. J. Inorg. Chem.* **2000**, 2131-2142.
27. *Ferrocenes*; Togni, A.; Hayashi, T., Eds.; VCH: Weinheim, New York, Basel, Cambridge, Tokyo, 1995.
28. Kabanov, B. K.; Zaitsev, V. A.; Varfolomeeva, N. A.; Baukova, G. G.; Kozlova, T. N. *Zh. Obshch. Khim.* **1972**, *42*, 956-957.
29. Kempe, R.; Spannenberg, A. *Z. Kristallogr. - New Cryst. Struct.* **1997**, *212*, 479-480.
30. Roberts, R. M. G.; Silver, J.; Azizian, J. *J. Organomet. Chem.* **1986**, *303*, 387-395.
31. Kabouche, Z.; Nguyen Huu, D. *J. Organomet. Chem.* **1989**, *375*, 191-195.
32. Dong, T. Y.; Hwang, M. Y.; Wen, Y. S.; Hwang, W. S. *J. Organomet. Chem.* **1990**, *391*, 377-385.
33. Herberhold, M.; Steffl, U.; Milius, W.; Wrackmeyer, B. *Z. Anorg. Allg. Chem.* **1998**, *624*, 386-392.
34. Herberhold, M.; Milius, W.; Steffl, U.; Vitzithum, K.; Wrackmeyer, B.; Herber, R. H.; Fontani, M.; Zanello, P. *Eur. J. Inorg. Chem.* **1999**, 145-151.
35. Altmann, R.; Gausset, O.; Horn, D.; Jurkschat, K.; Schurmann, M.; Fontani, M.; Zanello, P. *Organometallics* **2000**, *19*, 430-443.
36. Ruf, W.; Fueller, M.; Siebert, W. *J. Organometal. Chem.* **1974**, *64*, C45-C47.
37. Pebler, J.; Ruf, W.; Siebert, W. *Z. Anorg. Allg. Chem.* **1976**, *422*, 39-42.
38. Renk, T.; Ruf, W.; Siebert, W. *J. Organomet. Chem.* **1976**, *120*, 1-25.
39. Ruf, W.; Renk, T.; Siebert, W. *Z. Naturforsch.* **1976**, *31b*, 1028-1034.
40. Wrackmeyer, B.; Dörfler, U.; Herberhold, M. *Z. Naturforsch., B: Chem. Sci.* **1993**, *48*, 121-123.
41. Wrackmeyer, B.; Dörfler, D.; Milius, W.; Herberhold, M. *Polyhedron* **1995**, *14*, 1425-1431.
42. Wrackmeyer, B.; Dörfler, U.; Milius, W.; Herberhold, M. *Z. Naturforsch., B: Chem. Sci.* **1996**, *51*, 851-858.
43. Appel, A.; Nöth, H.; Schmidt, M. *Chem. Ber.* **1995**, *128*, 621-626.
44. Herberhold, M.; Dörfler, U.; Wrackmeyer, B. *J. Organomet. Chem.* **1997**, *530*, 117-120.

45. Silver, J.; Davies, D. A.; Roberts, R. M. G.; Herberhold, M.; Dörfler, U.; Wrackmeyer, B. *J. Organomet. Chem.* **1999**, *590*, 71-76.
46. Appel, A.; Jäkle, F.; Priermeier, T.; Schmid, R.; Wagner, M. *Organometallics* **1996**, *15*, 1188-1194.
47. Knabel, K.; Krossing, I.; Nöth, H.; Schwenk-Kircher, H.; Schmidt-Amelunxen, M.; Seifert, T. *Eur. J. Inorg. Chem.* **1998**, 1095-1114.
48. Jutzi, P.; Lenze, N.; Neumann, B.; Stammer, H.-G. *Angew. Chem., Int. Ed.* **2001**, *40*, 1424-1427.
49. Jäkle, F.; Berenbaum, A.; Lough, A. J.; Manners, I. *Chem. Eur. J.* **2000**, *6*, 2762-2771.
50. Jäkle, F.; Mattner, M.; Priermeier, T.; Wagner, M. *J. Organomet. Chem.* **1995**, *502*, 123-130.
51. Jäkle, F.; Priermeier, T.; Wagner, M. *Chem. Commun.* **1995**, 1765-1766.
52. Herdtweck, E.; Jäkle, F.; Opromolla, G.; Spiegler, M.; Wagner, M.; Zanello, P. *Organometallics* **1996**, *15*, 5524-5535.
53. Jäkle, F.; Priermeier, T.; Wagner, M. *Organometallics* **1996**, *15*, 2033-2040.
54. Herdtweck, E.; Jäkle, F.; Wagner, M. *Organometallics* **1997**, *16*, 4737-4745.
55. Starzewski, K. A. O.; Kelly, W. M.; Stumpf, A.; Freitag, D. *Angew. Chem. Int. Ed.* **1999**, *38*, 2439-2443.
56. Carpenter, B. E.; Piers, W. E.; McDonald, R. *Can. J. Chem.* **2001**, *79*, 291-295.
57. Fontani, M.; Peters, F.; Scherer, W.; Wachter, W.; Wagner, M.; Zanello, P. *Eur. J. Inorg. Chem.* **1998**, *10*, 1453-1465.
58. Grosche, M.; Herdtweck, E.; Peters, F.; Wagner, M. *Organometallics* **1999**, *18*, 4669-4672.
59. Dinnebier, R. E.; Wagner, M.; Peters, F.; Shankland, K.; David, W. I. F. *Z. Anorg. Allg. Chem.* **2000**, *626*, 1400-1405.
60. Herberich, G. E.; Fischer, A.; Wiebelhaus, D. *Organometallics* **1996**, *15*, 3106-3108.
61. Herberich, G. E.; Englert, U.; Fischer, A.; Wiebelhaus, D. *Organometallics* **1998**, *17*, 4769-4775.
62. Reetz, M. T.; Bruemmer, H.; Kessler, M.; Kuhnigk, J. *Chimia* **1995**, *49*, 501-503.
63. Bochmann, M.; Lancaster, S. J.; Robinson, O. B. *Chem. Commun.* **1995**, 2081-2082.
64. Shapiro, P. J. *Eur. J. Inorg. Chem.* **2001**, 321-326.
65. Cheng, X.; Slebodnick, C.; Deck, P. A.; Billodeaux, D. R.; Fronczek, F. R. *Inorg. Chem.* **2000**, *39*, 14921-14926.
66. Roling, P. V.; Rausch, M. D. *J. Org. Chem.* **1974**, *39*, 1420-1424.
67. Atwood, J. L.; Shoemaker, A. L. *Chem. Commun.* **1976**, 536-537.
68. Butler, I. R.; Drew, M. G. B. *Inorg. Chem. Commun.* **1999**, *2*, 234-237.
69. Cunningham, A. F. *J. Am. Chem. Soc.* **1991**, *113*, 4864-4870.
70. Dawoodi, Z.; Eaborn, C.; Pidcock, A. *J. Organomet. Chem.* **1979**, *170*, 95-104.

71. Lenze, N.; Neumann, B.; Salmon, A.; Stammler, A.; Stammler, H. G.; Jutzi, P. *J. Organomet. Chem.* **2001**, *619*, 74-87.
72. At higher temperature increasing amounts of the 1,3-isomer are formed. Gamboa, J. A.; Jäkle, F.; unpublished results.
73. Jäkle, F.; Lough, A. J.; Manners, I. *Chem. Commun.* **1999**, 453-454.
74. Cunningham, A. F. *Organometallics* **1994**, *13*, 2480-2485.
75. Cunningham, A. F. *Organometallics* **1997**, *16*, 1114-1122.
76. Mueller-Westerhoff, U. T.; Haas, T. J.; Swiegers, G. F.; Leipert, T. K. *J. Organomet. Chem.* **1994**, *472*, 229-246.
77. Mayor-Lopez, J., M.; Weber, J.; Mannfors, B.; Cunningham, A. F. *Organometallics* **1998**, *17*, 4983-4991.

Chapter 8

Polyfunctional Indium Lewis Acids with *o*-Phenylene Backbones

François P. Gabbaï

Department of Chemistry, Texas A&M University,
College Station, TX 77843-3255

This article deals with the synthesis and supramolecular chemistry of bifunctional indium Lewis acids. The systems under scrutiny incorporate the *o*-phenylene and *o*-tetrafluorophenylene backbones. The synthesis of these derivatives by transmetallation of organomercurials and their use in molecular recognition and coordination polymer synthesis is presented.

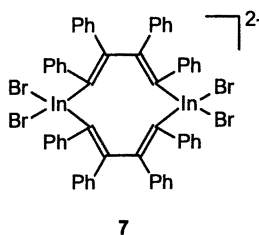
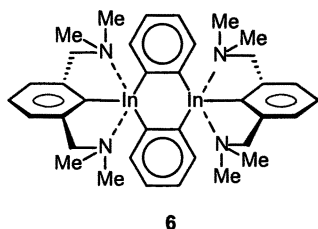
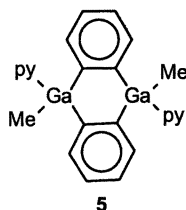
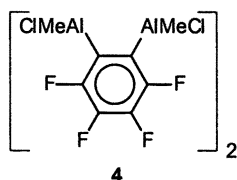
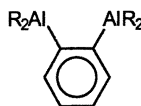
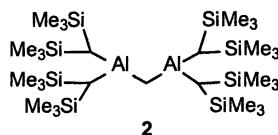
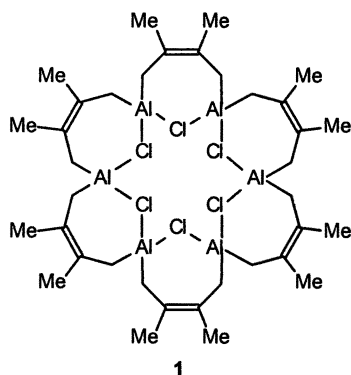
Introduction and background

Polyfunctional Lewis acids are molecular species containing several Lewis-acidic sites that can readily accept electron pairs from incoming basic substrates (*1*). Thus, their chemical nature is the opposite of polyfunctional Lewis-bases, which incorporate, in their molecular skeleton, a given number of Lewis-basic sites available for coordination of electrophilic substrates. In main-group-based systems, the Lewis-acidic sites are typically connected covalently to a molecular framework of well defined size and architecture. Recent applications discovered in the fields of molecular recognition as well as in catalysis have generated an increased interest in these compounds. The present report deals with recent results of our laboratory on the chemistry of polyfunctional organoindium Lewis acids.

Among the neutral polyfunctional Lewis acids, those containing weakly Lewis-acidic elements such as mercury (*1-4*) and tin (*5-11*) as electrophilic sites are by far the most developed and have been investigated for their ability to selectively bind anions and electron rich organic substrates. The majority of the tin- and mercury-based compounds are macrocycles containing up to five metal centers linked by organic or inorganic backbones. Interestingly, the study of the neutral polydentate

Lewis acids containing group 13 elements has attracted much less interest. A series of contributions dealing with the chemistry of polyfunctional boranes indicates (12-26), however, that the use of group 13 elements allows for the preparation of polyfunctional systems whose acidic properties outperform those of their tin- or mercury-containing analogs.

Polyfunctional Lewis acids that incorporate heavier group 13 elements remain relatively rare. This state of affairs certainly reflects the synthetic difficulties that might be encountered in the design and preparation of such systems. In addition to a series of α,ω -alkanedyl-bis(aluminum) complexes (27), earlier investigations have been concerned with the preparation and structural characterization of dialuminated derivatives (28,29). Cyclic (30,31) and macrocyclic structures have also been observed as in the case of the hexanuclear complex **1** formed by reaction of AlCl with 2,3-dimethylbutadiene (32). Recent investigations show that dialuminum complexes can be used for anion complexation. While the methylene-



bis(aluminum) complex **2** chelates a variety of anions including hydride, nitrate, nitrite, acetate and azide (33-35), *ortho*-bis(aluminum)phenylene complexes (36,37) (**3**) have been investigated for their activity as metallocene polymerization co-catalysts. Efforts to prepare fluorinated analogues of **3** have also been performed (38,39). The low stability of these complexes (**4**), however, has complicated their evaluation as co-catalysts. Polyfunctional Lewis acids with gallium at the active sites constitute an even more limited class of compounds. In this context, the recent synthesis of a digallacycle **5** (36) deserves mention.

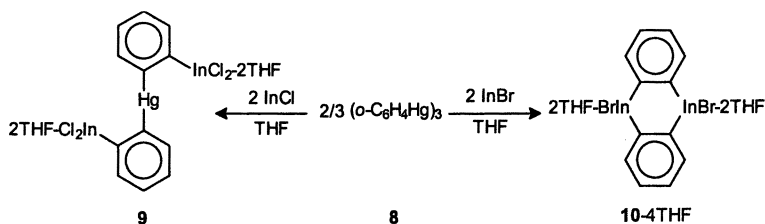
In addition to the work performed in our laboratory, several research groups have investigated the chemistry of polyfunctional organoindium species. The reaction of indium(I) halides with halomethanes proved to be a convenient approach to the synthesis of di(indium)methylene (**40**) and tri(indium)methylene complexes (**41**). Recently, cyclic derivatives have also been obtained. The diindacycles **6** (**42**) and **7** (**43**) are especially noteworthy and were both prepared by metathesis. Some of the results obtained in our laboratory on the chemistry of polyfunctional organoindium Lewis acids are presented in the following sections (44-51).

Synthesis of *ortho*-phenylene-indium complexes (47-49)

Following an investigation on flexible diindium-Lewis-acids (44,45), our work focused on derivatives in which the binding sites are embedded in a rigid molecular edifice. Such an approach presents some indisputable advantages since the Lewis-acidic centers can be purposefully arranged to match the geometry and chemical nature of the dedicated basic binding partner. It was therefore decided to study complexes incorporating the *ortho*-phenylene backbone. In an extension of earlier studies (44,45), it became important to determine whether or not *ortho*-phenylene indium complexes could be prepared by transmetalation of the corresponding poly-mercury derivatives with indium(I) halides. Such transmetalation reactions are very advantageous; they proceed smoothly and yield mercury metal as a sole by-product, which greatly facilitates the isolation of the products.

Trimeric *ortho*-phenylene-mercury (**8**) (**52**) is well known to undergo transmetalation reactions with a variety of main-group elements. The preparation of *ortho*-dilithiobenzene (**52**), tetrameric *ortho*-phenylenemagnesium (**53**) and dimeric *ortho*-phenylenzinc (**54**) are representative examples that demonstrate the importance of this synthetic method. In contrast to those clean transmetalations, the equimolar reaction of InCl with **8** takes an unexpected course and yields the heteronuclear trifunctional Lewis-acid **9** (Scheme 1).

Scheme 1



The molecular structure of **9** in the crystal consists of two *ortho*-phenylene indium dichloride moieties linked through a central Hg atom, giving rise to a pseudo-centric core (Figure 1). The mercury atom is as expected linearly coordinated. Each indium atom is penta-coordinated in a trigonal-bipyramidal fashion with two THF molecules at the axial positions and two chloride ligands as well as a phenylene ring at the equatorial sites. Two of the chloride ligands (Cl(2) and Cl(4)) as well as the oxygen atoms of two of the THF molecules (O(2) and O(3)) interact with the mercury centre. While the Hg...Cl and Hg...O distances are long (Hg-Cl(2) = 3.729 Å, Hg-Cl(4) = 3.914 Å, Hg-O(2) = 3.405 Å, Hg-O(3) = 3.302 Å), they are within the upper range for the implication of Van der Waals forces. Also, there is a detectable lengthening of the In-O(2) and In-O(3) bonds when compared to the In-O(1) and In-O(4) linkages, which indicates that two of the THF molecules are in a bridging situation. As a result, the structure of **9** contains weakly and asymmetrically chelated THF molecules.

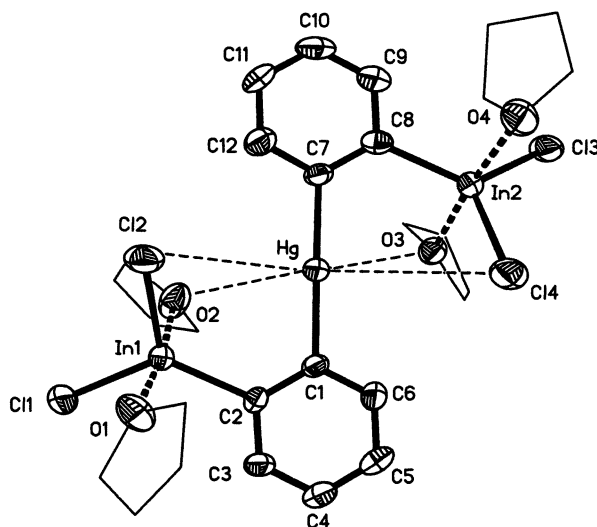


Figure 1: Structure of **9** in the crystal. Adapted with permission from reference 47. Copyright 1996 Royal Society of Chemistry.

Unlike InCl, InBr reacts cleanly with *ortho*-phenylene-mercury in THF to afford the tetrakis(THF) adducts of 9,10-dibromo-9,10-dihydro-9,10-diindaanthracene (**10**) in high yield (Scheme 1). Compound **10** crystallizes with two independent molecules in the unit cell. Both molecules are centrosymmetric and consist of 9,10-dibromo-9,10-dihydro-9,10-diindaanthracene tetrakis(THF) adducts (Figure 2). The median core of one of the two independent molecules is planar within experimental error. Each indium atom is pentacoordinate in a trigonal bipyramidal fashion, the equatorial sites being occupied by the two phenylene rings and the bromine atom while two molecules of THF occupy the axial positions. The second independent molecule does not approach such a high symmetry since the bromine atoms are displaced by 0.8 Å out of the plane containing the phenylene rings and the indium atoms.

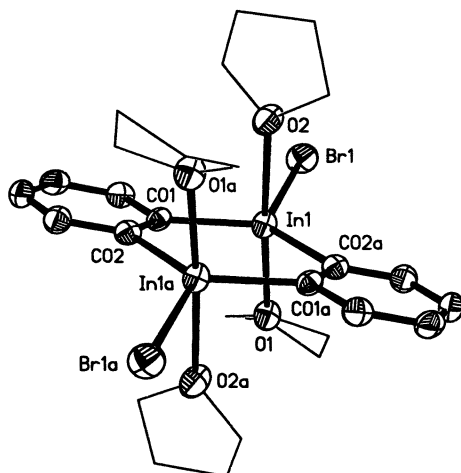
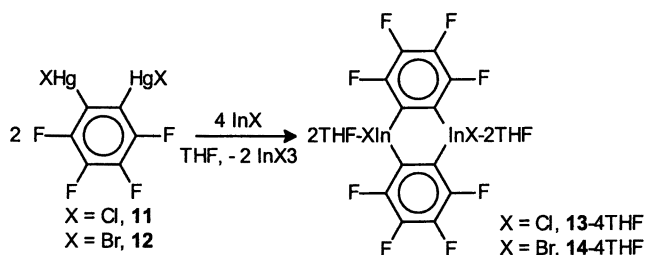


Figure 2: Structure of **10**·4 THF in the crystal (only one of the two independent molecules is shown)

In order to increase the Lewis acidity of the indium centers in compounds such as **10**, the preparation of derivatives that incorporate a tetrafluoronaphthalene backbone has also been pursued. 1,2-Bis(halomercuro)tetrafluorobenzene (halide = chloride (**11**) or bromide (**12**)) reacts with two equivalents of the corresponding indium(I)halide in THF at 25°C to afford the tetrakis(THF) adduct of the respective 9,10-dihalo-9,10-dihydro-9,10-diinda-octafluoroanthracene (halide = chloride (**13**) or bromide (**14**)) (Scheme 2). Compound **14** is also prepared by the reaction of (*o*-C₆F₄Hg)₃ with InBr in refluxing toluene followed by treatment with THF. The formation of the diindacycles **13** and **14** in the reaction of **11** and **12** with two equivalents of the corresponding indium(I) halide is surprising since, in principle, bis(indiumdihalide) complexes would be the expected products. Compounds **13** and **14** form stable tetrakis(THF) adducts which do not lose THF under normal conditions. Thus, their

behavior is different from that of **10**•4 THF, which was found to spontaneously lose two equivalents of THF at room temperature in an inert atmosphere. In the presence of a better donor, the THF ligands can be displaced. By addition of pyridine, the tetrakis(THF) adducts can be quantitatively converted into the tetrakis(pyridine) adducts.

Scheme 2



The ^{19}F NMR spectra of **13** and **14** exhibit two resonances whose multiplicity is consistent with the existence of a higher order AA'BB' spin system. The mass spectra of compounds **13**•4 THF and **14**•4 THF do not allow the detection of the molecular peaks, and the highest assignable peaks correspond to the naked diindacycles which result from the loss of the four coordinated THF molecules. Structural studies have been undertaken on several adducts of these diindacycles (Figure 3). While the structures resemble that of the perprotio-analog, the In-O bonds of **14**•4 THF are shorter by 0.08Å than those of **10**•4 THF. This reflects an increase in the Lewis acidity of the indium ligands which can be associated with the presence of perfluorinated ligands.

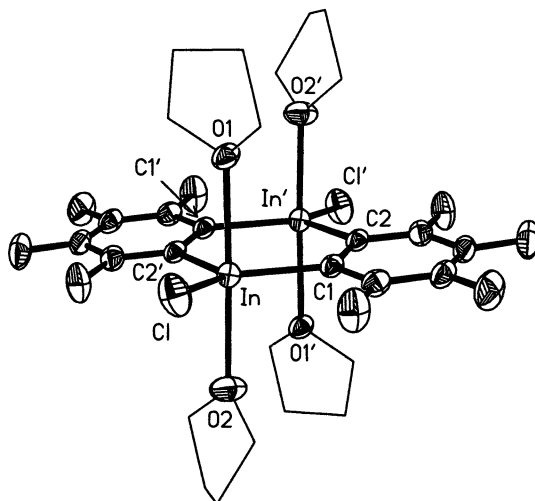
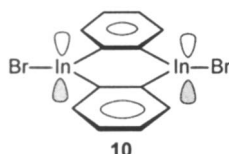


Figure 3: Structure of **13**•4 THF in the crystal

9,10-Diindaanthracenes in molecular recognition and coordination polymer synthesis (50,51)

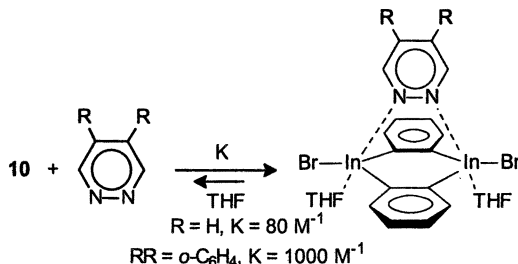
9,10-Dibromo-9,10-dihydro-9,10-diindaanthracene (**10**) contains two electrophilic indium centers positioned at the opposite apexes of a flat six-membered ring. The specific arrangement of the two indium centers in this molecule indicates that the cooperative binding of bifunctional bases with adjacent basic sites might be attainable. Also, since the potentially vacant indium p orbitals are oriented in a direction orthogonal to the plane containing the diindacycle, **10** appears well suited for the elaboration of coordination macromolecules with building-blocks assembled at 90° angles.



Recognition of 1,2-diazines (50)

In order to verify whether **10** could serve as a selective molecular receptor for bifunctional bases with adjacent basic sites, the coordination chemistry of **10** with different diazine structural isomers was investigated. There were no detectable changes in the ^1H NMR spectrum of **10** in a THF- d_8 solution when either pyrazine or pyrimidine were added in 1:1 or 1:2 mol ratios, which suggested that only weak interactions might occur between **10** and these bases. In contrast, incremental addition of pyridazine or phthalazine to a THF- d_8 solution of **10** at 25°C resulted in an up-field shift of the $\text{H}_{(2,3,6,7)}$ NMR resonances of the diindacycle **10** thus reflecting the formation of complexes between **10** and the 1,2-diazines. Analysis of the titration data clearly indicated the formation of 1:1 Lewis acid - diazine complexes **10**-pyridazine-2(THF) and **10**-phthalazine-2(THF) whose stability constants are equal to 80 (± 10) and 1000 (± 150) M^{-1} , respectively (Scheme 3). These data as a whole indicate that **10** is a selective receptor for 1,2-diazines.

Scheme 3



While the 1:1 complex **10**-phthalazine-2(THF) seems to be the preferred species in solution, colorless pale yellow crystals of the less soluble 1:2 complex **10**-2(phthalazine)-(THF) (**15**) spontaneously formed from a saturated THF solution containing equimolar amounts of **10** and phthalazine. As shown in Figure 4, the diindacycle acts as a ditopic receptor for one phthalazine molecule. Each indium atom adopts a trigonal bipyramidal coordination geometry. The two nitrogen atoms of the chelated phthalazine molecule (N(21) and N(22)) occupy one of the axial sites of

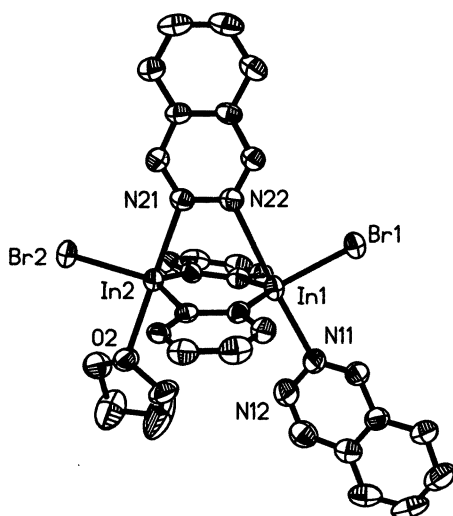


Figure 4: Structure of **15** in the crystal. Adapted with permission from reference 50. Copyright 1998 Royal Society of Chemistry.

each indium center (In(2) and In(1), respectively). The coordination sphere of each indium atom is completed by axial ligation of one THF molecule (In(2)) and one phthalazine (In(1)). The chelation of one phthalazine molecule by the diindacycle has some noteworthy structural consequences. The two indium atoms are displaced towards their respective coordinated nitrogen atoms N(21) and N(22), respectively. As a result, the six-membered ring containing the two indium atoms has a boat-like conformation rather than being planar as in **10**. The two phenylene rings of **15** are not coplanar (dihedral angle of 16.5°) and the dimeric *ortho*-phenylene indium moiety adopts a saddle shape.

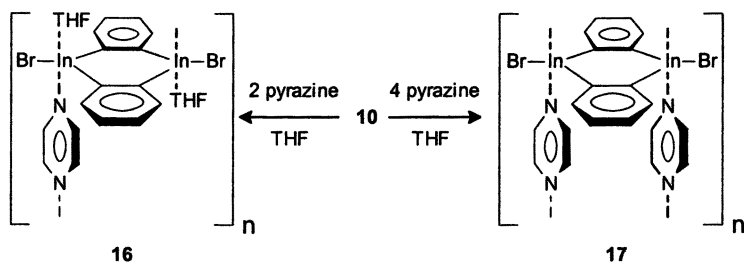
In conclusion, because of subtle structural variations, the indium *p*-orbitals of **10** can be brought to converge thus allowing chelation of bifunctional bases with adjacent electrophilic centers. The observed selectivity (phthalazine > pyridazine > pyrimidine \cong pyrazine) follows the basicity order phthalazine (pK_a 3.5) > pyridazine (pK_a 2.3) > pyrimidine

(pK_a 1.23) > pyrazine (pK_a 0.6) (55). It has however been noted previously that pK_a values are a poor indicator of the donor ability of nitrogen ligands (56). Hence, the ability of **10** to chelate 1,2-diazines can be taken as an alternative explanation for the observed selectivity.

Self-assembly of molecular stairs and ladders (51)

Although only weak association take place between compound **10** and pyrazine in solution, slow cooling of a THF solution of **10** containing one or two equivalents of pyrazine results in the crystallization of polymeric [**10**-(THF)₂-pyrazine]_n (**16**) (Scheme 4). The diindacyclic part of the complex is

Scheme 4



planar within experimental error. Each indium atom is in a trigonal bipyramidal coordination geometry. The axial positions are unsymmetrically occupied by one THF and one pyrazine molecule, respectively. The infinite chains run parallel to one another and do not form any short inter-chain contacts. The monomeric units [**10**-(THF)₂-pyrazine] are linked through a single In-N linkage. All diindacycles are parallel to one another and the Inⁿ...Inⁿ angle of 94.8° approaches normality (Figure 5). In turn, chains of **16** are reminiscent of stairs in which the diindacycles would constitute the steps.

Stoichiometric control of the assembly of **10** with pyrazine was achieved. When the ratio of pyrazine:**10** was increased to four, crystals of a novel compound (**17**) spontaneously precipitated (Scheme 4). The ¹H NMR spectrum revealed the presence of two molecules of pyrazine and two molecule of THF per molecule of **10**. Compound **17** crystallizes with two interstitial THF molecules and consists of polymeric [**10**-(pyrazine)₂]_n (Figure 5). Unlike in **16**, the monomeric units of **17** are assembled through two In-N linkages. Thus, chains of **17** resemble a ladder in which the diindacycles would constitute the rungs while the [In-pyrazine]_n sequences would constitute the parallel side-pieces (Figure 5). With Inⁿ...Inⁿ and

$\text{In}\cdots\text{In}'\cdots\text{In}''$ angles of 88.6° and 91.4° , the cavity generated between each step of the ladder approaches closely the shape of a rectangle of $7.8 \times 3.6 \text{ \AA}$ ($\text{In}\cdots\text{In}' \times \text{N1}'\cdots\text{N2}''$). The THF molecules are positioned half-way between the steps and do not penetrate the cavity deeply enough to be involved in short intermolecular contacts.

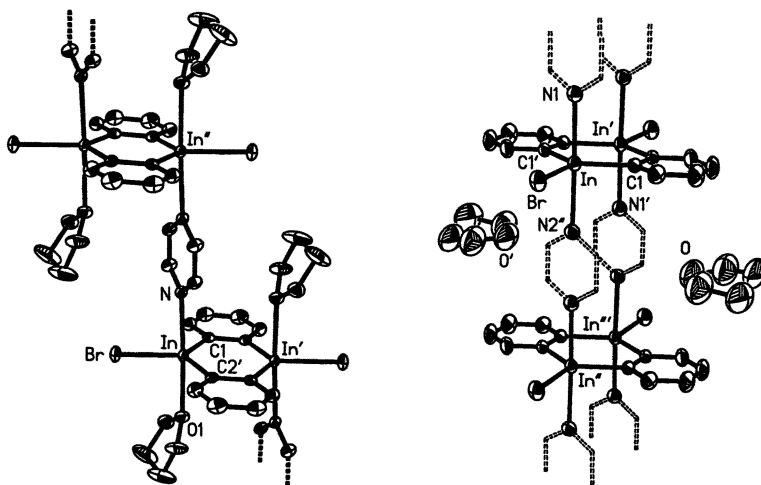


Figure 5: View of two monomeric units of **16** (left). View of two monomeric units of **17** with the interstitial THF molecules (right). Adapted with permission from reference 51. Copyright 1985 John Wiley & Sons.

Polymers **16** and **17** are insoluble in non-polar solvents. However, upon short reflux of the THF mother liquors from which they originate, complete dissolution of the polymers takes place. This process is reversible since both polymers spontaneously reform upon cooling. When heated in the solid state, compounds **16** and **17** first become brittle ($0\text{--}50^\circ\text{C}$) and decomposition of the solid occurs at temperatures of 380°C and 300°C , respectively.

The present results demonstrate that bifunctional Lewis acids such as **10** are useful building-blocks for coordination macromolecules and that they can be regarded as electrophilic spacers. The system **10**/pyrazine/THF is versatile since the stoichiometry and composition of the assembly can be controlled.

Conclusions

This contribution demonstrates that polyfunctional Lewis acids with indium atoms serving as electrophilic sites can be easily prepared by

the transmetalation reactions of polyfunctional organomercurials with indium(I) halogenides. Although this type of reaction can lead to the formation of unexpected products, it usually constitutes a useful synthetic method for making bifunctional Lewis-acids. The diindacycle **10** is a versatile bifunctional Lewis acid. It can be used as a selective receptor for bifunctional bases with adjacent basic centers such as 1,2-diazines, owing to the respective spatial arrangement of the indium centers. It is also a remarkable building-block for the synthesis of self assembled coordination supramolecules.

Acknowledgment: This work would not have been possible without the support of a number of people. In particular, I would like to thank Prof. Hubert Schmidbaur who allowed me to engage in this research at the Technische Universität Munchen. I am also indebted to Dr. Martin Tschinkl, Dr. Annette Schier and Jurgen Riede whose participation has been essential. Finally, I would like to thank the Department of Chemistry at Texas A&M where some of this work was completed.

References

1. (a) Vaugeois, J. ; Simard, M.; Wuest, J. D. *Coord. Chem. Rev.* **1995**, *145*, 55-73. (b) Hawthorne, M. F. Yang X. G., Zheng Z. P. *Pure Appl. Chem.* **1994**, *66*, 245-254.
2. Hawthorne, M. F.; Zheng, Z. *Acc. Chem. Res.* **1997**, *30*, 267-276.
3. Saikulova, L. N.; Bakhmutova, E. V.; Shubina, E. S.; Tikhonova, I. A.; Furin, G. G.; Bakhmutov, V. I.; Gambaryan, N. P.; Chistyakov, A. L.; Stankevich, I. V.; Shur, V. B.; Epstein, L. M. *J. Organomet. Chem.* **1999**, *585*, 201-210.
4. Chistyakov, A. L.; Stankevich, I. V.; Gambaryan, N. P.; Struchkov, Yu. T.; Yanovsky, A. I.; Tikhonova, I. A.; Shur, V. B. *J. Organomet. Chem.* **1997**, *536/537*, 413-424.
5. Horner, J. H.; Squatrito, P. J.; McGuire, N.; Riebenspies, J. P.; Newcomb, M. *Organometallics* **1991**, *10*, 1741-1750.
6. Newcomb, M.; Horner, J. H.; Blanda, M. T.; Squatrito, P. J. *J. Am. Chem. Soc.* **1989**, *111*, 6294-6301.
7. Altmann, R.; Gausset, O.; Horn, D.; Jurkschat, K.; Schuermann, M.; Fontani, M.; Zanello, P. *Organometallics* **2000**, *19*, 430-443.
8. Kuhn, S.; Hummeltenberg, R.; Schurmann, M.; Jurkschat, K. *Phosphorus, Sulfur Silicon Relat. Elem.* **1999**, *150-151*, 333-338.
9. Altmann, R.; Jurkschat, K.; Schurmann, M.; Dakternieks, D.; Duthie, A.; *Organometallics* **1998**, *17*, 5858-5866.
10. Altmann, R.; Jurkschat, K.; Schuermann, M.; Dakternieks, D.; Duthie, A. *Organometallics* **1997**, *16*, 5716-5723.
11. Dakternieks, D.; Jurkschat, K.; Zhu, H.; Tiekink, E. R. T. *Organometallics* **1995**, *14*, 2512-2521.
12. Schriver, D. F.; Biallas, M. J. *J. Am. Chem. Soc.* **1967**, *89*, 1078-1081.

13. Saturnino, D. J.; Yamauchi, M.; Clayton, W. R.; Nelson, R. W.; Shore, S. G. *J. Am. Chem. Soc.* **1975**, *97*, 6063-6070.
14. Katz, H. E. *J. Am. Chem. Soc.* **1985**, *107*, 1420-1421.
15. Katz, H. E. *J. Org. Chem.* **1985**, *50*, 5027-5032.
16. Katz, H. E. *Organometallics* **1987**, *6*, 1134-1136.
17. Jia, L.; Yang, X.; Stern, C.; Marks, T. J. *Organometallics* **1994**, *13*, 3755-3757.
18. For an attempt to use 1,1-diborylalkenes as co-catalysts, see: Köhler, K.; Piers, W. E.; Jarvis, A. P.; Xin, S.; Feng, Y.; Bravakis, A. M.; Collins, S.; Clegg, W.; Yap, G. P. A.; Marder, T. B. *Organometallics* **1998**, *17*, 3557-3566.
19. Piers, W. E.; Irvine, G. J.; Williams, V. C. *Eur. J. Inorg. Chem.* **2000**, *10*, 2131-2142.
20. You-Xian Chen, E.; Marks T. J. *Chem. Rev.* **2000**, *100*, 1391-1434.
21. Williams, V. C.; Piers, W. E.; Clegg, W.; Elsegood, M. R. J.; Collins, S.; Marder, T. B. *J. Am. Chem. Soc.* **1999**, *121*, 3244-3245.
22. Williams, V. C.; Irvine, G. J.; Piers, W. E.; Li, Z.; Collins, S.; Clegg, W.; Elsegood, M. R. J.; Marder, T. B. *Organometallics* **2000**, *19*, 1619-1621.
23. Williams, V. C.; Dai, C.; Li, Z.; Collins, S.; Piers, W. E.; Clegg, W.; Elsegood, M. R. J.; Marder, T. B. *Angew. Chem., Int. Ed. Engl.* **1999**, *38*, 3695-3698.
24. Metz, M. V.; Schwartz, D. J.; Stern, C. L.; Nickias, P. N.; Marks, T. J. *Angew. Chem., Int. Ed. Engl.* **2000**, *39*, 1312-1316.
25. Reilly, M.; Oh, T. *Tetrahedron Lett.* **1995**, *36*, 217-220.
26. Katz, H. E. *J. Org. Chem.* **1989**, *54*, 2179-2183.
27. Martin, H.; Bretinger, H.; Fürbach, F. *Angew. Chem.* **1985**, *97*, 323-324. Martin, H.; Bretinger, H.; *Z. Naturforsch.* **1985**, *40 b*, 182-186. Martin, H.; Bretinger, H. *Z. Naturforsch.* **1991**, *46 b*, 615-620. Ort, M. R.; Mottus, E. H. *J. Organomet. Chem.* **1973**, *50*, 47-52.
28. Atwood, J. L.; Shoemaker, A. L. *J. Chem. Soc., Chem. Commun.* **1976**, 536-537-538.
29. Reck, C. E.; Bretschneider-Hurley, A.; Heeg, M. J.; Winter, C. H. *Organometallics* **1998**, *17*, 2906-2911.
30. Hoberg, H.; Gotor, V.; Milchereit, A.; Krüger, C.; Sekutowski, J. C. *Angew. Chem.* **1977**, *89*, 563-564.
31. Üffing, C.; Ecker, A.; Köppe, R.; Merzweiler, K.; Schnöckel, H. G. *Chem. Eur. J.* **1998**, *4*, 2142-2147.
32. Dohmeier, C.; Mattes, R.; Schnoekel, H. *J. Chem. Soc., Chem. Commun.* **1990**, 358-359.
33. Uhl, W.; Layh, M. *Z. Anorg. Allg. Chem.* **1994**, *620*, 856-862.
34. Uhl, W.; Hannemann, F.; Saak, W.; Wartchow, R. *Eur. J. Inorg. Chem.* **1998**, *7*, 921-926.
35. Uhl, W.; Hannemann, F. *J. Organomet. Chem.* **1999**, *579*, 18-23.
36. Dam, M. A.; Nijbacker, T.; de Kanter, F. J. J.; Akkerman, O. S.; Bickelhaupt, F.; Spek, A. L. *Organometallics* **1999**, *18*, 1706-1709.

37. Eisch, J. J.; Mackenzie, K.; Windisch, H.; Krueger, C. *Eur. J. Inorg. Chem.* **1999**, *1*, 153-162.
38. Tschinkl, M.; Gabbai, F. P.; Bachman, R. E. *J. Chem. Soc., Chem. Commun.* **1999**, 1367-1368.
39. Tschinkl, M.; Cocker, T. M.; Bachman, R. E.; Taylor, R. E.; Gabbai F. P. *J. Organomet. Chem.* **2000**, *604*, 132-136.
40. Khan, M. A.; Peppe, C.; Tuck, D. G. *Organometallics* **1986**, *5*, 525-530.
41. Nobrega, J. A.; Peppe, C.; Brown, M. A.; Tuck, D. G. *J. Chem. Soc., Chem. Commun.* **1998**, 381-382.
42. Dam, M. A.; Nijbacker, T.; de Pater, B. T.; de Kanter, F. J. J.; Akkerman, O. S.; Bickelhaupt, F.; Smeets, W. J. J.; Spek, A. L. *Organometallics* **1997**, *16*, 511-512.
43. Beck, B. C.; Su, J.; Wei, P.; Li, X.-W.; Robinson, G. H. *Organometallics* **2000**, *19*, 1214-1215.
44. Tschinkl, M.; Schier, A.; Riede, J.; Schmidt, E.; Gabbai, F. P. *Organometallics* **1997**, *16*, 4759-4761.
45. Tschinkl, M.; Schier, A.; Riede, J.; Gabbai, F. P. *Inorg. Chem.* **1997**, *36*, 5706-5711.
46. Gabbai, F. P.; Schier, A.; Riede, J.; Sladek, A.; Görlitzer, H. W. *Inorg. Chem.* **1997**, *36*, 5694-5698.
47. Gabbai, F. P.; Schier, A.; Riede, J. *J. Chem. Soc., Chem. Commun.* **1996**, 1121-1122.
48. Gabbai, F. P.; Schier, A.; Riede, J.; Schichl, D. *Organometallics* **1996**, *15*, 4119-4121.
49. Tschinkl, M.; Schier, A.; Riede, J.; Gabbai, F. P. *Inorg. Chem.* **1998**, *37*, 5097-5101.
50. Gabbai, F. P.; Schier, A.; Riede, M.; Hynes, J. J. *J. Chem. Soc., Chem. Commun.*, **1998**, 897-898.
51. F. P. Gabbai, A. Schier, J. Riede *Angew. Chem. Int. Ed. Engl.* **1998**, *37*, 622-624.
52. Wittig, G.; Bickelhaupt, F. *Chem. Ber.* **1958**, *91*, 883.
53. Tinga, M. A. G. M.; Schat, G.; Akkerman, O. S.; Bickelhaupt, F.; Horn, E.; Kooijman, H.; Smeets, W. J. J.; Spek, A. L. *J. Am. Chem. Soc.* **1993**, *115*, 2808- 2817.
54. Schreuder Goedheijt, M.; Nijbacker, T.; Akkerman, O. S.; Bickelhaupt, F.; Veldman, N.; Spek, A. L. *Angew. Chem. Int. Ed. Engl.* **1996**, *35*, 1550-1552.
55. Albert, A.; Goldacre, R.; Phillips, J. J. *J. Chem. Soc.*, **1948**, 2240.
56. Reedijk, J. *Comprehensive Coordination Chemistry*, eds. G. Wilkinson, R. D. Gillard and J. A. McCleverty, Pergamon, Oxford, 1987; Vol. 2, Ch. 13.2, p. 80.

Chapter 9

Chelated Aluminum Anions

Melanie J. Harvey and David A. Atwood

Department of Chemistry, University of Kentucky,
Lexington, KY 40506-0055

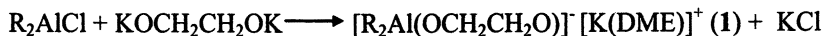
This chapter reviews structurally characterized chelated aluminum anions. These complexes are organized by the types of donor ligands: O, O'; N, N'; N, O; and N, N', O, O'. Although there exists a limited number of examples of chelated aluminum anions, they adopt a wide variety of structures depending on the ligand support; monomeric, dimeric, and polymeric anions of this type have been reported.

Introduction

Anionic aluminum complexes have become increasingly important in recent years. Aluminum anions have found wide use as reducing agents,(1) co-catalysts or counter ions in polymerization reactions(2) and in ionic liquids.(3) There is a much smaller amount of literature focusing on *chelated* aluminum anions. This review includes the structurally characterized chelated anionic aluminum complexes which have been reported. These complexes are organized by the type of chelating ligand. Grouped this way, there are four types of donor ligands represented; O, O'; N, N'; N, O; and N, N', O, O'.

Anions supported by O, O' ligands

Glycolate and binaphtholate ligands are bidentate ligands (of the type O, O') which have supported aluminum anions. One aluminum anion supported by one glycolate ligand and two other monodentate ligands was reported by Werner Uhl. It was synthesized in 28% yield by the reaction of a chloro aluminum complex with dipotassium glycolate.(4,5)



Compound **1** crystallizes as a coordination polymer with each aluminum atom in a distorted tetrahedral environment coordinated by two bis(trimethylsilyl)methyl ligands and chelated by a glycolate ligand (Figure 1). Each potassium is coordinated by a DME and is bridging between two

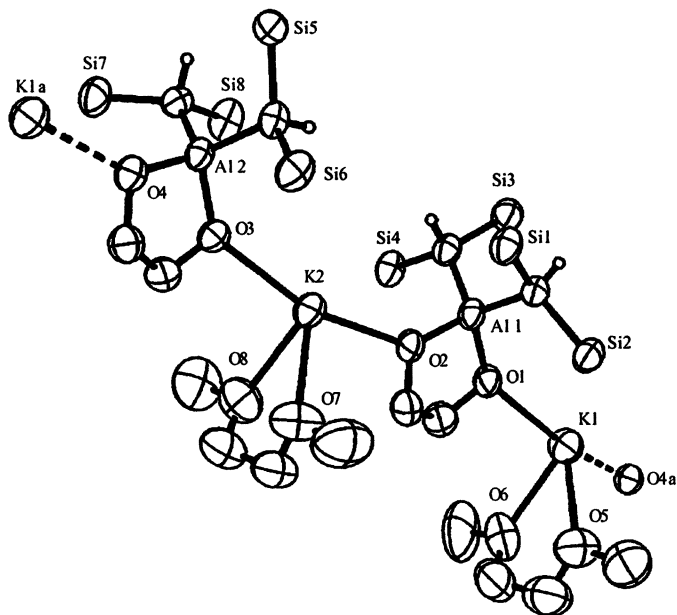


Figure 1. Structure of **1**. (Reproduced from reference 4. Copyright 1996 Elsevier Science S. A.)

aluminate groups through coordination to one oxygen on each of two glycolate units. The O-K-O units are slightly bent (160.8° and 160.0°).⁽⁴⁾

An Al-Li BINOL complex (**2**) can be prepared by the reaction of LiAlH_4 with (*R*)-BINOL.^(6,7) Compound **2** yields remarkably high enantiomeric



excesses for catalytic asymmetric Michael reactions. X-ray quality crystals were grown from cyclohexenone in THF which had the formula $[\text{C}_{40}\text{H}_{24}\text{O}_4\text{AlLi}/\text{C}_6\text{H}_8\text{O}/(\text{C}_4\text{H}_8\text{O})_3]$; based on that structure, the Li-Al-BINOL complex seems to adopt a structure where the lithium atom is coordinated through only one oxygen to the aluminate anion (Figure 2). These systems have been described as multifunctional heterobimetallic catalysts and are thought to be superior asymmetric catalysts because of the potential for cooperation

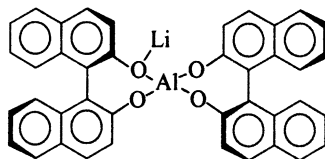


Figure 2. Structure of the Li-Al-BINOL complex (**2**). (Redrawn from reference 8. Copyright 1996 American Chemical Society.)

between the two metal centers, Li and Al. Compound **2** is also highly effective for the catalytic asymmetric synthesis of α -hydroxy phosphonates from aromatic aldehydes and α , β -unsaturated aldehydes.⁽⁸⁾ This catalyst yields the highest enantiomeric excess reported for the catalytic asymmetric hydrophosphonylation of benzaldehyde.

The same ligand is incorporated in Noyori's reagent, a highly effective reducing agent for ketones, which is a modified lithium aluminum hydride obtained by adding an alcohol or phenol and binaphthol to a THF solution. In a recent study of this reagent, several ligand redistribution products were isolated and structurally characterized, $[\text{LiAlH}_2(\text{BINOL})\cdot 2\text{THF}]_4$, $\text{Li}_3\text{Al}(\text{BINOL})_3\cdot 6\text{THF}$, $\text{Li}_2\text{Al}_2(\text{BINOL})_4\cdot 4\text{THF}$, $\text{LiAl}(\text{OR})_2\text{BINOL}\cdot 2\text{THF}$, and $\text{Li}_2\text{AlH}(\text{BINOL})_2\cdot 4\text{THF}$.⁽⁹⁾ In each of these structures, the binaphthol ligand binds in a bidentate fashion to an aluminum atom. In some cases, a lithium atom is also coordinated to one of the oxygen atoms of the binaphthol ligand. Although the identity of the active species in the reduction of ketones with this

reagent is still unclear, the identification of many of the species present in these solutions has provided significant insight into this important reaction.

Anions supported by N, N' ligands

The lithium aluminum tetraamide complex $[Li\{N(tBu)CH_2CH_2N-tBu\}_2Al]$ (**3**) is an example of an aluminum anion supported by a N, N' ligand. It was formed from the reaction of *n*-BuLi with $[HN(tBu)CH_2CH_2N-tBu]Al\{N(tBu)CH_2\}_2$ in hexanes (Figure 3).⁽¹⁰⁾ A variety of solvated derivatives of **3** can be formed in the presence of bases, such as diethyl ether

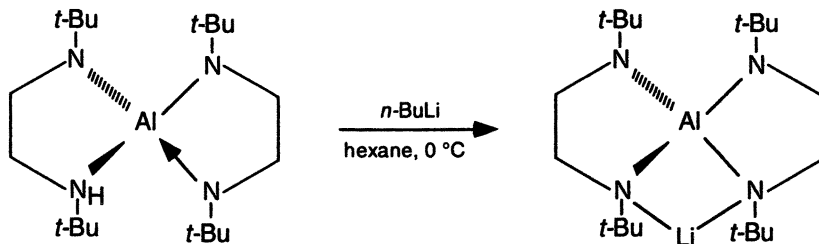


Figure 3. Synthesis of $[Li\{N(tBu)CH_2CH_2N-tBu\}_2Al]$ (**3**). (Redrawn from reference 10. Copyright 1997 American Chemical Society.)

and TMEDA. Compound **3** is monomeric and, based on spectroscopic data, the lithium centers migrate among the nitrogens in solution down to $-80\text{ }^\circ\text{C}$.⁽¹⁰⁾ Compound **3** crystallizes as two discrete monomeric molecules; however, there are no significant differences between them. The bidentate amide ligands coordinate to the aluminum atom and the lithium atom is coordinated by one of the nitrogen atoms from each ligand.

Anions supported by N, O ligands

Two structurally characterized chelated lithium aluminates were formed from the reaction of two equivalents of the bidentate N, O ligand 2,4-(R)₂-6-(CH₂NR')C₆H₂OH (where R' = alkyl and R = H (**4**) or tBu (**5**)) with LiAlH₄ in toluene and THF (Figure 4).⁽¹¹⁾ Spectroscopic data support a "rigid" solution state geometry at 25 °C. This has been attributed to the presence of two

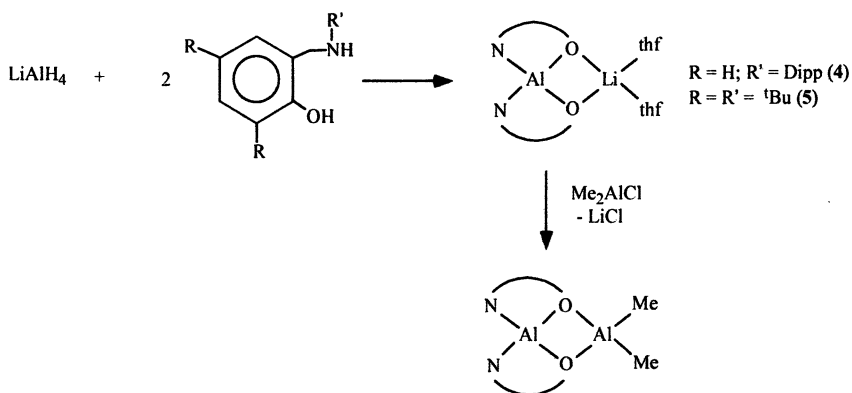


Figure 4. Synthesis of compounds 4 and 5.

chelating ligands along with the negative charge on aluminum. The lithium atoms may be labile since lithium chloride eliminates in the reaction of compound 5 with Me_2AlCl (Figure 4). The structures of 4 and 5 both feature an aluminum atom in a distorted tetrahedral geometry.⁽¹¹⁾ The lithium atoms in each structure are also in a tetrahedral environment as they bridge the oxygens of the two chelating ligands and are coordinated by two additional THF molecules. The Al-O distances in these structures are essentially equivalent (4, 1.784(3) Å and 1.783(3) Å; 5, 1.806(4) Å and 1.808(5) Å), so these compounds are described as containing lithium cations rather than lithium aryloxides.

Anions supported by N, N', O, O' ligands

The most developed support for chelated aluminum anions is the Salan class of ligands (N, N', O, O'). The Salan ligands afford a variety of chelated anions of aluminum. So far, these are the only ligands that have afforded anions supported by a single ligand. Using the Salpan H_4 and Salomphan H_4 ligands, two anions of this type have been formed.⁽¹²⁾

The Salan ligands can be deprotonated in four places, and the formation of aluminum anions requires that all four sigma binding sites be employed. The reaction of LiAlH_4 with Salpan (propyl backbone) or Salomphan (3,4-dimethylphenyl backbone) produces the dimeric lithium aluminates [$\text{SalanAlLi}(\text{thf})_2$]₂ (Salan = Salpan (6) or Salomphan (7))(Figure 5).⁽¹²⁾ Spectroscopic data supports the dimeric structure in solution. X-Ray crystallography confirmed that compounds 6 and 7 also exist as dimers in the

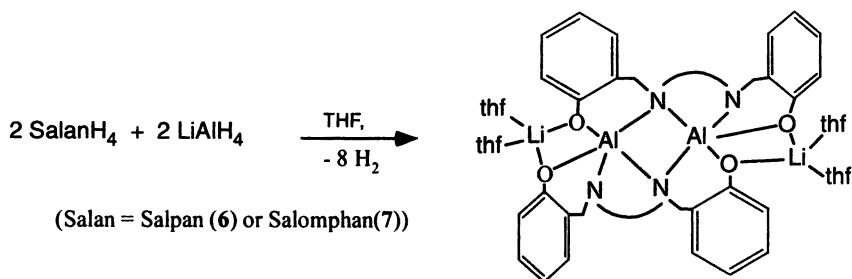


Figure 5. Synthesis of compounds 6 and 7. (Adapted from reference 13. Copyright 1997 Elsevier Science S.A.)

solid-state.⁽¹²⁾ In both structures the N atoms of the ligand bridge both Al atoms. The Li cations are bridged by two oxygen atoms from the same ligand and are coordinated by two thf molecules. The geometry around each Al atom is distorted trigonal bipyramidal. Compound 7 possesses a center of inversion which makes the two (SalomphanAl)Li(thf)₂ units equivalent to one another. The primary difference between 3 and 6 lies in the type and disposition of the amine backbone. In 6 the propyl amine backbones are oriented *cis* in relation to the Al₂N₂ four-membered ring. In 7, the phenylamine groups are oriented in a symmetrical, trans, configuration around the Al₂N₂ ring. This configuration also allows the center of symmetry that is found in the crystal structure of 7.

Salan ligands can easily be tuned by varying the backbone; for example, using Salban(tBu)H₄ the first uni-ligated monomeric aluminate has been accessed, Salban(tBu)Al{Li(thf)₂} (8).⁽¹⁴⁾ This ligand also gives the dimeric complex, Salban(tBu){AlH₂Li(thf)₂}₂ (9).⁽¹⁴⁾ The combination of the Salban(t)H₄ ligand with two moles of LiAlH₄ leads to the formation of a mixture of aluminum containing products, 8 and 9, with the latter predominating.

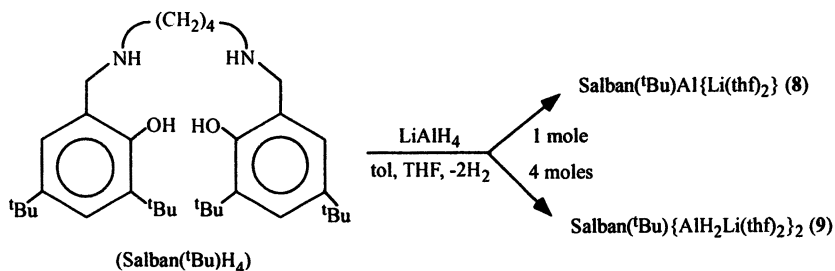


Figure 6. Synthesis of compounds 8 and 9. (Reproduced from reference 14. Copyright 2001 Royal Society of Chemistry.)

Reasonable yields of pure **8** and **9** could be obtained by using an excess (4 equivalents) and one equivalent of the aluminum reagent, respectively (Figure 6).⁽¹⁴⁾

The (CH₂)₄ linkage in the backbone of Salpan(tBu) is of sufficient flexibility to allow the ligand to coordinate just one metal. The structure of **8** (Figure 7) demonstrates the tetrahedral geometry that results for the aluminum atom when

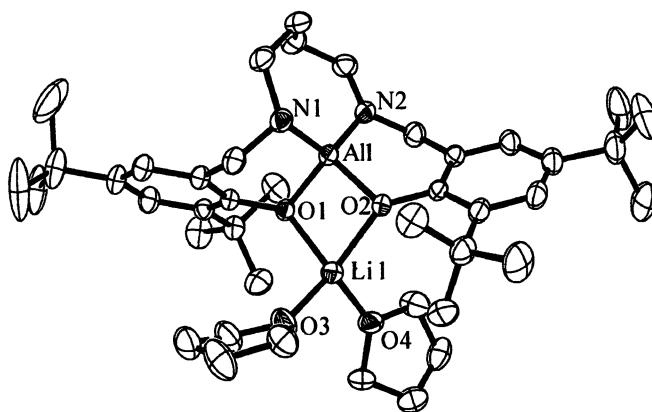


Figure 7. Molecular structure for **8**. (Reproduced from reference 14. Copyright 2001 Royal Society of Chemistry.)

this occurs.⁽¹⁴⁾ The angles range from 122.59(10)° (O2-Al1-N1) to 91.48(8)° (O2-Al1-O1). It is interesting to note that the Al-N and Al-O are surprisingly similar (Al1-N1 1.801(2) Å, Al1-N2 1.785(2) Å, Al1-O1 1.7997(18) Å, Al1-O2 1.7944(17) Å). These distances are also short for this type of complex (for comparison, [SalpanAl{Li(thf)₂}]₂ distances are Al1-O1 1.869(9) Å, Al1-O2 1.831(9) Å, Al1-N1 1.812(13) Å, Al1-N2 2.027(10) Å, Al1-N4 1.995(12) Å, Al2-O5 1.885(9) Å, Al2-O6 1.839(10) Å, Al2-N2 1.954(12) Å, Al2-N3 1.827(11) Å, and Al2-N4 2.035(10) Å).

The crystal structure of **9** reveals the compound is bimetallic with respect to aluminum (Figure 8). The aluminum atoms are in a five-coordinate trigonal bipyramidal geometry.⁽¹⁴⁾ In this arrangement the axial sites are occupied by oxygen and nitrogen atoms. These nitrogens form longer bonds to aluminum (Al1-N1', 2.113(3) Å) than the equatorial nitrogens (Al1-N1, 1.938(3) Å). Despite the charge on aluminum the Al-O and Al-N distances are comparable to those demonstrated in the neutral Salan derivatives (SalanAlR(AIR₂)₂).⁽¹³⁾ A similarity in these distances for related charged (cationic or anionic) and neutral

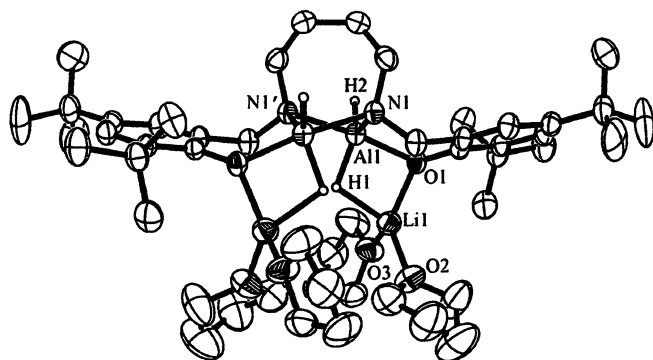


Figure 8. Molecular structure for 9. (Reproduced from reference 14. Copyright 2001 Royal Society of Chemistry.)

derivatives is common. The other equatorial sites are filled by hydrogens with Al-H distances that are longer for the bridging hydrides (Al1-H1, 1.5718 Å) than for the terminal ones (Al1-H2, 1.5175 Å).

A more unusual type of N,N' O,O' ligand are the N,N'-bis(alkyl)sulfamides. The alkali metal aluminates formed with these ligands are related to the alums which are double salts of these metals combined with sulfate anions. These diazasulfate alums form polymeric, dimeric, and monomeric structures as solids. The reaction of N,N'-bis(alkyl)sulfamides with MAlH_4 ($\text{M} = \text{Na}$ or Li) produces the alkali metal aluminates, $[\text{Li}(\text{thf})_2\{\text{Al}[\text{SO}_2(\text{NtBu})_2]_2\}]_\infty$ (10), $[\text{Na}(15\text{-crown-5})][\text{Al}\{\text{SO}_2(\text{NtBu})_2\}_2]$ (11), and $\{\text{Na}(15\text{-crown-5})\}[\text{O}_2\text{S}(\mu\text{-NBn})_2\text{Al}(\mu\text{-NBnSO}_2\text{NBn})]_2$ (12).⁽¹⁵⁾



(R = tBu, M = Li (10), Na(11); R = Benzyl, M = Na (12))

The X-ray structure of 10 shows it to be polymeric with alternating spirocyclic chelated aluminum anions and disolvated lithium cations (Figure 9). The diazasulfate ligand displays a tridentate bonding mode, with N, N' bonding to aluminum and the coordination of one oxygen to each lithium atom in the polymeric chain. The ligand forms two four-membered AlN_2S rings which are nearly planar ($4.1(2)^\circ$ torsion angle). The geometry around aluminum is a highly distorted tetrahedron with N-Al-N angles of 77.7° and 127.3° . In the crystal structure of compound 11 (Figure 10), the diazasulfate ligand adopts a tetra-

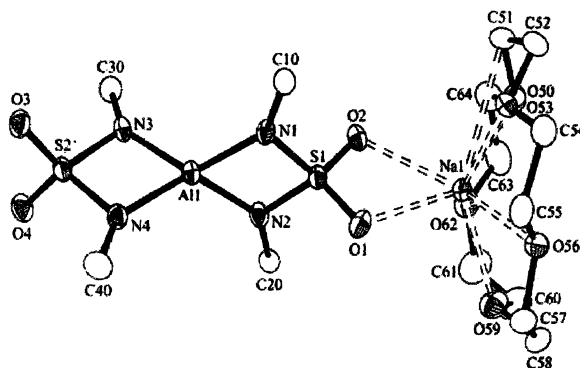


Figure 9. Molecular structure of **10**. (Reproduced from reference 15. Copyright 2001 American Chemical Society.)

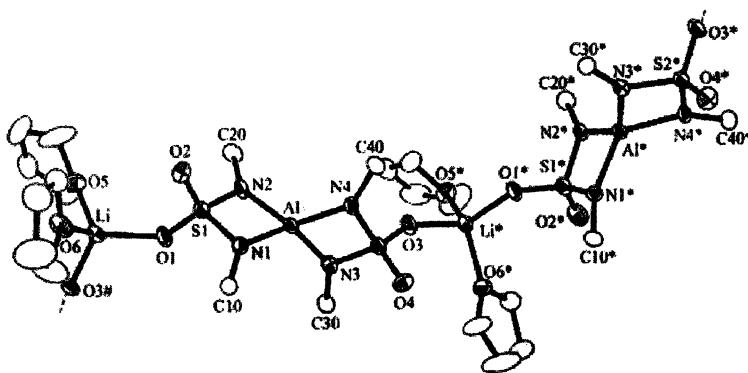


Figure 10. Molecular structure of **11**. (Reproduced from reference 15. Copyright 2001 American Chemical Society.)

dentate coordination mode.⁽¹⁵⁾ Compound **11** is monomeric with N, N' bonding to aluminum and O, O' bonding of one diazasulfate to a sodium atom encapsulated by a 15-crown-5 ligand. The AlN₂S rings are planar (< 1° torsion angle). The geometry around aluminum is the same as in compound **10** (identical N-Al-N angles). Compound **12** is dimeric with N, N' coordination of the terminal diazasulfate ligands to aluminum and O, O' coordination to the

sodium atoms which are each encapsulated by a 15-crown-5 ligand (Figure 11). The central diazasulfate ligands adopt N, O binding to one aluminum atom and N' binding to another aluminum atom forming a central 8-membered ring.

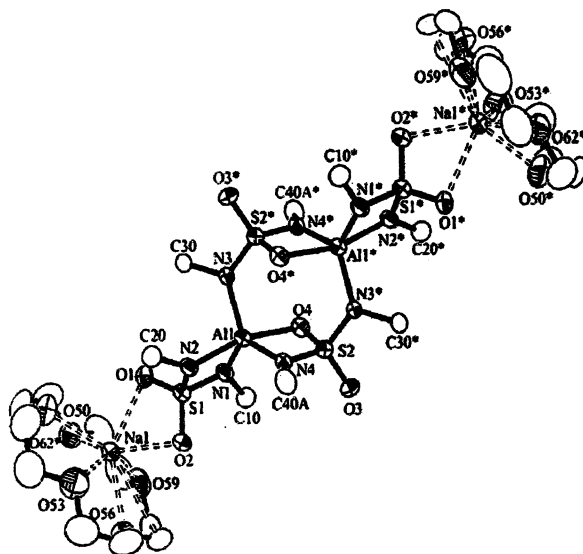


Figure 11. Molecular structure of 12. (Reproduced from reference 15. Copyright 2001 American Chemical Society.)

Summary

Although there exists a limited number of examples of chelated aluminum anions, they adopt a wide variety of structures depending on the ligand support. Monomeric, dimeric, and, in some cases, polymeric anions of this type have been reported. The Salan class of ligands has provided dimeric unligated aluminates, and in one case, the first monomeric unligated aluminum anion. Additionally, the Li-Al-BINOL complex and Noyori's reagent have found significant utility in asymmetric catalysis and as an excellent reducing agent (respectively).

References

1. Barron, A. R.; Wilkinson, G. *Polyhedron* **1986**, *5*, 1897; Bulychev, B. M. *Polyhedron* **1990**, *9*, 387; *Comprehensive Organic Synthesis*, Trost, B. M.; Fleming, I., Eds.; Pergamon Press: Oxford, 1991, 8; Yoon, N. M. *Pure Appl. Chem.* **1996**, *68*, 843.
2. Kobayashi, H. *J. Fluorine Chem.* **2000**, *105*, 201; Li, L.; Stern, C. L.; Marks, T. J. *Organometallics* **2000**, *19*, 3332; Li, L.; Marks, T. J. *Organometallics* **1998**, *17*, 3996; Chen, Y. -X.; Metz, M. V.; Li, L.; Stern, C. L.; Marks, T. J. *J. Am. Chem. Soc.* **1998**, *120*, 6287; Chen, Y. -X.; Stern, C. L.; Marks, T. J. *J. Am. Chem. Soc.* **1997**, *119*, 2582.
3. Wasserscheid, P.; Keim, W. *Angew. Chem., Int. Ed.* **2000**, *39*, 3772; Bradley, D.; Dyson, P.; Welton, T. *Chem. Rev.* **2000**, *9*, 18; Olivier, H. *J. Mol. Catal. A: Chem.* **1999**, *146*, 285.
4. Uhl, W.; Gerding, R.; Vester, A. *J. Organomet. Chem.* **1996**, *513*, 163.
5. A neutral trimetallic aluminum product also forms in this reaction presumably caused by a potassium glycolate impurity in the dipotassium glycolate reactant.
6. Arai, T.; Yamada, Y. M. A.; Yamamoto, N.; Sasai, H.; Shibasaki, M. *Chem. Eur. J.* **1996**, *2*, 1368.
7. Arai, T.; Sasai, H.; Aoe, K.; Okamura, K.; Date, T.; Shibasaki, M. *Angew. Chem. Int. Ed. Engl.*, **1996**, *35*, 104.
8. Arai, T.; Bougauchi, M.; Sasai, H.; Shibasaki, M. *J. Org. Chem.* **1996**, *61*, 2926.
9. Nöth, H.; Schlegel, A.; Suter, M. *J. Organomet. Chem.* **2001**, *621*, 231.
10. Gardiner, M.G.; Raston, C. L.; Skelton, B. W.; White, A. H. *Inorg. Chem.* **1997**, *36*, 2795.
11. Hill, M.S.; Atwood, D. A. *Main Group Chem.* **1998**, *2*, 285.
12. Atwood, D.A.; Rutherford, D. *Inorg. Chem.* **1995**, *34*, 4008.
13. Atwood, D.A. *Coord. Chem. Rev.* **1997**, *165*, 267.
14. Harvey, M. J.; Proffitt, M.; Wei, P.; Atwood, D. A., *Chem. Commun.*, in press.
15. Blais, P.; Brask, J. K.; Chivers, T.; Schatte, G. *Inorg. Chem.* **2001**, *40*, 384.

Chapter 10

Mono- and Dinuclear Olefin Polymerization at Aluminum

Peter H. M. Budzelaar¹ and Giovanni Talarico²

¹Institute of Metal-Organic Chemistry, University of Nijmegen,
The Netherlands (email: budz@sci.kun.nl)

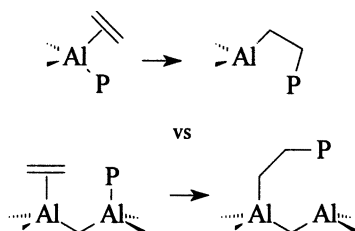
²Dipartimento di Chimica, Università degli Studi di Napoli,
Federico II, Italy (email: talarico@chemistry.unina.it)

Olefin polymerization is usually assumed to occur at a single metal atom, where the growing chain alternates between two adjacent coordination sites (modified Cossee mechanism). Using high-level ab initio and DFT calculations, we have compared this traditional mechanism with a dinuclear mechanism in which the chain alternates between neighbouring metal atoms. Surprisingly, insertion is not always more difficult than in a mononuclear system, suggesting that such a reaction might really occur. Moreover, the balance between chain transfer and propagation can be comparable to that for mononuclear systems, depending on the ligand environment. It appears that the possibility of such a dinuclear mechanism occurring in some of the known Al polymerization systems cannot be ruled out a priori.

Introduction

General

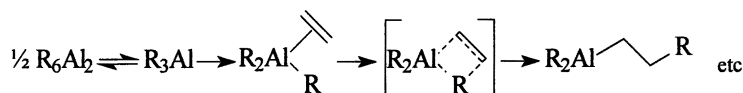
Coordination oligomerization and polymerization of olefins does not require a transition metal. Both reactions can also occur at e.g. aluminium. The Aufbau reaction ("living" *oligomerization* up to ≈ 100 monomers) has been known for a long time and is relatively well-understood (1). In contrast, the nature of the active species in most reported examples of *polymerization* at Al (2-7) is far less clear. This prompted us to consider the possibility that polymerization could occur between two metal centres of a dinuclear species, with switching of the chain at each insertion (8).



Surprisingly, calculations described here indicate that barriers for such a "new polymerization mechanism" (9) are not unduly high, suggesting that this possibility should also be taken into account when trying to interpret polymerization activity at Al.

Oligomerization at Al

At high pressure and temperature, Al trialkyls undergo insertion of ethene to give longer-chain alkyls (up to ≈ 100 monomers). These can be converted into alcohols by air oxidation, or into long-chain olefins by chain transfer at low pressure and even higher temperature. Kinetic studies indicate a mechanism involving monomeric Al alkyls:



Since the monomer-dimer equilibrium is much faster than propagation, all chains grow at the same rate (Poisson distribution of chain lengths).

Polymerization at Al

R_3Al

Polymerization with aluminium trialkyls has been described by Martin and Bretinger; they proposed the active species to be monomeric R_3Al (2). Under the conditions used, R exchange between R_3Al species is rapid, which is hard to reconcile with their observation that only 0.004 mol% of the Al is active. The authors claimed that, with the precautions taken, contamination by transition metals was very unlikely. This suggests that some other Al species, not participating in R exchange, is responsible for the polymerization.

(amidinate)AlR⁺

This was originally thought to be the active species in the (amidinate)AlMe₂/B(C₆F₅)₃ system. Later work showed the system to be more complicated (3). Calculations indicated that monomeric (amidinate)AlR⁺ should not polymerize because chain transfer is much easier than propagation (10).

(Pyridyl-imine-amide)AlR⁺

Gibson has used the addition of trialkylaluminium to pyridine-diimine ligands to generate dialkylaluminium complexes of anionic pyridine-imine-amide ligands. Reaction of these complexes was reported to produce cationic aluminium alkyls capable of polymerizing ethene (to rather low- M_w polymers) (7). This is remarkable, considering the fact that - assuming κ^3 -coordination of the ligand - the cation is formally coordinatively saturated. However, the reported M_w/M_n values (2.9-6.3) clearly show that this is not a well-defined single-site catalyst.

MAO

MAO, in the absence of transition metal catalyst precursors, is also frequently found to produce some polymer (though with much lower rates than the usual TM catalysts) (6).

Methods

Geometries of all complexes were optimized at the B3LYP level using 6-31G(d) basis set. Improved single-point energies were then calculated with the MP2/6-311G(d,p) basis. For several systems, CCSD(T) calculations were also performed, but these did not make a significant difference. DFT (all functionals) appears to underestimate the barriers for chain transfer to monomer at Al (10), therefore we do not report any DFT values here. All calculations were carried with the GAMESS-UK (11) and GAUSSIAN-98 programs (12).

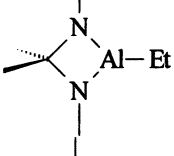
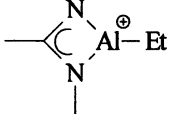
All geometries were optimized as local minima or saddle points without any symmetry restrictions, and the nature of each stationary point was checked by a frequency calculation. The reported energies do not include any zero-point energy or thermal corrections, nor are they corrected for BSSE.

Results and Discussion

Propagation

Table I compares propagation barriers for a number of mono- and dinuclear Al-ethyl species. Of the mononuclear species, Me_2AlEt has the lowest propagation barrier. Introduction of electron-withdrawing substituents or switching to a cationic species increases the olefin complexation energy *and* the insertion barrier. The barriers are much higher than those typical for transition-metal polymerization catalysts, but they are not so high that they exclude the possibility of aluminium-catalyzed olefin polymerization. Transition-metal catalysts typically have very early insertion transition states, with short C=C bond lengths and relatively long metal-olefin distances, as expected for exothermic reactions with low barriers. The Al transition states, in contrast, are more central, with nearly equal lengths for the Al-C bonds being formed and broken, and a rather long C=C bond. This is e.g. illustrated by the insertion transition state for Me_2AlEt in Figure 1.

Table I. Propagation barriers (ethene insertion into Al-Et bond) (kcal/mol).

<i>Mononuclear</i>	E_a	<i>Dinuclear</i>	E_a
$\text{Me}_2\text{Al-Et}$	21.9	$(\mu\text{-OH})(\text{AlH}_2)_2\text{-Et}$	26.4
$\text{F}_2\text{Al-Et}$	29.1	$(\mu\text{-OH})(\text{AlMe}_2)_2\text{-Et}$	26.6
$(\text{Me})(\text{NH}_3)\text{Al-Et}^+$	24.0	$(\mu\text{-F})(\text{AlMe}_2)_2\text{-Et}$	26.4
	33.0	$(\mu\text{-NH})[\text{AlMe}(\text{NH}_3)]_2\text{-Et}^+$	25.2
	28.9	$(\mu\text{-OH})_2(\text{AlH})_2\text{-Et}^+$	26.4

Barriers for dinuclear species tend to be somewhat higher than the lowest one for the mononuclear species, but the differences are not dramatic. Al-C and C-C bond lengths are also similar for the two kinds of transition states (Figure 1, left). Apparently, the higher number of bonds formally involved in the reaction does not make a large difference.



Chain transfer processes

Previous theoretical studies indicate that, of the relevant chain transfer processes, β -hydrogen transfer to monomer always has the lowest activation energy (10). This does not mean that it is always the dominant chain transfer pathway. Under conditions of high temperature and low monomer concentration, such as the "termination" phase of the Aufbau process for higher olefins, β -elimination (being a unimolecular reaction) may still occur because it is entropically favoured over the bimolecular hydrogen transfer reaction. In the present case, however, the only chain transfer process we will consider (for both mono- and dinuclear species) is β -hydrogen transfer to monomer.

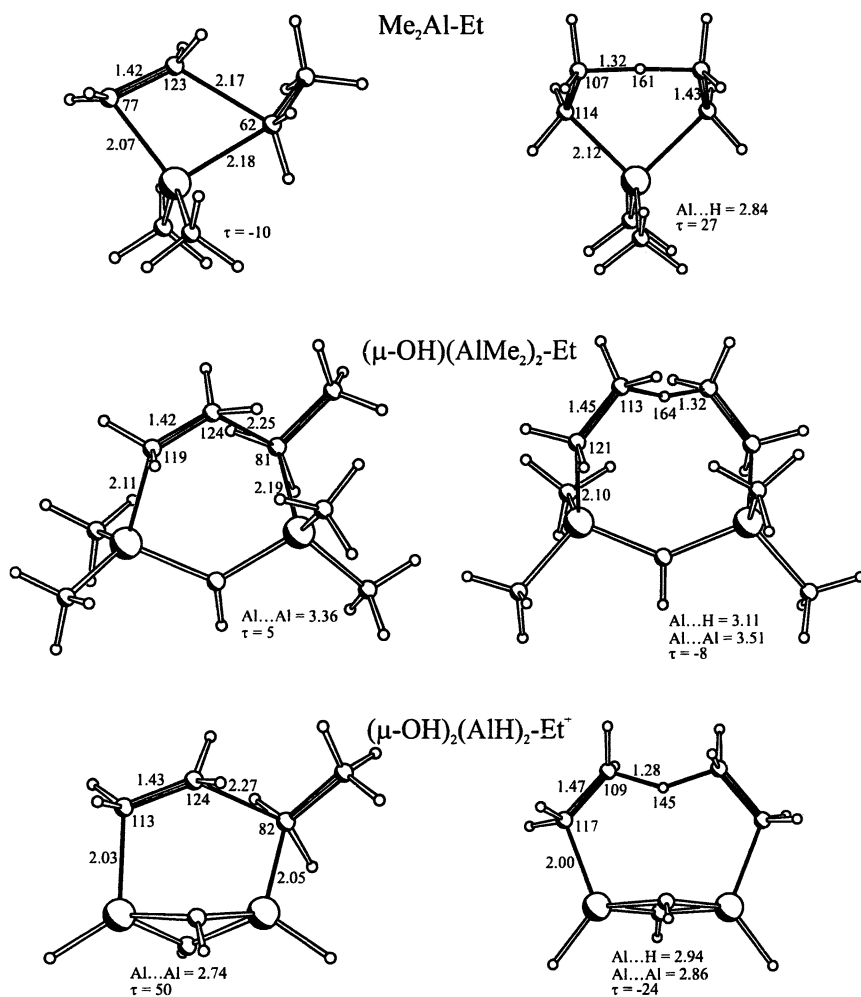
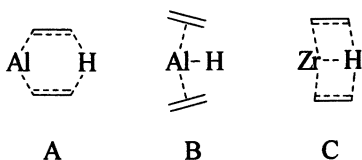


Figure 1. Representative examples of propagation (left) and chain transfer (right) transition states. Bond lengths in Å, angles in °. τ is the torsion angle along the double bond.

It is important to note that β -hydrogen transfer at aluminium differs fundamentally from the corresponding reaction at transition metals. In the Al case, the transfer is directly from carbon to carbon, without a significant Al-H interaction (structure A). Separate from this, there exists a local minimum or transition state (depending on the system) B in the path for associative olefin displacement from an aluminium hydride olefin complex. In contrast, for e.g.

Cp_2Zr there is only a single transition state for olefin displacement (C) (13) with a structure intermediate between structures A and B. Obviously, this makes it dangerous to draw parallels between chain transfer processes at Al and transition metals.

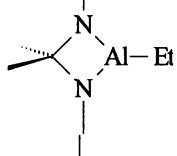
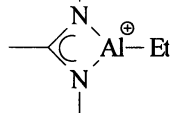


Propagation vs hydrogen transfer to monomer

Table II lists the calculated preferences for ethyl-to-ethene hydride transfer (relative to ethene insertion) for various aluminium ethyls. Among mononuclear species, Me_2AlEt has the highest preference for polymerization. Apparently, anything one does to this species (steric constraints, electronegative substituents, changing to a cationic analogue) makes things worse. For transition metals, steric hindrance appears to be very important in changing the balance between propagation and chain transfer (via associative displacement). For Al, however, the steric requirements around the metal for insertion and chain transfer are rather similar, so we would not expect bulky ligands to make much of a difference. Indeed, we found little impact on this balance on going from $[\text{HC}(\text{NH})_2\text{AlEt}]^+$ to $[t\text{-BuC}(\text{N-}i\text{-Pr})_2\text{AlEt}]^+$ (10).

The balance between propagation and chain transfer to monomer appears to be sensitive to the geometry of the "catalyst". We already reported a relation between balance and steric factors for some mononuclear systems (10). The rigid $(\mu\text{-OH})_2(\text{AlH})_2\text{Et}^+$ system has a short Al-Al distance and forms nearly parallel Al-C bonds. These constraints result in a strong twist around the C=C bond in the propagation TS (Figure 1, left) but are less of a problem in the chain transfer TS (Figure 1, right). Singly bridged binuclear species have a larger Al-Al distance and freedom of movement of the Al-C bonds. For these, propagation is easier (relative to chain transfer). We find several examples (including one cationic species) for which the balance is comparable to that of Me_2AlEt . However, we have not yet found a species with a balance much *better* than that.

Table II. Preference for propagation over chain transfer (Al-Et to ethene) (kcal/mol).

<i>Mononuclear</i>	ΔE_a	<i>Dinuclear</i>	ΔE_a
Me ₂ Al-Et	8.6	(μ -OH)(AlH ₂) ₂ -Et	6.6
F ₂ Al-Et	0.0	(μ -OH)(AlMe ₂) ₂ -Et	8.8
(Me)(NH ₃)Al-Et ⁺	-0.7	(μ -F)(AlMe ₂) ₂ -Et	8.3
	-1.1	(μ -NH)[AlMe(NH ₃)] ₂ -Et ⁺	6.8
	-7.5	(μ -OH) ₂ (AlH) ₂ -Et ⁺	-5.4

It should be noted here that the comparison of insertion with ethyl-to-ethene transfer does not give a direct measure of the actual propagation/chain transfer balance. Transfer from a longer chain than ethyl is always easier, because the product is a substituted (and therefore stabilized) olefin, and this is already felt in the transition state. Therefore, even the systems which here show the strongest preference for propagation (e.g. Me₂AlEt) have, after various corrections (basis set extension, entropy, ZPE, Et→Bu chain), only a modest preference for chain growth, corresponding to oligomerization rather than polymerization.

At aluminium, β -hydrogen transfer to unsaturated substrates appears to be a relatively facile reaction. This is true for transfer from alkyl to olefin in both mono- and dinuclear systems, as discussed in the present contribution; it also applies to transfer from alkyl to ketone (14) and from alcohol to ketone (Meerwein-Ponndorf-Verley reduction). In this respect, the main group metal Al differs markedly from transition metals, which more often have a definite preference for insertion. At present, we are unable to extract a trend from the model systems studied which would allow us to predict systems with a larger preference for propagation.

Conclusions

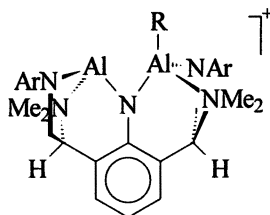
None of the Al-based polymerization systems reported in the literature are clearly well-defined, single-site catalysts, and for none of them has the nature of

the active species been unambiguously established. The substituent effects we calculate for the propagation/chain transfer balance indicate that, for mononuclear aluminium catalysts, it is not easy to do better than trialkylaluminium. Since experimentally several Al catalysts produce high molecular weights, one possibility is that polymerization there follows an unusual pathway, e.g. a dinuclear mechanism.

At least for aluminium, polymerization over two metal centres does not appear to be much more difficult than at a single metal centre. The spatial requirements for propagation and for chain transfer at a bimetallic species are rather different, resulting in a strong influence of the coordination environment on the propagation/chain transfer balance. Our results show that there are at least some binuclear species for which the balance favours propagation to a similar extent as in trialkylaluminium; in view of the large number of structures possible for binuclear systems, there might be some that actually have a better balance.

Of course, this does not constitute proof that any Al-based polymerization system actually involves the new dinuclear mechanism. However, the results do suggest that this possibility cannot be ruled out *a priori*.

As an elaborated version of $(\mu\text{-NH})[\text{AlMe}(\text{NH}_3)]_2\text{Et}^+$, the amide-bridged complex shown below or a related complex might be a "real" dinuclear polymerization catalyst. The challenge here would be to distinguish between a true dinuclear mechanism and one in which the chain grows at a single centre but can also (independently) move between metal centres.



References

1. Ziegler, K.; Gellert, H.-G. *Angew. Chem.* **1952**, *64*, 323. Ziegler, K.; Gellert, H.-G.; Zosel, K.; Holzkamp, E.; Schneider, J.; Söll, M.; Kroll, W.-R. *Justus Liebigs Ann. Chem.* **1960**, *629*, 121.
2. Martin, H.; Bretinger, H. *Makromol. Chem.* **1992**, *193*, 1283.
3. Coles, M.P.; Jordan, R.F. *J. Am. Chem. Soc.* **1997**, *119*, 8125; Dagorne, S.; Guzei, I.A.; Coles, M.P.; Jordan, R.F. *J. Am. Chem. Soc.* **2000**, *122*, 274.
4. Ihara, E.; Young Jr, V.G.; Jordan, R.F. *J. Am. Chem. Soc.* **1998**, *120*, 8277.

5. Kim, J.S.; Wojcinski II., L.M.; Liu, S.; Sworen, J.C.; Sen, A. *J. Am. Chem. Soc.* **2000**, *122*, 5668.
6. See e.g. ref 5: "as anticipated slight activity was exhibited by MAO".
7. Bruce, M.; Gibson, V.C.; Redshaw, C.; Solan, G.A.; White, A.J.P.; Willams, D.J. *J. Chem. Soc. Chem. Commun.* **1998**, 2523.
8. Here we mean a mechanism in which the chain switches metal in each insertion step, i.e. fundamentally different from the "standard" Cossee mechanism. We are not considering mechanisms in which a dimer is involved but where the polymerization still happens at a single metal centre according to the normal Cossee mechanism (see e.g. Meier, R.J.; Koglin, E. *J. Phys. Chem. A* **2001**, *105*, 3867), since in that case the second metal centre is just part of a larger, more complicated metalloligand.
9. There are clear similarities between our dinuclear insertion step and older proposals for chain growth between Ti and Al centers; see e.g. Natta, G.; Mazzanti, G. *Tetrahedron* **1960**, *8*, 86; Patat, P.; Sinn, H. *Angew. Chem.* **1958**, *70*, 496 and in particular Friedlander, H.N.; Resnick, W. *Adv. Pet. Chem. Refin.* **1958**, *1*, 526.
10. Talarico, G.; Budzelaar, P.H.M.; Gal, A.W. *J. Comp. Chem.* **2000**, *21*, 398; Talarico, G.; Budzelaar, P. H.M.; Barone, V.; Adamo, C. *Chem. Phys. Lett.* **2000**, *329*, 99; Talarico, G.; Budzelaar, P.H.M. *Organometallics* **2000**, *19*, 5691-5695; See also Reinhold, M.; McGrady, J.E.; Meier, R. *J. Chem. Soc. Dalton Trans.* **1999**, 484.
11. GAMESS-UK is a package of ab initio programs written by Guest, M.F.; Van Lenthe, J.H.; Kendrick, J.; Schoffel, K.; Sherwood, P. with contributions from Amos, R.D.; Buenker, R.J.; Van Dam, H.J.J.; Dupuis, M.; Handy, N.C.; Hillier, I.H.; Knowles, P.J.; Bonacic-Koutecky, V.; Von Niessen, W.; Harrison, R.J.; Rendell, A.P.; Saunders, V.R.; Stone, A.J.; De Vries, A.H.. The package is derived from the original GAMESS code due to Dupuis, M.; Spangler, D.; Wendoloski, J.: NRCC Software Catalog, Vol. 1, Program No. QG01 (GAMESS), 1980. DFT module by Young, P. under the auspices of EPSRC's Collaborative Computational Project No. 1 (CCP1) (1995-1997).
12. Frisch, M.J.; Trucks, G.W.; Schlegel, H.B.; Scuseria, G.E.; Robb, M.A.; Cheeseman, J.R.; Zakrzewski, V.G.; Montgomery, J.A. Jr., Stratmann, R.E.; Burant, J.C.; Dapprich, S.; Millam, J.M.; Daniels, A.D.; Kudin, K.N.; Strain, M.C.; Farkas, O.; Tomasi, J.; Barone, V.; Cossi, M.; Cammi, R.; Mennucci, B.; Pomelli, C.; Adamo, C.; Clifford, S.; Ochterski, J.; Petersson, G.A.; Ayala, P.Y.; Cui, Q.; Morokuma, K.; Malick, D.K.; Rabuck, A.D.; Raghavachari, K.; Foresman, J.B.; Cioslowski, J.; Ortiz, J.V.; Stefanov, B.B.; Liu, G.; Liashenko, A.; Piskorz, P.; Komaromi, I.; Gomperts, R.; Martin, R.L.; Fox, D.J.; Keith, T.; Al-Laham, M.A.; Peng, C.Y.; Nanayakkara, A.; Gonzalez, C.; Challacombe, M.; Gill, P.M.W.; Johnson,

- B.; Chen, W.; Wong, M.W.; Andres, J.L.; Gonzalez, C.; Head-Gordon, M.; Replogle, E.S.; and Pople, J.A., Gaussian, Inc., Pittsburgh PA, 1998.
13. Lorenz, J.C.W.; Woo, T.K.; Ziegler, T. *J. Am. Chem. Soc.* **1995**, *117*, 12793; Lorenz, J.C.W.; Woo, T.K.; Fan, L.; Ziegler, T. *J. Organomet. Chem.* **1995**, *497*, 91.
14. See e.g. Korolev, A.V.; Guzei, I.A.; Jordan, R.F. *J. Am. Chem. Soc.* **1999**, *121*, 11605.

Chapter 11

Nanostructural Element Modifications: Synthesis and Structure of Elementoid Gallium Clusters

Hansgeorg Schnöckel and Andreas Schnepf

Institute of Inorganic Chemistry, University of Karlsruhe, Engesserstrasse 15,
76128 Karlsruhe, Germany

The development of a novel technique – the cocondensation of the high temperature species GaX (X = halogen) together with a suitable solvent – was the basis for the synthesis of new types of metalloid clusters. Metalloid Ga – clusters, containing up to 84 Ga atoms were structurally characterized. The arrangement of the Ga atoms within the clusters exhibit strong similarities to one of the six allotropes of gallium. Therefore we introduced the more precise adjective *elementoid* for these metalloid clusters. This idea of bonding and structure is demonstrated by comparing the topology and atomic volume for the clusters and the corresponding allotrope.

Recently, a rapid development in the chemistry of gallium and aluminum compounds has been observed, mostly manifesting itself in the formation of new GaGa or AlAl bonds (1). Only Ga compounds are discussed here, of which there are two types. One compound type features unexpected multiple bonding (2) (c.f. chapter 1.6). In the second type Ga_n cluster compounds are formed, which will be the main concern of this article. Only molecular species will be discussed. The interesting Zintl-like species (3), which, with their highly negative charge, are stabilized in a „bath“ of positive alkaline metal cations with the help of lattice energy, will be omitted. The rapid development in all areas

far is best demonstrated by the fact that the first report of a molecular compound containing a direct GaGa bond stabilized by organic ligands (R_2GaGaR_2) came to light no longer than 12 years ago (4).

The basis for the renaissance of this chemistry which mostly deals with extremely sensitive compounds (e. g. to O_2 , H_2O , temperature) is the availability of suitable methods for their preparation. In principle, three routes were applied:

- Reduction of R_2GaX and $RGaX_2$ compounds with the help of alkaline metals (5, 6, 7).
- Reaction with solid "GaI" (8, 9, 10).
- Reaction with a metastable GaX solution ($X = Cl, Br, I$) (11).

The majority of Ga_n compounds which were synthesized recently applying one of these three methods are summarized in Table 1.

Table I. Ga_nR_m cluster compounds

Ga_nR_m	$R/D =$	Reference	Ga_nR_m	$R/D =$	Reference
$[Ga_3R_4]^*$	Si^iBu_3	7	$Ga_6R_8^{2-}$	$SiPh_2Me$	21
$[Ga_3R_4]^-$	Si^iBu_3	7	$Ga_8I_8D_6$	PEt_3	22
$[Ga_3R_3]^{2-}$	$2,6-C_6H_3Mes_2$	12	$[Ga_8R_8]^{2-}$	$C_{13}H_9$	23
$Ga_3I_5D_3$	PEt_3	9	$[Ga_8R_6]$	$C(SiMe_3)_3$	24
Ga_4R_4	$C(SiMe_3)_3$	13	$[Ga_9R_6]^-$	$Si(SiMe_3)_3$	10
	$C(SiMe_2Et)_3$	13	$Ga_{10}R_6$	$Si(SiMe_3)_3$	25
	$Si(SiMe_3)_3$	14	$[Ga_{10}R_6]^-$	Si^iBu_3	25
	$Ge(SiMe_3)_3$	14	$[Ga_{12}R_{10}]^{2-}$	$C_{13}H_9$	26
	Si^iBu_3	15	$[Ga_{13}R_6]^-$	Si^iBu_3	25
Ga_4R_6	$2,4,6-C_6H_2^iPr_3$	16	$Ga_{18}R_8$	Si^iBu_3	27
$[Ga_4R_6]^{2-}$	$2,4,6-C_6H_2^iPr_3$	16	$[Ga_{19}R_6]^-$	$C(SiMe_3)_3$	28
$[Ga_4R_2]^{2-}$	$2,6-C_6H_3Tip_2$	17	$Ga_{22}R_8$	Si^iBu_3	27
$[Ga_4R_4]^{2-}$	Si^iBu_3	18		$Si(SiMe_3)_3$	29
$[Ga_4I_3R_4]^-$	$Si(SiMe_3)_3$	10		$Ge(SiMe_3)_3$	30
$Ga_5Cl_7D_5$	Et_2O	19	$[Ga_{26}R_8]^{2-}$	$Si(SiMe_3)_3$	31
$(GaR)_6$	Cp^*	20	$[Ga_{84}R_{20}]^{4-}$	$(Me_3Si)_2N$	32

Here we will concentrate on those cluster compounds which have been prepared with the aid of a metastable GaX solution (c). Their generation has been described in detail before (1,11). In principle, GaX gas is quenched from ca. $1000^\circ C$ to $-196^\circ C$ together with a suitable solvent (e.g. toluene and a donor component resulting a metastable GaX solution which can be handled –

depending on the donor applied – up to room temperature without disproportionation ($3 \text{ GaX} \rightarrow 2 \text{ Ga} + \text{GaX}_3$), which is the thermodynamically favored process.

Under suitable conditions, intermediates can be trapped on the way from the GaX species towards elemental gallium, i. e. from Ga(I) to Ga(0). We have named these intermediates metalloid (1, 28) or, more generally, elementoid clusters (21). This new name is intended to distinguish these clusters from a broader classification by Cotton (33) in which non-metals are allowed in the cluster core. The name is also meant to emphasize that the topologies of metalloid (elementoid) clusters reflect the atomic arrangement within the metals (elements)ⁱ. In the following discussion the name elementoid and metalloid are used synonymously. For elemental Ga this view seems to be especially attractive, since so far four allotropes at normal pressure (α , β , γ , δ) and two high pressure allotropes (GaII, GaIII) have been described, which we have discussed in detail recently (1). In the following review we will point out that by variation of the preparation parameters, elementoid Ga_n clusters can be made which indeed reflect the formation principles of atoms within the arrangements of most of the above mentioned Ga allotropes. This means that just these arrangements of Ga atoms within the allotropes seem also to be stable arrangements favorable for molecular clusters. This relation will be explained with the help of the following examples.

1. Elementoid Ga-clusters

1.1 $[\text{Ga}_6(\text{SiPh}_2\text{Me})_8]^{2-} \cdot 2[\text{Li}(\text{THF})_4]^+$ (21)

The Ga₆R₈²⁻ anion **1** (R = SiPh₂Me) is the smallest Ga cluster, which due to its structure may be called a metalloid cluster (Figure 1). The six Ga atoms of the central Ga₆ moiety of **1** are arranged in a planar and rhomboid way (C_{2h} symmetry). Four of the six Ga atoms bear two ligands each; the remaining two Ga atoms are exclusively bonded to other Ga atoms [$d(\text{GaGa}) = 275 \text{ pm}$]. The other GaGa bonds within the gallium core range from 247 to 290 pm. At a first glance, this arrangement of metal atoms within the cluster core seems unusual, because for an alternatively formed Ga₆R₆²⁻ cluster ($\text{Ga}_6\text{R}_8^{2-} \rightarrow \text{Ga}_6\text{R}_6^{2-} + \text{R}_2$, s.b.) an octahedral structure would be expected. In contrast, a planar arrangement of the Ga atom is observed for **1** having similarities to a section of the β -Ga allotrope (Figure 1). As expected, the Ga-Ga distances in β -gallium are

ⁱ The suffix *-oid* is deduced from the Greek εἶδος which means idea, prototype.

larger than those of **1** since for the former one the coordination numbers are higher and the oxidation numbers are smaller, hence the radius of the Ga atoms increases. The same relation is valid for all other metalloids clusters, which will be compared in the following chapters to the solid state structures of the corresponding Ga allotropes.

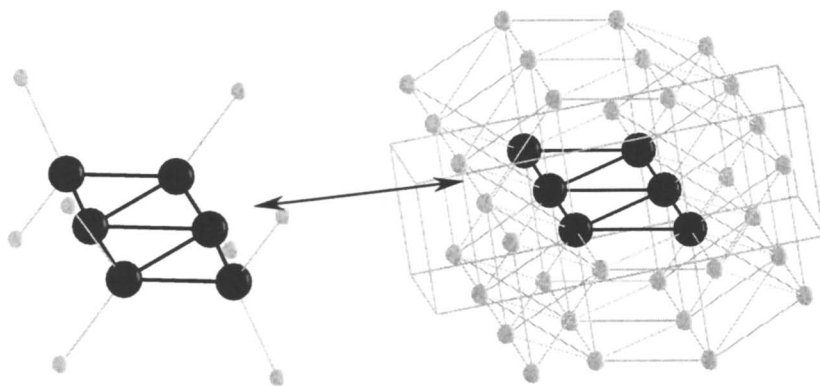
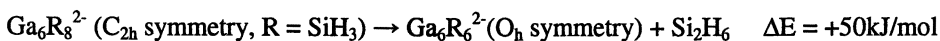


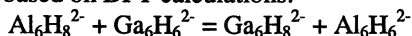
Figure 1: Molecular structure of $[Ga_6(SiPh_2)_8]^{2-}$ **1** (methyl and phenyl groups are omitted for clarity) and highlighted substructure in β -gallium.

With the help of DFT calculations it could also be demonstrated that the elementoid C_{2h} structure for $Ga_6R_8^{2-}$ units is favored, in opposition to an expected octahedral arrangement. (1)



On the other hand, calculations for the similar B and Al clusters ($R = SiH_3$) demonstrate that in both cases the octahedral $M_6R_6^{2-}$ species are favored [-135 kJ/mol ($B_6R_6^{2-}$) and -32 kJ/mol ($Al_6R_6^{2-}$)]. Thus only the gallium cluster **1** violates Wade's rules (34) and adopts a structure which resembles the Ga-Ga connections of β -gallium.ⁱⁱ (35)

ⁱⁱ Furthermore, the higher stability of $Ga_6H_8^{2-}$ (C_{2h}) and $Al_6H_6^{2-}$ (O_h) in contrast to $Al_6H_8^{2-}$ (C_{2h}) and $Ga_6H_6^{2-}$ (O_h) is obvious from the following exothermic reaction (-94 kJ/mol) based on DFT calculations:



1.2 $\text{Ga}_{12}(\text{C}_{13}\text{H}_9)_{10}^{2-} \cdot 2[\text{Li}(\text{THF})_4]^+$ (26)

The metalloid cluster anion $\text{Ga}_{12}\text{R}_{10}^{2-}$ (R = fluorenyl) **2** (Figure 2) exhibits a distorted icosahedral structure with relatively short GaGa distances within the Ga_5 rings (259 pm) as well as between the Ga_5 rings and the “naked” Ga atoms (265 pm). The distance between these two “naked” Ga atoms amounts to 527 pm.

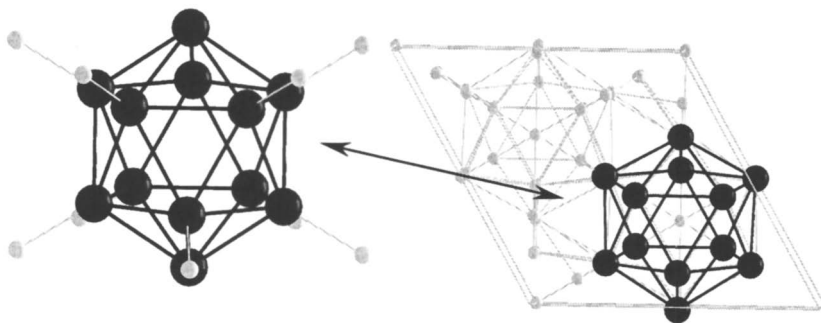


Figure 2: Molecular structure of $[\text{Ga}_{12}(\text{C}_{13}\text{H}_9)_{10}]^{2-}$ (of the fluorenyl ligands only the C atom directly bounded to the Ga atoms are shown for the sake of clarity) and highlighted substructure in δ -gallium

At a first glance, **2** is reminiscent of a classical icosahedral species like e. g. $\text{B}_{12}\text{H}_{12}^{2-}$, for which bonding follows Wade’s rules. A closer look, however, reveals that a structure like the one observed for **2** does not follow Wade’s rules, which predict a *nido* structure ($2n + 4$ electrons). Indeed, DFT calculations for the model compound $\text{G}_{12}\text{R}_{10}^{2-}$ (R = CH_3) confirm that Wade’s rules are not a suitable model to describe bonding for **2** (23, 26). On the other hand, the following view seems to be more adequate: After removal of two R’ substituents a hypothetical Ga_{12}R_8 species containing the same oxidation number as for the Ga atoms in **2** is formed. Such M_{12}R_8 species are indeed obtained for In (36) and Al (37) in which the metal atom core corresponds – although slightly distorted – to the closest packing of the metals. Since elemental Ga is not able to form a closest packing, a different structure is formed via addition of two R’ ligands which corresponds to the topology of δ -gallium (Figure 2). Therefore **2** should be called an elementoid cluster with respect to δ -Ga.

1.3 Ga₁₈(Si^tBu₃)₈ **3** (27)

Figure 3 shows that the arrangement of Ga atoms in **3** may be described as a section of the β-Ga allotrope. The cluster core of **3** is shielded by eight ligands and the eight ligand bearing Ga atoms form a strongly distorted square (quadratic) antiprism. Thus, **3** may be called an elementoid cluster with respect to β-Ga. A more sophisticated confirmation of this type of description will be presented in the next chapter.

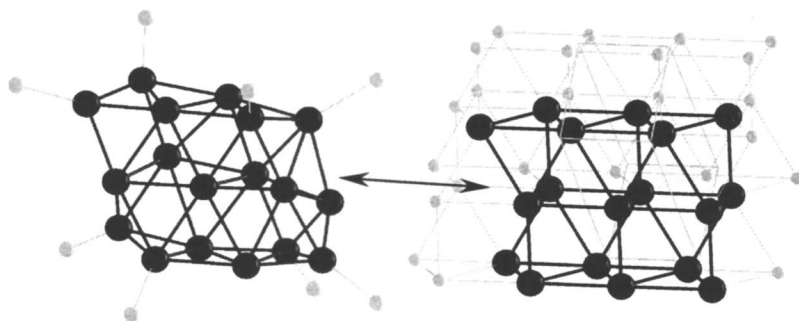


Figure 3: Molecular structure of Ga₁₈(Si^tBu₃)₈ (the ^tBu groups are omitted for the sake of presentation) and highlighted substructure in β-gallium

1.4 Ga₂₂R₈ [R = Si(SiMe₃)₃, **4a** (29); Ge(SiMe₃)₃, **4b** (30); Si^tBu₃, **4** (27)]

There are three known examples of metalloids clusters with the composition Ga₂₂R₈ (**4**, **4a**, **4b**). The cluster core of these three clusters is almost identical and can be described as follows: The central Ga atom is surrounded in a relatively long distance by a shell of 13 other Ga atoms (medium distance dGaGa = 294.2 pm). On the surface of the shell, eight Ga₄ planes are formed and each of these surfaces is capped by a GaR moiety. This unusual arrangement of Ga atoms within the cluster core of **4** can be described as a section of the Ga(III) high-pressure allotropeⁱⁱⁱ (Figure 4).

ⁱⁱⁱ More similar to Ga(III) is a Ga₁₈(GaR)₈²⁻ cluster anion **5** [R = Si(SiMe₃)₃] which can be prepared under special conditions starting from solid GaI (**31**)

The Ga_{14} core is surrounded by a distorted quadratic antiprism of 8 Ga atoms each bearing one cluster protecting ligand R. This shell containing 8 Ga atoms is similar to the one observed for the metalloid cluster **3**. However, in **3** there are 10 Ga atoms in this shell whereas 14 Ga atoms are in the same shell of **4**. Consequently, in comparison to **3** there is a higher “density” of the Ga atoms in **4** which is also reflected in the arrangement of the Ga atoms: the arrangements of Ga atoms in **3** and **4** correspond to topologies observed in the normal-pressure β -gallium (**3**) and in the high-pressure allotrope Ga(III) (**4**).

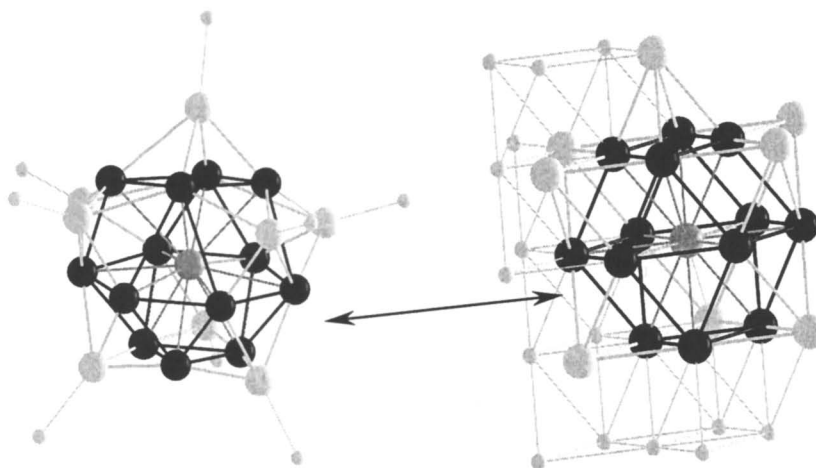


*Figure 4: Molecular structure of Ga_{22}R_8 [$\text{R} = \text{Si}(\text{SiMe}_3)_3$, **4a**; $\text{Ge}(\text{SiMe}_3)_3$, **4b**; Si^iBu_3 , **4**] (from the ligands only the atom directly bounded to the Ga atoms of the cluster core are shown to ease the presentation) and highlighted substructure in Ga(III)*

The close correlation between the topologies of the Ga atoms in **3** and **4** with $\text{R} = \text{Si}^i\text{Bu}_3$ for both cases with the structures of the β -Ga and Ga(III) allotropes can also be rationalized from their atomic volumes. The calculated atomic volume as deduced from BP(SVP) single point calculations using the COSMO solution model (27) is reduced in the direction from the metalloid clusters **3** to **4** by 4.7%.

A similar contraction of the atomic volume by 5.1% is observed for the transition from β -gallium to Ga(III). The less bulky Si(SiMe₃)₃ ligand in comparison to Si^tBu₃ evidently leads to a somewhat larger [Ga₈R'₈] cage and, therefore, to a pair of clusters Ga₁₄(GaR)₈ and [Ga₁₈(GaR)₈]²⁻ **5**, which are richer in gallium.

These correlations show that, based on the different Ga allotropes, a great variety of elementoid Ga clusters can be expected. The formation of a certain cluster type depends on the properties of the ligand as well as on the chemical conditions, which can be varied for the same reaction to give either **3** or a mixture of **4** and **3** (27).

Obviously there is a correlation between the average atomic volume within a certain Ga-cluster (e.g. **3** and **4**) (obtained via single point calculation on the basis of the measured geometry) and the atomic volume of the Ga allotrope which exhibits a similar topology. However, the correlation is between the relative volumes of the clusters and the relative volumes of the allotropes, not their absolute volumes. The discrepancies between the absolute volumes of the clusters and their corresponding allotropes could be an artifact of how these values are determined since the atomic volumes of the Ga-atoms in the allotropes are only based on experimental data while the atomic volumes in the clusters is derived from experimental geometries and from additional quantum chemical calculations.

1.5 [Ga₁₉(CSiMe₃)₆]⁻[Li₂Br(THF)₆]⁺ (28)

The Ga cluster anion Ga₁₉R₆⁻ [R = C(SiMe₃)₃] **6** is the smallest shell-structured metalloid gallium cluster prepared so far. The 19 Ga atoms are arranged within three sandwiched Ga₆ rings with the central planar ring containing the central Ga atom (Figure 5). The upper and lower Ga₆ rings are folded and contain 3 ligand-bearing Ga atoms each. The distances from the central Ga atom to the “naked” six Ga atoms in the central planar ring amount to 274 pm whereas there are longer distances of 295 pm to the three upper and three lower Ga atoms, completing the geometry of the distorted anticuboctahedron of “naked” Ga atoms.

A closer inspection shows that the structure of the shell of 12 “naked” Ga atoms is between an anticuboctahedron and an icosahedron similar to the situation within the first sphere of the Al₇₇R₂₀²⁻ - cluster (38). Anyway there is a coordination number of 12 (6+6) for the central Ga atom.

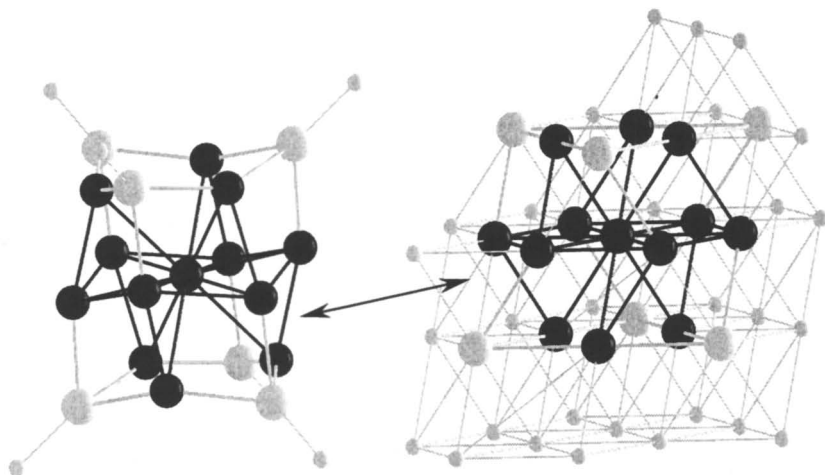


*Figure 5: Molecular structure of $[Ga_{19}(CSiMe_3)_6]$ **6** (the $SiMe_3$ groups are omitted for the sake of clarity) and highlighted substructure in Ga(III)*

As a consequence of the high steric demand of the $C(SiMe_3)_3$ ligands a large sphere of 6 GaR moieties is formed which provides enough space for the 14 Ga atoms arranged as in **6**. This description is confirmed by DFT calculations of the atomic volume of the Ga_{19} moiety (35); the average atomic volume of the Ga_{19} core of **6** is about 5.5% larger than that of the Ga_{22} core of **4**.^{iv} Since in **4** the arrangement of Ga atoms is similar to the topology of Ga(III) (Figure 5), it can be expected that the topology of a hypothetical allotrope with an atomic arrangement like in **6** should result in an atomic volume about 5.5% larger than that of Ga(III), i. e. the hypothetical allotrope should have an atomic volume similar to that of the normal-pressure allotropes β , γ or δ – Ga. However, at normal pressure no Ga allotrope with the coordination number of 12 typical for metals has been observed so far.

^{iv} An experimental confirmation of increasing GaGa distances is influenced by the steric demand of the $C(SiMe_3)_3$ ligand already provided by the first Ga_4R_4 [$R = C(SiMe_3)_3$] cluster (**13**), which exhibits the longest GaGa distances of all Ga_4R_4 clusters prepared so far.

1.6 $[Ga_{84}\{N(SiMe_3)_2\}_{20}]^{4-} \cdot 2[Li(THF)_4]^+ \cdot 2[Li_2Br(THF)_6]^+ \cdot 2 \text{ toluene}$ (32)

With respect to the “naked” metal atoms the metalloid cluster anion $Ga_{84}R_{20}^{4-}$ [$R = N(SiMe_3)_2$] **7** represents the largest metalloid cluster which has been structurally characterized^v. A detailed description of this cluster has already been given (1, 32). Here we will focus on two aspects which demonstrate that in **7** too, there are Ga_n moieties which are similar to certain Ga allotropes.

The center of **7** hosts a Ga_2 unit – a unique situation in the whole field of metal cluster chemistry – exhibiting a short GaGa distance of 233.5 pm. This distance is nearly as short as the so-called GaGa triple bond of 232 pm in $Ga_2R_2^{2-}$ (40) [$R = (2,4,6\text{-}iPr_3C_6H_2)_2C_6H_3$].^{vi} However, the GaGa distance in the typical Ga_2 moiety of α -gallium is 244.8 pm, as a consequence of the higher coordination number (7 instead of 5 in **7**). That means, for the first time the central Ga_2 unit in **7** represents a small but typical section of the thermodynamically stable α -allotrope (Figure 6).

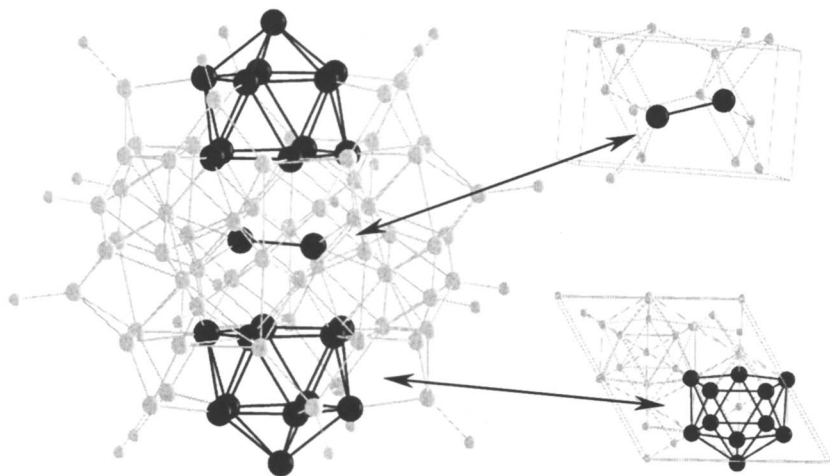


Figure 6: Molecular structure of $[Ga_{84}\{N(SiMe_3)_2\}_{20}]^{4-}$ **7** (the $SiMe_3$ groups are omitted for clarity) and highlighted substructures in δ - and α -gallium.

^v A $Pd_{145}(CO)_{60}(PEt_3)_{30}$ cluster, published recently, contains 55 “naked” Pd atoms (39).

^{vi} In this field there is a controversy about the so called triple bond in $RGaR^{2-}$ species, which, on the basis of the experimentally observed weak bonding (stretching force constant), should more precisely called a special type of a 6e2c bonding (41).

Furthermore, there are two Ga_{11} moieties of **7** which show a strong relationship to δ -gallium (Figure 6). Not only is the icosahedral arrangement of the Ga_{11} units similar to δ -Ga, as within **2**, but also the GaGa distances are similar to δ -Ga, unlike **2**. This greater similarity of **7** with elemental δ -Ga relative to **2** may be the consequence of their different formal oxidation state (0.19 for **7** and 0.66 for **2**). The formal oxidation state of **7** is much closer to the value of zero for elemental Ga. Apart from its topology, the metallic properties of **7** also hint at the similarity of metalloid clusters like **7** with elemental gallium. For example the single crystals of **7** show a metallic reflection like the bulk metal. Furthermore, electrical conductivity measurements on single crystals of **7** confirm that it is semiconducting in the range from -30°C to $+70^\circ\text{C}$ with a very small bandgap of 0.03 eV, consistent with the cluster's intermediacy between a molecular species and the bulk metal. At 7 K a transition to a superconducting phase is observed. The experimental upper critical field ($B_{c2} = 13$ T) is in a similar range as that of the high-temperature superconductors (42). This unexpected and so far unexplained physical property demonstrates impressingly that the synthesis and characterization of crystalline, nanostructured metalloid clusters – the diameter of the Ga_{84} cluster core is 1.4 nm – provides well-based possibilities to improve the knowledge of fundamental relationships between bulk metallic materials and nanoscaled molecular species.

2. Conclusions

For elemental Ga six allotropes have been characterized so far which exhibit a great variety of GaGa bonding between molecular and metallic bonds. Therefore, it is not surprising that for the metalloid (elementoid) Ga clusters, as intermediates on the way to the metal (element), a large variety of bonding motifs are also observed. This possibility to form different cluster types may increase if, as shown for **7**, structural moieties of different allotropes are present in the same cluster. Therefore, the prediction of any new Ga cluster is almost impossible. On the other hand, new structural motifs in Ga clusters may predict Ga allotropes that are as yet unknown. Since the bonding motifs for the connectivity in the different Ga allotropes are reflected in most of the Ga clusters discussed here, the term *elementoid cluster* as a generic term for metalloid clusters seems appropriate. In a more general, simplified way these elementoid clusters may be regarded as molecular nanostructural modifications (allotropes).

Furthermore, the structural variety of the elementoid Ga clusters shows that the classification according to the Wade-Mingos rules, which originally were developed for similar boron compounds, is not applicable for these Ga clusters.

The difficulty applying a single set of rules, such as the Wade-Mingos rules to even isovalent elements is seen in nature from the different number of allotropes found for Al (1), B (4) and Ga (6).

Through a combination of fundamental chemistry and the physics of diatomic high-temperature molecules (e. g. matrix isolation (11)), novel cluster compounds in the nano-metric scale could be prepared and structurally analyzed. In this way it is possible to develop an understanding of the bonding in intermediates during metal formation and solvation and possibly the mechanism of this fundamental reaction, which is not understood so far even though it is one of the oldest processes in the universe. Based on the unexpected properties of these clusters (e. g. the superconductivity of 7) an increasing interest in these kinds of clusters and their potential applications is expected in the future.

Acknowledgements

We thank the Deutsche Forschungsgemeinschaft and the Fonds der Chemischen Industrie for financial support and Dr. H. J. Himmel for discussions.

References

-
- 1 Schnöckel, H.; Schnepf, A. *Advances in Organometallic Chemistry*, **2001**, 47, 235.
 - 2 King, R. B.; Robinson, G. H. *J. Organomet. Chem.* **2000**, 597, 54.
 - 3 Corbett, J. D. *Angew. Chem.* **2000**, 112, 682; *Angew. Chem. Int. Ed.* **2000**, 39, 692.
 - 4 Uhl, W.; Layh, M.; Hildebrand, T. *J. Organomet. Chem.* **1989**, 364, 289.
 - 5 Uhl, W. *Angew. Chem.* **1993**, 105, 1449; *Angew. Chem. Int. Ed. Engl.* **1993**, 32, 1386.
 - 6 Uhl, W. *Coord. Chem. Rev.* **1997**, 163, 1.
 - 7 Wiberg, N.; Blank, T.; Amelunxen, K.; Nöth, H.; Knizek, J.; Habereeder, T.; Kaim, W.; Wanner, M. *Eur. J. Inorg. Chem.* **2001**, 1719.
 - 8 Green, M. L. H.; Mountford, P.; Smout, G.; Speel, S. *Polyhedron*, **1990**, 22, 2763.
 - 9 Schnepf, A.; Doriat, C.; Möllhausen, E.; Schnöckel, H. *Chem. Commun.* **1997**, 21, 2111.

- 10 Köstler, W.; Linti, G. *Angew. Chem.* **1997**, *109*, 2758; *Angew. Chem., Int. Ed.* **1997**, *36*, 2644.
- 11 Dohmeier, C.; Loos, D.; Schnöckel, H. *Angew. Chem.*, **1996**, *108*, 141; *Angew. Chem. Int. Ed. Engl.*, **1996**, *35*, 129.
- 12 Li, X.-W.; Pennington, W. T.; Robinson, G. H. *J. Am. Chem. Soc.* **1995**, *117*, 7578; Li, X.-W.; Xie, Y.; Schreiner, P. R.; Gripper, K. D.; Crittendon, R. C.; Campana, C. F.; Schaefer, H. F.; Robinson, G. H. *Organometallics* **1996**, *15*, 3798.
- 13 Uhl, W.; Hiller, V.; Layh, M.; Schwarz, W. *Angew. Chem.* **1992**, *104*, 1378; *Angew. Chem. Int. Ed. Engl.* **1992**, *31*, 1364; Uhl, W.; Jantschak, A. *J. Organomet. Chem.* **1998**, *555*, 263.
- 14 Linti, G. *J. Organomet. Chem.* **1996**, *520*, 107; Linti, G.; Rodig, A. *Chem. Commun.* **2000**, 127.
- 15 Wiberg, N.; Amelunxen, K.; Lerner, H.-W.; Nöth, H.; Ponikwar, W.; Schwenk, H. *J. Organomet. Chem.* **1999**, *574*, 246.
- 16 Wehmschulte, R. J.; Power, P. P. *Angew. Chem.* **1998**, *110*, 3344; *Angew. Chem., Int. Ed.* **1998**, *37*, 3154.
- 17 Twamley, B.; Power, P. P. *Angew. Chem.* **2000**, *112*, 3643; *Angew. Chem., Int. Ed.* **2000**, *39*, 3500.
- 18 Wiberg, N.; Blank, T.; Westerhausen, M.; Schneiderbauer, S.; Krossing, I.; Schnepf, A.; Schnöckel, H. *Organometallics* **2001** accepted for publication.
- 19 Loos, D.; Schnöckel, H.; Fenske, D. *Angew. Chem.* **1993**, *105*, 1124; *Angew. Chem. Int. Ed.* **1993**, *32*, 1059.
- 20 Loos, D.; Baum, E.; Ecker, A.; Schnöckel, H.; Downs, A. J. *Angew. Chem.* **1997**, *109*, 854; *Angew. Chem., Int. Ed.* **1997**, *36*, 860.
- 21 Donchev, A.; Schnepf, A.; Baum, E.; Stöber, G.; Schnöckel, H. *Z. Anorg. Allg. Chem.* **2001** accepted for publication.
- 22 Doriat, C.; Friesen, M.; Baum, M.; Ecker, A.; Schnöckel, H. *Angew. Chem.* **1997**, *109*, 2057; *Angew. Chem., Int. Ed.* **1997**, *36*, 1969.
- 23 Schnepf, A.; Stöber, G.; Schnöckel, H. *Z. Anorg. Allg. Chem.* **2000**, *626*, 1676.
- 24 Schnepf, A.; Köppe, R.; Schnöckel, H. *Angew. Chem.* **2001**, *113*, 1287; *Angew. Chem. Int. Ed.* **2001**, *40*, 1241.
- 25 Kehrwald, M.; Köstler, W.; Rodig, A.; Linti, G.; Blank, T.; Wiberg, N. *Organometallics* **2001**, in press.
- 26 Schnepf, A.; Stöber, G.; Köppe, R.; Schnöckel, H. *Angew. Chem.* **2000**, *112*, 1709; *Angew. Chem. Int. Ed.*, **2000**, *39*, 1637
- 27 Donchev, A.; Schnepf, A.; Stöber, G.; Baum, E.; Schnöckel, H.; Blank, T.; Wiberg, N. *Chemistry* **2001**, *7*, 3348.
- 28 Schnepf, A.; Stöber, G.; Schnöckel, H. *J. Am. Chem. Soc.* **2000**, *122*, 9178

-
- 29 Schnepf, A.; Weckert, E.; Linti, G.; Schnöckel, H. *Angew. Chem.* **1999**, *111*, 3578; *Angew. Chem., Int. Ed.* **1999**, *38*, 3381.
 - 30 Linti, G.; Rodig, A. *Chem. Commun.* **2000**, 127
 - 31 Rodig, A.; Linti, G. *Angew. Chem.* **2000**, *112*, 3076; *Angew. Chem., Int. Ed.* **2000**, *39*, 2952
 - 32 Schnepf, A.; Schnöckel, H. *Angew. Chem.* **2001**, *113*, 734; *Angew. Chem. Int. Ed.* **2001**, *40*, 711.
 - 33 Cotton, F. A. *Quart. Rev. Chem. Soc.*, **1966**, *20*, 397.
 - 34 Wade, K. *Adv. Inorg. Chem. Radiochem.* **1976**, *18*, 1; Mingos, D. M. P. *Nature*, **1972**, *336*, 99; Mingos, D. M. P. *Acc. Chem. Res.* **1984**, *17*, 311.
 - 35 Stöber, G.; Schnöckel, H. unpublished results.
 - 36 Wiberg, N.; Blank, T.; Nöth, H.; Ponikvar, W. *Angew. Chem.*, **1999**, *111*, 887; *Angew. Chem. Int. Ed. Engl.*, **1999**, *38*, 839.
 - 37 Purath, A.; Köppe, R.; Schnöckel, H. *Chem. Commun.*, **1999**, 1933.
 - 38 Ecker, A.; Weckert, E.; Schnöckel, H. *Nature*, **1997**, *387*, 379.
 - 39 Tran, N. T.; Powell, D. R.; Dahl, L. F. *Angew. Chem.* **2000**, *112*, 4287 *Angew. Chem. Int. Ed.* **2000**, *39*, 4121.
 - 40 Su, J.; Li, X.-W.; Crittendon, R. C.; Robinson, G. H. *J. Am. Chem. Soc.* **1997**, *119*, 5471.
 - 41 Linti, G. Schnöckel, H. *Coord. Chem. Review*, **2000**, *206*, 285; Köppe, R.; Schnöckel, H. *Z. Anorg. Allg. Chem.* **2000**, *626*, 1095.
 - 42 Hagel, J.; Kelemen, M. T.; Fischer, G.; Pilawa, B.; Wosnitza, J.; Dormann, E.; v. Löhneysen, H.; Schnepf, A.; Schnöckel, H.; Neisel, U.; Beck, J. *Euro. Phys. Lett.* submitted for publication.

Chapter 12

The Design, Syntheses, and Application of Group 13 Molecular and Polymeric Precursors to Advanced Ceramics

Mark J. Pender, Kersten M. Forsthoefel, and Larry G. Sneddon*

Department of Chemistry, University of Pennsylvania,
Philadelphia, PA 19104-6323

New decaborane-based single-source molecular and polymeric precursors to boron carbide have been developed that enable the formation of boron carbide and boron-carbide/silicon-carbide composites in processed forms, including nanostructured materials.

The development of efficient methods for the production of complex structural and electronic materials in usable forms with controlled structures, orders and porosities is one of the most important problems of modern solid state chemistry and materials science. The chemical precursor approach, in which a polymeric or molecular precursor is first formed into the desired shape and then decomposed to the final solid-state material with retention of this shape, has been shown to be an important new route for producing many ceramics in a wide range of processed forms and sizes (1). In our work, we have successfully employed this approach to design new processable precursors to technologically important boron- and silicon-nitride ceramic materials, including: (1) the polyborazylene precursor to boron nitride (2); (2) borazine-modified hydridopolysilazane (3) and borazine-silazane copolymer (4)

precursors to SiNCB ceramics; (3) second-generation dipentylamine-polyborazylene (5) and pinacolborane-hydridopolysilazane (6) polymeric precursors to BN and SiNCB ceramic fibers (7); and (4) precursors to both metal-boronitrides (8,9) and metal-borides (10).

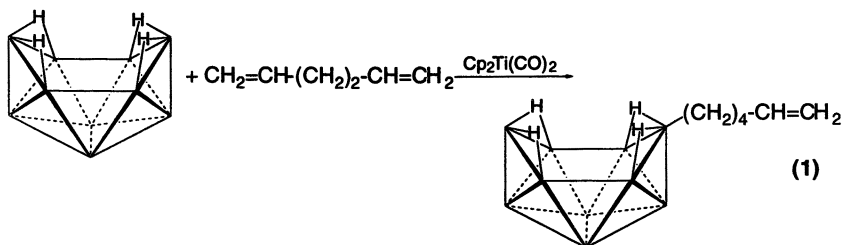
As described in the following sections, our most recent work has focused on the design of new single-source precursors to boron-carbide and boron-carbide/silicon-carbide composites that allow the formation of these ceramics in technologically important processed forms, including films, fibers and nanostructured materials.

Single-Source Boron Carbide and Boron-Carbide/Silicon-Carbide Precursors

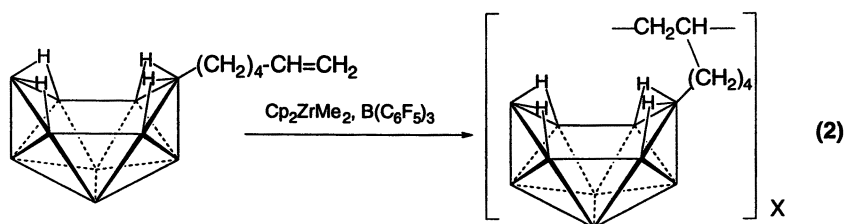
Boron carbide is a highly refractory material that is of great interest for both its structural and electronic properties (11). Of particular importance are its high-temperature stability, high hardness, high cross-section for neutron capture, and excellent high-temperature thermoelectric properties (12). This combination of properties gives rise to numerous applications, including uses as an abrasive wear-resistant material, ceramic armor, a neutron moderator in nuclear reactors, and, potentially, for power generation in deep space flight applications. Boron carbide is normally represented by a B_4C ($B_{12}C_3$) composition with a structure based on $B_{11}C$ icosahedra and C-B-C intericosahedral chains. However, single-phase boron carbides are also known with carbon concentrations ranging from 8.8 to 20 at%. This range of concentrations is made possible by the substitution of boron and carbon atoms for one another within both the icosahedra and the three-atom chains.

While boron carbide powders are easily made by the direct reaction of the elements at high temperatures, new synthetic methods that allow the formation of pure boron carbide in processed forms still need to be developed. Several investigations have found that boron carbide is indeed formed upon the pyrolysis of boron-based polymers suggesting that an efficient polymer-based route is possible. For example, Seyferth showed that pyrolysis of decaborane-diamine and -diphosphine polymers gave BN and BP, respectively, mixed with B_4C and carbon (13). Likewise, we showed (14) that pyrolysis of decaborane-dicyanopentane polymers yields predominately B_4C with a minor BN component (11). We also found that, upon pyrolysis, polyvinylpentaborane yields pure B_4C with high ceramic yields; however, due to the thermolytic and hydrolytic instability of this polymer, it has no significant technological potential. Thus, new efficient polymeric precursors to B_4C are needed that both give pure materials and have sufficient hydrolytic and thermal stabilities to enable processing.

We have now achieved the synthesis of the first decaborane-based polyolefin polymer, polyhexenyldecaborane, and demonstrated that it is, indeed, an excellent precursor to boron carbide in processed forms (15). The synthesis of the monomeric building block, 6-hexenyl-decaborane, that was needed for the construction of the polymer was made possible by our discovery of a new metal-catalyzed method (Eq. 1), involving the $\text{Cp}_2\text{Ti}(\text{CO})_2$ catalyzed reaction of hexadiene with decaborane (16).



The 6-hexenyl-decaborane monomer is isolated in high yield (>90%) as an air stable liquid. Polymerization of the compound was then achieved (Eq. 2) by employing the $\text{Cp}_2\text{ZrMe}_2/\text{B}(\text{C}_6\text{F}_5)_3$ catalyst system (17) to yield white polymeric materials which are both air stable for extended periods, and highly soluble in organic solvents.



The spectroscopic data for the polyhexenyldecaborane polymers are in excellent agreement with the inorganic/organic hybrid structure proposed in Eq. 2, consisting of a polyolefin-backbone with pendant decaboranes. The polymer Tgs are in the 50-60°C range and the TGA study in Figure 1 showed that polymer decomposition does not begin until ~225°C. Thus, the polymers are stable as melts. According to the TGA, the ceramic conversion reaction is essentially complete by 600°C. The observed TGA (65%) and bulk (60%) ceramic yields are close to the theoretical ceramic yield of 68% (Eq. 3).

As presented in Figure 2, XRD studies of the black, glassy ceramics obtained upon bulk pyrolyses of the polymer showed that samples heated to only 1000°C were amorphous, but those heated at 1250°C (1h) exhibited the onset of boron carbide crystallization.

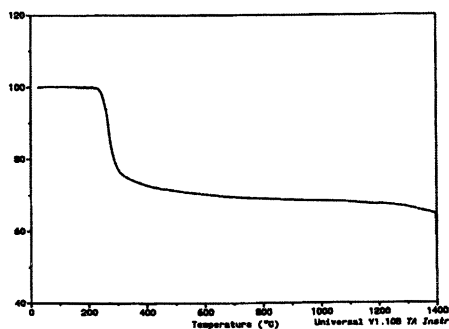
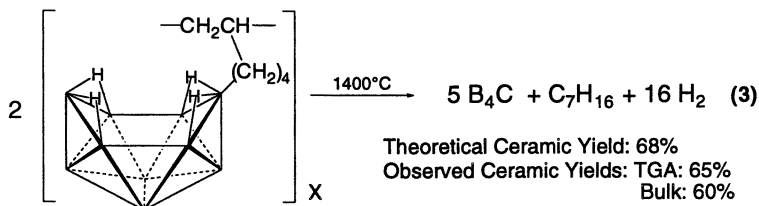


Figure 1. Thermogravimetric (TGA) study of polyhexenyldecaborane



Highly crystalline materials were obtained by heating the ceramics to 1850°C. The diffuse reflectance infrared spectrum, Figure 2, of a sample heated at 1250°C (1h) showed the characteristic boron carbide bands at 1605 and 1144 cm⁻¹ (18).

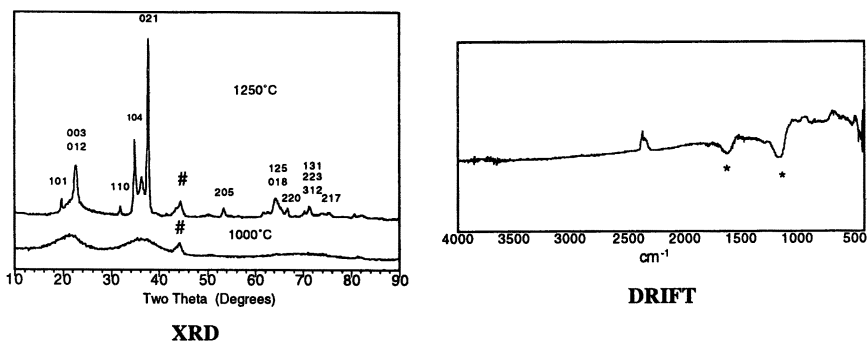
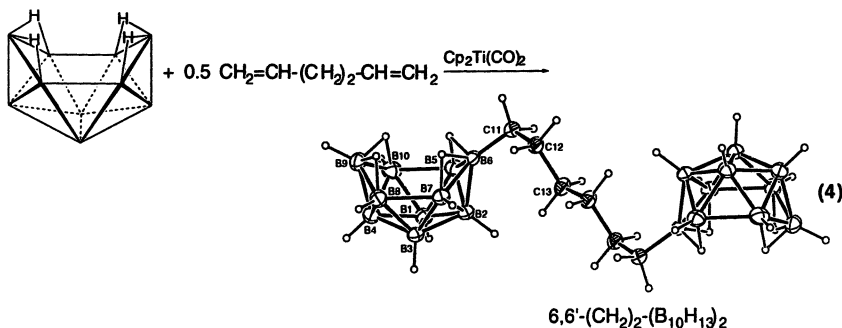


Figure 2. X-ray Diffraction (XRD) and diffuse reflectance infrared (DRIFT) studies of ceramics derived from polyhexenyldecaborane

Elemental analyses of the resulting boron carbide ceramics derived from polyhexenyldodecaborane indicate compositions in the range of B_4C . As discussed earlier, boron carbide can have a range of compositions ranging from 8.8 to 20 at.% carbon and it has been shown that solid-state properties, such as hardness and thermoelectric efficiency, vary with the boron:carbon ratio. The ceramics derived from the polyhexenyldodecaborane are thus on the carbon-rich side of the range of boron carbide compositions. However, by altering the boron to carbon ratio of the starting precursor, we have now also developed a new dodecaborane-based molecular precursor to boron-rich compositions.

The new precursor was synthesized by again employing the $Cp_2Ti(CO)_2$ catalyzed reaction of $B_{10}H_{14}$ with hexadiene, but the reactant ratios were altered to ensure hydroboration of both olefinic units. As shown in Eq. 4, the resulting $6,6'-(CH_2)_6-(B_{10}H_{13})_2$ product is obtained as an off-white, air stable solid in over 90% isolated yields.



The TGA study in Figure 3 of the $6,6'-(CH_2)_6-(B_{10}H_{13})_2$ ceramic-conversion reaction showed that decomposition begins near $220^\circ C$ and is essentially complete by $400^\circ C$.

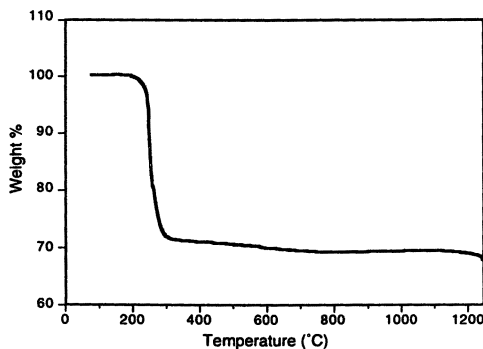


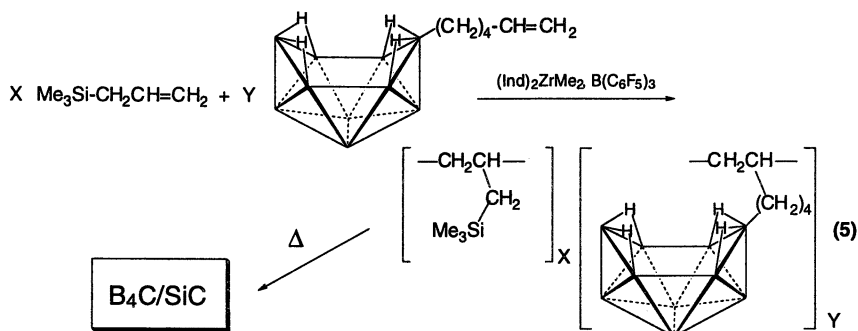
Figure 3. TGA study of $6,6'-(CH_2)_6-(B_{10}H_{13})_2$

The XRD spectra of bulk powder samples of $6,6'-(\text{CH}_2)_6-(\text{B}_{10}\text{H}_{13})_2$ pyrolyzed at 1000°C (3h) indicated that they were amorphous, but powders heated at 1025°C (3h) exhibited the characteristic boron carbide diffraction pattern. Likewise, DRIFT spectra of powders heated at 1025°C (3h) showed the major boron carbide bands.

Since the boron to carbon ratio (20:6) in $6,6'-(\text{CH}_2)_6-(\text{B}_{10}\text{H}_{13})_2$ is much higher than that in the polyhexenyldodecaborane (10:6), it was expected to provide access to boron-rich boron carbide compositions. Elemental analyses of the 1000°C (B, 88.39; C, 11.45%) and 1025°C (B, 89.04; C, 10.76%) pyrolyzed powders showed no measurable hydrogen and established $\text{B}_{7.7}\text{C}$ and $\text{B}_{8.3}\text{C}$ compositions, respectively. Thus, these studies (19) demonstrated that $6,6'-(\text{CH}_2)_6-(\text{B}_{10}\text{H}_{13})_2$ is, in fact, an excellent precursor to boron-rich boron carbide.

Both the polyhexenyldodecaborane polymer and the $6,6'-(\text{CH}_2)_6-(\text{B}_{10}\text{H}_{13})_2$ compound appear to be ideal precursors for the synthesis of boron carbide materials in processed forms: (1) they are readily synthesized in large amounts using metal catalyzed reactions; (2) they contain no other ceramic forming elements and have complementary boron to carbon ratios, thus yielding carbon-rich or boron-rich boron carbide compositions, respectively, upon pyrolysis; (3) they are stable as melts, thus allowing the use of melt-processing methods; and (4) upon pyrolysis, both precursors undergo a crosslinking reaction at relatively low temperatures ($\sim 220^\circ\text{C}$) that retards loss of material by volatilization, thereby generating high ceramic and chemical yields.

One of the limitations on the use of boron carbide is its relatively low oxidation temperature ($600^\circ\text{C} <$). However, recent work has shown that boron-carbide/silicon-carbide composites can exhibit oxidative stability up to 1200°C (19). We have now also developed new processable, single-source polymeric precursors to such composite material via the $(\text{Ind})_2\text{ZrMe}_2/\text{B}(\text{C}_6\text{F}_5)_3$ (21) catalyzed copolymerization of allylsilanes and hexenyldodecaborane. As shown in Eq. 5., a range of random copolymers has been produced in which their allyltrimethylsilane and hexenyldodecaborane contents can be controlled by the feed ratios.



Likewise, block copolymers have been achieved by alternate addition of the monomers to produce both allyltrimethylsilane and hexenyldecaborane blocks.

The polymers are air-stable solids and initial studies of their ceramic conversion reactions have shown that by varying the ratio of the allyltrimethylsilane and hexenyldecaborane components in the polymer, it is possible to control and tune the B₄C to SiC ratio in the final ceramic composite. Systematic studies of the optimum B₄C/SiC compositions for oxidative stability are underway.

Synthesis of Boron Carbide Nanofibers and Nanocylinders

Nanoscale ceramic-fibers, -nanocylinders and -nanoporous structures, just like their well-known carbon counterparts, have a tremendous number of potential applications, including uses as quantum electronic materials, structural reinforcements, and ceramic membranes to be utilized for catalyst supports or gas separations (22). Recently, Zhang et al. discussed the importance of nanoscale boron carbide materials and demonstrated the use of plasma-enhanced chemical vapor deposition to generate boron carbide nanowires and nanonecklaces (23). Han et al. have also recently reported the formation of mixtures of crystalline boron carbide nanorods and boron-doped nanotubes upon the reaction of boron oxide vapor with carbon nanotubes (24). Both of these methods are limited in their scales and there is a clear need for the development of new methods for the more efficient formation of such materials.

Because of their processability and high ceramic and chemical yields, the single-source polyhexenyldecaborane and 6,6'-(CH₂)₆-(B₁₀H₁₃)₂ precursors have now proven to be ideally suited for use in the generation of nanostructured materials. Some of our initial studies that utilize the unique properties of these precursors in conjunction with newly developed methods for nanofabrication are discussed below.

Porous alumina templates have recently been widely used to generate nanofibers from a variety of materials including polymers, carbon, metals, semiconductors and ceramics (25). This template method involves the absorption of a precursor material into the channels of the nanoporous alumina using either gas-phase or solution methods, conversion of the precursors to the final solid state material by thermolytic or chemical reactions, and then dissolution of the alumina membrane to leave the free standing fibers.

In our work using these templating methods, we used alumina membranes having a thickness of 60 μm and a nominal pore size of ~250 nm (± 50 nm) as the templates. As outlined in Figure 4, the membranes were immersed in liquid 6,6'-(CH₂)₆-(B₁₀H₁₃)₂ at 140°C until the membrane was saturated. The filled templates were then pyrolyzed to 1025°C to yield a boron carbide filled membrane. Immersing the sample in 48% hydrofluoric acid for 36 h dissolved the alumina template. The fact that the fibers were not attacked by the HF treatment is in agreement with the chemical inertness of boron carbide (26).

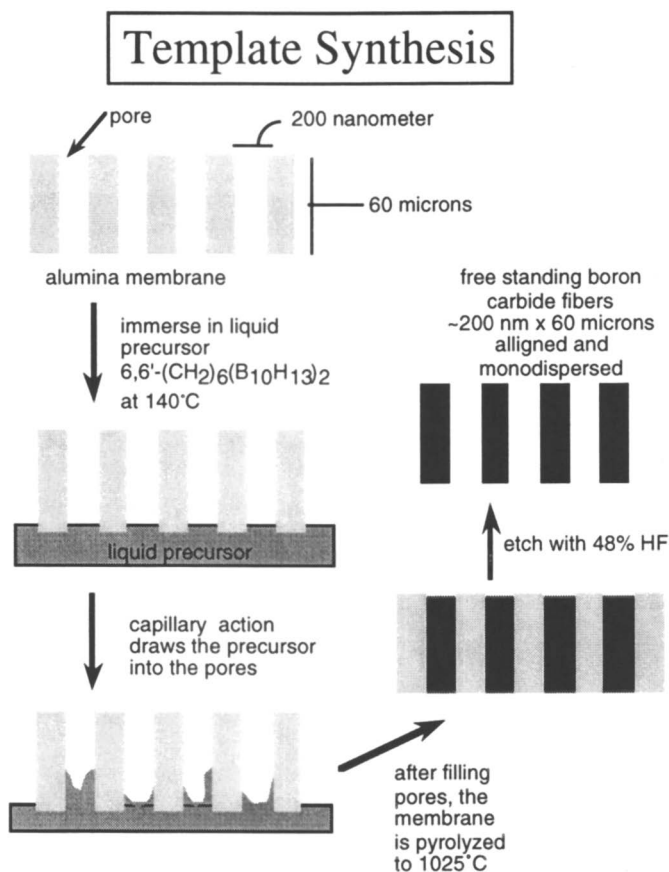


Figure 4. Schematic of template synthesis

The scanning electron microscopy (SEM) images in Figure 5 show a sample of nanofibers prepared as described above. The fibers are uniform with an ~ 250 nm diameter and ~ 45 μm length. A thin layer of boron carbide was allowed to remain on one end of the fibers. This layer serves to hold the fibers in their parallel arrangement giving the highly aligned, brush-like configuration that is apparent in the figures. Thus, as has been previously noted, one of the advantages of the templating technique over other methods for generating nanofibers is its natural ability to produce aligned, monodispersed ensembles of nanofibers (25).

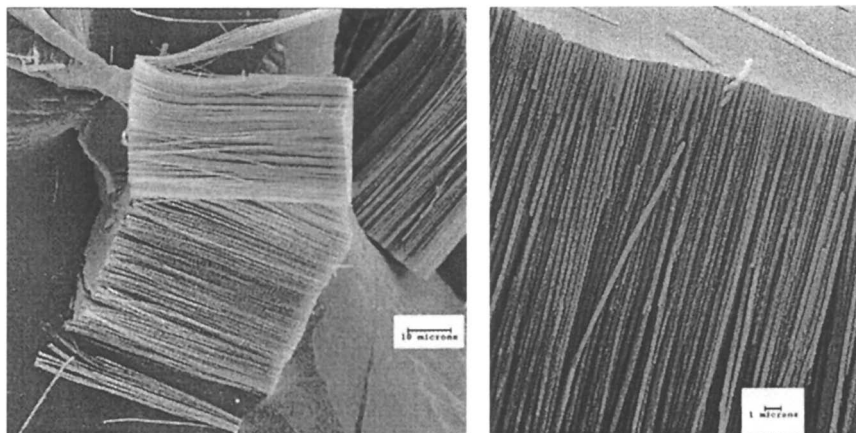


Figure 5. SEM images of boron carbide nanofibers

X-ray diffraction studies of these fibers showed that while the 1000°C fibers are largely amorphous, the 1025°C fibers are composed of crystalline boron carbide. In agreement with the XRD studies, analysis by transmission electron microscopy (TEM) confirmed that the nanofibers heated at 1000°C (3h) were amorphous, but those taken to 1025°C (3h) showed the onset of boron carbide crystallization.

The TEM studies also showed that while almost all of the nanofibers were solid, there were some, such as shown in the image in Figure 6, that had hollow cores.

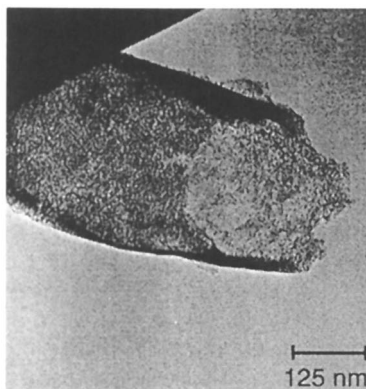


Figure 6. TEM image of the end of a boron carbide nanocylinder

Such hollow fiber structures are of great potential importance, since they could prove useful for the construction of multicomponent nanofibers. In the experiments above, the nanocylindrical fibers were only a minor component of material and probably arose from incomplete filling of a channel in the template by the neat liquid precursor. We have now developed an alternative synthesis method that enhances nanocylinder formation by initially forming only a thin coating of the precursor on the template walls. Thus, in order to avoid completely filling the channels, a precursor solution, rather than the neat liquid precursor employed above, is used to treat the membrane. In this process, a toluene solution of the polyhexenyldecaborane precursor is vacuum filtered through the template. The solvent is then completely evaporated to leave a thin precursor layer on the surfaces of the membrane. Pyrolysis of the coated membrane converts the precursor to a boron carbide coating.

Etching of the alumina membrane with HF then yields freestanding nanocylindrical boron carbide structures. The SEM images in Figure 7 and 8 show side and end views of an ensemble of boron carbide nanocylinders that are $\sim 50\ \mu\text{m}$ long and $\sim 250\ \text{nm}$ in diameter. Both the end view in the SEM image in Figure 8 and the TEM image of a single nanocylinder in Figure 9, clearly show the hollow cores of the cylindrical structures. The inside diameter and wall thickness of the nanocylinders can be controlled by the solution concentration and/or number of membrane treatments.

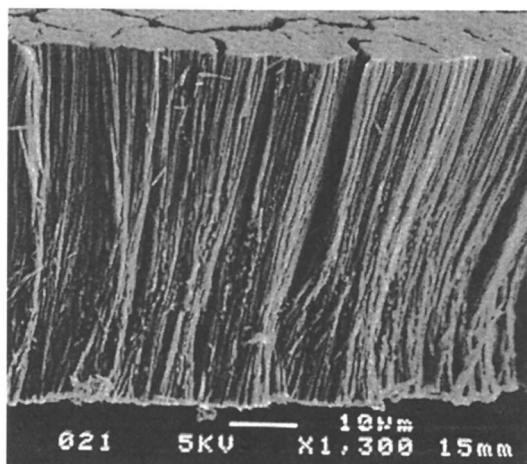


Figure 7. SEM image of a side view of the boron carbide nanocylinders

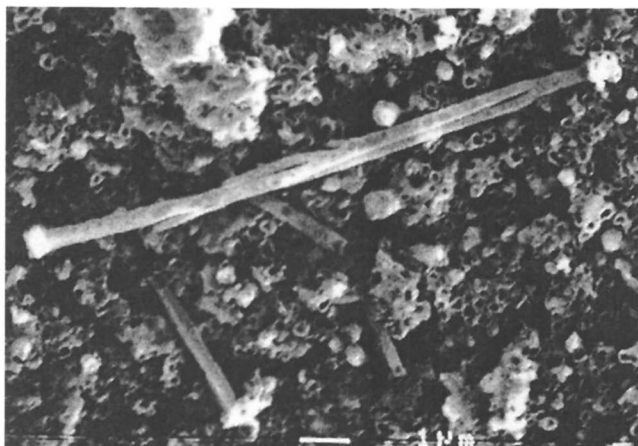


Figure 8. SEM image of an end view of the boron carbide nanocylinders showing their hollow cores

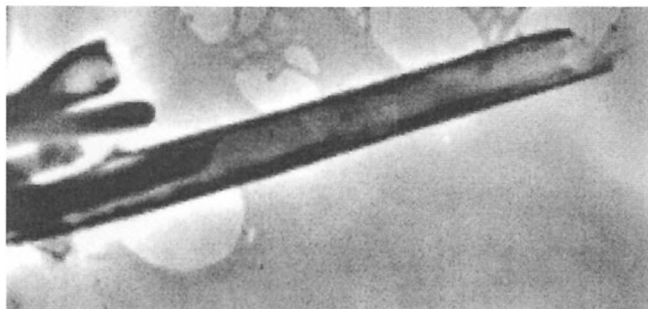


Figure 9. TEM image of a single boron carbide nanocylinder

In our initial studies of the syntheses of both nanofibers and nanocylinders, we have employed ~ 250 nm templates, but nanoporous alumina templates have been prepared with channels as small as 10-20 nm. We are now applying the methods that we developed in our initial work to generate and study these smaller dimension boron carbide fibers and nanocylinders.

In conclusion, the results discussed above have clearly demonstrated that nano-templating methods, in conjunction with the newly designed molecular and polymeric single-source boron carbide precursors, allow the systematic generation of aligned, monodispersed ensembles of both boron carbide nanofibers and nanocylinders. We are now investigating the structural and

electronic properties of these materials, as well as the use of these template methods for the production a wide range of other nanostructured ceramics.

Acknowledgements. We thank the National Science Foundation and the Air Force Office of Scientific Research, USAF, under grant number F49620-01-1-0443 for support of this work.

References

1. Wynne, K. J.; Rice, R. W. *Annu. Rev. Mater. Sci.* **1984**, *14*, 297-334.
2. (a) Fazan, P. J.; Remsen, E. E.; Carroll, P. J.; Beck, J. S.; Sneddon, L. G. *Chem. Mater.* **1995**, *7*, 1942-1956. (b) Fazan, P. J.; Beck, J. S.; Lynch, A. T.; Remsen, E. E.; Sneddon, L. G. *Chem. Mater.* **1990**, *2*, 96-97.
3. Su, K.; Remsen, E. E.; Zank, G. A.; Sneddon, L. G. *Chem. Mater.* **1993**, *5*, 547-556.
4. Wideman, T.; Su, K.; Remsen, E. E.; Zank, G. A.; Sneddon, L. G. *Chem. Mater.* **1995**, *7*, 2203-2212.
5. Wideman, T.; Remsen, E. E.; Carroll, P. J.; Sneddon, L. G. *Chem. Mater.* **1998**, *10*, 412-421.
6. Wideman, T.; Cortez, E.; Remsen, E. E.; Zank, G. A.; Carroll, P. J.; Sneddon, L. G. *Chem. Mater.* **1997**, *9*, 2218-2230.
7. Wideman, T.; Fazan, P. J.; Su, K.; Zank, G. A.; Remsen, E. E.; Sneddon, L. G. *Appl. Organomet. Chem.* **1998**, *12*, 681-693. (b) Wideman, T.; Remsen, E. E.; Zank, G. A.; Sneddon, L. G. in *Proceedings of the Ringberg Meeting on Grain Boundary Dynamics in Precursor Derived Ceramics*, Bill, J.; Aldinger, F. Eds., Wiley-VCR: New York, 1999, 103-112.
8. Wideman, T.; Cava, R. J.; Sneddon, L. G. *Chem. Mater.* **1996**, *8*, 2215-2217.
9. Su, K.; Nowakowski, M.; Bonnell, D.; Sneddon, L. G. *Chem. Mater.* **1992**, *4*, 1139-1141.
10. Su, K.; Sneddon, L. G. *Chem. Mater.* **1993**, *5*, 1659-1668.
11. For some recent reviews on the synthesis and properties of boron carbide, see: (a) Thevenot, F. *Key Eng. Materials* **1991**, *56-57*, 59-88. (b) *Boron Rich Solids*; Emin, D.; Aselage, T.; Beckel, C. L.; Howard, I. A.; Wood, C. eds.; AIP Conf. Proc 140, Am. Inst. Phys.: New York, 1986. (c) *Boron Rich Solids*; Emin, D.; Aselage, T.; Switendick, A. C.; Morosin, B.; Beckel, C. L. eds.; AIP Conf. Proc 231, Am. Inst. Phys.: New York, 1991.
12. See, for example, (a) Wood, C. In *Boron Rich Solids*; Emin, D.; Aselage, T.; Beckel, C. L.; Howard, I. A.; Wood, C. eds.; AIP Conf. Proc 140, Am. Inst. Phys.: New York, 1986, pp. 362-372 and references therein. (b) Aselage, T. L.; Tallant, D. R.; Gieske, J. H.; Van Deusen, S. B.; Tissot, R. G. *The Physics and Chemistry of Carbides; Nitrides and Borides*, 1990, 97.

13. (a) Rees, Jr., W. S.; Seyferth, D. *J. Am. Ceram. Soc.* **1990**, *71* (4), C194. (b) Seyferth, D.; Rees, Jr., W. S.; Haggerty, J. S.; Lightfoot, A. *Chem. Mater.* **1989**, *1*, 45.
14. Mirabelli, M. G. L.; Sneddon, L. G. *J. Am. Chem. Soc.* **1988**, *110*, 3305-3306.
15. Pender, M.; Sneddon, L. G. *ACS Polym. Prepr.* **2000**, *41*, 551-552.
16. Pender, M.; Wideman, T.; Carroll, P. J.; Sneddon, L. G. *J. Am. Chem. Soc.* **1998**, *120*, 9108-9109.
17. Yang, X.; Stern, C. L.; Marks, T. J. *J. Am. Chem. Soc.* **1994**, *116*, 10015-10031.
18. Becher, V. H. J.; Th venot, F. *Z. Inorg. Allg. Chem.* **1974**, *410*, 274-286.
19. Pender, M. J.; Sneddon, L. G. *Chem. Mater.* **2000**, *12*, 280-283.
20. See, for example: Blakely, K. A.; Shaffer, P. T. B. *Am. Ceram. Soc. Bull.* **1990**, *69*, 193-195.
21. (a) Zeigler, R.; Resconi, L.; Balbontin, G.; Guerra, G.; Venditto, V.; Rosa, C. D. *Polymer* **1994**, *35*, 4648-4655. (b) Habaue, S.; Baraki, H.; Okamoto, Y. *Macromol. Chem. Phys.* **1998**, *199*, 2211-2215.
22. For a review of the importance and applications of nanoscale structures, see: *Nanoscale Science, Engineering and Technology, Research Directions* report of the Basic Energy Sciences Nanoscience/Nanotechnology Group, US Department of Energy, 1999 and references therein.
23. (a) Zhang, D.; Kempton, B. G.; McIlloy, D. N.; Geng, Y.; Norton, M. G. *Mat. Res. Soc. Proc.* **1999**, *536*, 323-327. (b) Zhang, D.; McIlloy, D. N.; Geng, Y.; Norton, M. G. *Mat. Sci. Lett.* **1999**, *18*, 349-351.
24. Han, W.; Bando, Y.; Kurashima, K.; Sato, T. *Chem. Phys. Lett.* **1999**, *299*, 368-373.
25. See, for example: (a) Martin, C. R. *Science* **1994**, *266*, 1961-1966. (b) Martin, C. R. *Acc. Chem. Res.* **1995**, *28*, 61-68. (c) Martin, C. R. *Chem. Mater.* **1996**, *8*, 1739-1746 and references therein. (d) Lakshmi, B. B.; Patrissi, C. J.; Martin, C. R. *Chem. Mater.* **1997**, *9*, 2544-2550. (e) Cepak, V. M.; Hulteen, J. C.; Che, G.; Jirage, K. B.; Lakshmi, B. B.; Fisher, E. R.; Martin, C. R. *Chem. Mater.* **1997**, *9*, 1065-1067. (f) Che, G.; Lakshmi, B. B.; Martin, C. R.; Fisher, E. R.; Ruoff, R. S. *Chem. Mater.* **1998**, *10*, 260-267. (g) Klein, J. D.; Herrick, II, Robert, D.; Palmer, D.; Sailor, M. J. *Chem. Mater.* **1993**, *5*, 902-904. (h) Zelenski, C. M.; Dorhout, P. K. *J. Am. Chem. Soc.* **1998**, *120*, 734-742. (i) Zhang, Z.; Gekhtman, D.; Dresselhaus, M. S.; Ying, J. *Chem. Mater.* **1999**, *11*, 1659-1665.
26. Makarenko, G. N. In *Boron and Refractory Borides*; Matkovich, V. I., Ed., Springer-Verlag: New York, 1977, p 319.

Chapter 13

Molecular Phosphates and Phosponates of Aluminum and Gallium: Potential Applications in Materials Synthesis

Mark R. Mason, R. Mark Matthews, Alisa M. Perkins,
and Vira V. Ponomarova

Department of Chemistry, University of Toledo, Toledo, OH 43606

The potential for molecular phosphates and phosponates of the group 13 elements to serve as precursors to new materials is considered. Intermolecular exchange among dimeric and tetrameric gallophosponates and thermal and acetylaceton-promoted interconversion of $[\text{tBuAlO}_3\text{PMe}]_n$ ($n = 4, 6, 10$) are discussed in the context of the difficulties these rearrangements present for designed materials synthesis from molecular precursors. In addition, tetrameric alkylaluminophosponates bearing potentially ligating 4-cyanophenyl and 3-pyridyl substituents are used for the generation of coordination networks with transition metal ions. Presented are an example of a 1-D chain in which structural rearrangement of the precursor has occurred, and an example in which the molecular precursor remains intact in the final 2-D coordination network.

Molecular phosphates and phosponates of the group 13 elements have been investigated as soluble models of secondary building units (SBUs; Figure 1) in microporous alumino- and gallophosphate molecular sieves and as

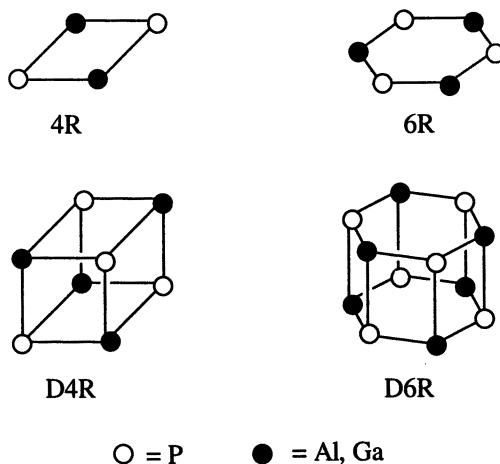


Figure 1. Secondary building units (SBUs) common to aluminophosphate and gallophosphate molecular sieves. μ_2 -Oxo bridges along each edge are omitted for clarity.

potential precursors to new group 13 phosphate materials (1,2). In this effort, organic-substituted derivatives of four-ring (4R), six-ring (6R), double-four-ring (D4R), and double-six-ring (D6R) SBUs have been prepared using several synthetic approaches (1-20).

Despite the interest in these potential precursors, there have been few reports on attempted conversion of molecular compounds to group 13 phosphate materials. Cassidy and coworkers at Imperial Chemical Industries Ltd. reported that pyrolysis of $[\text{Al}(\text{PO}_4)(\text{HCl})(\text{EtOH})_4]_4$ above 50°C is a useful method for depositing glassy films of aluminophosphate on a variety of substrates (20). More recently, Tilley and coworkers (21) converted $[\text{Me}_2\text{AlO}_2\text{P}(\text{O}^t\text{Bu})_2]_2$ and $[\text{Al}(\text{O}^i\text{Pr})_2\text{O}_2\text{P}(\text{O}^t\text{Bu})_2]_4$ to AlPO_4 via solution thermolysis and chemical vapor deposition. In both cases, dense phase materials were obtained and the structure of the inorganic core in the molecular precursor did not influence the final structure of the aluminophosphate material.

Preparation of new phosphate materials with intentional incorporation of specific SBUs will be a more challenging feat (1). The designed construction of phosphate molecular sieves from preformed molecular building blocks will require facile removal of organic substituents and linkage of SBUs into extended structures under mild conditions and without fragmentation or rearrangement of the SBUs. This has not yet been accomplished. In fact, we present here several examples of cage fragmentation and rearrangement in

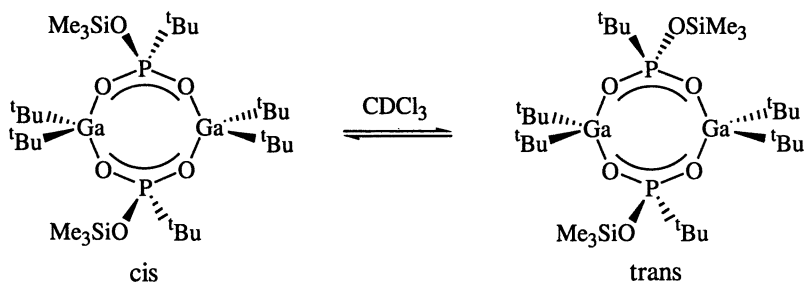
molecular phosphonates of aluminum and gallium that will frustrate efforts towards designed materials synthesis.

Undesired cage fragmentation and rearrangement would undoubtedly be exacerbated under the temperatures utilized for materials synthesis by solid-state pyrolysis, chemical vapor deposition, and solvothermal reactions. More plausible is the designed preparation of hybrid inorganic-organic materials from organic derivatized phosphate or phosphonate SBUs under mild reaction conditions. Phosphonate materials of aluminum, gallium, and indium have been reported by the groups of Bideau (22), Bruque (23), Bujoli (24), Clearfield (23,24), Hobday (25,26), Maeda (27-30), and Morris (31). However, these group 13 phosphonate materials were synthesized via solvothermal methods, not from preformed molecular precursors.

As an initial investigation of the stability of the inorganic cores of molecular phosphonates of aluminum and gallium during materials synthesis conditions, we report the preparation of phosphonate materials via coordination chemistry. Examples of intermolecular rearrangements, cage fragmentation, and generation of 1-D and 2-D coordination networks are discussed.

Intermolecular Rearrangements

Evidence for fragmentation or rearrangement of the inorganic cores of molecular group 13 phosphonates was first observed (4,5) for heterocyclic gallophosphonates $[\text{tBu}_2\text{GaO}_2\text{P(OR)R}]_2$ ($\text{R} = \text{H}, \text{SiMe}_3$; $\text{R}' = \text{H}, \text{Me}, \text{tBu}, \text{Ph}$). These 4R derivatives are obtained as either cis or trans isomers in the solid state, depending on the organic substituents on gallium and phosphorus. The trans arrangement of substituents appears most common. NMR (^1H , ^{31}P) spectroscopy reveals isomerization of these heterocycles to cis-trans mixtures in



solution. Monitoring of crossover experiments by NMR spectroscopy showed that these isomerization reactions may be explained, or at least accompanied, by an intermolecular rearrangement. Intermolecular exchange and isomerization

cannot be accounted for without invoking P–O and/or Ga–O bond cleavage in the $\text{Ga}_2\text{P}_2\text{O}_4$ heterocycle.

Similarly, NMR spectroscopy (^1H , ^{31}P) revealed that solutions of two D4R derivatives $[\text{}^t\text{BuGaO}_3\text{PR}]_4$ ($\text{R} = \text{Me}$, ^tBu , Ph , OSiMe_3) slowly undergo intermolecular exchange to give a mixture of tetrameric gallophosphonates (5). The resulting products differ only in the substituents on phosphorus. For a C_6D_6 solution of $[\text{}^t\text{BuGaO}_3\text{PPh}]_4$ and $[\text{}^t\text{BuGaO}_3\text{P}(\text{OSiMe}_3)]_4$, substantial rearrangement was observed within 2 d at 85°C (Figure 2).

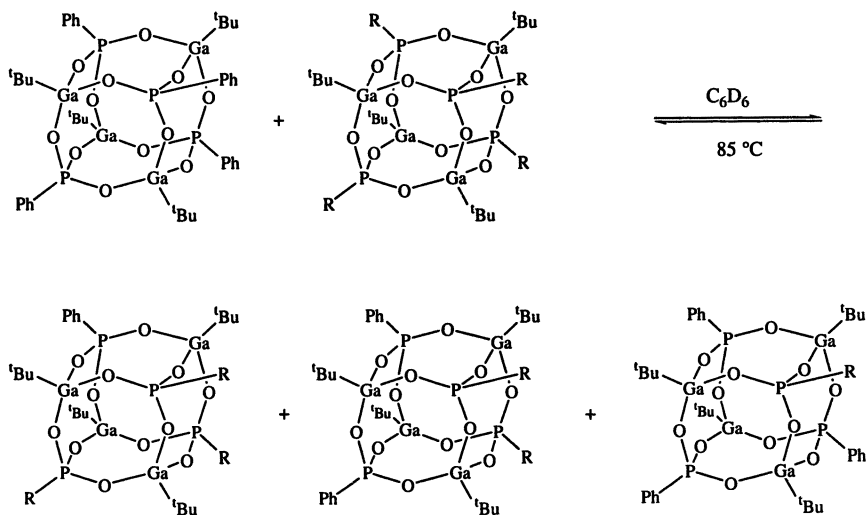
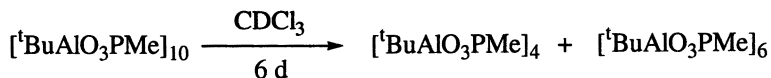


Figure 2. Intermolecular exchange among tetrameric gallophosphonates.

More dramatic examples of cage rearrangement were discovered during our detailed investigation of reactions of $^t\text{Bu}_3\text{Al}$ with methylphosphonic acid (7). These reagents react in refluxing toluene/THF to yield a mixture of $[\text{}^t\text{BuAlO}_3\text{PMe}]_4$, $[\text{}^t\text{BuAlO}_3\text{PMe}]_6$, and $[\text{}^t\text{BuAlO}_3\text{PMe}]_{10}$. Characterization of the D4R derivative $[\text{}^t\text{BuAlO}_3\text{PMe}]_4$ and the D6R oligomer $[\text{}^t\text{BuAlO}_3\text{PMe}]_6$ by NMR spectroscopy, IR spectroscopy, mass spectrometry, and X-ray crystallography was straightforward. Characterization of $[\text{}^t\text{BuAlO}_3\text{PMe}]_{10}$, however, was hindered by its low yield and by a room-temperature structural rearrangement in solution to a mixture of $[\text{}^t\text{BuAlO}_3\text{PMe}]_4$, $[\text{}^t\text{BuAlO}_3\text{PMe}]_6$, and $[\text{}^t\text{BuAlO}_3\text{PMe}]_{10}$.



X-ray crystallography verified the structure for $[\text{BuAlO}_3\text{PMe}]_{10}$ proposed based on spectroscopic data (1). The molecular structure (Figure 3) is comprised of two tetramers, each opened along an edge and linked via Al–O–P

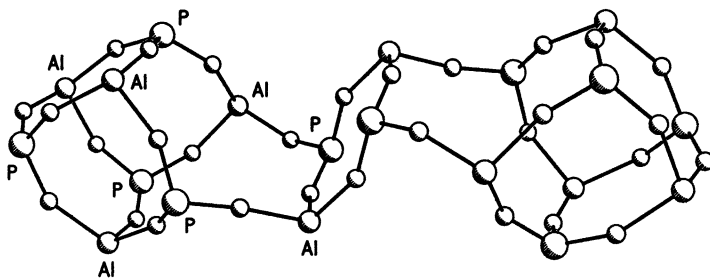
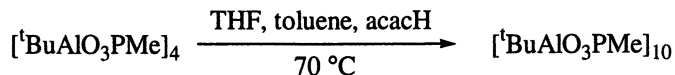


Figure 3. Molecular structure of the $\text{Al}_{10}\text{P}_{10}\text{O}_{30}$ core of $[\text{BuAlO}_3\text{PMe}]_{10}$. Methyl and tert-butyl substituents on phosphorus and aluminum are omitted for clarity.

linkages to an eight-membered $\text{Al}_2\text{P}_2\text{O}_4$ heterocycle. Furthermore, addition of acetylacetonate to $[\text{BuAlO}_3\text{PMe}]_4$ results in rearrangement and precipitation of pure $[\text{BuAlO}_3\text{PMe}]_{10}$! Although we cannot yet offer an explanation for the role of acetylacetonate in this unique reaction, this result nonetheless has significant implications for the robustness of the cage compounds under potential materials synthesis conditions.



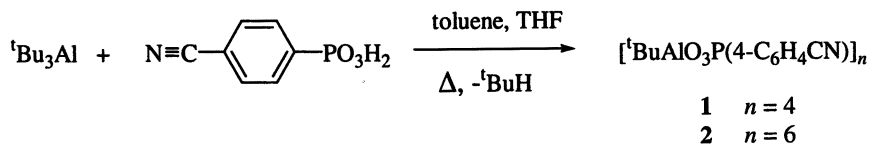
Cage Alkylaluminumphosphonates with Potentially Ligating Substituents

Considering the intermolecular exchange and rearrangement reactions just described, one must ask: Will molecular phosphates and phosphonates be sufficiently robust to be utilized as SBUs for the preparation of porous 3-D phosphate or phosphonate materials? To begin to address this question, we opted to investigate the stability of group 13 phosphonate compounds under the mildest possible conditions for materials synthesis. Hence, we chose to generate coordination networks by linkage of aluminumphosphonate SBUs with transition

metal ions at room temperature. This approach necessitated the preparation of alkylaluminumphosphonates decorated with potentially ligating substituents.

Our group (1), as well as that of Roesky (2), demonstrated that reactions of a phosphonic acid with an aluminum or gallium trialkyl yield dimeric heterocycles and trimeric, tetrameric, hexameric, and decameric cage compounds depending on reaction conditions and the organic substituents on phosphorus and the group 13 element. We have now used this procedure to incorporate potentially ligating 4-cyanophenyl and 3-pyridyl substituents into organic-soluble D4R and D6R aluminumphosphonate derivatives. These substituents were chosen based on their previous utility for generation of coordination networks (32,33) and the ease of synthesis of their phosphonic acid derivatives.

The requisite 4-cyanophenylphosphonic and 3-pyridylphosphonic acids were synthesized via palladium-catalyzed coupling of the corresponding aryl halide and diethylphosphite as described by Hirao and coworkers (34). Reaction of 4-cyanophenylphosphonic acid with ${}^t\text{Bu}_3\text{Al}$ produced $[\text{}^t\text{BuAlO}_3\text{P}(4\text{-C}_6\text{H}_4\text{CN})]_4$ (**1**) and $[\text{}^t\text{BuAlO}_3\text{P}(4\text{-C}_6\text{H}_4\text{CN})]_6$ (**2**) in yields of 66% and 28%, respectively. Compounds **1** and **2** have been characterized by NMR



spectroscopy, mass spectrometry, and X-ray crystallography (35). The molecular structures of **1** and **2** are shown in Figure 4. Compound **1** possesses a cubanoidal $\text{Al}_4\text{P}_4\text{O}_{12}$ D4R core with aluminum and phosphorus atoms alternating at vertex positions and with an oxygen atom bridging each edge. Each aluminum bears a *tert*-butyl substituent and each phosphorus a 4-cyanophenyl substituent. The 4-cyanophenyl substituents point away from the cubanoidal $\text{Al}_4\text{P}_4\text{O}_{12}$ core towards the corners of a tetrahedron, thus making **1** a potential tetrahedral building block for the construction of 3-D diamond-like coordination networks. Compound **2** possesses a drum-like $\text{Al}_6\text{P}_6\text{O}_{18}$ D6R core, also with one *tert*-butyl substituent per aluminum and a 4-cyanophenyl substituent per phosphorus.

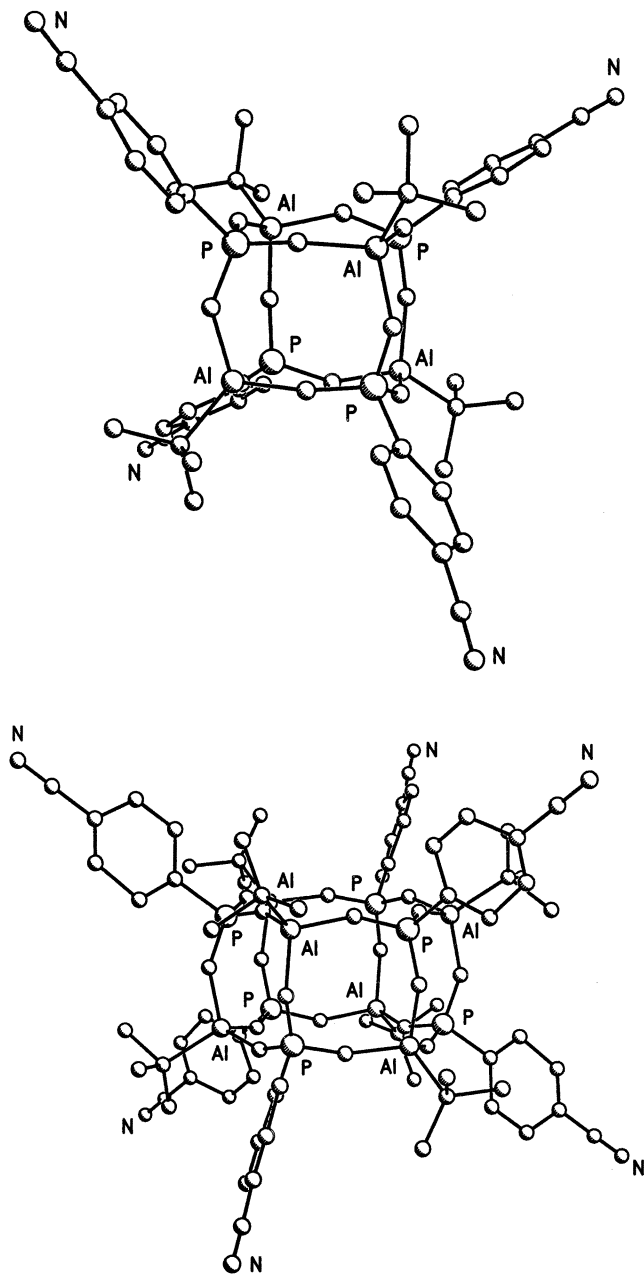
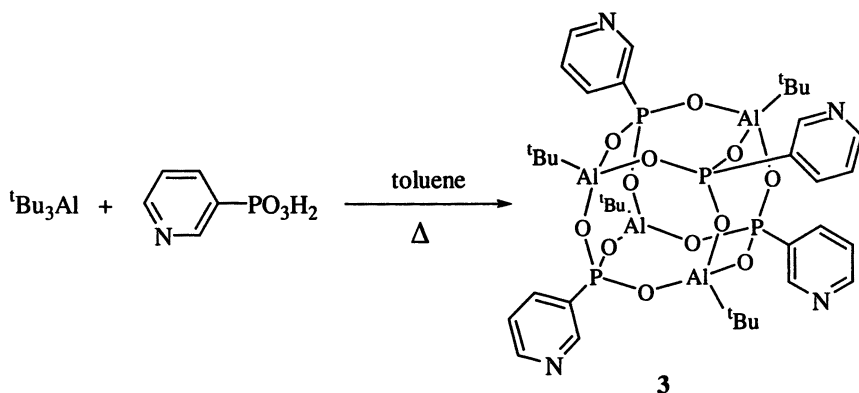


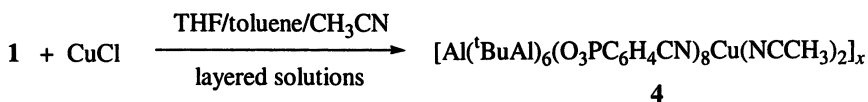
Figure 4. Molecular structures of 1 (top) and 2 (bottom).

Reaction of 3-pyridylphosphonic acid with ${}^t\text{Bu}_3\text{Al}$ similarly yielded $[\text{}^t\text{BuAlO}_3\text{P}(3\text{-C}_5\text{H}_4\text{N})]_4$ (**3**) in 64% yield. NMR spectroscopy and X-ray crystallography confirm that **3** has an $\text{Al}_4\text{P}_4\text{O}_{12}$ core with one *tert*-butyl substituent per aluminum and a 3-pyridyl substituent per phosphorus (36). Compound **3** differs from **1** in its potential ligating properties since **3** cannot coordinate to a metal ion linearly along the pseudo three-fold axes of the $\text{Al}_4\text{P}_4\text{O}_{12}$ cage.



1-D Coordination Network

Slow diffusion of a methylene chloride solution of **1** into an acetonitrile solution of CuCl , mediated by a layer of toluene, yielded a small quantity of tiny needles within 2 weeks, followed by formation of yellow prismatic crystals within 3 weeks. The identity of the needle-like crystals has not been determined. The prismatic crystals, isolated in approximately 35–45% yield, analyzed as $[\text{Al}({}^t\text{BuAl})_6(\text{O}_3\text{PC}_6\text{H}_4\text{CN})_8\text{Cu}(\text{NCCH}_3)_2]_n$ (**4**). From this structural formula, it is clear that there was rearrangement of the D_{4R} core of **1**. There is also no chloride counterion in this product.



X-ray crystallography determined the structure of **4** to be a 1-D zigzag chain (Figure 5) in which alkylaluminumphosphonate cage units of the formula

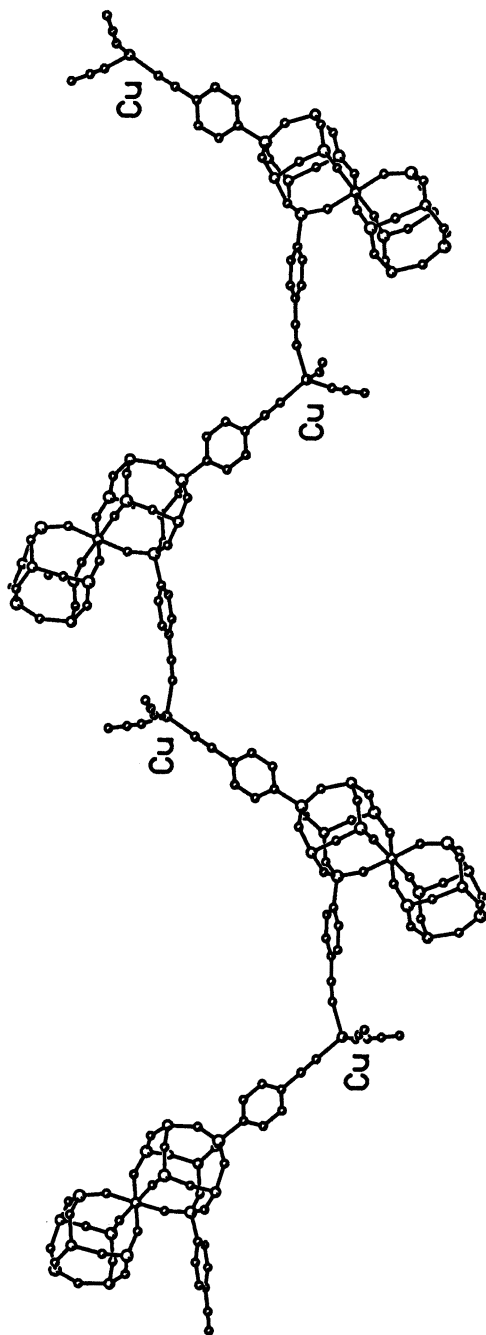


Figure 5. Molecular structure of a portion of the 1-D chain in 4. All *tert*-butyl and 4-cyanophenyl substituents are omitted for clarity except those coordinated to copper.

$[\text{Al}(\text{tBuAl})_6(\text{O}_3\text{PC}_6\text{H}_4\text{CN})_8]$ are linked via coordination of two cyanophenyl substituents per unit to two bridging $\text{Cu}(\text{NCCH}_3)_2^+$ moieties (35). Six cyanophenyl substituents per cluster remain uncoordinated, and there is no evidence for chloride counterions in the structure. Inspection of the $[\text{Al}(\text{tBuAl})_6(\text{O}_3\text{PC}_6\text{H}_4\text{CN})_8]$ units (Figure 6) reveals a core structure in which two $\text{Al}_4\text{P}_4\text{O}_{12}$ "cubes" share a common vertex. The shared vertex is occupied by an octahedral aluminum atom ligated by six phosphonate oxygen atoms. The fate of the original *tert*-butyl substituent on this aluminum center is not known. Charge-balancing requires the $[\text{Al}(\text{tBuAl})_6(\text{O}_3\text{PC}_6\text{H}_4\text{CN})_8]$ moiety to be anionic. This moiety then serves as counterion to the Cu^+ cations and accounts for the absence of chloride in the structure. This unique compound is the first example of octahedral aluminum and also vertex-shared cubanoidal units in the molecular phosphonate chemistry of the group 13 elements.

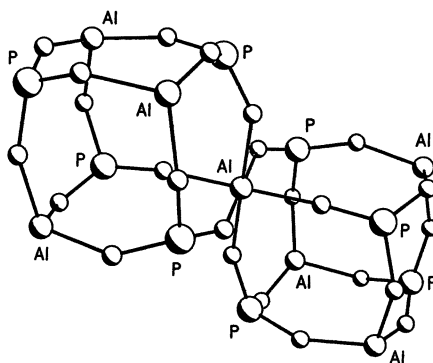
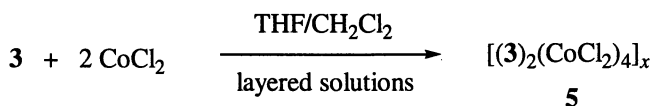


Figure 6. Molecular structure of the $[\text{Al}(\text{tBuAl})_6(\text{O}_3\text{PC}_6\text{H}_4\text{CN})_8]^-$ core of **4**. *Tert*-butyl and 4-cyanophenyl substituents are omitted for clarity.

Further investigation of the chemistry of **4** is underway. We aim to cleave the aluminophosphonate unit from Cu^+ , isolate the $[\text{Al}(\text{tBuAl})_6(\text{O}_3\text{PC}_6\text{H}_4\text{CN})_8]^-$ anion, and study its molecular chemistry and utility as a building block for new coordination networks. At this time, we do not understand the origin of the rearrangement that occurred in the formation of **4** under such mild conditions, nor have we identified any co-products of this reaction. This result does, however, substantiate our concern over cage fragmentation and rearrangement during reactions of these building blocks aimed at construction of new materials. These rearrangements may severely limit the utility of the molecular building block approach to new group 13 phosphate and phosphonate materials unless methods to circumvent fragmentation and rearrangements can be developed.

2-D Coordination Network

Slow diffusion of an acetonitrile solution of CoCl_2 into a solution of **3** in methylene chloride, mediated by a layer of nitromethane, yielded dark blue crystals within two days (36). Elemental analysis of these moisture-sensitive crystals was hindered by facile solvent loss in the absence of the mother liquor. Analysis of the resulting amorphous blue powder is consistent with the formula $\{[\text{tBuAlO}_3\text{P}(3\text{-C}_5\text{H}_4\text{N})]_4 \cdot 2\text{CoCl}_2\} \cdot \text{CH}_3\text{CN}$ (**5**).



Crystallographic data (36) collected on **5** at 150 K indicates the structural formula to be $\{[\text{tBuAlO}_3\text{P}(3\text{-C}_5\text{H}_4\text{N})]_4 \cdot 2\text{CoCl}_2\} \cdot 2\text{CH}_3\text{CN} \cdot 1.75\text{CH}_2\text{Cl}_2$, with additional solvent molecules trapped in the structural voids of the crystalline material as compared with the amorphous sample. Similar crystals obtained by layering of methylene chloride and THF solutions resulted in a molecular structure very similar to that of **5**. Gross features of the structure were virtually unchanged, but disorder in the solvate molecules lead to higher *R* factors and poorer structure solution. The molecular structure of **5** (Figure 7) consists of dimers of two molecules of **3** bridged by two tetrahedral CoCl_2 moieties. The CoCl_2 moieties are ligated by two 3-pyridyl substituents from adjacent

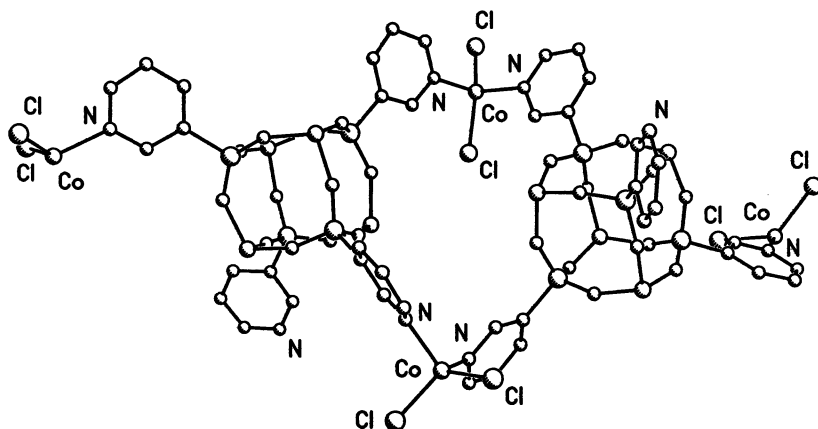


Figure 7. Molecular structure of a dimeric portion of **5**. Tert-butyl substituents and solvate molecules are omitted for clarity.

molecules of **3**. These dimeric units are further bridged by tetrahedral CoCl_2 units to generate a 2-D sheet. The structure exhibits no true porosity, but there are several small vacancies that are occupied by solvate molecules. Loss of a portion of these solvate molecules accounts for the loss of crystallinity upon removal of the crystals from the mother liquor. Although the layered structure of **5** exhibits no useful porosity, this result does demonstrate that molecular alkylaluminophosphonates can be utilized as building units for the construction of coordination networks without rearrangement of the inorganic core of the SBU.

Conclusions

This work demonstrates that cage alkylaluminophosphonates can be modified with ligating substituents and used as SBUs for the construction of extended coordination networks upon reaction with metal ions. Examples of 1-D and 2-D materials were presented, and 3-D diamond-like frameworks should be accessible with the appropriate choice of SBU and metal ion.

The more obvious and important conclusion, however, is that use of the molecular phosphonates as precursors in designed materials synthesis is limited due to relatively facile cage fragmentation and rearrangement, even at room temperature. Further understanding of factors which influence cage interconversions in these systems and methods to preclude fragmentation are required. Encapsulation of fluoride or oxide in D4R SBUs, as is so prominent in gallophosphate molecular sieves (37), may offer one strategy to address this limitation.

Acknowledgements

Acknowledgement is made to the donors of the Petroleum Research Fund, administered by the American Chemical Society (Grants 29723-G3 and 34890-AC3), for support of this research. The authors are grateful to Dr. James D. Fisher, Dr. Mark S. Mashuta, Dr. John F. Richardson, and Dr. Ashwani Vij for previous synthetic work and crystallographic studies that laid the foundation for the research reported here. Details of their contributions are found in the references. Dr. Thomas S. Barnard is acknowledged for his assistance with the preparation of Figures 3-7.

References

1. Mason, M. R. *J. Cluster Sci.* **1998**, *9*, 1.
2. Walawalkar, M. G.; Roesky, H. W.; Murugavel, R. *Acc. Chem. Res.* **1999**, *32*, 117.
3. Mason, M. R.; Matthews, R. M.; Mashuta, M. S.; Richardson, J. F. *Inorg. Chem.* **1996**, *35*, 5756.
4. Mason, M. R.; Mashuta, M. S.; Richardson, J. F. *Angew. Chem., Int. Ed. Engl.* **1997**, *36*, 239.
5. Mason, M. R.; Perkins, A. M.; Matthews, R. M.; Fisher, J. D.; Mashuta, M. S.; Vij, A. *Inorg. Chem.* **1998**, *37*, 3734.
6. Mason, M. R.; Perkins, A. M.; Matthews, R. M.; Fisher, J. D.; Mashuta, M. S.; Vij, A. *Organometallics*, manuscript in preparation.
7. Mason, M. R.; Perkins, A. M.; Ponomarova, V.; Vij, A. *Organometallics* **2001**, in press.
8. Diemert, K.; Englert, U.; Kuchen, W.; Sandt, F. *Angew. Chem., Int. Ed. Engl.* **1997**, *36*, 241.
9. Keys, A.; Bott, S.; Barron, A. R. *J. Chem. Soc., Chem. Commun.* **1996**, 2339.
10. Chakraborty, D.; Horchler, S.; Roesky, H. W.; Noltemeyer, M.; Schmidt, H.-G. *Inorg. Chem.* **2000**, *39*, 3995.
11. Yang, Y.; Pinkas, J.; Noltemeyer, M.; Roesky, H. W. *Inorg. Chem.* **1998**, *37*, 6404.
12. Yang, Y.; Schmidt, H.-G.; Noltemeyer, M.; Pinkas, J.; Roesky, H. W. *J. Chem. Soc., Dalton Trans.* **1996**, 3609.
13. Walawalkar, M. G.; Murugavel, R.; Roesky, H. W.; Schmidt, H.-G. *Organometallics* **1997**, *16*, 516.
14. Walawalkar, M. G.; Murugavel, R.; Roesky, H. W.; Schmidt, H.-G. *Inorg. Chem.* **1997**, *36*, 4202.
15. Yang, Y.; Walawalkar, M. G.; Pinkas, J.; Roesky, H. W.; Schmidt, H.-G. *Angew. Chem., Int. Ed. Engl.* **1998**, *37*, 96.
16. Walawalkar, M. G.; Murugavel, R.; Voigt, A.; Roesky, H. W.; Schmidt, H.-G. *J. Am. Chem. Soc.* **1997**, *119*, 4656.
17. Pinkas, J.; Wessel, H.; Yang, Y.; Montero, M. L.; Noltemeyer, M.; Fröba, M.; Roesky, H. W. *Inorg. Chem.* **1998**, *37*, 2450.
18. Yang, Y.; Pinkas, J.; Schäfer, M.; Roesky, H. W. *Angew. Chem., Int. Ed. Engl.* **1998**, *37*, 2650.
19. Chakraborty, D.; Horchler, S.; Krätzner, R.; Varkey, S. P.; Pinkas, J.; Roesky, H. W.; Usón, I.; Noltemeyer, M.; Schmidt, H.-G. *Inorg. Chem.* **2001**, *40*, 2620.
20. Cassidy, J. E.; Jarvis, J. A. J.; Rother, R. N. *J. Chem. Soc., Dalton Trans.* **1975**, 1497.

21. Lugmair, C. G.; Tilley, T. D.; Rheingold, A. L. *Chem. Mater.* **1999**, *11*, 1615.
22. Chaplais, G.; Bideau, J. L.; Leclercq, D.; Mutin, H.; Vioux, A. *J. Mater. Chem.* **2000**, *10*, 1593.
23. Cabeza, A.; Aranda, M. A. G.; Bruque, S.; Poojary, D. M.; Clearfield, A.; Sanz, J. *Inorg. Chem.* **1998**, *37*, 4168.
24. Fredoueil, F.; Massiot, D.; Poojary, D.; Bujoli-Doeuff, M.; Clearfield, A.; Bujoli, B. *Chem. Commun.* **1998**, 175.
25. Morizzi, J.; Hobday, M.; Rix, C. *J. Mater. Chem.* **2000**, *10*, 1693.
26. Morizzi, J.; Hobday, M.; Rix, C. *J. Mater. Chem.* **1999**, *9*, 863.
27. Maeda, K.; Hashiguchi, Y.; Kiyozumi, Y.; Mizukami, F. *Bull. Chem. Soc. Jpn.* **1997**, *70*, 345.
28. Maeda, K.; Akimoto, J.; Kiyozumi, Y.; Mizukami, F. *J. Chem. Soc., Chem. Commun.* **1995**, 1033.
29. Maeda, K.; Akimoto, J.; Kiyozumi, Y.; Mizukami, F. *Angew. Chem., Int. Ed. Engl.* **1995**, *34*, 1199.
30. Maeda, K.; Kiyozumi, Y.; Mizukami, F. *Angew. Chem., Int. Ed. Engl.* **1994**, *33*, 2335.
31. Carter, V. J.; Wright, P. A.; Gale, J. D.; Morris, R. E.; Sastre, E.; Perez-Pariente, J. *J. Mater. Chem.* **1997**, *7*, 2287.
32. Stang, P. J.; Olenyuk, B. *Acc. Chem. Res.* **1997**, *30*, 502.
33. Eddaoudi, M.; Moler, D. B.; Li, H.; Chen, B.; Reineke, T. M.; O'Keefe, M.; Yaghi, O. M. *Acc. Chem. Res.* **2001**, *34*, 319.
34. Hirao, T.; Masunaga, T.; Oshiro, Y.; Agawa, T. *Synthesis* **1981**, 56.
35. Mason, M. R.; Ponomarova, V.; Matthews, R. M., manuscript in preparation.
36. Mason, M. R.; Ponomarova, V., unpublished result.
37. Wragg, D. S.; Morris, R. E. *J. Am. Chem. Soc.* **2000**, *122*, 11246.

Chapter 14

Polyimido Anions of Group 13 Elements

P. Blais, J. K. Brask, T. Chivers, C. Fedorchuk, and G. Schatte

Department of Chemistry, University of Calgary, Calgary,
Alberta T2N 1N4, Canada

Polyimido anions of the type $E(NR)_3^{3-}$ ($E = B, Al$) are isoelectronic with the common oxo-anions EO_3^{3-} . This article reviews the unexpected chemistry involved in the attempted synthesis of these trianions by the lithiation of trisamido derivatives of group 13 elements. The reaction of $B(NH^tBu)_3$ with three equivalents of organolithium reagents RLi ($R = Me, ^nBu, ^iBu, Ph$) generates the boraamidinates $\{Li_2[RB(N^tBu)_2]\}_x$, which have been shown by X-ray crystallography to have dimeric or trimeric cluster structures. The coordination chemistry of the dianionic boraamidinate ligands $[RB(NR)_2]^{2-}$ is reviewed. The reaction of the dimeric trisamido derivatives $[M(NH^tBu)_3]_2$ ($M = Al, Ga$) with RLi reagents results in the entrapment of monomeric or dimeric organolithium fragments by partially lithiated M_2N_6 templates.

Polyimido anions with p-block element centres, e.g. $[C(N^tBu)_3]^{2-}$ (1), have attracted attention recently as multidentate ligands with unique electronic and/or stereochemical properties that may engender novel metal-centered chemistry (1, 2). These anions are isoelectronic with common oxo anions, e.g. CO_3^{2-} , BO_3^{3-} .

Structures of Dilithium Alkyl/Aryl Boraamidates

The structures of complexes **4a-d** are derived from a simple building block in which an RB unit bridges a distorted four-membered Li_2N_2 ring (**5** in Figure 1). The face-to-face dimerization of two units of **5** generates the ten-atom cluster, with a distorted Li_4N_4 cube, that has been structurally characterized for **4b**, **4c** and **4d** (9). In the case of **4a** a trimeric cluster is also obtained. As indicated in Figure 1 this oligomer is derived from the edge-on (Li-N) interactions of three units of **5** to give a distorted hexagonal prism. It is possible that the use of groups smaller than ^tBu attached to nitrogen will result in the formation of larger oligomeric clusters or even polymeric open-ladder structures via lateral Li-N interactions.

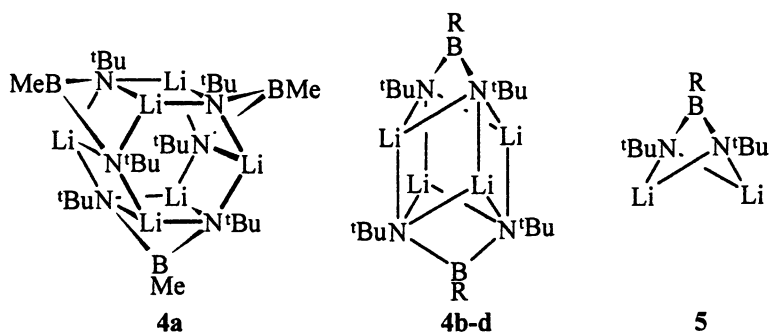
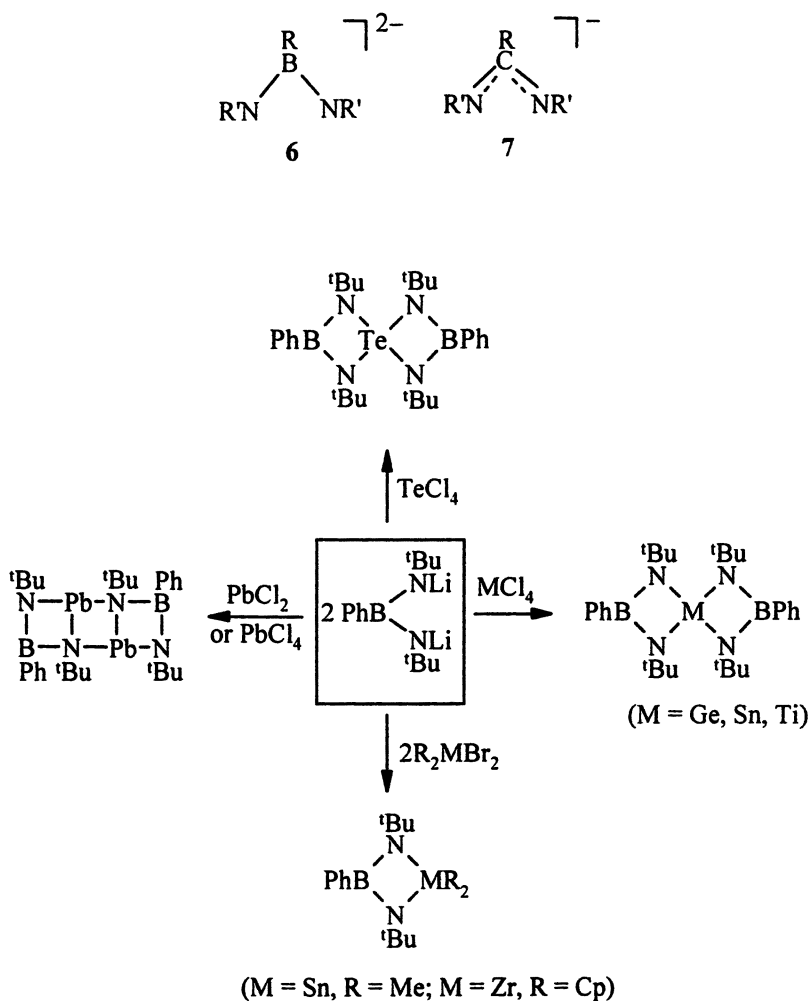


Figure 1. The monomeric unit **5** and the dimeric and trimeric clusters formed by dilithium alkyl/aryl boraamidates.

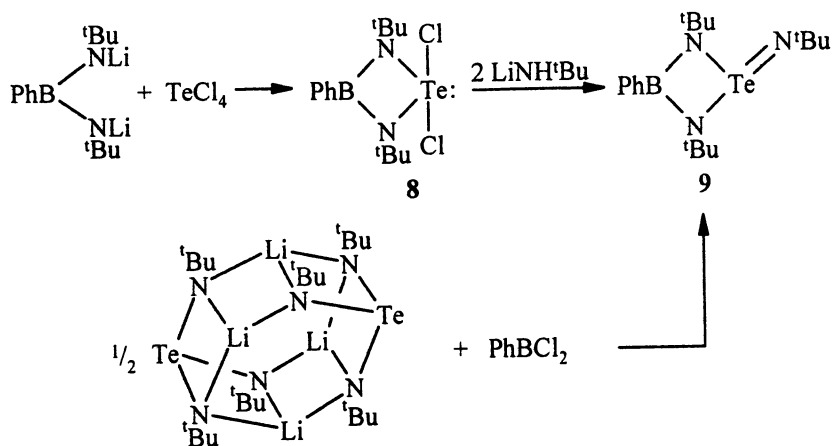
Metal Complexes of Boraamidates

The boraamidate ligand $[\text{RB}(\text{NR}')_2]^{2-}$ (**6**) is isoelectronic with the extensively studied amidinate anions $[\text{RC}(\text{NR}')_2]^-$ (**7**) (11). Metal complexes of the dianionic ligand **6** are readily obtained by metathetical reactions between $\text{Li}_2[\text{PhB}(\text{NR})_2]$ and metal halides. Early studies were primarily limited to Group 4 or 14 metals for which complexes containing one or two boraamidate ligands have been obtained (10b) (Scheme 1). This approach has been extended to the synthesis of the pentafluorophenyl derivative $\text{C}_6\text{F}_5\text{B}(\text{N}^t\text{Bu})_2\text{SnMe}_2$ (10c).

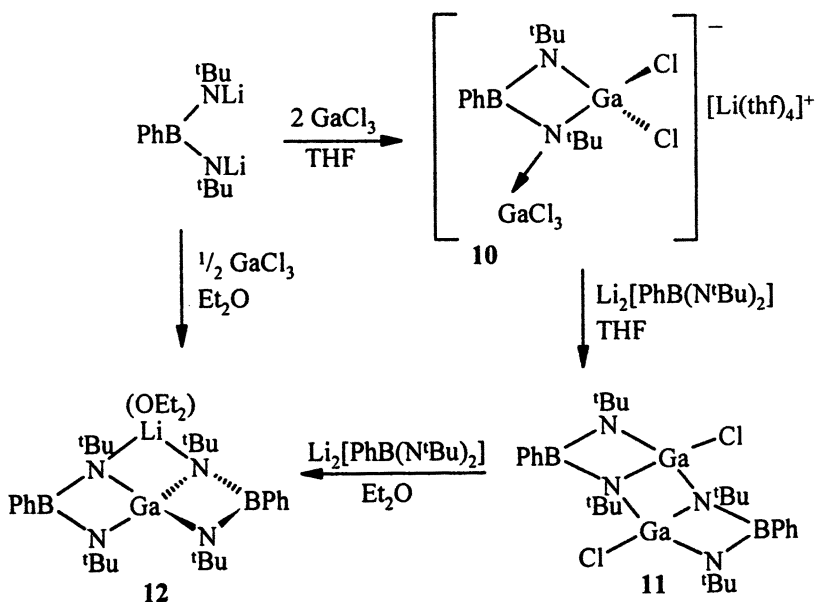


Scheme 1.

The metathetical reaction between $\text{Li}_2[\text{PhB}(\text{N}^t\text{Bu})_2]$ and TeCl_4 in a 2:1 molar ratio produces a spirocyclic tellurium (IV) complex (12) (Scheme 1). More recently we have shown that this reaction produces the boraamidinato tellurium dichloride **8** in excellent yield when a 1:1 molar ratio is employed (13). Subsequent treatment of this dimeric complex with lithium *tert*-butylamide produces the tellurium imide $\text{PhB}(\mu\text{-N}^t\text{Bu})_2\text{TeN}^t\text{Bu}$ (**9**) (13). Apparently the boraamidinato ligand inhibits the dimerization of the $\text{Te}=\text{N}^t\text{Bu}$ functionality. Complex **9** may also be obtained, though less conveniently, from the reaction of PhBCl_2 with $\{\text{Li}_2[\text{Te}(\text{N}^t\text{Bu})_3]_2\}_2$ (Scheme 2) (5a).



Scheme 2.



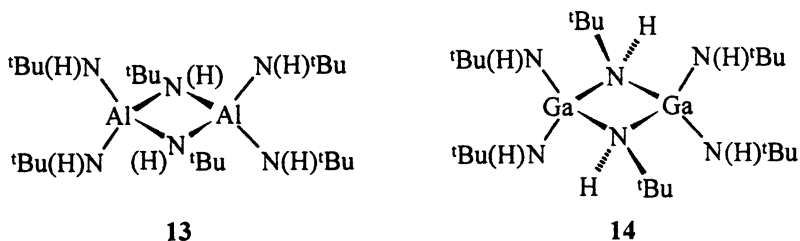
Scheme 3.

Preliminary investigations of Group 13 complexes of boraamidates have led to the structural characterization of **10**, **11** and **12** in which the chloride ligands in GaCl_3 are successively replaced (Scheme 3) (13a). The indium analogue of **12**, prepared in a similar manner, also has a spirocyclic structure (13b).

Although the use of reagents of the type $\text{Li}_2[\text{RB}(\text{NR}')_2]$ in metathetical reactions is the most versatile route to boraamidate complexes, several other synthetic approaches have been reported. These include the preparation of (a) the dimeric Sn(II) complex $[\text{PhB}(\text{N}^{\text{tBu}})_2\text{Sn}]_2$ by the reaction of SnCl_2 with $\text{Me}_3\text{SiN}(\text{Li})\text{BMe}_2$ (14), (b) sulfur(II) complexes of the type $\text{RB}(\mu\text{-NR}')(\mu\text{-NR}'')\text{S}$ by treatment of sulfur(IV) diimides with $\text{RB}(\text{SME})_2$ (15), (c) $\text{C}_6\text{F}_5\text{B}(\text{N}^{\text{tBu}})_2\text{CPh}_2$ (16) and ${}^{\text{tBu}}\text{B}(\text{N}^{\text{tBu}})_2\text{P}^{\text{tBu}}(\text{N}^{\text{tBu}})$ (17) by [2 + 2] cycloaddition reactions of the appropriate iminoborane with ${}^{\text{tBu}}\text{N}=\text{CPh}_2$ or ${}^{\text{tBu}}\text{N}=\text{P}^{\text{tBu}}$, respectively, (d) $\text{MesB}(\text{N}^{\text{tBu}})_2\text{Si}(\text{Mes})\text{SiMe}_3$ by the reaction of the iminoborane $\text{Me}_3\text{Si}(\text{tBu})\text{NB}=\text{N}^{\text{tBu}}$ with the photochemically generated silylene SiMes_2 (18) and (e) $\text{MeB}(\text{NAr})_2\text{SiMe}_2$ (Ar = 2,6-diisopropylphenyl) from the isomerization of $\text{ArN}=\text{BN}(\text{Ar})\text{SiMe}_3$ formed by the lithiation of $\text{Ar}(\text{H})\text{NB}(\text{F})\text{N}(\text{R})\text{SiMe}_3$ with Li^{tBu} (19). Metathesis reactions could undoubtedly be applied to synthesis of the aforementioned Sn(II), S(II) and $\text{Me}_2\text{Si}(\text{IV})$ derivatives, but the cycloaddition reaction with iminoboranes provides a method of generating boraamidate complexes that are not accessible via halide/metal exchange.

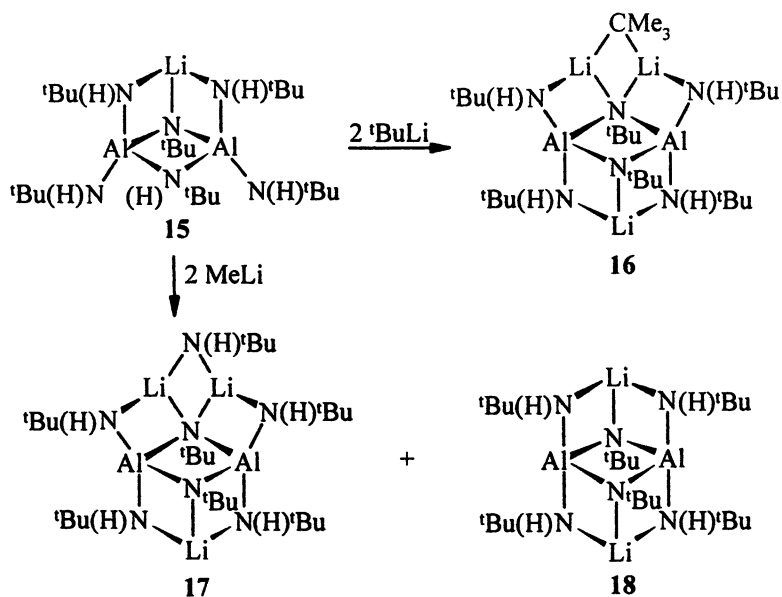
Lithiation of $[M(\text{NH}^t\text{Bu})_3]_2$

The dimeric trisamido complexes $[M(\text{NH}^t\text{Bu})_3]_2$ (**13**, $M = \text{Al}$; **14**, $M = \text{Ga}$) are prepared by the reaction of lithium *tert*-butylamide with AlCl_3 or GaCl_3 , respectively, in diethyl ether. Complex **13** is obtained as a mixture of *cis* and *trans*-isomers that is not readily separated by fractional crystallization (7) whereas the gallium analogue **14** is isolated as the *cis*-isomer (8).



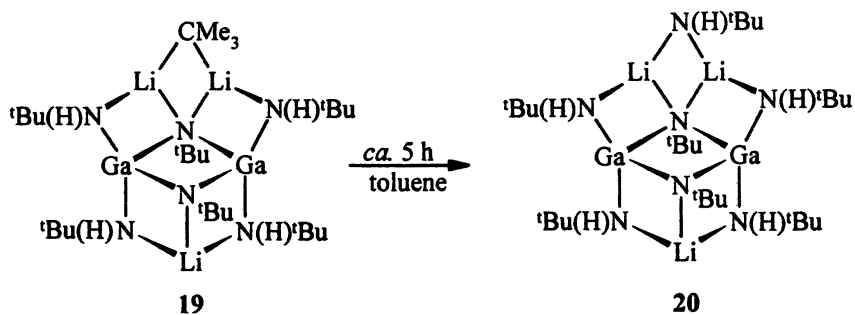
The outcome of the reaction of **13** with an excess of an organolithium reagent is different for the three RLi reagents ($\text{R} = \text{Me}$, ${}^t\text{Bu}$, ${}^n\text{Bu}$) that have been studied (20). In all three cases the initial monolithiation occurs at one of the bridging amido groups to give complex **15** on the basis of the ${}^1\text{H}$ NMR spectrum, which exhibits four resonances attributed inequivalent bridging N^tBu and NH^tBu groups and inequivalent pairs of terminal NH^tBu groups with the appropriate relative intensities (Scheme 4). Subsequent lithiation with *tert*-butyllithium yields a complex that shows four ${}^t\text{Bu}$ resonances with relative intensities 1:2:2:2 in the ${}^1\text{H}$ NMR spectrum. An X-ray structure revealed this complex (**16**) to contain a monomeric ${}^t\text{BuLi}$ unit entrapped by a dilithium derivative of **13** consistent with the NMR data.

By contrast, the reaction of **13** with methyllithium generates two products **17** and **18** in isolated yields of 44% and 19%, respectively (20) (Scheme 4). Complex **17** was shown by X-ray crystallography to involve the entrapment of a monomeric LiNH^tBu unit by a dilithium derivative of **13**. The minor product **18** showed two ${}^t\text{Bu}$ resonances in the ${}^1\text{H}$ NMR spectrum with relative intensities 1:2 consistent with the lithiation of both bridging NH^tBu groups of **13**. Thus it appears that, in addition to acting as a lithiation reagent, methyllithium also acts as a nucleophile generating LiNH^tBu which is trapped by the dilithiated complex **18**.



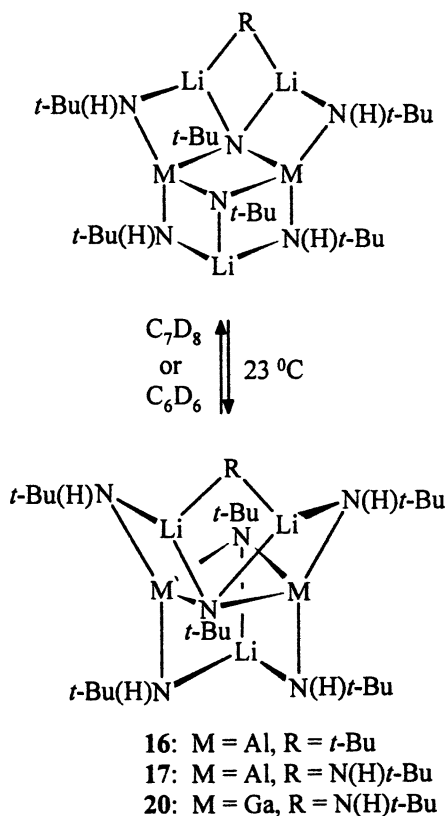
Scheme 4.

Interestingly the gallium complex 19, which was identified by the close similarity of the ¹H NMR pattern with that of the aluminum analogue 16, converts over a period of *ca.* 5 hours at room temperature to 20, the gallium analogue of 17, which was characterized by X-ray crystallography (20) (Scheme 5).



Scheme 5.

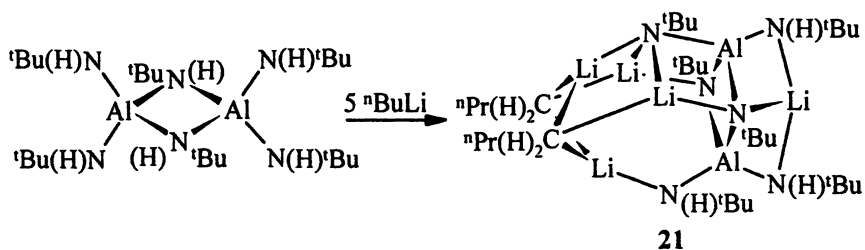
The complexes **16**, **17** and **20** exhibit fluxionality in aromatic solvents, as monitored by ^1H NMR. Only four $t\text{Bu}$ resonances with relative intensities 1:2:2:2 are observed for such solutions at room temperature (**20**). Variable temperature ^1H NMR studies indicate that the fluxional process involves concerted Li-N bond breaking and formation as depicted in Scheme 6.



Scheme 6.

The third organolithium reagent investigated was *n*-butyllithium. In this case the trapped organolithium fragment is in the form of the dimer $(\text{Li}^n\text{Bu})_2$, which is stabilized by coordination to a trilitiated derivative of **13** in the complex **21** (**7**) (Scheme 7). Entrapment of a solvated $(\text{Li}^n\text{Bu})_2$ unit has been

observed recently in the complex $(\text{Ph}_2\text{NLi})[\text{Ph}(\text{C}_6\text{H}_4\text{Li})\text{NLi}]_2(\text{Li}^t\text{Bu})_2(\text{Et}_2\text{O})_4$ (21), but 21 is unique in incorporating an *unsolvated* $(\text{Li}^t\text{Bu})_2$ dimer. Variable temperature ^1H NMR studies indicate that 21 is fluxional in solution (7).



Scheme 7.

In summary, the reactions of the trisamidoalane or gallane dimers, 13 and 14, with organolithium reagents result in the stabilization of monomeric or dimeric organolithium fragments by a partially lithiated M_2N_6 ($\text{M} = \text{Al}, \text{Ga}$) framework. Alternative metallating agents, or a different synthetic approach, will be necessary for the generation of $\text{Al}(\text{NR})_3^{3-}$, an isoelectronic analogue of AlO_3^{3-} .

Reactions of MAlH_4 ($\text{M} = \text{Li}, \text{Na}$) with Primary Amines

The reactions of secondary amines with LiAlH_4 have been studied extensively (22-25). Several complexes of the type $[\text{L}_2\text{LiAl}(\text{NR}_2)_4]$ ($\text{L} =$ electron-pair donor ligand) (22, 23) as well as the intermediate lithium amidohydridoaluminates formed in this process, e.g. $[\text{H}_3\text{AlN}(\text{SiMe}_3)_2\text{Li}(\text{Et}_2\text{O})_2]_2$ (24) and $[\text{Li}(\text{THF})_4][\text{HAl}(\text{NPh}_2)_3]$ (25) have been structurally characterized. Intermediates containing one or two Al-H functionalities have also been isolated from the reaction of LiAlH_4 with the sterically demanding primary amine DippNH_2 ($\text{Dipp} = 2,6$ -diisopropylaniline) (26).

Tetrakisimido anions of the type $[\text{E}(\text{NR})_4]^{x-}$ [$\text{E} = \text{S}, x = 2$ (27); $\text{E} = \text{P}, x = 3$ (28); $\text{E} = \text{Si}, x = 4$ (29)] have been characterized. As yet no examples of the pentaanion $[\text{Al}(\text{NR})_4]^{5-}$, the fourth member of this isoelectronic series, have been reported, although the corresponding oxo anion is well known, e.g. Na_5AlO_4 (30). Tetrakisamido aluminates of the type $\text{Li}[\text{Al}(\text{NHR})_4]$ ($\text{R} = ^t\text{Bu}, ^i\text{Pr}, p\text{-tolyl}$), which are potential precursors of $[\text{Al}(\text{NR})_4]^{5-}$, are readily prepared by the reaction of the appropriate primary amine with LiAlH_4 (31).

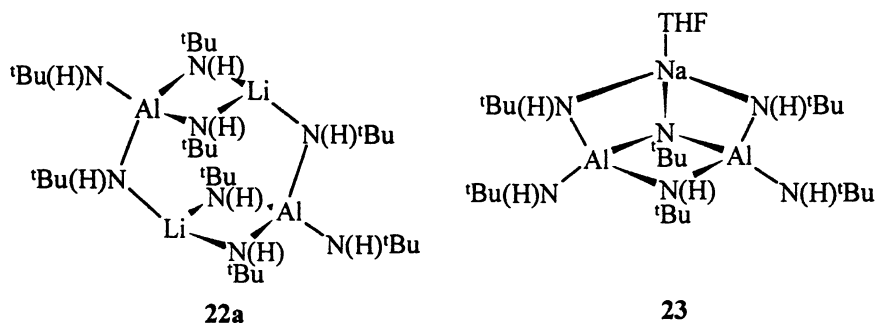


(22a, R = ^tBu)

(22b, R = ⁱPr)

(22c, R = *p*-tolyl)

Complex 22a is also obtained from the reaction of AlCl₃ with LiNH^tBu (32). Recrystallization from a non-coordinating solvent generates a dimeric species whereas the aryl derivative 22c has been characterized as the ion-separated complex [Li(THF)₄][Al(NH*p*-tolyl)₄] (31). Interestingly, the reaction of *tert*-butylamine with NaAlH₄ in THF yields the bimetallic complex 23. As in the case of 15 monometallation occurs at one of the bridging ^tBuN(H) groups.



Finally, we note that the reaction of H₃Al·N(Me)C₃H₈ with LiNHPH generates the intriguing ion-separated complex [Li(OEt₂)₃]⁺{(HAl)₄(NPh)₆[Li(OEt₂)₃]₃}⁻ (24) (33). The imidoalane anion in 24 consists of an adamantoid [(HAl)₄(NPh)₆]⁴⁻ tetraanion with three of the four six-membered Al₃N₃ rings asymmetrically capped by μ₃-Li⁺ centers.

References

- Chivers, T.; Parvez, M.; Schatte, G. *J. Organomet. Chem.* **1998**, *550*, 213.
- Brask, J. K.; Chivers, T. *Angew. Chem., Int. Ed. Engl.* **2001**, in press.
- (a) Veith, M.; Lisowsky, R. *Angew. Chem., Int. Ed. Engl.* **1988**, *27*, 1087;
(b) Bailey, P. J.; Blake, A. J.; Kryszczuk, M.; Parsons, S.; Reed, D. *J. Chem. Soc., Chem. Commun.* **1995**, 1647.
- Edwards, A. J.; Paver, M. A.; Raithby, P. R.; Rennie, M.-A.; Russell, C. A.; Wright, D. C. *Angew. Chem., Int. Ed. Engl.* **1994**, *33*, 1277.

5. (a) Chivers, T.; Gao, X.; Parvez, M. *Angew. Chem., Int. Ed. Engl.* **1996**, *35*, 2549; (b) Fleischer, R.; Freitag, S.; Pauer, F.; Stalke, D. *Angew. Chem., Int. Ed. Engl.* **1996**, *35*, 204; (c) Chivers, T.; Parvez, M.; Schatte, G. *Inorg. Chem.* **1996**, *35*, 4094.
6. Aubrey, D. W.; Lappert, M. F. *J. Chem. Soc.* **1959**, 2927.
7. Brask, J. K.; Chivers, T.; Yap, G. P. A. *Chem. Commun.* **1998**, 2543.
8. Atwood, D. A.; Atwood, V. O.; Cowley, A. H.; Jones, R. A.; Atwood, J. L.; Bott, S. G. *Inorg. Chem.*, **1994**, *33*, 3251.
9. (a) Brask, J. K.; Chivers, T.; Schatte, G. *Chem. Commun.* **2000**, 1805; (b) Brask, J. K.; Chivers, T.; Fedorchuk, C.; Schatte, G. unpublished results.
10. (a) Heine, A.; Fest, D.; Stalke, D.; Habben, C. D.; Meller, A.; Sheldrick, G. M. *J. Chem. Soc., Chem. Commun.* **1990**, 742; (b) Fest, D.; Habben, C. D.; Meller, A.; Sheldrick, G. M.; Stalke, D.; Pauer, F. *Chem. Ber.* **1990**, *123*, 703; (c) Habben, C. D.; Heine, A.; Sheldrick, G. M.; Stalke, D. *Z. Naturforsch.* **1992**, *47b*, 1367.
11. (a) Edelmann, F. T. *Coord. Chem. Rev.* **1994**, *137*, 403; (b) Barker, J.; Kilner, M. *Coord. Chem. Rev.* **1994**, *133*, 219.
12. Koch, H.-J.; Roesky, H. W.; Besser, S.; Herbst-Irmer, R. *Chem. Ber.* **1993**, *126*, 571.
13. (a) Chivers, T.; Schatte, G. unpublished results; (b) Chivers, T.; Fedorchuk, C.; Schatte, G. unpublished results.
14. Fußstetter, H.; Nöth, H. *Chem. Ber.* **1979**, *112*, 3672.
15. Habben, C. D.; Heine, A.; Sheldrick, G.M.; Stalke, D.; Bühl, M.; von R. Schleyer, P. *Chem. Ber.* **1991**, *124*, 47.
16. Paetzold, P.; Richter, A.; Thijssen, T.; Wurtenburg, S. *Chem. Ber.* **1979**, *112*, 3811.
17. Gudat, D.; Niecke, E.; Nieger, M.; Paetzold, P. *Chem. Ber.* **1988**, *121*, 565.
18. Paetzold, P.; Hahnfeld, D.; Englert, U.; Wojnowski, W.; Dreczewski, B.; Pawelec, Z.; Walz, L. *Chem. Ber.* **1992**, *125*, 1073.
19. Luthin, W.; Stratmann, J.-G.; Elter, G.; Meller, A.; Heine, A.; Gornitzka, H. *Z. Anorg. Allg. Chem.* **1995**, *621*, 1995.
20. Brask, J. K.; Chivers, T.; Schatte, G.; Yap, G. P. A. *Organometallics* **2000**, *19*, 5683.
21. Davies, R. P.; Raithby, P. R.; Snaith, R. *Angew. Chem., Int. Ed. Engl.* **1997**, *36*, 1215.
22. (a) Böck, S.; Nöth, H.; Rahm, P. *Z. Naturforsch.* **1988**, *43b*, 53; (b) Linti, G.; Nöth, H.; Rahm, P. *Z. Naturforsch.* **1988**, *43b*, 1101.
23. Andrianarison, M. M.; Ellerby, M. C.; Gorrell, I. B.; Hitchcock, P. B.; Smith, J. D.; Stanley, R. D. *J. Chem. Soc., Dalton Trans.* **1996**, 211.
24. Heine, A.; Stalke, D. *Angew. Chem., Int. Ed. Engl.* **1992**, *31*, 854.
25. Pauls, J.; Neumüller, B. *Inorg. Chem.* **2001**, *40*, 121.

26. Montero, M. L.; Wessel, H.; Roesky, H. W.; Teichert, M.; Usón, I. *Angew. Chem., Int. Ed. Engl.* **1997**, *36*, 629.
27. Fleischer, R.; Rothenberger, A.; Stalke, D. *Angew. Chem., Int. Ed. Engl.* **1997**, *36*, 1105.
28. Raithby, P.R.; Russell, C.A.; Steiner, A.; Wright, D.S. *Angew. Chem., Int. Ed. Engl.* **1997**, *36*, 649.
29. Brask, J. K.; Chivers, T.; Parvez, M. *Inorg. Chem.* **2000**, *39*, 2505.
30. Barker, M.G.; Gadd, P.G.; Begley, M. J. *J.C.S. Chem. Comm.* **1981**, 379.
31. Blais, P.; Chivers, T.; Schatte, G. *Can. J. Chem.*, submitted.
32. Silverman, J. S.; Carmalt, C. J.; Neumayer, D. A.; Cowley, A. H.; McBurnett, B. G.; Decken, A. *Polyhedron* **1998**, *17*, 977.
33. Henderson, K. W.; Kennedy, A. R.; McKeown, A. E.; Mulvey, R. E. *Angew. Chem., Int. Ed. Engl.* **2000**, *39*, 3879.

Chapter 15

A Density Functional Theory Study of Distortions from Octahedral Symmetry in Hypoelectronic Six-Vertex Polyhedral Clusters of the Group 13 Elements Boron, Indium, and Thallium

R. B. King¹, I. Silaghi-Dumitrescu², and A. Kun²

¹Department of Chemistry, University of Georgia, Athens, GA 30602

²Faculty of Chemistry and Chemical Engineering, Babes-Bolyai University, Cluj-Napoca, Roumania

Density functional theory (DFT) has been applied to the six atom icosogen clusters (Ic_6^z : $z = 4, 6, 8$; $\text{Ic} = \text{B, In, Tl}$). Convergence to energy minima was obtained with the following optimized structures: (a) Ic_6^{8-} : Regular octahedral geometry (O_h) for these 14 skeletal electron clusters in accord with the expected absence of Jahn-Teller effects and the known geometry of Tl_6^{8-} ; (b) Ic_6^{6-} : Oblate (flattened) tetragonal bipyramidal (D_{4h}) and oblate trigonal antiprismatic (D_{3d}) geometries in accord with the experimentally observed oblate tetragonal bipyramidal geometry for Tl_6^{6-} in CsTl ; (c) Ic_6^{4-} : C_{2v} bicapped tetrahedral ($\text{Ic} = \text{B}$) or D_{3d} prolate (elongated) trigonal antiprismatic ($\text{Ic} = \text{In, Tl}$) geometries. The shapes of the frontier orbitals in the optimized structures have been determined.

Introduction

Experimental work in recent years by Corbett and co-workers¹ on intermetallics containing alkali metals and the heavier group 13 elements indium and thallium (icosogens or triels) has led to the discovery of a number of unusual deltahedra quite different from the deltahedra found in the boranes $B_nH_n^{2-}$ ($6 \leq n \leq 12$).^{2,3} This appears to be related to the skeletal electron counts of the deltahedra since borane deltahedra contain $2n + 2$ skeletal electrons whereas the deltahedra of the heavier icosogens in their alkali metal intermetallics contain less than $2n + 2$ apparent skeletal electrons and thus may be regarded as hypoelectronic. Such hypoelectronic deltahedra (Figure 1) are known for icosogen clusters containing six,^{4,5} seven,⁶ nine,⁷ ten,^{8,9,10} and eleven^{11,12,13,14,15} atoms. An analysis of the topology of these hypoelectronic polyhedra^{16,17} suggests that the apparent electron deficiency is relieved by a distortion consisting of flattening selected degree 4 vertices of the parent deltahedron. This has been attributed to participation of the flattened vertex d orbitals in addition to the sp^3 orbitals.^{16,17} Such d orbital participation provides a way for otherwise non-bonding external electrons in these d orbitals to participate in the deltahedral skeletal bonding in order to relieve the apparent extreme electron deficiencies of the hypoelectronic deltahedra. Alternatively the flattened vertices of the hypoelectronic deltahedra can be regarded as "inverted" vertices similar to the bridgehead vertices in tricyclo-[1.1.1]-pentane, in which all four orbitals of the sp^3 valence orbital manifold can be internal orbitals.¹⁸ This avoids the need for d orbital participation in these post-transition element clusters similar to the use of multicenter bonding models for hypervalent coordination compounds of the heavier main group elements as an alternative to d orbital participation in their chemical bonding.^{19,20,21}

This chapter presents some details of our initial attempt to study computationally by modern density functional theory (DFT) methods the phenomenon of flattening in hypoelectronic icosogen deltahedra. Previous computational work on these deltahedra, largely by Corbett and co-workers,¹ have been limited to extended Hückel methods. The six-vertex system was selected for this initial DFT study since it represents by far the least complicated of the icosogen deltahedra exhibiting flattening. The experimentally known examples of hypoelectronic six-vertex deltahedra are found in the intermetallics KTI^4 and $CsTI^5$, both of which were found to contain isolated oblate tetragonal bipyramidal Tl_6^{6-} anions of ideal D_{4h} symmetry derived from the axial compression of a regular octahedron thereby destroying its C_3 axes. The system is modeled computationally by DFT calculations on the isolated anions Ic_6^{n-} ($Ic = B, In, Tl; z = 4, 6, 8$). The anions Ic_6^{8-} have the $14 = 2n + 2$ skeletal electron

count expected for a regular octahedron and found in well-known octahedral clusters such as $B_6H_6^{2-}$. The anions Ic_6^{6-} represent the electronic configuration found in the experimentally known^{4,5} Tl_6^{6-} whereas the anions Ic_6^{4-} represent a still greater degree of electron deficiency.

A recent note²² provides a summary of these calculations including the optimized structures. This more detailed paper discusses the underlying topology and group theory and presents pictures of the skeletal bonding molecular orbitals of the various types of six-vertex icosogen clusters.

Computational Methods

Density functional theory was used at the following two levels:

(1) B3LYP/LANL2DZ, which includes Becke's 3 parameter functional²³ with LYP type non-local correlation functionals²⁴ as implemented in Gaussian 94.²⁵ The basis functions include Los Alamos ECP's and are of DZ quality.²⁶

(2) A BP86 density functional with nonlocal corrections introduced in a perturbative manner coded in Spartan as pBP86/DN* using Becke's 1988 functional²⁷ with a numerical basis set (DN*) implemented in Spartan.²⁸

Except for Tl_6^{8-} , which converged towards the isolated atoms, all other structures have been fully optimized at both levels of approximation within the default convergence criteria found in these programs (rms gradient = 10^{-4} in Spartan, maximum force = 0.000450, rms force = 0.000300, maximum displacement = 0.001800, rms displacement = 0.001200, respectively, in Gaussian). The optimized structures are depicted in Figure 1. Orbital shapes are based on the Gaussian outputs and have been drawn by using the Molekel package.²⁹ The computed total energies of the optimum structures of the Ic_6^{n-} species are given in Table 1.

Results

The computed total energies of the optimum structures of the Ic_6^{n-} species are given in Table 1. The computed energies for individual molecular orbitals (MOs) in the Ic_6^{n-} species are given in Tables 2, 3, and 4 for $Ic = B, In,$ and Tl , respectively. In these tables the MOs are listed in order of increasing energies with the highest occupied molecular orbitals (HOMOs) being in bold boxes. Orbitals listed above the HOMOs are occupied bonding orbitals whereas orbitals listed below the HOMOs are unoccupied antibonding orbitals.

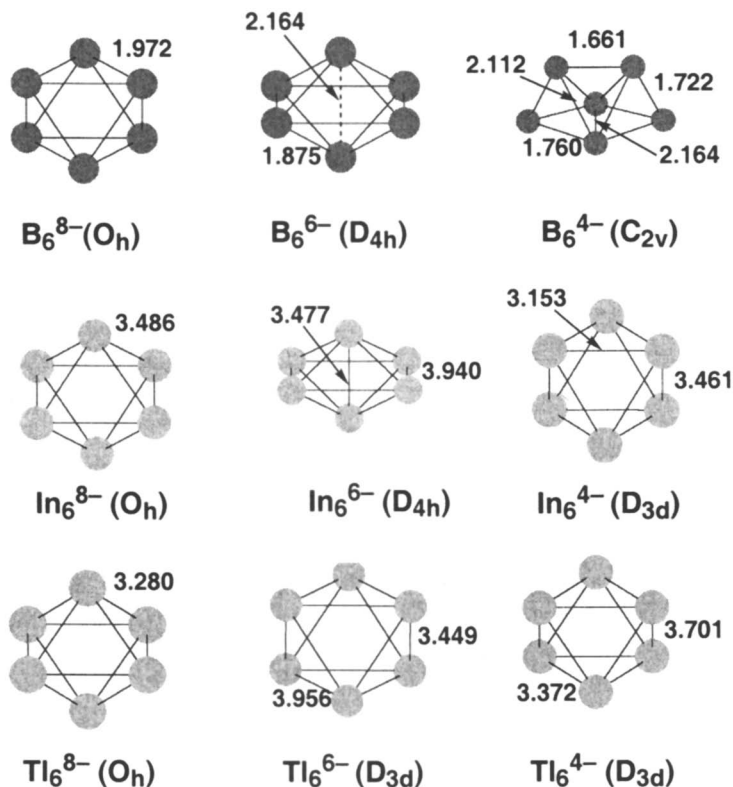


Figure 1: Optimized structures for the nine species Ic_6^{n-} ($n = 8, 6, 4$; $Ic = B, In, Tl$).

The significance of the Kohn-Sham (KS) orbitals obtained within the limits of various DFT functionals has been addressed in recent years by several papers.^{36,37,38,39,40,41} It appears that the shapes, symmetry properties, and energy orders of the occupied MOs are similar to those calculated by Hartree-Fock and extended Hückel methods. This supports the idea of using the KS orbitals as the basis for qualitative and quantitative (after a linear scaling) interpretation of MOs.³⁵

Table I: Total Energies (a. u.) of the Optimum Structures of Ic_6^{z-} Species

z	Method	B_6^{z-}	In_6^{z-}	Tl_6^{z-}
4	B3LYP/LANL2DZ	-147.8860165	-10.8247947	-309.2358056
4	LSDA/pBP86/DN*	-148.00215	-34458.81919	
6	B3LYP/LANL2DZ	-146.5265194	-9.8979723	-308.2994419 ^d
				-308.2891499 ^e
6	LSDA/pBP86/DN*	-147.09378 ^a	-34457.90383	
		-146.62782 ^b		
		-146.61358 ^c		
8	B3LYP/LANL2DZ	-144.618819	-8.484888	-306.9061411 ^f
8	LSDA/pBP86/DN*	-144.65176	-34456.56989	

^a Linear ($D_{\infty h}$).^b Bicapped tetrahedron (C_{2v}).^c Oblate tetragonal bipyramid (D_{4h}).^d Oblate trigonal antiprism (D_{3d}).^e Single point calculation of a D_{4h} oblate tetragonal antiprism obtained from the octahedron by applying the same ratio of compression as achieved by optimized In_6^{6-} relative to In_6^{8-} .^f Single point value calculated at the experimental geometry (O_h).

Discussion

Topological and Group Theoretical Background

The relevant six-vertex polyhedra can all be derived from the regular octahedron in one of two different ways as follows (Figure 2):

- (1) Topology-preserving distortions involving descent of symmetry from octahedral (O_h) to a subgroup of O_h (Figure 2a). This can occur either by tetragonal distortion or trigonal distortion. Tetragonal distortion results in loss of the C_3 axes to give a tetragonal bipyramid of D_{4h} symmetry, which can be either oblate (flattened along the C_4 axis) or prolate (elongated along the C_4 axis). Trigonal distortion results in loss of the C_4 axes to give a trigonal antiprism of D_{3d} symmetry, which likewise can be either oblate or prolate.
- (2) Conversion of an octahedron to a bicapped tetrahedron through a single diamond-square-diamond process (Figure 2b). The bicapped tetrahedron

has the same numbers of vertices (6), edges (12), and faces (8) as the regular octahedron but is topologically different. Thus the six vertices of the bicapped tetrahedron are partitioned into three symmetry-related pairs with degrees 3, 4, and 5 in contrast to the regular octahedron where all six vertices are equivalent with degree 4. This partitioning of the vertices of the bicapped tetrahedron lowers the symmetry to C_{2v} so that no pair or triplet of molecular orbitals is required to be degenerate by group theory.

Table II: Energies of the Molecular Orbitals in B_6^{z-}

Orbital no.	B_6^+	B_6^4	B_6^6	B_6^6	B_6^8	B_6^8
	B3LYP/ LANL2DZ	LSDA/ pBP86/DN*	B3LYP/ LANL2DZ	LSDA/ pBP86/DN*	B3LYP/ LANL2DZ	LSDA/ pBP86/DN*
1/7	0.00490	0.0734	0.30735	0.3978	0.60889	0.7106
2/8	0.19796	0.2568	0.53723	0.6116	0.83582	0.9254
3/9	0.25324	0.3220	0.53734	0.6117	0.83583	0.9254
4/10	0.32299	0.3724	0.59367	0.6689	0.83584	0.9254
5/11	0.39335	0.4303	0.70519	0.7534	0.98485	1.0459
6/12	0.42119	0.4629	0.73054	0.7891	1.01114	1.0840
7/13	0.42925	0.4807	0.75165	0.8018	1.01115	1.0841
8/14	0.44794	0.4818	0.75171	0.8019	1.02650	1.0877
9/15	0.49184	0.5039	0.76575	0.8040	1.02650	1.0877
10/16	0.50133	0.5320	0.77081	0.8142	1.02651	1.0877
11/17	0.50567	0.5389	0.77649	0.8143	1.05538	1.1041
12/18	0.55702	0.5523	0.77652	0.8300	1.05538	1.1041
13/19	0.60009	0.6147	0.86092	0.8806	1.05539	1.1042
14/20	0.62865	0.6426	0.92388	0.9586	1.18877	1.2466
15/21	0.64803	0.6700	0.93832	0.9586	1.18877	1.2466
16/22	0.68168	0.6958	0.93894	0.9699	1.21210	1.2466
			0.93892			
17/23	0.68797	0.6983	1.01032	0.9933	1.21209	1.2827
			1.01034		1.21210	1.2827
						1.2827
18/24	0.69010	0.7124		1.0062		
				1.0063		
				1.0064		

Table III: Energies of the Molecular Orbitals in In_6^{z-} .

Orbital no.	In_6^{4-}		In_6^{6-}		In_6^{8-}	
	B3LYP/ LANL2DZ	LSDA/ pBP86/DN*	B3LYP/ LANL2DZ	LSDA/ pBP86/DN*	B3LYP/ LANL2DZ	LSDA/ pBP86/DN*
1/139	0.08778	0.1119	0.32634	0.3486	0.56461	0.5818
2/140	0.16034	0.1766	0.39757	0.4160	0.62870	0.6396
3/141	0.19004	0.2031	0.39758	0.4161	0.62870	0.6396
4/142	0.19004	0.2146	0.42807	0.4435	0.62870	0.6396
5/143	0.24629	0.2548	0.42962	0.4480	0.67155	0.6783
6/144	0.24629	0.2596	0.45942	0.4743	0.67155	0.6785
7/145	0.31709	0.3232	0.54690	0.5473	0.75742	0.7534
8/146	0.33414	0.3298	0.54691	0.5475	0.77453	0.7609
9/147	0.34347	0.3327	0.54700	0.5477	0.77453	0.7609
10/148	0.34347	0.3414	0.55985	0.5527	0.77453	0.7609
11/149	0.35399	0.3447	0.55986	0.5548	0.77914	0.7742
12/150	0.38506	0.3525	0.56092	0.5548	0.77914	0.7742
13/151	0.38506	0.3779	0.61588	0.5937	0.77914	0.7744
14/152	0.43246	0.3879	0.62062	0.5940	0.84589	0.8082
15/153	0.43246	0.4024	0.62063	0.6002	0.84589	0.8082
16/154	0.43441	0.4138	0.62085	0.6029	0.84836	0.8082
17/155	0.44926	0.4204	0.62415	0.6031	0.84836	0.8238
18/156	0.44926	0.4265	0.64069	0.6099	0.84836	0.8236

The bonding in Ic_6^{8-} , like that in the isoelectronic $\text{B}_6\text{H}_6^{2-}$, can be considered to be that of a three-dimensional deltahedral aromatic system.⁴² In such systems the three internal orbitals from the four-orbital sp^3 manifold of each vertex atom are partitioned into two twin internal orbitals (tangential orbitals) and a unique internal orbital (radial orbital) leading to a total of $2n$ tangential orbitals and n radial orbitals for a deltahedron having n vertices such as the six-vertex octahedra discussed in this paper. Pairwise overlap between the tangential orbitals in the surface of the deltahedron (surface bonding) is responsible for the deltahedral framework and leads to the splitting of the $2n$ tangential orbitals into n bonding and n antibonding orbitals. The resulting equal numbers of bonding and antibonding molecular orbitals from overlap of the tangential atomic orbitals are supplemented by additional bonding and antibonding orbitals arising by the global mutual overlap of the n radial orbitals leading to an additional bond centered in the core of the deltahedron. In this core bonding the n radial orbitals overlap to form a single bonding orbital and $n - 1$ antibonding orbitals in an

n -center two-electron bond. The resulting combination of $2n$ skeletal electrons for the surface bonding and an additional two-electrons for the core bonding leads to the observed $2n + 2$ skeletal electrons for the closed deltahedral boranes $B_nH_n^{2-}$ ($6 \leq n \leq 12$)^{43,44,45,46} as well as other isoelectronic and isolobal species including the cluster anions Ic_6^{8-} (e.g., the regular octahedral Tl_6^{8-} anion found⁴⁷ in the intermetallics $Na_{14}K_6Tl_{18}M^{II}$ where $M^{II} = Mg, Zn, Cd, Hg$).

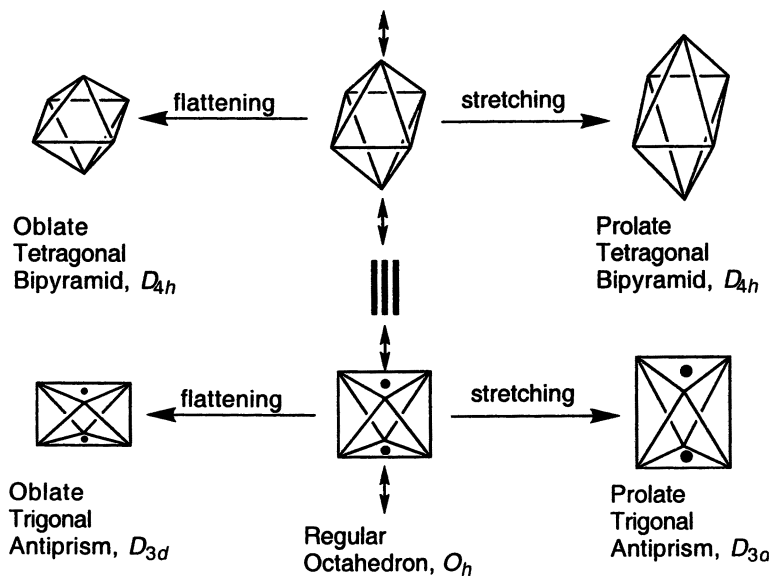
Table IV: Energies of the Molecular Orbitals in Tl_6^{z-} .

Orbital no.	Tl_6^{4-} B3LYP/ LANL2DZ	Tl_6^{6-} B3LYP/ LANL2DZ	Tl_6^{8-} * B3LYP/ LANL2DZ
	31	0.07080	0.29890
32	0.12385	0.34360	0.57402
33	0.14929	0.34366	0.57403
34	0.14930	0.37547	0.57404
35	0.18560	0.38876	0.63477
36	0.18560	0.38877	0.63478
37	0.32458	0.53872	0.73766
38	0.33695	0.54289	0.76403
39	0.34365	0.54291	0.76404
40	0.34365	0.55084	0.76405
41	0.35249	0.55086	0.76675
42	0.38079	0.55610	0.76681
43	0.38079	0.58562	0.76690
44	0.40778	0.60103	0.82187
45	0.41258	0.60103	0.82200
46	0.41259	0.60141	0.83793
47	0.42149	0.60142	0.83795
48	0.42150	0.60387	0.83799

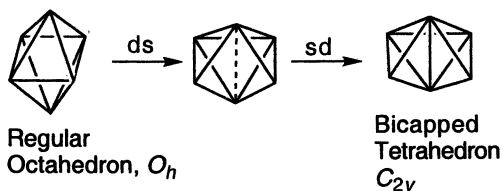
- Single point calculation at the experimental geometry

The 14-skeletal Electron Systems Ic_6^{8-}

The optimized calculated structures for Ic_6^{8-} ($Ic = B, In$) and the experimental structure⁵³ for Tl_6^{8-} were all found to be regular octahedra in accord with their 14 skeletal electrons corresponding to the $2n + 2$ skeletal electrons required for a globally delocalized deltahedron with six vertices, namely the regular octahedron. The computed structure for Tl_6^{8-} could not be



(a) Topology-preserving distortions involving descent of symmetry



(b) Diamond-square-diamond (dsd) process

Figure 2: (a) Topology-preserving distortions of a regular octahedron involving descent of symmetry from O_h to D_{4h} and D_{3d} to give tetragonal bipyramids and trigonal antiprisms, respectively; (b) A diamond-square-diamond (dsd) process to convert a regular octahedron into a bicapped tetrahedron (C_{2v} symmetry).

optimized so that a single point calculation was done at the experimental geometry.⁵³

The bonding orbitals in the octahedral Ic_6^{8-} structures (Figure 3) correspond to six fundamental types in increasing order of energy as follows:

- (1) A single low-lying a_{1g} orbital which is mainly core bonding with symmetry corresponding to the S molecular orbital of TSH.
- (2) A degenerate triplet of t_{1u} orbitals which is heavily surface bonding but with some external bonding corresponding to P molecular orbitals of TSH.
- (3) A degenerate doublet of e_g orbitals which contains the external lone pairs and resemble $d_{x^2-y^2}$ and d_{z^2} atomic orbitals.
- (4) A single a_{1g} orbital which mainly contains the external lone pairs but mixed with some core bonding of opposite phase.
- (5) A degenerate triplet of t_{2g} orbitals which is exclusively surface bonding corresponding to a triplet of D molecular orbitals resembling the triplet of d_{xy} , d_{xz} , and d_{yz} atomic orbitals.
- (6) A degenerate triplet of t_{1u} orbitals which is a combination of surface and external bonding resembling a degenerate triplet of f atomic orbitals.^{54,55,56,57}

Core bonding appears to be much more significant in B_6^{8-} than in its heavier congeners In_6^{8-} and Tl_6^{8-} as suggested by the following:

- (1) The greater distance of the lowest lying a_{1g} orbital, corresponding almost entirely to core bonding, below the next lowest lying set of orbitals, namely the degenerate t_{1u} triplet, corresponding only to surface and external bonding.
- (2) The reversal of the relative energies of the e_g and second a_{1g} orbitals in going from B_6^{8-} to In_6^{8-} and Tl_6^{8-} . The second a_{1g} orbital obviously contains some core bonding whereas the e_g orbitals involve exclusively the external lone pairs.

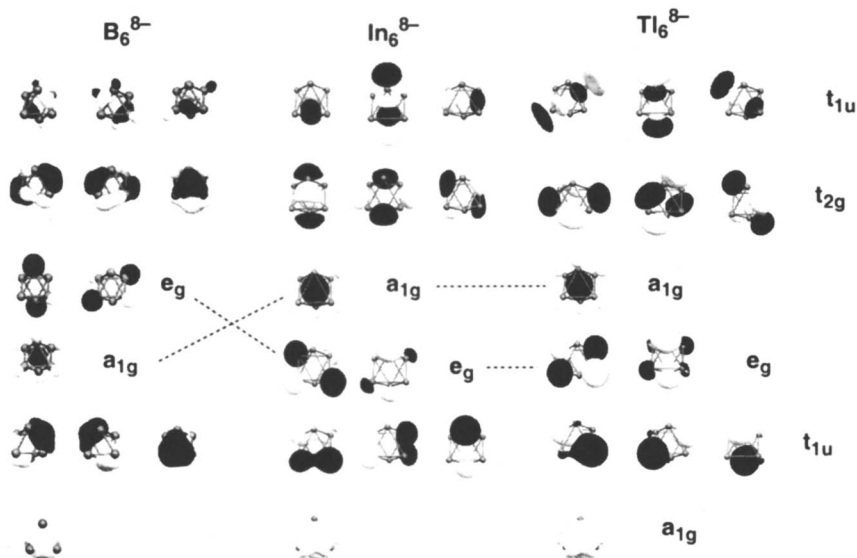


Figure 3: Bonding MOs for the regular octahedral (O_h) clusters Ic_6^{8-} .

The 12-skeletal Electron Systems Ic_6^{6-}

Removal of two skeletal electrons from Ic_6^{8-} to give Ic_6^{6-} would be expected to occur from the degenerate t_{1u} triplet HOMOs necessarily leading to a Jahn-Teller distortion corresponding to an oblate (flattened) polyhedron of some type. The optimized structures for B_6^{6-} and In_6^{6-} as well as the experimental structures for Tl_6^{6-} in KTI^4 and $CsTI^5$ were found to be oblate tetragonal bipyramids of D_{4h} symmetry. In the oblate tetragonal bipyramids for Ic_6^{6-} the axial (*trans*) $Ic-Ic$ distance in the flattened direction is similar to the length of an edge (Figure 1) suggesting direct interactions between this pair of axial atoms.

Optimization of the structure of Tl_6^{6-} , like that of Tl_6^{8-} discussed above, presented some difficulties and attempted optimization of Tl_6^{6-} starting from D_{4h} geometry failed completely. However, we were able to find an energy minimum for Tl_6^{6-} with D_{3d} oblate trigonal antiprismatic geometry (Figure 1) in contradiction to the experimental preference for D_{4h} oblate tetragonal antiprismatic geometry in KTI^4 and $CsTI^5$. In order to clarify this discrepancy we performed a single point calculation of the energy of a D_{4h} oblate tetragonal bipyramidal Tl_6^{6-} configuration obtained from the octahedron by applying the same ratio of compression as achieved by optimized In_6^{6-} relative to In_6^{8-} . This calculation

indicated that D_{4h} oblate tetragonal bipyramidal TI_6^{6-} was approximately 6 kcal/mole higher in energy than D_{3d} oblate trigonal antiprismatic TI_6^{6-} . This suggests that the oblate polyhedra for Ic_6^{6-} are of very similar energies so that the polyhedron of choice can be affected by the counterion and solid state environment.

Figure 4 shows the bonding MOs for oblate tetragonal bipyramidal B_6^{6-} and In_6^{6-} , respectively, indicating the splittings of the degenerate t_{1u} , t_{2g} , and e_g orbitals upon reduction of the symmetry from O_h to D_{4h} (Table 5). The compression along the unique (z) axis of the oblate tetragonal bipyramid raises the energies of the MOs with electron densities concentrated along this axis including the b_{1g} component of the split e_g doublet of the original octahedron and the a_{2u} components of the t_{1u} bonding orbitals. This pattern is clearest for B_6^{6-} (Figure 6), in which the frontier t_{1u} triplet is split into an a_{2u} singlet LUMO and an e_u doublet HOMO.

The distribution of Mulliken atomic charges is particularly interesting for the two D_{4h} Ic_6^{6-} species. In the octahedral Ic_6^{8-} systems the excess negative charge is equally divided among the substituents in accord with the symmetry ($-1.333/\text{atom}$). However in the B_6^{6-} and In_6^{6-} systems there is a distinction between the charges of the equatorial and axial atoms ($-0.895/\text{axial}$; $-1.052/\text{equatorial}$ for B_6^{6-} and $-0.311/\text{axial}$ and $-1.345/\text{equatorial}$ for In_6^{6-}). This might be related to the short axial-axial distances calculated for B_6^{6-} and In_6^{6-} (Figure 1) since the smaller charges on the axial atoms reflect a smaller electrostatic repulsion between them, which in turn allow for the shorter *trans* distances between the axial atoms.

Figure 4 also shows the bonding MOs computed for oblate trigonal antiprismatic TI_6^{6-} indicating the splittings of the degenerate t_{1u} and t_{2g} triplets upon reduction of the symmetry from O_h to D_{3d} . Note that for the D_{3d} symmetry of the trigonal antiprism, the e_g doublet of O_h remains unsplit. Again the frontier t_{1u} triplet is split into an a_{2u} singlet LUMO and an e_u doublet HOMO suggesting that the frontier orbitals of TI_6^{6-} are about the same whether the oblate polyhedron is a D_{4h} tetragonal bipyramid or a D_{3d} trigonal antiprism.

The 10-skeletal Electron Systems Ic_6^{4-}

In order to gain greater insight into the geometry of hypoelectronic six-vertex deltahedra, computations were also performed on the hypoelectronic 10-skeletal electron systems Ic_6^{4-} ($\text{Ic} = \text{B}, \text{In}, \text{TI}$), which represent a greater degree of electron deficiency than has yet been realized experimentally. The

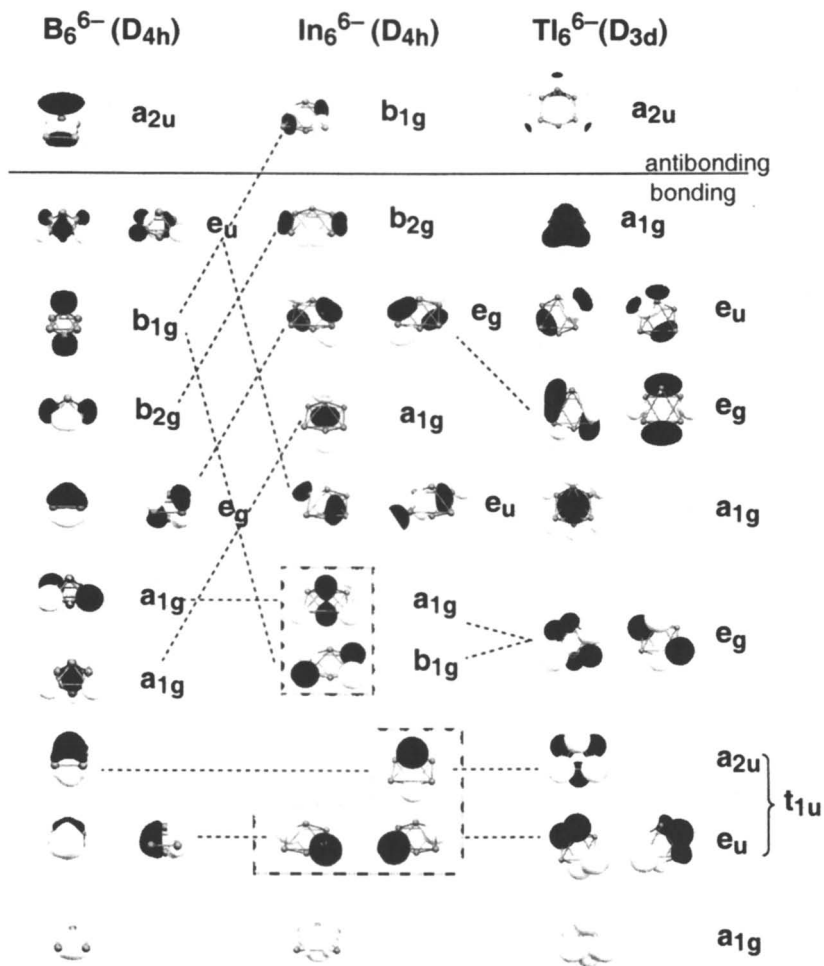


Figure 4: Bonding MOs for the clusters Ic_6^{6-} with oblate tetragonal bipyramidal (D_{4h}) or trigonal antiprismatic (D_{3d}) geometries, respectively.

optimized structures of the anions In_6^{4-} and Tl_6^{4-} were both found to be prolate (elongated) deltahedra with D_{4h} (tetragonal bipyramid) and D_{3d} (trigonal antiprism) symmetries, respectively. In both cases the frontier t_{1u} triplets of the corresponding regular octahedra are split into antibonding e_u doublet LUMOs and a bonding a_{2u} singlet HOMO (Figure 5). This corresponds to higher energy MOs originating from the octahedral t_{1u} components along the two shorter axes of the prolate deltahedra than that of the MO originating from the third component along the longer axis.

The optimized structure for the boron analogue B_6^{4-} was found to be quite different than those of In_6^{4-} and Tl_6^{4-} , namely a C_{2v} bicapped tetrahedron. This structure is derived from a regular octahedron through a single dsd process as noted above (Figure 2b). Conversion of an octahedron to a bicapped tetrahedron generates two degree 5 vertices, which appear to be a particularly favorable environment for boron atoms in cluster structures. This is indicated by the high stability of B_{12} icosahedra in diverse structures^{58,59} and the presence of B_6 pentagonal bipyramidal building blocks in a number of optimized computed structures for large boron clusters.⁶⁰

The C_{2v} symmetry of the bicapped tetrahedral structure computed for B_6^{4-} means that each of its 11 bonding orbitals is non-degenerate with a unique energy. Despite this low symmetry, the shapes and symmetries of most of the bonding MOs of B_6^{4-} (Figure 5) are readily seen to correspond to MOs in the regular octahedral B_6^{8-} (Figure 3). The frontier orbitals of B_6^{4-} obviously originate from the frontier t_{1u} triplet of B_6^{8-} with the b_2 component becoming the HOMO, the a_1 component becoming the LUMO, and the remaining component (b_2) being an unoccupied MO of still higher energy. A bicapped tetrahedron with equivalent edge lengths has an unsymmetrical elongated structure related to the prolate deltahedra found in the optimized structures of In_6^{4-} and Tl_6^{4-} . A bicapped tetrahedron thus does not appear to be unreasonable for an Ic_6^{4-} structure lacking two electron pairs for the 14-skeletal electron closed shell configuration of the globally delocalized octahedra of the optimized Ic_6^{8-} structures.

Summary

DFT calculations on the six-atom cluster anions Ic_6^{8-} (Ic = B, In, Tl) lead to regular octahedral optimized structures in accord with their 14 skeletal electrons obeying the $2n + 2$ rule^{49,50,51,52} for a six-vertex deltahedron. The computed molecular orbital shapes are in accord with the six-center two-electron core bonding and the surface bonding expected for a three-dimensional aromatic octahedron. DFT calculations on the hypoelectronic cluster ions Ic_6^{6-} lead to

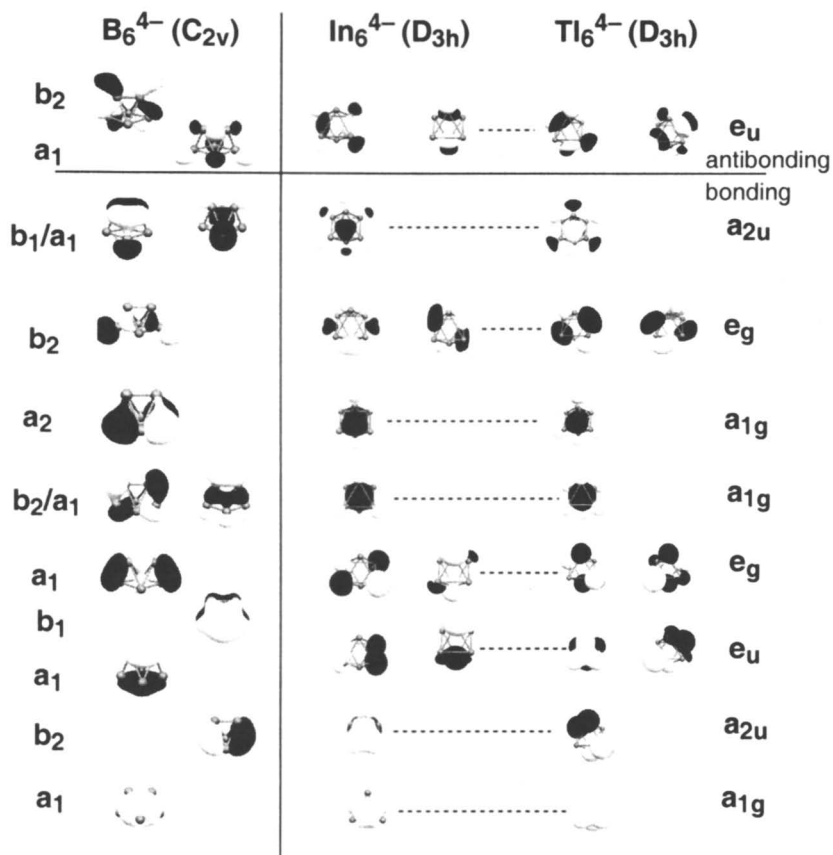


Figure 5: Bonding MOs for the bicapped tetrahedral B_6^{4-} and the prolate trigonal antiprismatic In_6^{4-} and Tl_6^{4-} .

optimized oblate (flattened) deltahedral structures which may be either tetragonal bipyramidal (D_{4h}) for $Ic = B, In$ or trigonal antiprismatic (D_{3d}) for $Ic = Tl$. In either of these Ic_6^{6-} structures the degenerate triplet t_{1u} HOMO of the octahedral Ic_6^{8-} is split into a degenerate doublet bonding e_u HOMO and a non-degenerate antibonding a_{2u} LUMO. DFT calculations on the even more hypoelectronic clusters Ic_6^{4-} lead either to prolate (elongated) deltahedra ($Ic = In, Tl$) or a bicapped tetrahedron ($Ic = B$). In these cases the splitting of the degenerate triplet t_{1u} HOMO of the octahedral Ic_6^{8-} is the opposite to that of Ic_6^{6-} leading to a non-degenerate bonding a_{2u} HOMO and a degenerate doublet antibonding e_u HOMO for Ic_6^{4-} ($Ic = In, Tl$). The bicapped tetrahedron is also an unsymmetrical prolate deltahedron that is of too low symmetry, i.e., C_{2v} , to have any MO degeneracies required by group theory. However, the splitting of the degenerate triplet t_{1u} HOMO of the octahedral B_6^{8-} into a single bonding HOMO and two antibonding LUMOs in bicapped tetrahedral B_6^{4-} is similar to the splitting pattern of the other prolate deltahedra.

Acknowledgment: One of us (R. B. K.) is indebted to the Petroleum Research Fund of the American Chemical Society for partial support of this work. In addition part of this work was undertaken with the financial support from CNSIS-Roumania, through Grant 176/4C. We are also indebted to Prof. H. F. Schaefer, III, of the University of Georgia Center for Computational Quantum Chemistry, who provided financial support for a visit of one of us (I. S.-D.) to the University of Georgia in summer 2000.

References

1. Corbett, J. D.; *Structure and Bonding*, **1997**, 67, 175.
2. Muetterties, E. L.; Knoth, W. H., *Polyhedral Boranes*, Marcel Dekker, New York, 1968.
3. Muetterties, E. L., Ed., *Boron Hydride Chemistry*, Academic Press, New York, 1975.
4. Dong, Z.; Corbett, J. D., *J. Am. Chem. Soc.*, **1993**, 115, 11299.
5. Dong, Z.; Corbett, J. D., *Inorg. Chem.*, **1996**, 35, 2301.
6. Kaskel, S.; Corbett, J. D., *Inorg. Chem.*, **2000**, 39, 778.
7. Huang, D.; Dong, Z.; Corbett, J. D., *Inorg. Chem.*, **1998**, 37, 5881.
8. Sevov, S. C.; Corbett, J. D., *J. Am. Chem. Soc.*, **1993**, 115, 9089.
9. Sevov, S. C.; Corbett, J. D., *Inorg. Chem.*, **1993**, 32, 1059.
10. Dong, Z.; Henning, R. W.; Corbett, J. D., *Inorg. Chem.*, **1997**, 36, 3559.
11. Sevov, S. C.; Corbett, J. D., *Inorg. Chem.*, **1991**, 30, 4875.
12. Sevov, S. C.; Ostenson, J. E.; Corbett, J. D., *J. Alloys and Compounds*, **1993**, 202, 289.
13. Dong, Z.; Corbett, J. D., *J. Cluster Sci.*, **1995**, 5, 187.

14. Dong, Z.; Corbett, J. D., *Inorg. Chem.*, **1995**, *34*, 5042.
15. Henning, R. W.; Corbett, J. D., *Inorg. Chem.*, **1997**, *36*, 6045.
16. King, R. B., *Inorg. Chim. Acta*, **1995**, *228*, 219.
17. King, R. B., *Inorg. Chim. Acta*, **1996**, *252*, 115.
18. Wiberg, K. B., *Accts. Chem. Res.*, **1994**, *17*, 379.
19. Kutzelnigg, W., *Angew. Chem. Int. Ed.*, **1984**, *23*, 272.
20. Reed, A. E.; Schleyer, P. v. R., *J. Am. Chem. Soc.*, **1990**, *112*, 1434.
21. Buslaev, Ya. A.; Klyagina, A. P., *Coord. Chem. Rev.*, **1993**, *126*, 149.
22. King, R. B.; Silaghi-Dumitrescu, I.; Kun, A., *Inorg. Chem.*, **2001**, *40*, 0000.
23. Becke, A. D., *J. Chem. Phys.*, **1993**, *98*, 5648.
24. Lee, C.; Yang, W.; Parr, R. G., *Phys. Rev.*, **1988**, *B37*, 785.
25. Frisch, M. J.; Trucks, G. W.; Schlegel, H. B.; Gill, P. M. W.; Johnson, B. G.; Robb, M. A.; Cheeseman, J. R.; Keith, T.; Petersson, G. A.; Montgomery, J. A.; Raghavachari, K.; Al-Laham, M. A.; Zakrzewski, V. G.; Ortiz, J. V.; Foresman, J. B.; Peng, C. Y.; Ayala, P. Y.; Chen, W.; Wong, M. W.; Andres, J. L.; Replogle, E. S.; Gomperts, R.; Martin, R. L.; Fox, D. J.; Binkley, J. S.; Defrees, D. J.; Baker, J.; Stewart, J. J. P.; Head-Gordon, M.; Gonzalez, C.; Pople, J. A., *Gaussian 94, Revision B.3*; Gaussian, Inc.: Pittsburgh PA, 1995.
26. Hay, P. J.; Wadt, W. R., *J. Chem. Phys.*, **1985**, *82*, 270, 284, 299.
27. Becke, A. D.; *Phys. Rev.*, **1988**, *A38*, 3098.
28. Spartan version 5.1, Wavefunction, Inc., 18401 Von Karman Avenue, Suite 370, Irvine, CA 92612 USA
29. Flückiger, P. F., Portman, S., *MOLEKEL, Advanced Interactive 3D-Graphics for Molecular Sciences*, Revision 3.04. Developed at the University of Geneva; <http://figc.ethz.ch/molekel/>.
30. Zhao, Q.; Parr, R. G., *Phys. Rev.*, **1992**, *46A*, 2337.
31. Zhao, Q.; Parr, R. G., *J. Chem. Phys.*, **1993**, *98*, 543.
32. Kohn, W.; Becke, A. D.; Parr, R. G., *J. Chem. Phys.*, **1996**, *100*, 12974.
33. Baerends, E. J.; Gritsenko, O. V., *J. Phys. Chem.*, **1997**, *101*, 5383.
34. Hoffmann, R., *J. Mol. Struct. (THEOCHEM)*, **1998**, *424*, 1.
35. Stowaser, R.; Hoffmann, R., *J. Am. Chem. Soc.*, **199**, *121*, 3414.
36. Zhao, Q.; Parr, R. G., *Phys. Rev.*, **1992**, *46A*, 2337.
37. Zhao, Q.; Parr, R. G., *J. Chem. Phys.*, **1993**, *98*, 543.
38. Kohn, W.; Becke, A. D.; Parr, R. G., *J. Chem. Phys.*, **1996**, *100*, 12974.
39. Baerends, E. J.; Gritsenko, O. V., *J. Phys. Chem.*, **1997**, *101*, 5383.
40. Hoffmann, R., *J. Mol. Struct. (THEOCHEM)*, **1998**, *424*, 1.
41. Stowaser, R.; Hoffmann, R., *J. Am. Chem. Soc.*, **199**, *121*, 3414.
42. King, R. B.; Rouvray, D. H., *J. Am. Chem. Soc.*, **1977**, *99*, 7834.
43. Williams, R. E., *Inorg. Chem.*, **1971**, *10*, 210.

44. Williams, R. E., *Adv. Inorg. Chem. Radiochem.*, **1976**, *18*, 67.
45. Wade, K., *Chem. Comm.*, **1971**, 792.
46. Wade, K., *Adv. Inorg. Chem. Radiochem.*, **1976**, *18*, 1.
47. Dong, Z.; Corbett, J. D., *Angew. Chem. Int. Ed.*, **1996**, *35*, 1006.
48. King, R. B.; Rouvray, D. H., *J. Am. Chem. Soc.*, **1977**, *99*, 7834.
49. Williams, R. E., *Inorg. Chem.*, **1971**, *10*, 210.
50. Williams, R. E., *Adv. Inorg. Chem. Radiochem.*, **1976**, *18*, 67.
51. Wade, K., *Chem. Comm.*, **1971**, 792.
52. Wade, K., *Adv. Inorg. Chem. Radiochem.*, **1976**, *18*, 1.
53. Dong, Z.; Corbett, J. D., *Angew. Chem. Int. Ed.*, **1996**, *35*, 1006.
54. Freedman, H. G., Jr.; Choppin, G. R.; Feuerbacher, D. G., *J. Chem. Educ.*, **1964**, *41*, 354.
55. Becker, C., *J. Chem. Educ.*, **1964**, *41*, 358.
56. Smith, W.; Clack, D. W., *Rev. Roum. Chim.*, **1975**, *20*, 1243.
57. King, R. B., *J. Phys. Chem. A*, **1997**, *101*, 4653.
58. Jemmis, E. D.; Pavankumar, P. N. V., *Proc. Indian Acad. Sci.*, **1984**, *93*, 479.
59. King, R. B., in *Contemporary Boron Chemistry*, eds. Davidson, M.; Hughes, A. K.; Marder, T. B.; Wade, K., Royal Society of Chemistry, 2000, pp. 506–509.
60. Boustani, I., *Phys. Rev. B*, **1997**, *B55*, 16426.
61. Jemmis, E. D.; Pavankumar, P. N. V., *Proc. Indian Acad. Sci.*, **1984**, *93*, 479.
62. King, R. B., in *Contemporary Boron Chemistry*, eds. Davidson, M.; Hughes, A. K.; Marder, T. B.; Wade, K., Royal Society of Chemistry, 2000, pp. 506–509.
63. Boustani, I., *Phys. Rev. B*, **1997**, *B55*, 16426.

Chapter 16

Molecular Understanding of Aluminum Bioinorganic Chemistry in Relevance to the Pathology of Alzheimer's Disease

S. Anitha¹, P. Shanmugavelu², Valeswara-Rao Gazula³,
S. K. Shankar⁴, Rani B. Menon², R. V. Rao², Jagannatha K. S. Rao^{1,*},
and Luigi Zecca⁵

¹Department of Biochemistry and Nutrition, Central Food Technological Research Institute, Mysore-570013, India

²Analytical Control Section, Chemical Engineering and Technology Group, BARC, Mumbai-400085, India

³Department of Neurology, Yale University School of Medicine, New Haven, CT 06520

⁴Department of Neuropathology, National Institute of Mental Health and Neurosciences, Bangalore-560029, India

⁵Department of Molecular Neurobiology, IATB, CNR, Milan, Italy

Aluminum (Al) is a suspected etiological factor in neurological disorders like Alzheimer's, Parkinson's, Huntington's diseases etc. The understanding of Al neurobiochemistry was hampered due to Al speciation chemistry and differential sensitivity animal models for Al toxicity. Experimental and circumstantial evidence provided a great deal of information on the complex inorganic biochemistry of Al in relevance to pathological events observed in Alzheimer's brains. In this contribution, the speciation chemistry of Al in relevance to neurobiology, role of Al, in modulating trace elemental homeostasis in human brains, Al-induced changes in animal brains mimicking Alzheimer's human brains, and its interaction with DNA are discussed.

Introduction

Alzheimer's Disease (AD) is a neurodegenerative disorder characterized by progressive impairments of memory and cognition. It typically occurs in later stages of life and is associated with a multiplicity of structural, chemical and functional abnormalities involving brain regions concerned with cognition and memory. Alois Alzheimer first reported this form of dementia in 1907 when he described a disease of the cerebral cortex in a 51-year old woman suffering from an inexorably progressive disorder of dementia. Although other forms of dementia had been well characterized at the time of Alzheimer's clinical report, his patient was clinically and pathologically unusual because of her relatively young age and the presence of the then newly-described intracellular inclusions which have subsequently come to be known as neurofibrillary tangles (NFT). In recognition of this unique combination of clinical and pathological features, the term "Alzheimer's Disease" subsequently came into common usage. Today, Alzheimer's disease is considered to be one of the forthcoming scourges of the 21st century. Epidemiological studies suggest that the dementia presently occurs in up to 10% of individuals over the age of 65. It has been estimated that there are between 2.5 and 3 million patients suffering from Alzheimer's disease in the USA and 0.6 million in the UK. These figures have been projected to increase by 20% over the next 20 years as the proportion of the elderly in the population increases. The cost of caring for such individuals is well over 80 billion dollars annually and is increasing rapidly.

AD is characterized by initial memory loss followed by progressive loss of neurons, leading to dementia and loss of all nervous function, and eventually death. The neuropathologic characteristics include cortical and subcortical atrophy, formation of intraneuronal neurofibrillary tangles (NFT), deposition of A β peptide in neuritic plaques, formation of neuropil threads, loss of synaptic function, oxidative stress, and apoptosis leading to neuronal loss. These events are observed mostly in the hippocampal and cortical regions of AD brains.

Aluminum has never been demonstrated to have definite biological function, suggesting that the ion possesses properties which are incompatible with fundamental life processes. In the last few years, many scientific studies have brought to light the potential toxicity of Al to humans. It is usually excluded from normal biochemical and metabolic processes because of low solubility of its chemical forms, namely silicates, phosphates and oxides, which

render the Al physiologically unavailable. Living organisms are carefully and effectively protected from Al aggression by different ways and one of the studies suggests that naturally occurring silicon species might play a sort of planetarian antidote effect to the ecotoxic potency of natural Al. Most of the understanding of Al toxicity in humans was established as a result of studies of disorders experienced by dialysis patients when the dialysis fluid contained Al at above 0.5 micromoles/l. In such patients, Al accumulated in various tissues including kidney, liver, bone, and heart (1,2), giving rise to pathological conditions. The pathological conditions include i) dialysis encephalopathy that can lead to dementia and death and ii) dialysis osteomalacic osteodystrophy in which there is defective mineralization of pre-bone collagen accompanied by bone pain and spontaneous fracture. Al accumulation in the heart is also a contributory factor in the cardiac hypertrophy often observed in hemodialysis patients. In fact, the element might be implicated in the pathogenesis of Alzheimer's disease.

The potential role of Al in the pathogenesis of human neurodegenerative disorders remains controversial. Recent studies in experimental animals as well as circumstantial evidence, strongly provided clue that Al might be one of the factors causing neuronal cell death in devastating disorders like Alzheimer's disease, Parkinson's disease, Huntington's disease, Guam and amyotrophic lateral sclerosis. No defined mechanism has been proposed for the cell death in the AD brain. Al is the only trivalent metal ion in the periodic table that appears capable of inducing progressive encephalopathy leading to neurological disorders (3). Normally, Al is prevented from entering the central nervous system (CNS) by the blood-brain barrier. Under pathological conditions, however an increased amount of Al has been found in the brain tissue and cerebrospinal fluid (4). The perturbing mechanism is not clearly known, but may be related to blood-brain barrier breakdown as a result of vascular damage (ischemia and/or inflammation) and by the iron transport pathway. In order to understand the possible role of Al in such disorders, it is important to understand the complex hydrolysis chemistry of Al under various biological conditions (5). This chapter mainly deals with Al speciation chemistry in biological systems, its role in modulating trace-element homeostasis in the human brains, aluminum maltolate induced changes in aged rabbit brain that mimic Alzheimer's in the human brains, its modulation in DNA conformation, and the possible hypothetical mechanism for neuronal cell death induced by Al.

Aluminum Bio-inorganic Chemistry

Aluminum Loading in Humans

Although Al is ubiquitous, its bioavailability is limited due to its insoluble nature. Because of the insoluble nature of aluminum compounds, naturally occurring surface and subsoil water is extremely low in Al content and biosystems have little exposure to soluble aluminum. This has played a major role in maintaining low Al burden in animals and most plants. Under certain pathological conditions, an increased amount of Al has been found in biological systems. Its wide use in day-to-day life, however, is increasing Al intake on the part of man through several routes. One of the possible major sources of human aluminum consumption is through food, drinking water, beverages and Al- containing drugs. Aluminum sulfate is used extensively as a flocculation agent to remove organic substances. It is estimated that the dietary intake of aluminum may vary from 3 to 30 mg/day, but a reasonable average dietary intake is probably about 5 mg/day. Al is naturally present in tealeaves. Tea plants have been found with as much as 0.3% Al in older leaves and about 0.01% in younger ones. Typical tea infusions contain 50 times as much as Al as do infusions from coffee. Levels of Al in brewed tea are commonly in the range of 2-6 mg/l (6). Other possible sources of Al are food additives, containers, cookware, utensils and food wrappings. Dietary intake of Al from food is small compared with the amounts consumed through the use of Al containing antacids that may provide 50-1000 mg/day of Al. In order to investigate the potential toxicity of Al in the pathogenesis of neurological disorders, it is not only essential to establish its role in neurodegenerative disorder, but also modes of transport into the human body and its distribution pattern in various parts of the brain.

Potential Biological Carriers of Aluminum

Aluminum may gain access to the human body through the gastrointestinal tract, lung tissue and nose. It is generally accepted that about 1% of the intake enters the body, with the remaining excreted by the renal system. The following four factors have been clearly shown to modulate Al absorption: (a) amount of Al ingested, (b) solubility of Al

compounds, (c) integrity of the tight junctions of the small intestine, and (d) the uremic state.

The definite mechanism by which Al is transported into body parts is not clearly understood. It was initially thought that inorganic phosphate (1.1 mM), citrate (0.1 mM), transferrin (50 μ M) and lactate (0.9 mM) present in plasma were the possible carriers of Al. The binding of Al with citrate in aqueous medium has been extensively studied (7). Though the stability constant of aluminum-citrate complex is high, experiments demonstrated that lipid bilayer permeation by the neutral aluminum-citrate complex is remarkably slow (8). This could possibly suggest that Al enhancement in brain is not due to the involvement of neutral aluminum-complexes.

Albumin is present in the plasma at a concentration of 40 g/l. It is a weak Al binder at physiological pH and is unable to effectively compete with other stronger carriers. The glycoprotein transferrin is recognized as the major plasma iron transport protein. It is only 30% saturated with iron and regarded as a potential carrier of Al under physiological conditions, without interference with the sites occupied by iron (9). The stability constant of transferrin with Al is less than that of iron by half. Transferrin-mediated brain uptake of Al is confirmed by the postmortem study of the brains of patients with chronic renal failure (10). A high proportion of Al is bound to transferrin in the blood plasma. This might suggest that Al absorption is interlinked with the pathway of iron's absorption. The uptake of Al appears to be determined largely by the distribution of transferrin receptors, which occur in greatest densities in regions of the brain that are selectively vulnerable to Alzheimer's disease. Further studies provided evidence that Al distribution in the brain in various disorders reflects the regional distribution of transferrin receptors, suggesting that transferrin and transferrin receptors on endothelia are involved. Thus it is possible that Al may use the system of uptake and transport of iron involving transferrin and its receptor-mediated endocytosis.

The Al transport across the yeast cells in the presence of citrate and EDTA using 27 Al NMR has been studied by our group (11). The results showed that Al, as a nitrate salt, could enter the cells within 15 minutes, and that, over a period of 4 hrs, an equilibrium sets in between outside and inside the cell. Aluminum- citrate does not favor Al transport into the cells above pH 5.0 and EDTA could bring out all Al that entered the cells within 30 min.

The role of Aluminum in Metal Homeostasis in Human AD Brain

Trace element homeostasis plays a crucial role in the normal functioning of the human brain. The distribution of trace elements is not homogenous in different regions of the brains, and their concentration varies significantly (12). In biological systems there is an interdependency among the concentrations of certain elements for homeostasis of trace elements. Direct correlation with respect to the changes in the concentration of trace elements in some regions of the brain was observed. A recent study (13) showed a marked difference in trace level metal concentration in different regions of AD brains compared to control brains. The total metal concentration also showed a marked difference in AD brain. Frontal cortex and hippocampus of normal brain contain about 258 $\mu\text{M/g}$ and 269 $\mu\text{M/g}$ respectively. In AD brain it has elevated significantly. Frontal cortex regions of AD brain showed an elevated level of about 1423 $\mu\text{M/g}$ and hippocampal regions showed a still higher level of about 1903 $\mu\text{M/g}$. The rise in the total metal concentration in AD brain is mainly due the elevation of Al and Fe. Al alone is present to the extent of 50-65% in AD brain over other elements as shown in Figure 1. The comparative study indicated that the concentration of Al and Fe have increased by several fold in both the hippocampal and frontal cortex regions of AD brain compared to normal brain, while Na, K and P have been significantly reduced. Co-localization of Al and Fe at high levels in AD brain perhaps confirms the concept of the same Al transport route as that of Fe. The increased level of Al drastically decreased K and Na levels thereby affecting the homeostasis, as the binding of Al with the channel forming proteins could interfere with gating mechanisms. The trivalent ions (Al, Fe) replaced divalent (Mg, Ca, Cu, Zn) and monovalent (Na, K) ions in severe AD brains as shown in Table I. The data indicated that, during the progression of AD, the percentage of singly charged ions decreased by 2500-fold, while the percentage of triply charged ions increased by 10-fold.

Table I. Percentage elemental charge distribution in normal and Alzheimer's brain

Charge	Frontal Cortex			Hippocampus		
	Control	Moderate AD	Severe AD	Control	Moderate AD	Severe AD
1+	80	17.6	0.02	86.6	19.5	0.01
2+	9.4	50.4	0.1	7.1	34.7	0.09
3+	10.6	32	99.9	6.3	45.8	99.9

1+, 2+ and 3+ charge includes ions of (Na, K), (Cu, Zn, Mg, Ca) and (Al, Fe) respectively.

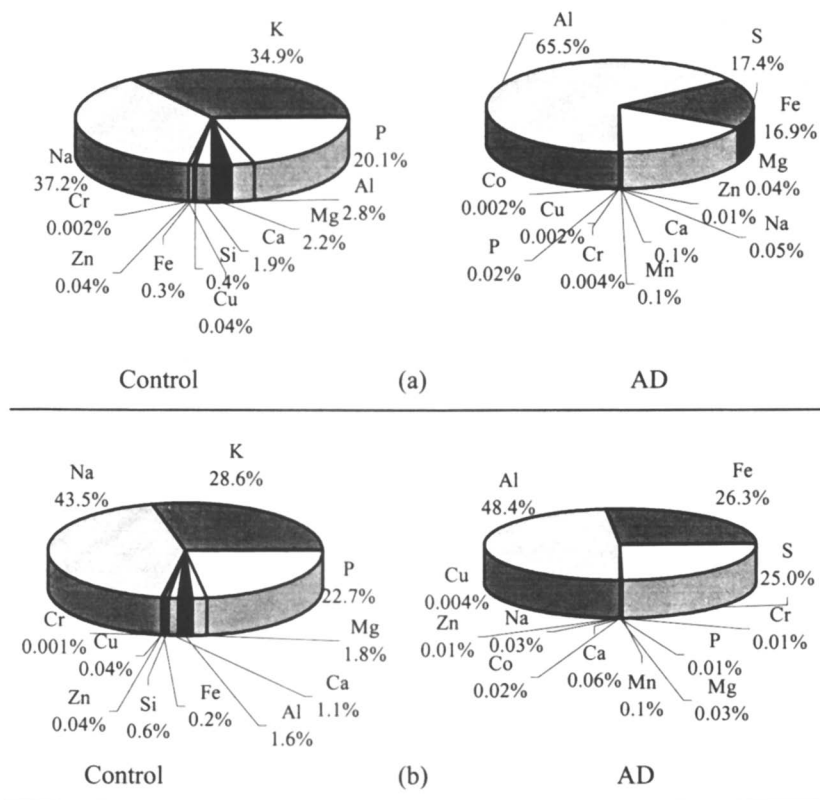
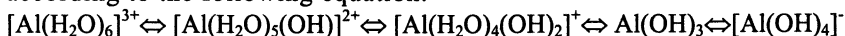


Figure 1 Comparison of relative mole% of trace elements in control and AD human brain in (a) Frontal cortex (b) hippocampus. (Reproduced with permission from reference 13. Copyright 1999)

Aluminum Speciation Chemistry and Neurotoxicity

Aluminum Toxicity Studies

The toxic effects of Al are very diverse and have been extensively investigated both *in vivo* and *in vitro*. For proof of the hypothesis that Al may be a significant risk factor for Alzheimer's disease, approximately fifty different neurotoxic effects of Al have been demonstrated (14). They include aluminum's action on the cell nucleus, effect on enzymes metabolic processes, interference with cytoskeletal mechanisms, effect on membranes and effect on neurotransmission. A number of groups (Savory et al, (USA), Zatta et al, (Italy) and Rao et al, (India)) have studied the effects of different inorganic salts of Al in causing neurodegeneration. All these studies have clearly shown that most of the inorganic Al salts can cause only localized effects at the site of injection. Generally, Al is prevented from entering the CNS through the blood brain barrier; under pathological conditions, however, an increased amount of Al has been found (4). In order to investigate any possible role of Al in such disorders, it is important to understand the complex hydrolysis chemistry of Al as a function of pH (5). The speciation chemistry of Al is especially important in the experimental design of research investigations into Al toxicity. Al speciation in the stock solutions must be evaluated, since it hydrolyzes readily and at pH 7.0 there is a strong tendency for the precipitation of Al(OH)₃ which makes the preparation of Al stock solutions difficult. Aluminum is a strongly hydrolyzing element, and is generally insoluble at neutral pH. Its solubility is enhanced under acidic or alkaline conditions, and in the presence of complexing agents. In aqueous solution at pH < 5.0, aluminum exists as an octahedral hexahydrate, [Al(H₂O)₆]³⁺, usually abbreviated as Al³⁺. As the solution becomes less acidic, [Al(H₂O)₆]³⁺ undergoes successive deprotonations to yield different species such as [Al(OH)]²⁺, [Al(OH)₂]⁺ and Al(OH)₃. Neutral solutions give Al(OH)₃ precipitate that re-dissolves, owing to the formation of tetrahedral aluminates, [Al(OH)₄]⁻, the primary soluble Al (III) species at pH > 6.2, the biological pH. The overall deprotonation reactions will take place according to the following equation.



One cannot compute the soluble Al concentration of the solution simply by adding a known quantity of an Al compound to water, without taking hydrolysis reactions into account. For example, when Al inorganic salts such as chloride,

sulfate, hydroxide or perchlorate are dissolved in water at a calculated concentration of 10 mM, the exact Al concentration after pH adjustment and filtration is about 50 μM . The use of aluminum-lactate or aluminum-aspartate, however, increases the soluble Al concentration to $\sim 55\text{-}330 \mu\text{M}$, and use of aluminum-maltolate or gluconate increases the soluble Al concentration to 4000-6000 μM . Aluminum-maltolate is particularly suitable for toxicological studies because of its defined molecular structure in solution, its neutral charge, high solubility and hydrolytic stability at pH 7.0. For *invitro* studies to investigate the Al interaction with DNA, it is of utmost importance to have a higher free Al^{3+} ion concentration at physiological pH. This cannot be achieved by using any inorganic Al salt due to the insolubility problem at physiological pH. Aluminum-maltolate provides higher free Al concentrations over a wide range of pH, rendering it the most efficient compound for biological studies. At this pH, the total soluble Al ion, 'r' is given by $(\text{Al}^{3+})/[(\text{Al}^{3+} + \text{Al}(\text{OH})^{2+} + \text{Al}(\text{OH})_2^+ + \text{Al}(\text{OH})_4^-)]$ and $1/r=1+[(10^{5.5}/\text{H}^+) + (10^{-11.1}/(\text{H}^+)^2 + (10^{-23.2}/(\text{H}^+)^4)]$. Using the above distribution pattern of Al species at pH 7.4, free Al concentration is expressed (9) according to the following equation.



a. Aluminum Toxicity: *Invitro* Study

Studies were extensively carried out to understand the preferential interaction of different Al compounds like AlCl_3 , $\text{Al}(\text{OH})_3$, AlF_3 , $\text{NaAl}(\text{PO}_4)_3$ etc on ATPase complexes of synaptosomes and hexokinase in the brain. It has been reported that aluminum fluoride exerts a greater inhibitory effect on Ca-ATPase in synaptosomes than on acetylcholinesterase, Mg-ATPase, and Na-K-ATPase compared to other inorganic salts (15). Al preferentially binds to astrocytes over synaptosomes and neurons (16). For the first time, the presence of Al_{13} polymer $[\text{Al}_{13}(\text{OH})_{24}\text{O}_4(\text{H}_2\text{O})_{12}]^{7+}$ in brain cells has been evidenced using ^{27}Al NMR (17). In this polymer, four coordinated Al ions are presumed to be located at the center of a structure, within a symmetrical environment. The tetrahedron of oxygen atoms in the center of the group contains the four-coordinated Al atoms.

b. Role of Aluminum in the Dynamic Nature of DNA and Oligomers

The DNA molecule is dynamic and polymorphic in nature. Though

the right-handed B-form is the most predominant conformation, non-B-DNA-type conformations also occur in biological systems under various conditions; examples include Z-DNA, triple helix, tetraplexes, hairpin cruciform etc. Not only the sequence but also the topology of DNA have been proposed to have a crucial role in its functional aspects such as replication, transcription and susceptibility of DNA for oxidative damage and mutations. By virtue of its high charge density and low ionic radius Al can induce considerable changes in chromatin structure at micromolar level (18). The role of Al in the changes in the in gene expression associated with Alzheimer's disease has been extensively studied by McLachlan' group (19). We, for the first time, evidenced altered helical nature of DNA in AD brain hippocampus (20). This altered DNA topology in Alzheimer's brain will have tremendous implications in gene expression activity, nucleosome organization and assembly, susceptibility of DNA to damage, and terminal differentiation. Though various causes have been proposed for the topological changes in AD, the factors that are actually responsible have yet to be established. The focus is whether cells can adapt different DNA conformations in the presence of Al.

Various studies have been carried out to understand the interaction of Al with DNA and oligomers under physiological pH with different levels of free Al concentrations (10^{-7} to 10^{-9} M) using aluminum-maltolate. These studies are of great biological significance and have provided new information. Studies (21) with Al concentrations in these ranges with calf thymus genomic DNA indicated that Al strongly binds to right-handed B-DNA and the binding constant is $2.3 \times 10^3 \text{ M}^{-1}$ and at sufficiently high concentrations, it caused precipitation of DNA. Studies on interaction of Al with synthetic DNA, namely d(GCGTACGC), d(CCGGGCCCGG) and d(GCCCATGGC), indicated the following novel information. Al caused a B to Ψ DNA transition in d(GCGTACGC), while in the case of d(GCCCATGGC), Al strongly binds to the B-DNA conformation with no structural transition. In the case of d(CCGGGCCCGG), Al caused a Z to A transition. This is the first report indicating that Al causes structural transitions in sequence-specific oligomers rich with GC* (22). But Al strongly binds to AT*-rich oligomers with no structural transition (23). Al could also induce a B to Z-DNA conformation for the CCG repeats (CCG)₁₂. Interestingly, Al also could be able to uncoil supercoiled DNA and topoisomers. Early addition of EDTA prevented Al-induced uncoiling. But once Al initiated uncoiling, EDTA could not reverse it (24). The uncoiled DNA has a typical Ψ DNA conformation.

The Relevance of Aluminum Neurotoxicity to Alzheimer's Disease

Al neurotoxicity studies are hampered due to Al speciation chemistry problems and lack of animal models that are very sensitive to Al toxicity. Recently our team and that of Savory from the USA clearly demonstrated that aged rabbit is the best animal model for aluminum-maltolate toxicity studies. Our teams showed that aluminum-maltolate-treated aged rabbit perfectly mimics AD brain in terms of neurofibrillary tangles, A β deposition, neuropeptide Y, neuropeptide amino acids, racemization pattern of L- to D-amino acids, oxidative stress, apoptosis, etc. These findings clearly showed that Al could induce neurodegeneration similar to that found in AD brain. The following studies support the above argument.

a. Role of Aluminum in NFT Production

Neurofibrillary tangle formation is the hallmark of Alzheimer's neuropathology. Studies showed that Al could induce NFT formation both in cell and animal models. Extensive studies have been carried out in understanding Al neurotoxicity and its relevance to Alzheimer's disease using aluminum-maltolate. Both *invitro* and *invivo* (25-33) experiments have been carried out using aluminum-maltolate via oral, intravenous, and intracerebral routes of administration. With intracerebral administration, the effect of aluminum-maltolate is dramatic, even at sites in the CNS distant to the injection site. As little as 2 mM of Al can trigger vigorous NFT production. This experimental system bypasses the physiological barrier(s) that prevent Al from entering the CNS but effectively produces the effects of increased Al load in the CNS, similar to Alzheimer's disease.

Studies from the Rao (India), Savory (USA) and Zatta (Italy) groups provided information on aluminum-maltolate complex-induced neurodegeneration, which perfectly mimics AD brain pathology. Recently two significant contributions (34,35) provided an important clue on the application of aluminum-maltolate in understanding Al neurotoxicity and also for the use of it as a compound to develop Alzheimer's animal models. These two groups showed that aluminum-maltolate, injected intracisternally into aged rabbits, could produce significant AD pathology events like NFT formation, A β deposition, oxidative stress, apoptosis and paired helical filaments (PHF) in the hippocampal and frontal cortex regions of aged rabbits. Furthermore, they also showed co-localization of oxidative stress and apoptosis, NFT and apoptosis and PHF and apoptosis in the same neurons in the hippocampal region of aged rabbit brain (34,35). To the best of our knowledge, these findings are the first of their kind to evidence that aluminum-maltolate could cause neurodegeneration similar to that of the neuropathology of AD brain. The

apoptotic mechanism and NFT formation in single neurons using confocal imaging and the gel profile of DNA damage were also studied (35). All of these indicated that Al could induce apoptosis in both the frontal cortex and the hippocampus of aged rabbit, mimicking AD brain.

b. The Role of Aluminum in Anti-Apoptotic and Pro-Apoptotic Proteins Expression

Bcl 2 is an anti-apoptotic protein expressed to save cells in the initial phases of cell death. Bax is a pro-apoptotic protein expressed to stimulate cells to undergo death. The ratio of Bcl 2 to Bax indicates the fate of cells by protection or promotion of cell death. In AD brain cells, the Bcl 2:Bax ratio is very low, indicating that the cells are undergoing death. Studies (34, 35) have shown that Al induces cell death events in brain cells similar to those observed in postmortem AD brain. A time sequence study of various apoptotic events in CA1 region of hippocampal region of aged rabbit brain showed clearly that aluminum-maltolate can induce Bax expression, and thus favor the initiation of programmed cell death, following the accumulation of redox-active iron, and oxidative stress (34). This contribution is considered to be a milestone work in understanding the mechanism involved in AD pathology.

c. Modulation of Neuropeptide by Aluminum

The major secondary symptoms observed in AD patients after memory loss are reduction in appetite and change in feeding behavior. Recent studies clearly indicate that neuropeptide Y (NPY) present in the hypothalamic region plays a key role in regulating feeding behavior and food intake. NPY is a 36-amino acid, C-terminal amidated peptide and is widely distributed in the central and peripheral nervous systems. It has been found that NPY concentration is reduced in cerebrospinal fluid, plasma, cerebral cortex, hippocampus and hypothalamus of AD brain (36). The reduction of NPY in AD hypothalamus may be responsible for the altered feeding behavior in AD patients. It was shown that any decrease in α -helical content would decrease the NPY interaction with receptors and its regulatory ability as a vasoconstrictor and neuromodulator. Our recent study with animal models indicated that Al caused structural destabilization in NPY by decreasing the α -helical content of the protein from 80% to 30% as confirmed by ELISA study. NMR study has clearly showed that Al strongly binds to NPY thus making the molecule functionally inactive by modulating its structural stability. This is the first report to show modulation of NPY by Al (37).

d. Modulation of NAAG by Aluminum

Glutamic acid and aspartic acid are important acidic neurotransmitters in the CNS. N-Acetyl-L-aspartyl-L-glutamate (NAAG) belongs to this class of neurotransmitters and is known to be present in high concentrations (0.5-5.0 mM) in the nervous system. Immunohistochemical evidence shows that it is present within the neurons of the peripheral and central nervous systems. It has also been identified in retinal neurons of several species including rats, monkeys and humans. NAAG has been shown to selectively activate the N-methyl-D-aspartate receptor-1 (NMDAR-1) in the family of NMDA receptors. The understanding of the role of NAAG in neurodegenerative disorders indicated that both NAA and NAAG concentrations and the activity of NAALADase were significantly reduced in the hippocampus (by 38 and 24%) and amygdala (28 and 22%) of AD brains, but not in the cerebral cortex and olfactory bulb (38). Recently our group showed that aluminum-maltolate could reduce NAAG concentrations in aged rabbits. Similar to NPY, this neuropeptide has been shown to be decreased in AD brain. NMR studies clearly showed that Al binds strongly to NAAG thus making it functionally inactive by modulating structural stability (39).

e. Aluminum-Induced Amino Acid Racemization

Excitatory amino acids play a crucial role in brain functioning. Nature prefers L-amino acids rather than D-forms for the construction of proteins. With a few exceptions, all proteins comprise L-amino acids. But studies have shown mild accumulation of D-aspartate and D-glutamate as an aging phenomenon and significantly higher levels in Alzheimer's disease-affected brain regions and cerebrospinal fluid. It has also been shown that D-amino acids are preferentially incorporated into AD-specific hallmark protein complexes like NFT and A β peptide, and thus possibly favor tangle and plaque formation. Recently it was reported that Al complexes of D-amino acids favor more A β aggregation compared to L-amino acid-Al complexes implicating the stereospecific involvement (40). It was also shown that Al ingestion favors D-aspartate racemization in rat brain (41). This study provided clue that Al-treated aged rabbit brain mimics AD human brain in terms of the accumulation of D-aspartate and D-glutamate in the hippocampal region along with other hallmark events involved in the pathology.

Our group (unpublished results) showed that Al-maltolate could favor the racemization from L- to D- amino acids in the hippocampal region of aged rabbit brain. By NMR spectroscopy, it was clearly shown that Al preferentially binds to L-amino acids over D-amino acids. Nevertheless the exact chemistry involved in the racemization needs to be explored. The possible catalytic role of Al in the racemization of L- to D- amino acids is due to the chelation of amino acids by the

positively charged metal ion, which stabilizes the intermediate carbanion formed by loss of the α -hydrogen, thus increasing racemization rates from L- amino acid to the D-amino acid.

New Hypothesis on the role of Aluminum in Cell Death

It is apparent that accumulation of metals in AD brain might play a significant role in cell death and neuronal loss. Al, with an ionic radius of 54 pm, could compete with other metal ions in binding with biomolecules and thus replace other essential metals. Martin (5) reported that Al is likely to replace Ca, Mg and Zn. It has been reported (13) that Al and Fe concentrations were elevated in AD brain while levels of other elements such as Na, K, Cu, Mg, Zn and Ca were significantly reduced. The co-localization of Fe and Al may be attributed to the similar ionic radius to charge ratio of Al and Fe (Al: 0.16; Fe 0.169). Based on these results, we have proposed three pathways for the cell damage due to the presence of high levels of Fe and Al. The three pathways are described below (Figure 2).

i. Aluminum-Enhanced A β Peptide-Mediated Oxidative Stress

There is controversy over the issue of whether oxidative damage increases A β peptide production, or A β peptide increases the oxidative stress. Evidence (42) strongly suggests that A β peptide and oxidative stress are inextricably linked to each other. It has been shown that Al³⁺, Zn²⁺ and Fe³⁺ promote the aggregation of A β peptide in very dilute solutions. They also promote aggregation of physiological concentrations of A β peptide. So both Al and A β peptide may enhance amyloid-mediated oxidative stress. Since both Al and A β peptide cause increased production of H₂O₂, this favors redox-active iron, leading to oxidative stress and cell death.

ii. Bcl2:Bax Ratio Modulation Pathway

Experiments (35) with aged rabbits showed that aluminum-maltolate was able to develop oxidative stress in hippocampal neurons leading to apoptosis. The studies further indicated that Al-treated aged rabbit hippocampal neurons first express Bcl2 (anti-apoptotic) protein in the first 3 hrs. Later, however, Al favors expression of Bax (pro-apoptotic) protein, accumulation of redox-active iron, presence of oxidative stress and final cumulative apoptosis.

iii. Aluminum-Enhanced Fe-Mediated Oxidative Stress

The mitochondrial damage caused by Al leads to the production of highly reactive oxy and hydroxy free radicals. These findings clearly indicated that Al enhances oxidative stress through enhanced iron-mediated Fenton reactions by increasing the redox-active iron concentration. Further study (13) clearly showed that Al causes accumulation of H_2O_2 and also activates superoxide dismutase (SOD), while it inhibits catalase. The increased H_2O_2 pool enhances the presence of redox active iron either from loosely bound Fe or by modulating the electron transport chain. This provides a clue in proposing the role of Al in enhancing Fe-mediated oxidative stress.

All these three events lead to the generation of hydroxy free radicals and results in neuronal cell death by way of damage to DNA, proteins and lipids.

Conclusion

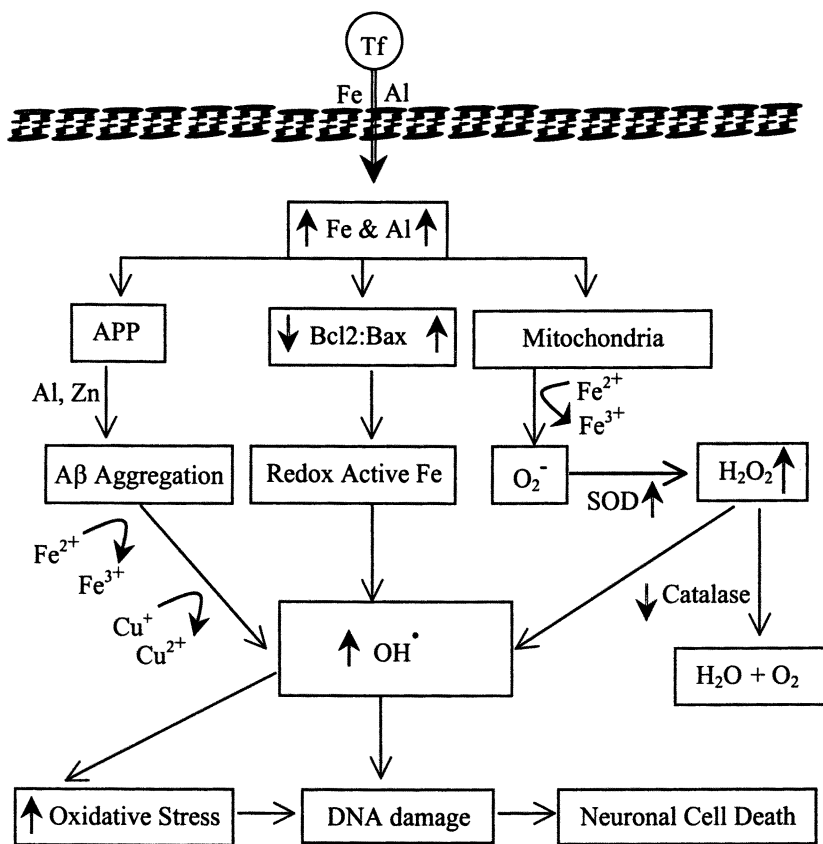
Aluminum's association with AD neuropathology is due to the presence of elevated aluminum levels in AD brain and Al localization in NFT and plaques. Our studies, as explained above, clearly showed that Al deposits greatly in severely affected AD brain while iron preferentially deposits in moderately affected AD brain. These two metals could sequentially displace monovalent and divalent ions, thus leading to mitochondrial dysfunction, which ultimately paves the pathway to neuronal cell death as explained below. Three pathways explain the high points on how the Al causes neuronal cell death below.

- A-beta ($A\beta$) aggregation,
- Bcl2:Bax ratio alteration, and
- Free radical generation through redox action of iron in mitochondria.

All these studies clearly indicated that the group 13 element Al could cause neurodegeneration mimicking AD neuropathology through multifaceted pathways. This is a new hypothesis on how Al could cause neurodegeneration.

Acknowledgements

The authors wish to thank Dr.V.Prakash, Director, CFTRI, Shri.B.Bhattacharjee, Director, BARC and Shri. T.K. Bera, Project Manager, BARC Unit, Mumbai, for their encouragement and support. This work was done under CSIR (India) and CNR (Italy) Joint collaborative project.



Legend: Tf-Transferrin; SOD- Superoxide dismutase; The upward and downward arrows indicate increasing and decreasing trends due to the elevation of Al in the cell.

Figure 2. Aluminum induced cell death through three possible pathways

References

- 1 Kerr, D.N.S.; Ward, M.K.; Aluminum and its role in biology; Sigel, H.; Sigel, A.; Marcel Dekker Inc., New York, **1988**, Vol. 24, 217-258.
- 2 London, G.M. *Amer. J. Kidney Disease*. **1989**, XIII, 75-83.
- 3 Lukiw, W.J.; Yasui, M.; Strong, M.J. Mineral and Metal Neurotoxicology; Ota, K.; Verity, M.A.; Boca Raton, FL, CRC Press, **1997**; 113-125.
- 4 Savory, J.; Huang, Y.; Herman, M.M.; Wills, M.R. *Brain Res*. **1996**, 707, 272-281.
- 5 Martin, B.R.; Mineral and Metal Neurotoxicology, Ota, K.; Verity, M.A.; Boca Raton, FL, CRC Press, **1997**, 123-130,
- 6 Flaten, T.P.; Odegard, M. *Food. Chem. Toxic*. **1988**, 26, 959.
- 7 Martin, B.R. *Clin Chem*. **1986**, 32, 1797-1806.
- 8 Akesson, M.A.; Munns, D.N. *Biochim. Biophys. Acta*. **1986**, 984, 200.
- 9 Cochran, M.; Coates, J.; Neoh, S. *FEBS. Lett*. **1987**, 176, 129.
- 10 Morris, C.M.; Candy, J.M.; Oakley, A.E.; Taylor, G.A.; Mountfort, S.; Bishop, H.; Ward, M.K.; Bloxham, C.A.; Edwardson, J.A. *J.Neurol Sci*. **1989**, 94, 295-306.
- 11 Rao, K.S.J.; Eswaran, K.R.K. *Mol. Cell. Biochem*. **1997**, 175, 59-63.
- 12 Rajan, M.T.; Rao, K.S.J.; Mamatha, B.M.; Rao, R.V.; Shanmugavelu, P.; Rani Menon.; Pavithran. *J.Neurol Sci*. **1997**, 146, 153-166.
- 13 Rao, K.S.J.; Rao, R.V.; Shanmugavelu, P.; Menon. R.B. *Alz.Rep*. **1999**, 2, 241-246.
- 14 Crapper McLachlan, D.R.; Lukiw, W.J.; Kruck, T.P.A. *Environ. Geochem. Health*. **1990**, 12, 103-114.
- 15 Rao, K.S.J. *Biochem.Int*. **1990**, 22, 725-734.
- 16 Rao, K.S.J. *Biochem.Int*. **1992**, 28, 51-56.
- 17 Rao, K.S.J.; Rao, G.V. *FEBS.Lett*. **1992**, 311, 49-50.
- 18 Walker, P.R.; LeBlanc, J.; Sikorska, M. *Biochemistry*. **1989**, 28, 3911-3915.
- 19 Crapper McLachlan, D.R.; Lewis, P.N.; Lukiw, W.J.; Sima, A.; Bergeron, C.; De Boni, U. *Ann.Neurol*. 1884, 15, 329-334.
- 20 Anitha, S.; Rao, K.S. J.; Viswamitra, M.A. *Biochem Soc Trans*. **2000**, 28, A454, Number: 1848,
- 21 Rao, K.S.J.; Divakar, S. *Bull.Environ.Contamn.Toxicol*. **1993**, 50, 92-99.
- 22 Champion, C.S.K.; Rajan, M.T.; Rao, K.S.J.; Viswamitra. M.A. *Cell. Mol. Life. Sci*. **1998**, 54, 488-496.

- 23 Rajan, M.T.; Champion, C.S.K.; Vishnuvardhan, D.; Rao K.S.J.; Viswamitra, M.A. *Mol.Biol.Rep.* **1996**, *22*, 47-52.
- 24 Rao, K.S.J.; Rao B.S.; Vishnuvardhan, D.; Prasad, K.V.S. *Biochem.Biophys. Acta.* **1993**, *1172*, 17-20.
- 25 Bertholf, R.L.; Nicholson, J.R.P.; Wills, M.R.; Savory, J. *J. Ann.Clin. Lab. Sci.* **1989**, *17*, 418-423.
- 26 Wills, M.R.; Hewitt, C. D.; Savory, J.; Herman, M.M. *Ann. Clin. Lab. Sci.* **1993**, *23*,17-22
- 27 Katsetos, C.D.; Savory J.; Herman M.M.; Carpenter, R.M.; Frankfurter, A.; Hewitt, C.D.; Wills, M.R. *Neuropathol. Appl.Neurobiol.* **1990**, *16*, 511-528
- 28 Erasmus, R.T.; Savory, J.; Wills, M.R.; Herman, M.M. *Ther. Drug Monitor.* **1993**, *15*, 588.
- 29 Huang, Y.; Savory, J.; Herman, M.M.; Nicholson, J.R.; Reyes, M.R.; Boyd J.C.; Wills, M.R. *NeuroToxicol*, **1995**, *16*, 291-296.
- 30 Savory, J.; Herman, M.M.; Hundley, J.C. *NeuroToxicol*, **1993**, *14*, 9-12.
- 31 Savory, J.; Herman, M.M.; Erasmus, R.T. *Neuropathol.Appl. Neurobiol*, **1994**, *20*, 31-37.
- 32 Savory, J.; Huang, Y.; Herman, M.M.; Reyes, M.R.; Wills, M.R. *Brain. Res.* **1995**, *669*, 325-329.
- 33 Huang, Y.; Herman, M.M.; Liu, J.; Katsetos, C.D.; Wills, M.R.; Savory, J. *Brain. Res.* **1997**, *771*, 213-220.
- 34 Savory, J.; Rao, K.S.J.; Huang, Y.; Lateda, P.R.; Hermann, M.M. *NeuroToxicology.* **1999**, *20*, 805-818.
- 35 Rao, K.S.J.; Anitha, S.; Latha, K.S. *Alz.Rep.* **2000**, *3*, 83-88.
- 36 Koide, S.; Onishi, H.; Hashimoto, H.; Kai, T.; Yamagami, S. *Neurosci Lett.***1995**, *198*, 149-151.
- 37 Rao, K.S.J.; Ramesh, J.; Easwaran, K.R.K. *Alz. Rep.***1999**, *2*, 99-103.
- 38 Passani, L.A.; Vonsattel, J.P.; Carter, R.E.; Coyle, J.T. *Mol. Chem. Neuropathol.* **1997**, *31*, 97-118.
- 39 Ramesh, J.; Rao, K.S.J.; Easwaran, K.R.K. *Alz Rep.* **2001**, *4*, 87-92.
- 40 Ramesh, J.; Madhav, T.R.; Vatsala, S.; Ramakrishna, T.; Easwaran, K.R.K. *Alz. Rep.* **1999**, *2*, 31-35.
- 41 Anderson, K.K.; Perez, G.L.; Fisher, G.H.; Man, E.H. *Neurosci. Res. Commun.* **1989**, *6*, 45-49
- 42 Smith, M.A.; Hirai, K.; Hsiao, K.; Pappolla, M.A.; Harris, P.L.; Siedlak, S.L.K.; Pappolla, M.A.; Tabaton, M.; Perry G.. *J Neurochem.* **1998**, *70*, 2212-2215.

Chapter 17

Advancement of Studies on the Formation of Polynuclear Hydroxyl Aluminum Species and Their Transformation Laws in Aqueous Systems and Soil Solutions: A Review

C. Y. Wang^{1,2}, S. P. Bi^{1,*} and M. B. Luo¹

¹Department of Chemistry, Nanjing University, Nanjing 210093, China

²Department of Chemistry, Xuzhou Normal University 221009, China

*Corresponding author: email: bisp@nju.edu.cn

In this paper, the research progress about the formation of polynuclear hydroxyl Al species and their transformation laws in the last decade will be reviewed. All kinds of reactions about hydrolysis, polymerization, flocculation and precipitation of soluble Al occurring in aqueous systems, soil solutions and on the interface of water and mineral have been systematically summarized including: Al polymerization via coalescence of the hexamer units according to the "gibbsite-fragment" model. The proposed structure of various polymeric Al species according to the "core-link" model will be made. The effects of some important parameters, such as the sort of clay minerals, the OH/Al molar ratios, the type and amount of different complexing anions, as well as the temperature will also be examined. All kinds of hydroxyl monomer and

polymer species of Al, their methods of measurement, thermodynamic stability and structures will be summarized, appraised and tabulated.

Introduction

Aluminum (Al) is the most abundant metallic element in the lithosphere, and of all elements only superceded by oxygen and silicion, making up approximately 6.62% the solid matter in soil. Al has some special chemical natures. It has been considered non-toxic for quite a long time and has been widely applied in many areas: military flying materials, building materials, and as articles for daily use. Some Al salts (such as polyaluminum chloride, polyaluminum sulfate, polyaluminum sulfate silicate) are an important coagulant in waste especially for potable water treatment. $\text{Al}(\text{OH})_3$ has been used in drugs to treat gastric and duodenal ulcers, excessive blood phosphorus of renal failure patients, and some others symptoms in clinic. However, this situation has changed since 1980's with the global acidic deposition and the discharging of acidic waste waters. Al is released from aluminosilicate minerals and sediment into soil solutions and water systems, which increases the amount of soluble Al in the environment. Al species and some highly dispersed granule combined Al in natural waters and soil solutions play an important environmental ecological role in the hydrosphere. The physicochemical reactions of aquatic Al on the interfaces of minerals/water determine the biogeochemical cycling of many others elements by hydrolysis-polymerzation-flocculation-subsidence and adsorption-complexation-electro-neutralization. Especially the direct biological toxicity and indirect physiological ability obstacle of some Al species to aquatic organisms, flora, and human body have received increasing exposure (1,2). Some polynuclear Al species appear to be more toxic to aquatic and terrestrial biota than mononuclear species (3). The aim of this review is to summarize the present status of studies on the formation of hydroxyl polynuclear Al species and their transformation laws in aquatic environments and soil solutions.

Hydrolysis and Polymerization of Soluble Aluminum in Aquatic Systems and Soil Solutions

The concentration of Al is low in natural water: the average concentration is $10 \mu\text{g} \cdot \text{l}^{-1}$ for the hydrosphere, and is $100\text{-}500 \mu\text{g} \cdot \text{l}^{-1}$ for fresh water (4) . The environmental Al originates, to a large extent, from input of acids into the environment, mainly through fossil fuels containing sulfur or nitrogen. This

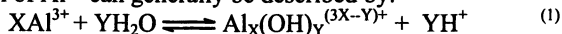
leads to the decomposition and the corrosion of bauxite and to a greater mobility of Al in the environment into water systems. Much of our present understanding about the nature of hydroxyl Al species in environmental systems has been derived from the study of laboratory-hydrolyzed solutions prepared by adding a base to Al salt solutions.

Hydrolysis and polymerization reactions of soluble Al and the resultant hydrolytic products have been studied for more than a century. At present, the emphasis of this study is focused on the following four aspects: (i) Al species and their pathway of transformation; (ii) The major mechanism(s) of hydrolysis, polymerization of hexaaquaaluminum(III) and its control and optimization; (iii) The stable conditions and the measurement of thermodynamic stability constants of the hydrolysis and polymerization of Al; (iv) As a new cause toxin element, its effects on other elements in the biogeochemical cycle and direct and/or indirect toxicity to life systems.

An understanding of these aspects, however, tend to remain elusive because of the complexity of natural systems, for which it is not possible to precisely identify all reactants and products, Furthermore there is a lack of information regarding the kinetics and thermodynamics of these reactions. Therefore, these items remain front-line areas of very active investigation.

The Hydrolytic and Polymeric Species of Aluminum

Hydrolysis and polymerization reactions of aqueous Al and the various components have been reported (5). However it is difficult to identify unequivocally the species that are produced by Al hydrolysis because of the apparent diversity of reaction condition and number of coexisting species. Generally speaking, the octahedral complex $\text{Al}(\text{H}_2\text{O})_6^{3+}$ is a proton donor. It takes place in a series of hydrolyses in aqueous solutions and forms monomeric Al species (Al_a), polymeric Al species (Al_b), or polyaluminum, and amorphous sol (Al_c). The soluble Al include Al^{3+} , Al_a , and Al_b . The overall hydrolysis and polymerization of Al^{3+} can generally be described by:



Correspondingly, $1 \leq X \leq 54$, $1 \leq Y \leq 144$ (6). Its hydrolysis products are a series of metastable species from Al^{3+} to $\text{Al}_m(\text{OH})_{3m}$ (see Table I. among it, the OH/Al molal ratios $B = \text{OH}/\text{Al}$ or called alkalinity; z takes 0 or 2; $Y/X \approx 2.7$ (15); $m > 54$). Of all the polynuclear species proposed, those having the most convincing experimental support, albeit usually indirect, are the $\text{Al}_2(\text{OH})_2^{4+}$, $\text{Al}_6(\text{OH})_{12}(\text{H}_2\text{O})_{12}^{6+}$, $\text{Al}_8(\text{OH})_{20}(\text{H}_2\text{O})_x^{4+}$, $\text{Al}_{13}\text{O}_4(\text{OH})_{24}(\text{H}_2\text{O})_{12}^{7+}$ and

Table I. polymeric Al species and their analytical methods

code	Al species	lg β	method	define	condition	ref.
Al ₁	Al(OH)(H ₂ O) ²⁺	-5.52	c,e	**	pH=4.0- 5.5	8
		-5.0	--			7
	Al(OH) ₂ (H ₂ O) ₄ ⁺	-8.71	c,e	**	9	
		-10.1	--		7	
		-11.3	--		8	
Al ₂	Al(OH) ₄ ⁻	-23.46	c,e,	**	pH>9	7, 10
	Al(OH) ₅ ²⁻	--	c,e,	0		7
	Al ₂ (OH) ₂ (H ₂ O) ₈ ⁴⁺	-6.3	ab,N,u,sx	**		9, 16
Al ₃	Al ₂ (OH) ₅	--	--	0	11	
	Al ₃ (OH) ₄ (H ₂ O) ₁₀ ⁵⁺	-13.57	ab	**	8	
Al ₄		-13.74	ab		9	
	Al ₃ (OH) ₈ ⁺	--	I	0	11	
	Al ₄ (OH) ₈ ⁴⁺	--	I	0	7	
Al ₅	Al ₄ (OH) ₁₀ (H ₂ O) ₈ ²⁺	--	I	0	7	
	Al ₅ (OH) ₁₃ ²⁺	--	I	0	7	
Al ₆	Al ₆ (OH) ₁₅ ³⁺	-47.0	ab,u	**	[Al ³⁺]> 10 ⁻² mol/l B<2.2	9, 17
	Al ₆ (OH) ₁₂ (H ₂ O) ₁₂ ⁶⁺	--	c,d	**		7
	Al ₆ (OH) ₁₀ ⁴⁺	--	--	0		7
Al ₇	Al ₇ (OH) ₁₇ ⁴⁺	-48.8	ab	*	7, 9	
	Al ₇ (OH) ₁₅ ⁵⁺	--	--	0	11	
Al ₈	Al ₈ (OH) ₂₀ (H ₂ O) _x ⁴⁺	-68.70	ab,IR,N	**	7, 9	
	Al ₈ (OH) ₁₂ (H ₂ O) ₁₂ ⁶⁺	--	--	0	13	
Al ₉	Al ₉ (OH) ₁₈ ⁸⁺	--	I	0	7, 13	
Al ₁₀	Al ₁₀ (OH) ₂₂ (H ₂ O) ₁₆ ⁸⁺	--	--	0	13	
Al ₁₃	Al ₁₃ O ₄ (OH) ₂₄ (H ₂ O) ₁₂ ⁷⁺	-97.6	f,N,sx	**	14, 20	
		-109.2	N,sx		8	
	Al ₁₃ O ₄ (OH) ₂₈ ³⁺	-105	N,sx	0	7	
	Al ₁₃ (OH) ₃₂	--	ab,sx,u,	0	7	
	Al ₁₃ (OH) ₃₀ (H ₂ O) ₁₈ ⁹⁺	--	sx	0	13	
	Al ₁₃ (OH) ₃₄	-97.60	sx	*	7	
	Al ₁₃ O ₄ (OH) _{24+z} ^{(7-z)+}	--	N	0	[Al ³⁺]> 10 ⁻² mol/l	
	Al ₁₄	Al ₁₄ (OH) ₃₂ ⁸⁺	--	ab	0	15
		Al ₁₄ (OH) ₃₄ ⁷⁺	--	ab	*	1.5<B< 2.8
		Al ₁₅ (OH) ₃₈ ¹⁰⁺	--	--	0	7
Al ₁₆	Al ₁₆ (OH) ₃₈	--	--	0	18	
Al ₂₄	Al ₂₄ (OH) ₆₀ (H ₂ O) ₂₄ ¹²⁺	--	--	*	13	
Al ₅₄	Al ₅₄ (OH) ₁₄₄ (H ₂ O) ₃₆ ¹⁸⁺	--	t	*	13	
	Al(OH) ₃ (aq)	-16.0	d,u	**	8, 9	
Al _X	Al(OH) ₃ (am)	-10.4	d,u	**	pH>7, B>3	
	Al _X (OH) _Y ^(3X-Y)	--	N	*	6, 15	
Al _m	Al _m (OH) _{3m}	--	N	*	13	

- The meaning of the symbol of analytical methods, ab: potentiometric acid- base titration; c: cation ion exchange; d: dialysis technique; e: ion- selective electrode; f: flow injection analysis; IR: infrared spectroscopy; I: light scattering; N: ²⁷Al-NMR; t: model inferring; u: ultracentrifugation; sx: the small-angle x-ray diffraction;
- ** : this species exists certainly under relevant conditions; * : maybe exists; 0 : uncertain; -- : unknown.

$\text{Al}_{54}(\text{OH})_{144}(\text{H}_2\text{O})_{36}^{18+}$ (7), but those species can't exist at the same time, their superior species vary with the conditions.

The Mechanisms of the Hydrolysis-Polymerization of Aluminum Species

Many researchers using both experiment (21) and computer simulation (5,22,23) have studied the species and speciation of Al in aqueous systems and soil solutions. So far, the following model has been favored by many investigators:

(1) "core—link" or hexameric ring model (Figure 1), which can elucidate a series of possible species (Figure 2). In Figure 2, "†" is the schematic representation of the double OH-bridge $[\text{Al}_2(\text{OH})_2]^{4+}$. The basic unit of this model for Al polynuclear formation is either the $[\text{Al}_6(\text{OH})_{12}(\text{H}_2\text{O})_{12}]^{6+}$ (single ring) (12), or the $[\text{Al}_{10}(\text{OH})_{22}(\text{H}_2\text{O})_{16}]^{8+}$ (double ring) (13) species. These polynuclear units are believed to coalesce with aging via deprotonation of edge-group water molecules, which then form all kinds of species. Thus, it is envisaged that the polymerization process involves continued bidimensional growth of the hexameric ring units. With the subsequent formation of the sheet structure of gibbsite or bayerite. The observation that hydrogen ion activities of partially neutralized Al salt solutions generally increase on aging has been taken as support of this polymerization process. Yet, there has been some disagreement (7) among the proponents of the hexameric ring model as to the smallest polynuclear species present in the same solutions. Moreover, there is no direct or indirect convincing evidence supporting all these sheet structures.

(2) "Al₁₃ polynuclear species model" (Figure 3). This model holds that in Al solution there are monomer, dimer, trimer and Al₁₃ tridecamer, or larger polymerized Al species. These species can transform from one to another directly. The Al₁₃ polymer consists of a central tetrahedral Al symmetrically surrounded by 12 octahedrally coordinated Al ions disposed in groups of three at each apex of the tetrahedron. Therefore it is usually described as $\text{AlO}_4\text{Al}_{12}(\text{OH})_{24}(\text{H}_2\text{O})_{12}^{7+}$. At present, more and more scholars deem that $\text{Al}(\text{OH})_4^-$ is a required precursor to Al₁₃ polymer (7). That is, Al₁₃ constitutes six dimeric species nucleated around an $\text{Al}(\text{OH})_4^-$. They argue that the Al₁₃ structure could be viewed as comprised of six oxygen sharing dimeric units which bridge the edges of the central tetrahedron.

Others consider that Al₁₃ polymer isn't the dominant species in soil solutions, because of comparing to AlO₆ tetrahedron, the central tetrahedral AlO₄ of Al₁₃ is thermodynamically unstable system. Furthermore, according to the reactive equation (1), the production of Al₁₃ makes great demands on more base. The Al₁₃ model can't explain the formation and transformation of all kinds

of Al species in dilute solution also. Kato et al. (17) consider that the Al_{13} is very low in concentration by chemical equilibrium calculations, and hence can be ignored in soil solutions. Moreover, there is no consensus on the forming mechanism, the metastable state conditions, and some important influence factors related to Al_{13} .

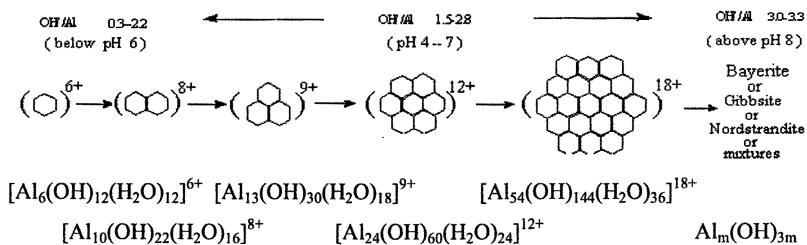


Figure1. Aluminum polymerization via coalescence of the hexamer units according to the "gibbsite-fragment" model (Adapted with permission from reference 13. Copyright 1988 Hsu, P. H.)

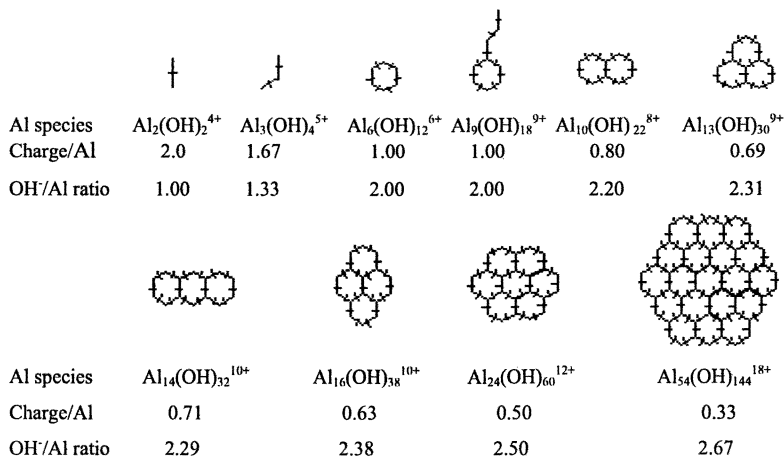


Figure2. Proposed structures of polymeric aluminum species according to the "core-link" model (Adapted with permission from reference 15, Copyright 1990 Letterman & Asolekar; from reference 22, Copyright 1976 Stol & Van Helden; from reference 24, Copyright 1986 Beijing: Science Press.)

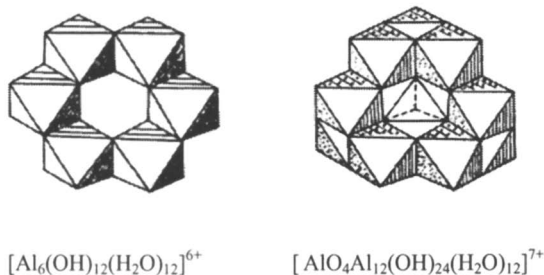


Figure 3. The structures of the hexamer units model and the Al_{13} polynuclear species model (Adapted with permission from reference 12, Copyright 1987 Schutz & Stone; and from reference 26, Copyright 1989 Parker, Kinraide & Zelazny.)

Hunter and Ross (19) reported the presence of Al_{13} in organic horizons of a forested spodosol. Several investigators, however, have suggested that its presence in soil solutions of agricultural fields is doubtful, because the coexistence of phosphate (26), sulfate (27), and silicate (28, 29) in soil solutions decreases the concentration of Al_{13} . In addition, desorption of the highly charged Al_{13} (+7) from negatively charged soil colloids into soil solutions is doubtful.

Formation of polynuclear Al species involving polymerization at the mineral/water interfaces and the mineral interlayers has received considerable attention (20). It is found by some researchers that even when Al concentration in bulk solutions are low, the surface Al concentration is several orders of magnitude greater, presumably making polymer formation a very favorable process. Another important finding is that some Al species may exchange with other cations, making clay minerals a potential source of Al polynuclear complexes in soil solutions and aquatic systems (7).

Flocculation and Precipitation of Polynuclear Aluminum Species (Polyaluminum)

In fact, polynuclear Al species are a set of kinetic medium products in hydrolysis, polymerization, gelation, and precipitation of Al solution (Figure 4), which have got extensive research in the physico-chemical treatment of water

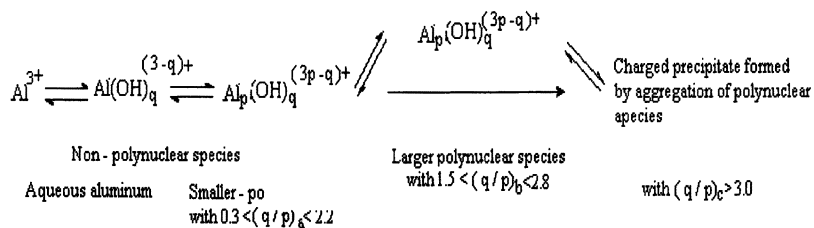


Figure 4. Proposed pathway for the reactions involved in base and acid titrations (Adapted with permission from reference 15. Copyright 1990 Letterman & Asolekar.)

and waste water (9). But the research in the multimedium environmental interfaces of water/sediment and water/minerals is not enough. Particulate phase are clearly important Al components in soil solution and natural water systems. They may be transformed into some very fine particulates or monomeric Al species that pass easily through membrane filters in acidic surface waters, potentially causing major errors in the determination of “dissolved” Al (7). There are many factors influencing the flocculation and precipitation of polynuclear Al species. These factors and their influential laws include five aspects as follows:

(1) The sort of clay minerals. The Al concentration and the form of Al species in soil solutions are related to the type of clay minerals, the pH value of soil, and the depth of soil (30,31). Clay minerals are important sources of environmental Al. Different geology conditions have different dissolution mechanisms for minerals, thereby having dissimilar effects. Some researchers consider that Al activity is controlled by gibbsite, jurbanite, or both in terms of mineral stability (32). In fact, It is controlled by multiform bauxite in acidic natural waters, such as kaolinite, montmorillonite, illite, aluminite, basaluminite, imogolite, allophanes, taranakite, etc. (33). The main exchangeable Al in all of the soils is Al^{3+} . The Al in montmorillonite is almost exchangeable Al, and yet there is little in vermiculite and kaolinite. Syuntaro H. et al. (29) consider by means of ^{27}Al -NMR that the concentrations of Al_{13} decrease with increasing Si/Al molar ratio of soil solutions, and Al_{13} is not detected at Si/Al ≥ 0.28 . In the KCl extracts from soils, the Al_{13} is not detected at all. This result suggests that Al_{13} is not formed in these soils, or that the persistence of Al_{13} in the soil solutions is strongly inhibited by adsorption or precipitation reactions. The Al in montmorillonite has a greater degree of hydrolysis than that of kaolinite, because the interstitial matter in

montmorillonite interlayer is labile and has a tendency of expansion. Some smaller polynuclear species form at clay interfaces, and Al_{13} and larger polynuclear species have been detected in the interlayers of swelled aluminosilicates.

(2) pH, or OH^-/Al^{3+} molar ratio (let $B = OH^-/Al^{3+}$). B is a key factor of controlling the polyaluminum content. In general, the main species at $B < 1.5$ are the monomeric and oligomer; the predominant species at $B = 1.5-2.2$ are Al_{13} and/or other larger polynuclear species, and the amorphous $Al(OH)_3$ precipitation detectable forms at $B > 3.0$. The ^{27}Al -NMR evidence presented indicates that the precipitate contains some Al_{13} , which due to Al_{13} complexation nucleation within all kinds of Al_{13} units and gelation even precipitation. It is demonstrated employing a quantitative ^{27}Al -NMR technique that the Al_{13} species forms in detectable quantities in solutions only at the concentration $> 3.4 \times 10^{-2} mol \cdot l^{-1}$ and $B > 0.25$. Its concentration increases linearly along with the raise of B . Correspondingly, the Al monomeric species decreased at the same time. The percentage of Al_{13} in total Al (Al_T) and B have a simply linear relation $Al_{13} = (B/2.46) \times 100$ (34). Other information (35) about this shows that Al_{13} polymer may form at the inhomogeneous site of pH while injecting base or the interfaces of undissolved solid phase and solution. As far as soil systems, when pH ranges from 2.8-4.2, Al performs a main buffering function and the effects of exchangeable Al are very notable. When pH ranges from 4.2-5.0, there are hydroxyl Al ions forming in soil and most of them are polymer.

(3) Coexistence ions, especially all kinds of organic or inorganic complexation ions, such as OH^- , F^- , Cl^- , SO_4^{2-} , PO_4^{3-} , SiO_4^{4-} , CO_3^{2-} , humus, low molecular mass organic acids and the like (7, 36). It was testified by some experiment that anions influence the observed flocculation and precipitation behavior, character, and the crystallization rate of Al polynuclear species with the relative effectiveness following the general order: $PO_4^{3-} > SiO_4^{4-} > SO_4^{2-} > Cl^- > NO_3^- > ClO_4^{4-}$. Some strongly complexing ligands, such as F^- or $C_2O_4^{2-}$ etc., generally increase the pH value of maximum precipitation, other anions, such as SO_4^{2-} , SeO_4^{2-} , Cl^- , NO_3^- , usually increase the pH value of maximum precipitation, and yet PO_4^{3-} , SiO_3^{2-} etc. can combine polyaluminum anions to form many kinds complex crystals which make Al in water move to sediment. Organic acids in soil react with Al to form organic Al complexes, which hinder or delay the hydrolysis and polymerization of soluble Al (37-39). The inhibiting effects of different dissolved organic constituents on Al's flocculation and precipitation reactions have been studied extensively according to the following sequence: tartaric acid > citric acid > malic acid = salicylic acid > oxalic acid > tannic acid > aspartic acid > p-hydroxybenzoic. Moreover, the addition of organic ligands not only hinders the formation of the tridecamer, but also provokes its depolymerization into oligomers, and then into monomers. This

was studied by combining ^{27}Al -NMR and small-angle x-ray scattering technology (40).

However, there is no consensus about the mechanism of the influence of anions on the flocculation of polyaluminum species. Presently, there are the following explanations: anion inclusion in polyaluminum species leads to supersaturation and then precipitation. Reducing the electrostatic repulsion between Al polynuclear centers makes it physical flocculation. Reducing of repulsion between polynuclear centers catalyzes further growth of the gibbsite fragments along the a and b crystallographic axes, which makes it grow up continually and then coagulation. It must be explained that the result of the sequence of anions introduction into the Al salt solution are different, the studies when the anions are introduced prior to neutralization have generally demonstrated the inhibitory influence of complexing anions on the hydrolysis-precipitation reactions of hexaaquaaluminum cation (41), whereas the studies employing the latter approach have substantiated that even the addition of F^- to some partially neutralized Al solutions can also cause rapid precipitation of polyaluminum species (7).

(4) The sequence, way, rate and mingling condition of base injection. The mechanisms of hydrolysis and polymerization of aqueous Al vary with the method of base introduction. When inject the amount of alkali of $B > 2.2$, the dynamic mechanism of alkali addition once is sedimentation-dissolution-hydrolysis- polymerization. Whereas, that of step by step is hydrolysis-polymerization-sedimentation. Some of the initial solid phase formed on rapid neutralization of Al solution redissolves with aging, and the Al_b fraction increases continually. Until now, the formation of Al_{13} has been reported to require special conditions such as vigorous stirring (34) or very rapid neutralization rates (7).

(5) Temperature. Temperature affects the solubility, the hydrolysis and the pH value of the Al solution (42, 43). At 25°C the degree of Al hydrolysis and the sedimentation of high molecular weight species are more rapid obviously than that observed at 2°C , the polymerization processes seem more advanced also, i.e., more of the combined deprotonation/condensation reactions are involved in the polymerization processes at 25°C compared to that at 2°C . This may explain why pH in the solutions were significantly lower at 25°C compared with at 2°C . Precipitation may occur even at lower B values. While $\text{Al}_T > 0.01 \text{ mol.l}^{-1}$ and B is big, the higher the temperature is, the greater degree of polymerization. The formation of polymeric Al species at low temperature may be hindered (44). Heating is favorable for the clarification of soil suspension and for the flocculation and precipitation of polynuclear Al species.

Conclusions

The exact nature of the polymeric Al species which are found in aqueous systems and soil solutions is still a matter of debate. Aqueous Al exhibits a plethora of chemical forms that vary with the sort of clay minerals, the OH/Al molar ratios, the presence and concentration of organic and inorganic ligands, and the experimental conditions etc. Lots of research about the speciation of the monomeric and polymeric Al species can only be limited to lab due to the complexity of nature systems. Many of the seemingly inconsistent and even paradoxical reports derive from the utilization of different experimental methods, conditions, and approaches, which have hindered the application of these ambiguous conclusions to pure minerals and/or nature waters. Future studies should emphasize the studies of the kinetic course, the transformation conditions, and the thermodynamic stability, pay attention to the surface complexation, hydrolysis, polymerization, flocculation, and precipitation on the interface or surface of water/mineral, as well as the effect of the natural complexing ligands such as all kinds of organic and inorganic anions on the distribution, transformation, and structure of polynuclear hydroxyl Al species.

Acknowledgements

This project is financially supported by the Natural Science Foundation of China (Key project No.49831005 & 29777013), Research Funding of The State Key Laboratory of Pollution Control and Resource Reuse of China (Nanjing University). Great thanks are given to Profs. Hongyuan Chen, Xiaorong Wang for their encouragements and help. Appreciation is extended to Prof. David Atwood (University of Kentucky) for helpful comments.

References

1. Fuente, J. M.; Rodriguez, V. R. Ponce, J. L. C., Estrella, L. H. *Science*. **1997**, 276, 1568-1568.
2. Desroches, S.; Dayde, S.; Berthon, G.; *J. Inorg. Biochem.* **2000**, 81(4), 301-312.
3. Shann, J. R.; Bertsch, P. M. *Soil Sci. Soc. Am. J.* **1993**, 57, 116-120.
4. Clarke, N.; Danielsson, L. G. *Anal. Chim. Acta.* **1995**, 306, 5-21.
5. Lydersen, E; Salbu, B. *Studies of Aluminum Species in Fresh Water: The Surface Water Acidification Program*; Mason, B. T. Ed., 1992; 245.

6. Akitt, J. W.; Elders, J. *J. Chem. Soc., Dalton Trans.* **1988**, 1347-1355.
7. Sposito, G. *The Environmental Chemistry of Aluminum*; CRC Press; Inc. 2nd; Boca Raton, Florida, 1995 pp. 87-116.
8. David, J. S.; Nordin, J. P.; Phillips, B. L.; and Casey, W. H. *Geochem. Cosmochim. Acta.* **1999**, 63(10), 1471-1480.
9. Luan, Z. K.; Tang, H. X. *Huanjing Kexue Xuebao.* **1995**, 15(1), 39-44.
10. Wesolowski, D. J.; Palmer, D. A. *Geochim. Cosmochim. Acta.* **1994**, 58, 2947.
11. Tang, H. X. *Huanjing Kexue Xuebao.* **1998**, 18(1), 1-11.
12. Schutz, A.; Stone, W. E. E. *Clays Clay Miner.* **1987**, 35, 251-262.
13. Hsu, P. H. *Aluminum Hydroxides in Minerals in Soil Environments*; 2nd, Eds, Dixon, J. B.; Weed, S. B., Soil Sci. Soc. of Am., Madison, WI, 1988.
14. Furrer, G.; Ludwig, C. *J. Colloid Interface Sci.* **1992**, 149(1), 56-67.
15. Letterman, R. D.; Asolekar, S. R. *Wat. Res.* **1990**, 24(8), 931-948.
16. Huertas, F. J.; Chou, L. *Geochim. Cosmochim. Acta.* **1998**, 62:417-431.
17. Kato, H.; et al. *Nippon Dojo Hiriyogaku Zasshi.* **1999**, 70(3), 291-296.
18. Liu, W. X.; Luan, Z. K.; Tang, H. X. *Shengtai Xuebao.* **1996**, 16(2), 211-214.
19. Hunter, D.; and Ross, D. S. *Science.* **1991**, 251(4997), 1056-1058.
20. Simpson, S. L.; Powell, K. J. *Analytica Chimica Acta.* **1997**, 343, 19-32.
21. Hem, J. D. *Aluminum Hydrolysis Reaction and Products in Mildly Acidic Aqueous Systems Chemical Modelling of Aqueous System*; In: Melchior, D. C; Basset, R. L., Eds. American Chemical Society, 1990, Ch. 33:430.
22. Stol, R. J.; Van Helden, A. K. *J. Colloid and Interface.* **1976**, 57(1), 115-131.
23. Bi, S. P.; Wei, Y. *Analyst.* **1995**, 120, 2805-2811.
24. Xu, B. H. *Soil Chemical Florilegium.* Beijing: Science Press, 1986, 19.
25. Baes, C. F.; *The Hydrolysis of Cations*; John Wiley & Sons, New York, 1976.
26. Parker, D. R.; Kinraide, T. B.; and Zelazny, L. W. *Soil Sci. Soc. Am. J.* **1989**, 53, 789-796.
27. Kerven, G. L.; Larsen, P. L.; and Edwards D. G. *Soil Sci. Soc. Am. J.* **1995b**, 59, 765-771.
28. Larsen, P. L.; Kerven, L. C.; Bell, L. C.; and Edwards, D. G. Effects of Sulfate Acids on the Chemistry of Monomeric and Polymeric (Al₁₃) Aluminum Species in Solutions. Proc. Int. Symp. Plant Soil Interactions at Low pH (3rd). 1995, 617-621.
29. Syuntaro, H.; et al. *Soil Sci. Soc. Am. J.* **1998**, 62, 630.
30. Godbold, D. L.; Jentschke, G. *Physiol. Plant.* **1998**, 118, 553.
31. Tombacz, E.; Dobos, A.; *Colloid and Polymer Sci.* **2000**, 78(4), 337-345.
32. Merino, A.; Macias, F. Grodeja, E. G. *Chemosphere.* **1998**, 36, 1137-1142.
33. Maitat, O. *Water, Air and soil Pollut.* **2000**, 117(1-4), 217-243.
34. Parker, D. R.; Bertsch, P. M. *Environ. Sci. Technol.* **1992**, 26, 908-921.
35. Phillips, D. L.; Casey, W. H.; Karlsson, M. *Nature.* **2000**, 404(23), 379-382.
36. Boisvert, J. P.; Jolicoeur, C. *Colloid Surf: A.* **1999**, 155(2-3), 161-170.

37. Krishnamurti, G. S. R.; Wang, M. K.; and Huang, P. M. *Clays and Clay Minerals*. **1999**, 47(5), 658-663.
38. Narayanan, R.; Laine, R. M. *J. Mater. Chem.* **2000**, 10(9), 2097-2104.
39. Tombacz, E.; Filipcsei, G.; *Colloids and Surfaces*. **1999**, 151(1-2), 233-244.
40. Masion, A.; Thomas, F.; Tchoubar, D.; Bottero, J. Y.; and Tekely, P. *Langmuir*. **1994**, 10, 4353-4356.
41. Yang, X. D.; Bi, S. P. *Wuji Huaxue Xuebao*. **2001**, 17, 168-180.
42. Busch, M.; Seubert, A. *Analytica Chimica Acta*. **1999**, 399, 223-235.
43. Lydersen, E.; Salbu, B.; Poleo, A. B. S. and Muniz, I. P. *Water, Air, and Soil Pollut.* **1990**, 51, 203-215.
44. Roy, R. L.; Campbell, P. G. C; *Environ. Toxicol. Chem.* **2000**, 19, 2457-2466.

Chapter 18

Chemistry of the Tetrafluoroaluminate Anion

**B. D. Conley, U. Dutta, C. Fridh, A. L. Gilliam, B. C. Yearwood,
J. P. Selegue, and D. A. Atwood***

Department of Chemistry, University of Kentucky, Lexington, KY 40506

A review of the chemistry of the tetrafluoroaluminate anion is presented. The uses, synthesis, characterization, and biological action of AlF_4^- are examined. Aluminum fluoride complexes, especially tetrafluoroaluminate, stimulate various guanosine nucleotide binding proteins (G-proteins), and inhibit P-type ATPases. Tetrafluoroaluminate complexes serve as precursors to aluminum trifluoride, which is used as a solid state catalyst for chlorofluorocarbon isomerizations and fluorinations.

Introduction

Fluorometallic complexes have been shown to interfere with the activity of G-proteins and P-type ATPases. G-proteins take part in an enormous variety of biological signaling systems, helping control almost all important life processes

(1). Moreover, fluoroaluminate complexes influence the activity of a variety of phosphatases, phosphorylases, and kinases. Hence the potential impact of fluorometallic complexes on life is immense, especially when one considers the ubiquitous nature of aluminum and the increasing use of fluoride in today's world.

Aluminum is the most abundant metal in the earth's crust, and exists in many common igneous minerals like feldspars and micas. Aluminum has a wide variety of industrial applications including construction, the aerospace industry, packaging, and cooking utensils. Fluorine is the thirteenth element in order of abundance in the earth's crust (2). Fluorine also has a wide variety of uses including nuclear reactors (as UF_6), the aluminum industry (as AlF_3 and Na_3AlF_6), fluorinated oils, greases, and polymers (e.g. Teflon), and fluoridation of water supplies (at concentrations less than 1 ppm). As a hard metal ion aqueous Al^{3+} interacts most strongly with hard donors, and therefore its complexes with O^- and F^- donor ligands are very stable. Out of 60 metal species, Al^{3+} binds to fluoride the strongest (except for the marginally stronger Sc^{3+}) (3). Aluminum forms stronger complexes with fluoride than with the other halides. The Al-F bond strength is about 655 kJ mol^{-1} , which is very strong compared to common bonds like H-H (432 kJ mol^{-1}), H-C (411 kJ mol^{-1}), C-C (346 kJ mol^{-1}), Si-O (452 kJ mol^{-1}). The effect of the high bond strength can be observed in the extremely high lattice energy of AlF_3 . The stability of NaAlF_4 has been investigated by differential scanning calorimetry. The disproportionation reaction:



takes place at elevated temperatures (between 700 and 900 K). The enthalpy of this reaction has been calculated to be -66.9 kJ (4). The most stable aluminum fluoride species is AlF_3 .

In view of the many studies involving the tetrafluoroaluminate anion's influence on G-proteins, and the industrial applications of AlF_4^- described in the patent literature, a review of the uses, synthesis, characterization, and biological activity of the tetrafluoroaluminate anion is appropriate.

Uses

Aluminum fluoride complexes, especially tetrafluoroaluminates [AlF_4^-], are currently of major importance because of their ability to act as phosphate analogues and thereby stimulate various guanosine nucleotide binding proteins (G-proteins) (5,6), and inhibit P-type ATPases (7). As a result of the ubiquitous nature of G-proteins, tetrafluoroaluminates are used in laboratory studies to

investigate the physiological and biochemical changes caused in cellular systems by aluminofluoride complexes.

Tetrafluoroaluminates are used in the preparation of AlF_3 . Aluminum trifluoride is important in the industrial production of Al metal, as it increases the conductivity of electrolytes in the electrolysis process. Aluminum trifluoride is also used as a solid state catalyst for chlorofluorocarbon isomerization and fluorination. High surface area AlF_3 dispersed onto carbon, organic, or inorganic supports may be a useful catalyst for these or other reactions (8). For example, a fluoroaluminum species (obtained from ammonium bifluoride in anhydrous methanol slurried with calcined alumina) generated on a support of alumina was treated with chromium to obtain active olefin polymerization catalysts (9). The AlF_4^- species can be converted to the different phases of AlF_3 by thermolysis. For example, the beta phase of $[\text{NH}_4^+][\text{AlF}_4^-]$ can be thermolyzed at 550°C to form the kappa phase of AlF_3 (10). Fluoroaluminum catalysts can also be prepared from pyrolysis of precursors obtained from aqueous solution, treatment of Al_2O_3 with HF at elevated temperatures, and treatment of AlCl_3 with HF or chlorofluorocarbons (10). The advantage of AlF_4^- over these other methods is AlF_4^- can be thermolyzed to AlF_3 without any oxide or hydroxide contamination.

Potassium tetrafluoroaluminate can be used as a flux when soldering aluminum. A flux is added in order to remove oxides and other disruptive covering films on the metal surface (11). A mix of fluoroaluminates (including KAlF_4 and KAlF_6) can be used as a flux in the brazing of aluminum and aluminum alloy parts. The flux containing the mix of fluoroaluminates allows brazing of aluminum at temperatures lower than what could be accomplished with fluoride fluxes, thus saving heating energy (12). Another method utilizes a flux-coated soldering rod that is used to deliver a solder alloy and a flux compound to the region to be repaired. The flux compound has a higher melting temperature than the solder alloy, and is present as a coating that sufficiently thermally insulates the alloy to cause the flux compound and the solder alloy to melt nearly simultaneously during the soldering operation. The solder alloy is preferably a zinc-aluminum alloy, while the flux coating preferably contains a cesium-aluminum flux compound such as potassium cesium tetrafluoroaluminate, dispersed in an adhesive binder that will readily volatilize or cleanly burn off during the soldering operation. The flux compound and binder form a hard coating that tenaciously adheres to the solder alloy and thermally insulates the solder alloy until the flux compound melts during the soldering operation. By controlling the relative amounts of preferred flux compounds and binders, the flux coating remains protective and thermal-insulating on the alloy until melting of the flux compound begins (14).

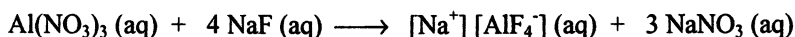
LiAlF_4 can be incorporated into the carbon cathode current collector of non-aqueous lithium batteries. LiAlF_4 is also used as the non-aqueous electrolyte, which can be dispersed throughout the cathode collector (13).

Synthesis

Tetrafluoroaluminate complexes may be synthesized in a number of ways. Aluminofluoride complexes are formed spontaneously in a water solution containing fluoride and trace amounts of aluminum. The most direct method of synthesis is a combination of aluminum trifluoride and a metal fluoride, usually under aqueous conditions.

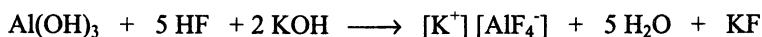


For most of the biochemical and physiological studies involving AlF_4^- , the fluoride source is usually sodium fluoride, and the aluminum source is aluminum nitrate or aluminum chloride. Solutions are usually made up with millimolar concentrations of sodium fluoride, and micromolar concentrations of the aluminum source.



However, the aqueous aluminofluoride complexes are not permanent, as equilibria exist between the various possible multifluorinated species. This is further discussed later in this chapter.

Belt *et al.* prepared KAlF_4 from aluminum hydroxide, hydrogen fluoride, and potassium hydroxide (14). The precipitate of KAlF_4 was recovered and dried under vacuum at 80°C . It was found to have a melting point of 546 to 550°C by differential scanning calorimetry.

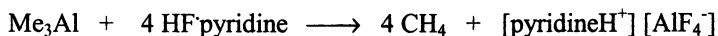


Petrosyants *et al.* extracted the AlF_4^- anion from mixtures of aluminum and sodium fluoride into dimethylsulfoxide (DMSO) and acetonitrile (AN) solutions containing benzo-15-crown-5 (B15C5) (15). They found varying the concentration of B15C5 from 0.2 to 0.7 M both in DMSO and AN solutions, and the ratio of NaF/Al from 4 up to 50 , had no significant effect on the extraction. However in DMSO, six-coordinate aluminum fluoride complexes (detected by NMR) were also present.

Sengupta and Sen have prepared fluoroaluminates of organic base cations (16). The compounds were prepared by evaporating a mixture of Al(OH)_3 dissolved in HF and the organic base. The organic bases used were hydroxylamine, pyridine, quinoline, morpholine, 2-aminipyridine, and α,α' -bipyridyl. The fluoroaluminates formed were highly hygroscopic solids. Unfortunately, thermal decomposition of the fluoroaluminates produced a

mixture of aluminum fluoride and oxide, indicating that either hydrated [baseH⁺] [AlF₄⁻] or a mixed fluoro/aquo/hydroxo species was formed.

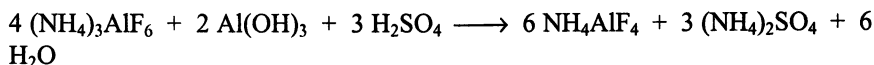
An anhydrous synthesis of the AlF₄⁻ species, also using organic cations, has been developed by Herron *et al* (17). In a glovebox, trimethylaluminum dissolved in pyridine was added to HF (as its pyridine adduct).



The 1,8-bis(dimethylamino)naphthalene (Proton Sponge, PS, (Aldrich)) tetrafluoroaluminate has also been prepared and characterized by x-ray crystallography (see discussion below) (8). It was prepared in a glove box by slurring [pyridineH⁺] [AlF₄⁻] into a solution containing excess PS dissolved in dry acetonitrile. Slurring the pyridinium salt in neat collidine (collidine = 2,4,6-trimethylpyridine) in a glove box, and heating to 120°C for 30 minutes produced [collidineH⁺] [AlF₄⁻], which was characterized by x-ray, IR, and multinuclear NMR.

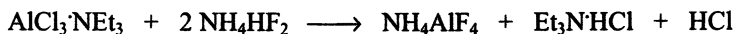
Harlow *et al.* prepared [tetraphenylphosphonium⁺] [AlF₄⁻] under anhydrous conditions using collidine tetrafluoroaluminate dissolved in methanol and (C₆H₅)₄PBr. The product was recrystallized from hot acetone or acetonitrile, and characterized by x-ray, IR, and multinuclear NMR. The arsonium derivative [(C₆H₅)₄As⁺] [AlF₄⁻] was prepared (using (C₆H₅)₄AsCl) and characterized in a similar manner.

Ammonium tetrafluoroaluminate has been prepared in a number of ways. Aramaki *et al.* added an inorganic acid (e.g. H₂SO₄) to an aqueous slurry of (NH₄)₃AlF₆ and either Al(OH)₃ or Al₂O₃ to precipitate out [NH₄⁺] [AlF₄⁻] (18). The reaction system was kept under atmospheric pressure and at 70 to 100°C. To neutralize the free ammonia in the slurry and maintain the solubility of the formed ammonium tetrafluoroaluminate, the inorganic acid was added in such an amount that the pH of the slurry after completion of the reaction was 4 to 7. Varying the method in which the inorganic acid is added to the slurry can vary the particle size of the NH₄AlF₄ produced. When the total amount of the acid is poured into the slurry at one time, the particle size of the crystalline NH₄AlF₄ is in the range from about 10 to 20 μm. The particle size increases to the range 20 to 50 μm when the acid is added intermittently.



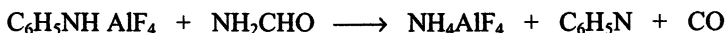
Marlett prepared NH₄AlF₄ by adding an alkylamine-aluminum trichloride complex to a bifluoride (e.g. NH₄HF₂ or NaHF₂) in toluene (19). The reaction can be carried out under anhydrous conditions. After reaction completion, the

toluene was distilled off. The product was purified by washing with water (to remove NH_4Cl) and drying in an oven. The product was analyzed by XRD.



Ammonium tetrafluoroaluminate has also been prepared by neutralization of an aqueous solution of hydrated aluminum trifluoride in 40% HF with $\text{N}(\text{CH}_3)_4\text{OH}$ (20). This gave $[(\text{CH}_3)_4\text{N}^+][\text{AlF}_4^-]\text{H}_2\text{O}$. Dehydration of this solid at $< 120^\circ\text{C}$ gave the hygroscopic $[(\text{CH}_3)_4\text{N}^+][\text{AlF}_4^-]$.

Harlow *et al.* prepared NH_4AlF_4 (beta phase) by heating pyridine HAlF_4 (under N_2) to about 180°C in formamide solvent (10). Pyridine is evolved from the solution and HAlF_4 remains behind. The HAlF_4 reacts with the formamide solvent eliminating CO gas.



Another synthesis using an AlF_4^- starting material involves reacting collidine HAlF_4 in dry methanol with a solution of $\text{N}(\text{CH}_3)_4\text{Cl}$ in dry methanol (21). The by-product collidine HCl was sublimed away in flowing nitrogen at $< 200^\circ\text{C}$, and the $[(\text{CH}_3)_4\text{N}^+][\text{AlF}_4^-]$ left behind was characterized by x-ray and IR.

Characterization

Aluminum halide chemistry has several examples of tetrahedral $[\text{AlX}_4^-]$ species when $\text{X} = \text{Cl}, \text{Br}, \text{I}$ (22-24). The $[\text{AlF}_4^-]$ species had however been controversial due to lack of structural proof, although there was indirect evidence for the tetrahedral $[\text{AlF}_4^-]$ anion, including IR (21-25), Raman (in molten salts) (26-28), and NMR data (29-30). Tetrahedrally coordinated AlF_4^- compounds had been proposed to exist in a hot melt form or in vapor phase, but upon cooling reassembled into six-coordinate forms. In 1993, Herron *et al.* crystallized $[\text{PSH}^+][\text{AlF}_4^-]$ (where PS = Proton Sponge) (17). The tetrahedral nature of the anion was confirmed with average Al-F distances of 1.62 \AA and a F-Al-F bond angle of 109° . The closest contact between the coordinated fluoride and the chelated proton of the cation was 2.77 \AA , which is too long to be considered a hydrogen bond. Thus the $[\text{AlF}_4^-]$ anion exists with only Van der Waals contacts to either the cations or other anions of the lattice.

The same group also determined the structure of $[\text{collidineH}^+][\text{AlF}_4^-]$ (17). The backbone of the structure consists of a series of infinite $[\text{AlF}_4^-]_\infty$ chains that extend along the c axis. The collidinium cations form strong hydrogen bonds to the terminal fluoride ions of the chain, effectively forming a sheath around these chains. In between the chains and residing in a hydrophobic region defined by

the collidinium sheaths are two independent, discrete, tetrahedral $[\text{AlF}_4^-]$ species. As before, the $[\text{AlF}_4^-]$ species have no contact, other than Van de Waals, with other species in the lattice. The crystal structure of [tetraphenylphosphonium⁺] $[\text{AlF}_4^-]$ and [tetraphenylarsonium⁺] $[\text{AlF}_4^-]$ has also been reported (8). Both structures are similar to that of [PSH] $[\text{AlF}_4^-]$ with discrete cations and anions.

Multinuclear NMR experiments demonstrated the presence of the tetrafluoroaluminate species in solution. Herron observed aluminum-fluorine coupling for $[\text{PSH}^+][\text{AlF}_4^-]$ in CD_3CN (a sextet from ^{19}F - ^{27}Al in ^{19}F NMR, and a quintet from ^{27}Al - ^{19}F in ^{27}Al NMR). Peaks at -187 to -194 ppm (^{19}F NMR) and 49 to 52 ppm (^{27}Al NMR) were observed for the PSH, collidineH, $(\text{CH}_3)_4\text{N}$, $(\text{CH}_3)_4\text{P}$, $(\text{CH}_3)_4\text{As}$, and $(\text{CH}_3\text{CH}_2)_4\text{P}$ tetrafluoroaluminate species. Similar NMR data was observed by Tsivadze *et al* for the AlF_4^- anion stabilized by benzo-15-crown-5 in solutions of donor solvents (15).

The ^{19}F MAS NMR showed a single, sharp line at -187 and -188 ppm for $[\text{PSH}^+][\text{AlF}_4^-]$ and $[\text{collidineH}^+][\text{AlF}_4^-]$ respectively (17). The Raman spectra showed a sharp band at 635 cm^{-1} . The IR spectra for these compounds showed a sharp band at 785 cm^{-1} , attributed to the Al-F stretching frequencies. Sengupta and Sen prepared a series of tetrafluoroaluminates with organic base cations (including pyridine, quinoline, and morpholine) (21,25). They report IR values in the range of $410 - 675\text{ cm}^{-1}$ for the Al-F stretch. However, as noted before, these compounds may have been a mix of fluoro/aquo/hydroxo aluminate species. In our lab we have obtained IR values of $567 - 825\text{ cm}^{-1}$ for hydrated tetrafluoroaluminate anions with inorganic cations (Na^+ , Li^+ , K^+ , Rb^+ , Cs^+ , and Tl^+).

In aqueous solutions, there is a rapid, pH dependant exchange between H_2O , OH^- , and F^- ligands binding to the aluminum cation. The solution behavior of fluoroaluminate complexes in aqueous solutions has been studied using ^{27}Al and ^{19}F NMR (31). The question of coordination of the fluoroaluminate species in aqueous solutions has also been investigated. The coordination of the fluoroaluminate species is an important one with regards to its ability to interfere with the activities of nucleoside-binding proteins. As noted before, the tetrafluoroaluminate anion has been proposed to stimulate G-proteins and P-type ATPases by assuming a tetrahedral geometry that is similar to a γ -phosphate. The AlF_4^- -nucleoside diphosphate (NDP) complex is thought to mimic the size and shape of a nucleoside triphosphate (32). However, theoretical studies have ruled out any tetracoordination for AlF_x in aqueous solutions (33), although it is possible that ternary species such as AlOH_yF_x may be tetrahedral. A reversible equilibria exist between the different fluoroaluminate species. The proportions of multifluorinated species, such as $\text{AlF}_x(\text{H}_2\text{O})_{6-x}^{(3-x)+}$ (where $x = 3-6$) or $\text{AlF}_x\text{OH}(\text{H}_2\text{O})_{5-x}^{(2-x)+}$ (where $x = 3-5$), depend on the excess concentration of free fluoride ions and on the pH of the solution (34).

Multinuclear NMR spectroscopy has been used to study the ternary system Al^{3+} , F⁻, and NDP in aqueous solutions (pH = 6) without protein (35,36). Ternary complexes (NDP) AlF_x ($x = 1-3$) were found, but no (NDP) AlF_4^- was detected. Further multinuclear NMR studies of fluoroaluminate species in aqueous solutions over a wider pH range (2-8) with varying $[\text{F}^-]/[\text{Al}]$ ratios have been conducted (31). It was concluded that all the fluoroaluminate complexes observed in aqueous solution are hexacoordinated with an octahedral geometry. This contrasts with the situation in organic solvents where Herron observed the tetrahedral AlF_4^- species. Crystallographic studies have provided further evidence for the octahedral coordination of the tetrafluoroaluminate complex in the active sites of proteins such as the G-protein $\text{Gi}\alpha_1$ (37), transducin (38), NDP kinase (39), nitrogenase (40), the Ras-RasGAP complex (41), and the G-protein RhoA (42).

Biological Activity

Transfer of phosphate groups is the basic mechanism in the regulation of the activity of numerous enzymes, energy metabolism, cell signaling, movement, and regulation of cell growth. Phosphate is an important component of phospholipids in the cell membranes. AlF_4^- acts as a high affinity analog of the γ -phosphate (Figure 1) (43,44). AlF_4^- mimics the role of γ -phosphate only if the β -phosphate is present and remains unsubstituted. The effect is more readily seen with G proteins because guanosine diphosphate (GDP) is always tightly bound at the site after the hydrolysis of guanosine triphosphate (GTP).

The tetrafluoroaluminate complex was proposed to act as an analogue of the terminal phosphate of GTP because the Al-F bond length is close to the P-O phosphate bond length, and the AlF_4^- and PO_4^{3-} structures are both tetrahedral. Fluorine and oxygen have nearly the same size and the same valence orbitals, but fluorine is more electronegative and has an even greater capacity than oxygen for forming hydrogen bonds. Aluminum and phosphorus both have their valence electrons in the same third shell. Chabre (44) explained an important functional difference between a phosphate group and the structurally analogous tetrafluoroaluminate. In phosphate, oxygen is covalently bound to the phosphorus and does not exchange with oxygen from solvent. In $[\text{AlF}_4^-]$ the bonding between the electropositive aluminum and the highly electronegative fluorine is more ionic in character. The reaction of a bound phosphate compound with orthophosphate is endergonic and slow, whereas the corresponding reaction with $[\text{AlF}_4^-]$ is rapid and spontaneous. Fluorides in the bound complex can also exchange with free fluoride ions in solution.

G protein-mediated cell responses are of key importance in the processes of neurotransmission and intercellular signaling in the brain (45), and

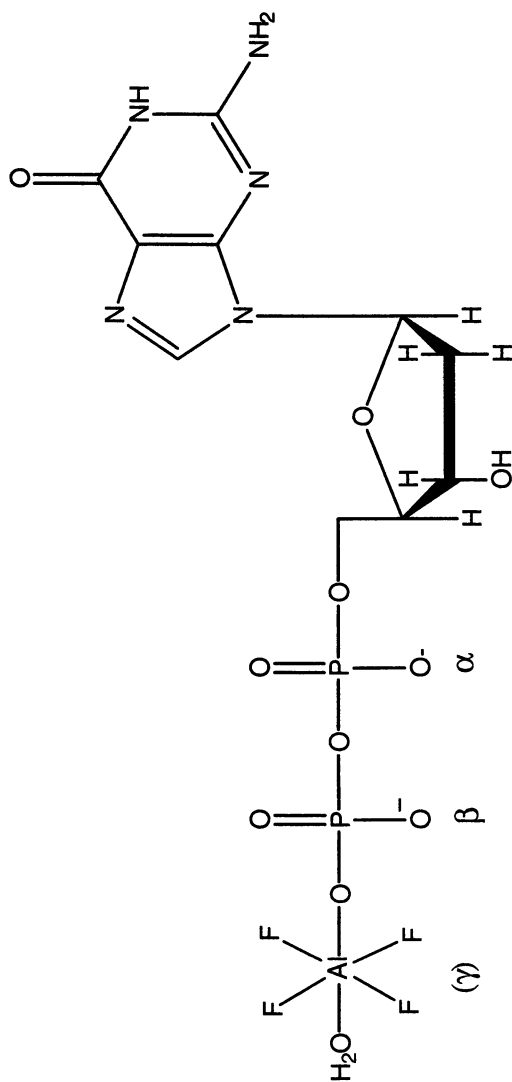


Figure 1. AlF_4^- binds strongly to the β -phosphate.

AlF_4^- acts as an active stimulatory species (46). Aluminofluoride complexes mimic the action of many neurotransmitters, hormones, and growth factors. Exposure of osteoclasts to AlF_4^- resulted in a marked inhibition of bone resorption (47). Brief exposure to aluminum fluoride complexes induced prolonged enhancement of synaptic transmission (48) and can affect the activity of many other ion channels and enzymes in the kidney (49). Rapid and dynamic changes of the actin network are of vital importance for the motility of human neutrophils. AlF_4^- induction expressed a pronounced and sustained increase in a filamentous form of actin in intact human neutrophils (50). It should be noted that the human body does possess natural barrier systems to aluminum intake. There are various physiological ligands, such as transferrin, citrate, and silicic acid, which are efficient buffers in preventing the intake of aluminum under natural conditions (51). However, the formation of AlF_4^- only requires trace amounts of aluminum, and the increased bioavailability of aluminum in the environment can certainly lead to increased absorption of aluminum by the body.

Conclusions

In view of the ubiquity of phosphate in cell metabolism together with the dramatic increase in the amount of aluminum and fluoride now found in our ecosystem, aluminofluoride complexes represent a strong potential danger for living organisms, including humans (1). One area of future research will be the investigation of the long term pharmacological and toxicological effects of exposure to tetrafluoroaluminate complexes on animals and plants. Another area of future research will be the determination of the relationship, if any, between aluminum in everyday products (cooking utensils, deodorants, antacids, food and beverage packaging), the increasing use of fluoride (water fluoridation, dental products, industrial fertilizers), and the health of humans.

In the industrial arena, continued AlF_4^- research will be seen in the development of better AlF_4^- precursors which provide for cleaner decomposition at lower temperatures to AlF_3 . The deposition of AlF_4^- onto organic or inorganic supports for subsequent decomposition to AlF_3 continues to be investigated. Future research will also be conducted with the view of preparing purer $\text{M}^+ \text{AlF}_4^-$ (M = metal or organic cation) with less dangerous starting materials, lower temperatures, and better cost effectiveness. Preparation of better fluxes containing AlF_4^- for the soldering of aluminum and aluminum alloys will also be a continuing area of research and development.

The future of the chemistry of tetrafluoroaluminate complexes continues to be bright. This brief review of some aspects of AlF_4^- chemistry hopefully provided a glimmer of the past, present, and future of this important area of research.

References

1. Strunecka, A.; Patocka, J. *Fluoride* **1999**, 32, 230.
2. Greenwood, N. N.; Earnshaw, A. *Chemistry of the Elements*, 2nd ed.; Butterworth-Heinemann, Woburn, MA, **1998**.
3. Bond, A. M.; Hefter, G.T. *Critical Survey of Stability Constants and Related Thermodynamic Data of Fluoride Complexes in Aqueous Solution*; IUPAC Chemical Data Series, No. 27; Pergamon, New York, **1980**.
4. Bruno, M.; Herstad, O.; Holm, J. L. *J. Thermal Analysis and Calorimetry* **1999**, 56, 57.
5. Sternweis, P.C.; Gilman, A. G. *Proc. Natl. Acad. Sci. U.S.A.* **1982**, 78, 4888.
6. Gilman, A.G. *Annu. Rev. Biochem.*, **1987**, 56, 615.
7. Troullier, A.; Girardet, J. L.; Dupont, Y. *J. Biol. Chem.* **1992**, 267, 22821 and references therein.
8. Harlow, R. L.; Herron, N.; Thorn, D. L. U.S. Patent No. 5,986,023, **1999**.
9. McDaniel, M.P.; Klendworth, D. D.; Johnson, M. M. U.S. Patent No. 5,171,798, **1992**.
10. Harlow, R. L.; Herron, N. U.S. Patent No. 5,417,954, **1995**.
11. Conn, P. J.; Bowling Jr., J. H. U.S. Patent No. 6,244,497, **2001**.
12. Ono, M.; Hattori, M.; Itaya, E.; Yanagawa, Y. U.S. Patent No. 6,010,578, **2000**.
13. Zajack Jr, W. V.; Bis, F. F.; DeBold, F. C.; Kowalchik, L. A.; Barnes, J. A. U.S. Patent No. 5,714,279, **1998**.
14. Belt, H. J.; Sander, R.; Rudolph, W. U.S. Patent No. 5,985,233, **1999**.
15. Petrosyants, S. P.; Maliarik, M. A.; Tolkacheva, E. O.; Tsvadze, A. Y. *Main Group Chemistry* **1998**, 2, 183.
16. Sengupta, A.K.; Sen, K. *Indian J. Chem.* **1979**, 17A, 107.
17. Herron, N.; Thorn, D.L.; Harlow, R.L.; Davidson, F. *J. Am.Chem. Soc.* **1993**, 115, 3028.
18. Aramaki, M.; Etsuo, U. U.S. Patent No. 4,034,068, **1977**.
19. Marlett, E. U.S. Patent No. 5,045,300, **1991**.
20. Bukovec, P; Siftar, J. *Monatsh. Chem.* **1975**, 106, 483.
21. Herron, N.; Harlow, R.L.; Thorn, D.L. *Inorg. Chem.* **1993**, 32, 2985.
22. Zaworotko, M. J.; Cameron, T.S.; Linden, A.; Sturge, K. C. *Acta Crystallogr* **1989**, C45, 996.
23. Jones, D.E.H. *J. Chem. Soc. Dalton Trans.* **1972**, 567.
24. Kidd, R.G.; Truax, B.R. *J. Am. Chem. Soc.* **1968**, 90, 6867.
25. Sengupta, A.K.; Sen, K. *Indian J. Chem.* **1979**, 17A, 107.
26. Gilbert, B.; Mamantov, G. *J. Chem. Phys.* **1975**, 62, 950.
27. Gilbert, B.; Mamantov, G.; Begun, G.M. *Inorg. Nucl. Chem. Letts.* **1974**, 10, 1123.

28. Gilbert, B.; Williams, S.D.; Mamantov, G. *Inorg. Chem.* **1988**, *27*, 2359.
29. Matwiyoff, N. A.; Wageman, W.E. *Inorg. Chem.* **1970**, *9*, 1031.
30. Colton, R.; Eller, P. G. *Aust. J. Chem.* **1989**, *42*, 1605.
31. Martinez, E. J.; Girardet, J. L.; Morat, C. *Inorg. Chem.* **1996**, *35*, 706
32. Chabre, M. *Trends Biochem. Sci.* **1990**, *15*,6.
33. Martin, R. B. *Biochem. Biophys. Res. Commun.* **1988**, *155*, 1194.
34. Goldstein, G. *Anal. Chem.* **1964**, *36*, 243.
35. Nelson, D. J.; Martin, R. B. *J. Inorg. Biochem.* **1991**, *43*, 37.
36. Wang, X.; Simpson, J. H.; Nelson, D. J. *J. Inorg. Biochem.* **1995**, *58*, 29.
37. Coleman, D. E.; Berghuis, A. M.; Lee, E.; Linder, M. E.; Gilman, A. G.; Sprang, S. R. *Science* **1994**, *265*, 1405.
38. Sondak, J.; Lambright, D. G.; Noel, J. P.; Hamm, H. E.; Sigler, P. B. *Nature* **1994**, *372*, 276.
39. Xu, Y. W.; Morera, S.; Janin, J.; Cherfils, J. *Proc. Natl. Acad. Sci. U.S.A.* **1997**, *94*, 3579.
40. Schindelin, H.; Kisker, C.; Schlessman, J. L.; Howard, J. B.; Rees, D. C. *Nature* **1997**, *387*, 370.
41. Scheffzek, K.; Ahmadian, M. R.; Kabsch, W.; Wiesmüller, L.; Lautwein, A.; Schmitz, F.; Wittinghofer, A. *Science* **1997**, *277*, 333.
42. Rittinger, K.; Walker, P. A.; Eccleston, J. F.; Smerdon, S. J.; Gamblin, S. J. *Nature* **1997**, *389*, 758.
43. Bigay, J.; Deterre, P.; Pfister, C.; Chabre, M. *EMBO J.* **1987**, *6*, 2907.
44. Chabre, M. *TIBS* **1990**, *15*, 6-10.
45. Rana, R.S.; Hokin, L.E. *Physiol. Rev.* **1990**, *70*, 115-164.
46. Candura, S.M.; Castoldi, A.F.; Manzo, L.; Costa, L.G. *Life Sci.* **1991**, *49*, 1245.
47. Moonga, B.S.; Pazianas, M.; Alam, A.S.; Shankar, V.S.; Huang, C.L.; Zaidi, M. *Biochem. Biophys. Res. Commun.* **1993**, *190*, 496.
48. Publicover, S.J. *Exp. Brain Res.* **1991**, *84*, 680.
49. Zhou, J.; Sims, C.; Chang, C.H.; Mattera, B.L.; Hopfer, U.; Douglas, J. *Proc. Natl. Acad. Sci. USA* **1990**, *87*, 7532.
50. Bengtsson, T.; Sarndahl, E.; Stendahl, O.; Andersson, T. *Proc. Natl. Acad. Sci. USA* **1990**, *87*, 2921.
51. Wilhelm, M.; Jager, D. E.; Ohnesorge, F. K. *Pharmacol. Toxicol.* **1990**, *66*, 4.

Chapter 19

Aluminofluoride Complexes: A Useful Tool in Laboratory Investigations, but a Hidden Danger for Living Organisms?

Anna Strunecka¹ and Jiri Patočka²

¹Charles University Prague, Faculty of Sciences, Department of Physiology
and Developmental Biology, 128 43 Prague 2, Vinicna 7, Czech Republic

²Military Medical Academy, Department of Toxicology, 500 01 Hradec
Kralove, Simkova 878, Czech Republic

Aluminofluoride complexes are used in many laboratory investigations of guanine nucleotide binding proteins (G proteins). Reflecting on many studies, a new view on the toxicity of aluminum and fluoride can be suggested. The hidden danger of their long-term synergistic action is not fully recognized at this point.

Fluoride anions, generally introduced as NaF solutions, have long been known to influence the activity of various enzymes and the purified guanine nucleotide-binding regulatory component of adenylylase (1). Sternweis and Gilman (2) have reported that fluoride activation of adenylylase depends on the presence of trace aluminum. This fact had at first been ignored because aluminum is a normal component of glass from which it is etched by a solution with fluoride. The requirement for aluminum is highly specific: of 28 other metals tested, only beryllium promoted activation of the guanine nucleotide-binding regulatory component of adenylylase by fluoride (2,3).

In aqueous solutions, the fluoride anions bind to the metal cation and are exchangeable with free fluoride or hydroxyl ions. The complexes are not permanent; and the proportions of multifluorinated species such as AlF_3 , $\text{AlF}_3(\text{OH})$ and AlF_4^{1-} depend on the excess concentration of free fluoride ions and on the pH of the solution (4). Further studies demonstrated that slow equilibration kinetics between various aluminofluoride complexes could give rise to puzzling kinetics that had caused misinterpretation of results.

The idea that aluminofluoride complexes act as a high affinity analogue of the terminal phosphate of GTP was suggested (3, 5). Guanine nucleotide binding proteins (G proteins) take part in an enormous variety of biological signaling systems, helping control almost all important life processes (6). Moreover, aluminofluoride complexes also influence the activity of a variety of phosphatases, phosphorylases and kinases (5). Reflecting on many studies, which utilize aluminofluoride complexes, the effects of fluoride in the presence of aluminum on various cells and tissues as observed, can be reviewed.

A knowledge of mechanism of action of aluminofluoride complexes on the molecular and cellular level will draw us nearer to an understanding of the detrimental effects of aluminum and fluoride combinations in the environment.

Aluminofluoride Complexes

The exact structure of the activator complex able to simulate a phosphate group in many biochemical reactions has been disputed. Aluminofluoride complexes are easily soluble in water. Calculations based on existing equilibrium data (4) predicted that in the millimolar range of fluoride concentration and physiological pH the major species is AlF_4^{1-} . According to the model of Bigay et al. (3) and Chabre (5), the proposed biologically active state resulted from the binding of tetrahedral AlF_4^{1-} . Martin (7) recalculated the equilibrium of aluminofluoride complexes and suggested that the predominant species are the neutral complex AlF_3 and the mixed complex $\text{AlF}_3(\text{OH})$. These complexes should be hexacoordinated, with water molecules occupying the free sites; only the hydroxylated and the ternary fluorohydroxylated complexes would be tetrahedral. For aluminum, it is uncertain whether the complex that enters the site is an AlF_3 that becomes tetrahedral by losing its three bound water molecules and contracting a fourth bond with the β -phosphate oxygen, or if it is an already tetrahedral $\text{AlF}_3(\text{OH})$ that exchanges its hydroxyl for the β -phosphate oxygen or an AlF_4^{1-} that exchanges a fluorine. Many of the crystal structures of nucleotide binding proteins complexed with AlF_x show AlF_4^{1-} (8). It seems that the different coordination numbers originate mainly from the difference in pH at which the enzymes were crystallized. The bound AlF_x occurs as AlF_3 at pH 7.5 – 8.5 but as AlF_4^{1-} at pH below 7 (7, 8).

AlF_x : The Phosphoryl Transfer Transition State Analog

Transfer of phosphate groups is the basic mechanism in the regulation of the activity of numerous enzymes, energy metabolism, cell signaling, movement, and regulation of cell growth. Phosphate is an important component of phospholipids in the cell membranes.

Analogies between a phosphate group and aluminofluoride complex consist in atomic and molecular similarities. The fluorine atom has the same size and the same valence orbitals as oxygen. Of course, fluorine is more electronegative than oxygen and with a similar capacity for forming hydrogen bonds. Aluminum is close to phosphorus in the periodic table, and their valence electrons are in the same shell. An Al-F bond is the same length as a P - O bond in phosphate, i.e. 1.5 to 1.6 Å (5). Like phosphorus, aluminum has possible coordination numbers of 1 - 6, due to the possible hybridization of its outer shell 3p electrons with the 3d orbitals. These complexes can bind to proteins by hydrogen bonds to the fluorine atoms just as oxygen atoms of a phosphate ion.

However, an important functional difference between a phosphate group and the structurally analogous AlF_x complexes exist (3,5). In phosphate, oxygen is covalently bound to the phosphorus and does not exchange with oxygen from solvent. In AlF_x , ionic bonds are formed between the electropositive aluminum and the highly electronegative fluorine. While the reaction of a bound phosphate compound with orthophosphate is endergonic and slow, the corresponding reaction with AlF_x is rapid and spontaneous. AlF_x bind ionically to the terminal oxygen of GDP β -phosphate. Enzyme-bound GDP or ADP could therefore form a complex with AlF_x that imitates ATP or GTP in its effect on protein conformation. This effect often causes a structural change that locks the site and prevents the dissociation of the trisphosphate.

AlF_x in Laboratory Studies

The low cost and availability of these fluorometallic complexes has probably contributed to their widespread use as a tool in laboratory studies (5, 9). They have been used as evidence for involvement of a G protein in a system. The phosphate-analogue models of AlF_x action have been accepted for G-proteins but may be extended to all enzymes that bind phosphate or nucleoside-polyphosphate (5). Phosphoryl transfer reactions are involved in processes such as energy transduction, regulation of cell growth, activation of metabolites, and cytoskeletal protein assembly. It has been reported that aluminofluoride complexes impair the polymerization-depolymerization cycle of tubulin (5). Shape changes and disorganization of the spectrin network were observed after addition of 1 mM NaF and 10 μM AlCl_3 in human red blood cells (10). Rapid and dynamic changes of the cytoskeletal network are of vital importance for many cells.

ATP generation in mitochondria requires the association of an F_1 subunit with an F_0 transmembrane subunit transporting protons. The binding of ADP

and inorganic phosphate in a catalytic site of F_1 triggers conformational changes, which lock both of them into the site and induce the formation of pyrophosphate bonds by eliminating a water molecule. So can arise an aluminofluoride analog of pyrophosphate, $R-O-PO_2-O-AlF_3$, which may be bound at the site for the γ -phosphate. The inhibition of mitochondria ATPase activity in the presence of AlF_4^- was reported (11). This inhibition was not reversed by elution of fluoride from solution or by the addition of strong aluminum chelators. No significant release of the complex occurred over a period of days. Aluminofluoride complexes inhibit many ATPases, phosphatases, and phosphorylases. The intervention of aluminofluoride complexes in the energy transformation processes may thus affect the energy metabolism of the entire organism (9).

The description of laboratory investigations using aluminofluoride complexes during the past decade would involve hundreds of references. They bring evidence that aluminofluoride complexes influence most cells and tissues of the human body with powerful pharmacological efficacy. It is surprising that numerous laboratory findings of adverse effects of trace amounts of aluminum in the presence of fluoride have not been reported until recently. Aluminofluoride complexes affect all blood elements and blood circulation,, endothelial cells, the function of the immune system, bone cells, fibroblasts, keratinocytes, ion transport, processes of neurotransmission, growth and differentiation of cells, protein phosphorylation, and cytoskeletal protein assembly (9). Enormous possibilities for multiple molecular interactions of aluminum and fluoride exist in the brain and clearly warrant further investigation. Regarding the role of phosphates in cell metabolism and life processes, we can predict hundreds of reactions which might be influenced. The endocrine glands such as the parathyroid gland, the thyroid, the pituitary gland, and the pineal gland, are extremely sensitive to aluminofluoride complexes. Regarding the crucial role of the thyroid in regulation of growth, development, and metabolism of many tissues, AlF_x might influence the proper function of the entire human body. A phosphoryl transfer transition state analog might thus represent a useful tool for laboratory investigations, but also a strong potential danger for living organisms including humans.

AlF_x : The Messenger of False Information

Laboratory investigations support the hypothesis that G proteins are potential fluoride and aluminum targets. The heterotrimeric G proteins mediate the transfer of information from heptahelical receptors to effector molecules. Physiological agonists of G protein-coupled receptors include neurotransmitters and hormones, such as dopamine, epinephrine, norepinephrine, serotonin, acetylcholine, glucagon, vasopressin, melatonin, TSH, neuropeptides, opioids, excitatory amino acids, prostanoids, purines, photons and odorants (6). Aluminofluoride complexes may therefore clone or potentiate the action of many neurotransmitters, hormones and growth factors.

In the liver, for example, the effects of submaximal doses of AlF_x were potentiated by submaximal doses of glucagon, vasopressin, angiotensin II, and α_1 -adrenergic agonists (12). Using phorbol myristate acetate, the activator of protein kinase C, the conclusion was made that aluminofluoride complexes mimic the effects of Ca^{2+} mobilizing hormones by activating the G protein which couples the hormone receptor to phospholipase C. Fluoride anions in the presence of aluminum thus affect the liver as an organ involved in glycogenolysis, fatty acid oxidation, and lipolysis.

The aluminofluoride complex acts as the first messenger triggering processes of neurotransmission and potentiating the action of various hormones. Numerous laboratory results demonstrate that micromolar AlCl_3 in the presence of fluoride affect the levels of the second messenger molecules, such as cAMP, inositol phosphates, and cytosolic free calcium ions, in various cells and tissues, as shown in Table I. Such biochemical changes induce various functional responses. The false information of AlF_x is greatly amplified. The principle of amplification of the initial signal during its conversion into the functional response has been a widely accepted tenet in cell physiology.

The discoveries of receptor diversity, numerous G proteins, and phospholipase C families broadens enormously the possibilities of interactions of signal transduction pathways. The diversity of molecules involved in these processes is manifested at all levels of molecular signalling.

Understanding the role of G proteins in cell metabolism allows an acceptance of the fact that fluoride together with reactive aluminum now found in the environment, water, and food chain, can evoke numerous pathophysiological symptoms. Every molecule of AlF_x is the messenger of false information.

Aluminofluoride Complexes in Ecosystems

Aluminum, the most abundant metal in the earth's lithosphere, is everywhere: in soil, water sources, air, plants and animals. The natural barrier systems have for aluminum and various physiological ligands are efficient buffers, preventing the increased intake of this metal in natural conditions. Until relatively recently, it existed in forms not generally available to living organisms, and was therefore regarded as non-toxic. With the appearance of acid rain and the massive use of aluminum in industry, there has been an increase in

Table I. Some effects of AIF_x observed in laboratory investigations

Type of Cell Or Tissue	Biochemical Response	Functional Response	References
Liver -hepatocytes	Free cytosolic Ca ²⁺ ↑ Inositol 1,4,5,P ₃ ↑ cAMP ↓	Activation of glycolysis, Fatty acid oxidation, catabolic processes	12, 28
Kidney	Free cytosolic Ca ²⁺ ↑ cAMP ↑ ion channels	Glomerular cell proliferation Renal mesangial proliferation Transport of ions affected	29, 30
Thrombocytes	Free cytosolic Ca ²⁺ ↑ Inositol 1,4,5,P ₃ ↑	Aggregation Shape changes	31
Red blood cells	Inositol 1,4,5,P ₃ ↑	Shape changes Cytoskeletal disorganization	10
Fibroblasts	Free cytosolic Ca ²⁺ ↑ Inositol 1,4,5,P ₃ ↑	Increased proliferation	32, 33
Osteoblasts	PG synthesis ↑ Tyrosine phosphorylation ↑	Mitogenic effect proliferation ↑ Life span ↑	34
Osteoclasts	cAMP ↓ Free cytosolic Ca ²⁺ ↑	Inhibition of bone resorption Cellular retraction	35
Neurons	Inositol 1,4,5,P ₃ ↑ Ca ²⁺ ↑	Changes of spike amplitude	36

Brain	Inositol 1,4,5, P_3 ↑ Free cytosolic Ca^{2+} ↑	Enhancement of synaptic transmission and spike amplitude	37, 38
-------	---	--	--------

NOTE: Fluoride was used as NaF in millimolar concentrations, aluminum as $AlCl_3$ (micromolar).

the amount of aluminum in ecosystems, nourishment and water sources. It is now more bioavailable.

In aqueous solutions with a pH of less than 3, aluminum exists as the $\text{Al}(\text{H}_2\text{O})_6^{3+}$ ion, usually abbreviated to Al^{3+} . In a less acidic water, $\text{Al}(\text{H}_2\text{O})_6^{3+}$ undergoes successive deprotonation, becoming $\text{Al}(\text{H}_2\text{O})_5(\text{OH})^{2+}$ etc. Minimum solubility occurs in neutral solutions with the precipitation of $\text{Al}(\text{OH})_3$. In basic solution this solid redissolves, due to the formation of tetrahedral $\text{Al}(\text{OH})_4^-$. Since large aluminum concentrations only occur at a pH <5 and about 95% of natural waters have a pH >6, it might be predicted that human exposure to aluminum from water is not great.

For the general population, the major sources of aluminum are drinking water, residues in foods, cooking utensils, food and beverage packaging, and aluminum-containing medications (e.g., antacids and buffered aspirins). Vaccines, allergy skin tests, 25% human serum albumin, baby skin creams, baby diaper wipes, and antacids, which are frequently given to infants, are extremely high in aluminum. Such items as deodorants, vaginal douches and baby wipe not only have high aluminum content, but are applied to areas where there is a far greater tendency for absorption through the skin.

Fluoridation of water supplies and the use of fluoride in industry started the era of supplementation of living organisms with fluoride, providing the possibility its combined action with aluminum. Toxic effects of increased aluminum concentration have already been observed in some animal and plant species living in freshwaters with aluminum concentrations of between 0.1 and 0.8 mg/L (13).

Fluoride Enhances Aluminum Intake

Fluoride comes from fluoridated water, from crops grown with fluoridated water, from medicines, dental products, and fuels. Industrial fertilizers and pesticides increase the amount of this element in agricultural products and food sources (14). Several studies reported a high content of fluoride and aluminum in all tested Chinese, Indian and herbal tea (15). Tea is the second most-consumed beverage after water in the world. That the aluminum present in tea is indeed resorbed in the simultaneous presence of fluoride was demonstrated in healthy male volunteers after drinking equal volumes of tea, coffee or tap water on separate days. In every case the amount of the urinary excreted aluminum increased on the day when tea was taken. The results indicated that tea consumption must be considered in any assessment of the total dietary intake of aluminum in human beings (15).

Minute quantities of aluminum injected intracerebrally into animals will induce severe neurological symptoms and neuropathological features of neurodegeneration. The presence of fluoride caused more aluminum to cross the blood-brain barrier and be deposited in the brain of rats (16). Aluminum-induced neural degeneration in rats is greatly enhanced when the animals were fed low

doses of fluoride (17). Some animal studies compared behavior, body weight, plasma, and brain fluoride levels after NaF exposures during late gestation, at weaning or in adults. Rats exposed as adults displayed behavior-specific changes typical of cognitive deficits, whereas rats exposed prenatally had dispersed behaviors typical of hyperactivity.

Aluminofluoride Complexes: Hidden Danger for Human Health

No one can predict what happens in the human body after a truly chronic exposure to an increased content of fluoride and aluminum in body fluids and in various tissues. Chronic exposure of humans to AlF_x begins in the foetus. The severity and the development of the symptoms depend on a person's age, genetic background, nutrition status, kidney function, and many other factors. For example, we need to determine the mechanisms by which aluminum crosses epithelia, such as those of the gastrointestinal tract and the central nervous system, and how these mechanisms influence both the subsequent transport and fate of the absorbed aluminum and the concomitant nature and severity of the biological response to the accumulation of aluminum (18).

Most of the ill effects caused by the synergistic action of aluminum and fluoride were first recognized among workers in aluminum factories, where fluoride and aluminum are present in high concentrations. Occupational exposure in aluminum potroom workers has been reported since the 1930s (19). Also persons living near an enamel factory that emitted hydrogen fluoride into the air had a distinct decline in mental acuity, memory loss, inability to coordinate thoughts, and reduced ability to write.

There are many examples of aluminum-induced neurotoxicity. Elevated aluminum levels have been implicated as the cause of dialysis encephalopathy in renal failure patients undergoing long term hemodialysis (20). Since many hemodialysis units rely on systems to purify fluoridated tap water, it is likely that many patients are being exposed inadvertently to increased concentrations of fluoride (21). Some patients used aluminum-containing medications. Moreover, patients with renal failure cannot remove aluminum from the blood. Dialysis dementia can arise after three to seven years of hemodialysis treatment. Uremic adults and premature infants not on dialysis treatment also can develop encephalopathy, dementia, and convulsions due to aluminum neurotoxicity.

The hypothesis that the accumulation of aluminum in the brain is the cause of Alzheimer's disease (AD) has been postulated and discussed very often (22, 23). This suggestion was further supported by a positive correlation between the incidence of AD and concentrations of aluminum in drinking water. In areas where the mean aluminum concentrations exceeded 0.11 mg/l (4 μ mol/l), the incidence was reported to be 1.5 times higher than that in districts where the concentrations were lower (24). Some authors reported that aluminum is accumulated in some parts of postmortem brains of AD patients. However, results obtained from extensive analysis of the presence of aluminum in

postmortem brains, senile plaques and neurofibrillary tangles are controversial. Neither the increased content of aluminum in the brain nor the results of ecological studies can explain whether and why aluminum constitutes a risk. The question as to whether aluminum presents a contributing factor to Alzheimer's disease is still the subject of debate (25). At present, aluminum is regarded as a putative risk factor along with alcohol consumption, stressful life events, and manual occupation.

We suggest that most of pathologic changes may be raised by synergistic action of aluminum with fluoride (26) may induce various changes observed in the brain of patients with AD. Aluminofluoride complexes may affect processes of neurotransmission, β amyloid generation and plaque formation. They can influence protein tau phosphorylation and organization of cytoskeletal proteins, transport of ions, energy metabolism and calcium homeostasis. AD could be an example demonstrating the diversified and multidimensional nature of the integration of the nervous system. However, aluminofluoride complexes may act as the initial signal stimulating impairment of homeostasis, degeneration and death of the cells. By influencing energy metabolism these complexes can accelerate aging and impair the functions of the nervous system. In respect to the etiology of AD, the long term action of aluminofluoride complexes may represent a serious and powerful risk factor for the development of this devastating disease.

Conclusions

The discovery of AlF_x as a new class of phosphate analogue has brought numerous demonstrations of their powerful efficacy. It is not surprising when considering the role of G proteins in signal transduction and the ubiquity of phosphate in cell metabolism.

It might seem difficult to decide if numerous laboratory experiments demonstrate a potential ecotoxicological risk of fluoride and aluminum for living organisms including humans. However, the results of laboratory investigations using isolated animal and human cells or tissues must be integrated into the functional whole. It is evident that AlF_x is a molecule giving false information, which is amplified by processes of signal transmission. The origins of many human diseases are in the malfunctioning of signaling components. Pharmacologists estimate that up to 60% of all medicines used today exert their effects through G protein signaling pathways (27).

In light of the published findings, responsible scientists and physicians should not neglect the potential of AlF_x 's to harm human health. Understanding the mechanism of action of fluorometallic complexes could allow us to explain numerous observations about the effects of increased amount of fluoride and aluminum in the environment and food chain. Numerous published reports bring us at least a strong warning.

This work has been supported by the Internal Grant Agency of the Ministry of Health of the Czech Republic.

References

1. Rall, T. W.; Sutherland, E. W. *J. Biol. Chem.* **1958**, 232, 1065-1076.
2. Sternweis, P.C.; Gilman, A. G. *Proc. Natl. Acad. Sci. USA* **1982**, 79, 4888-4891.
3. Bigay, J.; Deterre, P.; Pfister, C. ; et al. *EMBO J* **1987**, 6, 2907-2913.
4. Goldstein, G. *Anal. Chem.* **1964**, 36, 243-244.
5. Chabre, M. *Trends Biochem. Sci.* **1990**, 15, 6-10.
6. Gilman, A. G. *Annu. Rev. Biochem.* **1987**, 56, 615-649.
7. Martin, R. B. *Biochem. Biophys. Res. Commun.* **1988**, 155, 1194-1200.
8. Schlichting, I.; Reinstein, J. *Nat. Struct. Biol.* **1999**, 8, 721-723.
9. Strunecka, A.; Patocka, J. *Fluoride* **1999**, 32 (4), 230 – 242.
10. Strunecka, A.; El Dessouki, N. I.; Palecek, J.; et al. *Receptor* **1991**, 1, 141-154.
11. Lunardi, J.; Dupuis, A.; Garin, J.; et al. *Proc. Natl. Acad. Sci. USA* **1988**, 85, 8958-8962.
12. Blackmore, P. J.; Exton, H. *J. Biol. Chem.* **1986**, 261, 11056-11063.
13. Jones, K. C.; Bennett, B. G. *Monit. Asses. Res. Centr.* **1985**, 4(33), 1-35.
14. Schuld, A. www.bruha.com/fluoride/html/
15. Nabrzycki, M.; Gajewska, R. *Z. Lebensm. Unters. Forsch.* **1995**, 201(4), 307-315.
16. Varner, J. A.; Jensen, K. F.; Horvath, W. J.; Isaacson, R. L. *Brain Res.* **1998**, 784, 284 – 298.
17. Mullenix, P. J.; Denbesten, P. K.; Schunior, A.; Kernan, W. J. *Neurotoxicol. Teratol.* **1995**, 17(2), 169-177.
18. Exley, C.; Burgess, E.; Day, J. P.; et al. *J. Toxicol. Environ. Health* **1996**, 48(6), 569-584.
19. Spittle, B. *Int. Clin. Psychopharmacol. J.* **1994**, 9, 79-82.
20. Alfrey, C.; Le Gendre, G. R. ; Kachny, W. D. *N. Engl. J. Med.* **1976**, 294, 184 -188.
21. Arnow, P. M.; Bland, L. A.; Houchins, G. S.; Fridkin, S.; Fellner, S. K.; *Annu. Intern. Med.* **1994**, 121, 339-344.
22. Crapper, M. C.; Lachlan, D. R. *Neurobiol. Aging* **1986**, 7, 525-532.
23. Harris, W.R.; Berthon, G.; Day, J. P.; et al. *J. Toxicol. Environ. Health* **1996**, 48(6), 543-568.
24. Martyn, C. N.; Osmond, C.; Edwardson J. A. *Lancet* **1989**; ii, 59-62.
25. *Aluminium and Alzheimer's Disease. The Science that Describes the Link*; Ed. Exley, C. Elsevier Science, Amsterdam, New York, NL, USA , **2001**.
26. Strunecka, A.; Patocka, J. *Cs. Physiol.* **1999**, 48, 9-15.
27. Roush, W. *Science* **1996**, 271 (5252), 1056.
28. Blackmore, P. F.; Lynch, C. J.; Uhing, R. J.; et al. *Adv. Exp. Med. Biol.* **1988**, 232, 169-182.

29. Zhou, J. ; Sims C. ; Chang, C. H. ; et al. *Proc.Natl. Acad. Sci. USA* **1990**, 87 7532-7535.
30. Brunskill, N. J. ; Morrissey, J. J.; Klahr, S. *Kidney Int.* **1992**, 42, 11-17.
31. Deckmyn, H. *Vergh. K. Acad. Geneesk. Belg.* **1991**, 53, 589-604.
32. Paris, S.; Poysegur, J. *J. Biol. Chem.* **1987**, 262, 1970-1976.
33. Harootunian, A. T.; Kao, J. P.; Paranjape, S.; et al. *Cell Calcium.* **1991**, 12, 153-164.
34. Caverzasio, J.; Imai, T.; Ammann, P. P.; et al. *J. Bone Miner. Res.* **1996**, 11, 46-55.
35. Moonga, B. S.; Pazianas, M.; Alam, A. S.; et al. *Biochem.Biophys.Res. Co.* **1993**, 190, 496-501.
36. Nadakavukaren, J. J.; Welsh, D. K.; Peppert, S. M. *Brain Res.* **1990**, 507, 181-188.
37. Candura, S. M.; Castoldi, A. F.; Manzo, L.; Costa, L. G. *Life Sci.* **1991**, 49, 1245-1252.
38. Publicover, S. J. *Exp.Brain Res.* **1991**, 84, 680-684.

Author Index

- Anitha, S., 228
Atwood, David A., 131, 259
Baker, R. Tom, 70
Bi, S. P., 246
Bishop, Karyn L., 70
Blais, P., 195
Brask, J. K., 195
Broene, Richard D., 70
Budzelaar, Peter H. M., 142
Cameron, Thomas M., 70
Carter, Charles A. G., 70
Chivers, T., 195
Conley, B. D., 259
Dutta, U., 259
Eisch, John J., 88
Fedorchuk, C., 195
Fehlner, Thomas P., 49
Forsthoefel, Kersten M., 168
Fridh, C., 259
Gabbai, François P., 118
Gazula, Valeswara-Rao, 228
Gilliam, A. L., 259
Hardman, Ned J., 2
Harvey, Melanie J., 131
Jäkle, Frieder, 104
Jutzi, P., 16
John, Kevin D., 70
King, R. B., 208
Kotowicz, Boguslaw W., 88
Kun, A., 208
Luo, M. B., 246
Mackenzie, Katrin, 88
Mann, Grace, 70
Martin, Richard L., 70
Mason, Mark R., 181
Matthews, R. Mark, 181
Menon, Rani B., 228
Otieno, Peter O., 88
Patocka, Jiri, 271
Pender, Mark J., 168
Perkins, Alisa M., 181
Phillips, Andrew D., 2
Ponomarova, Vira V., 181
Power, Philip P., 2
Rao, Jagannatha K. S., 228
Rao, R. V., 228
Schatte, G., 195
Schebaum, L. O., 16
Schnepf, Andreas, 154
Schnöckel, Hansgeorg, 154
Selegue, J. P., 259
Shapiro, Pamela J., 31
Shankar, S. K., 228
Shanmugavelu, P., 228
Silaghi-Dumitrescu, I., 208
Sneddon, Larry G., 168
Strunecka, Anna, 271
Talarico, Giovanni, 142
Wang, C. Y., 246
Westcott, Stephen A., 70
Yearwood, B. C., 259
Zecca, Luigi, 228

Subject Index

A

- N*-Acetyl-L-aspartyl-L-glutamate, modulation by aluminum, 240
- 1,4-Addition to α,β -enones in diboration reaction, 71-72*f*
- Alkyl-aryl boraamidates, dilithium, structure, 197*f*
- Alkylaluminophosphonate cage units two-dimensional sheet with no structural rearrangement of precursor, 191-192
zigzag chain with structural rearrangement of precursor, 188-189*f*
- Alumina templates in boron carbide nanocylinder preparation, 177-178
nanofiber preparation, 174-175, 178
- Aluminofluoride complex as phosphoryl transfer transition state analog, 273-274
- Aluminofluoride complexes in ecosystems, 275, 278
- Aluminofluoride effects observed in laboratory investigations, 273-274, 276*t*
- Aluminofluorides as messengers in biological systems, 274-275
- Aluminofluorides, possible danger for living organisms, 271-282
- Aluminophosphate molecular sieves, structure, 182*f*
- Aluminum alkyls as Lewis acids in olefin polymerization, 89
- Aluminum anions, chelated, 131-141
- Aluminium anions supported by
N,N' ligands, 134
N,O ligands, 134-135
N,N',O,O' ligands, 135-140
O,O' ligands, 132-134
- Aluminum aqueous polymeric species, 248-250
- Aluminum bioinorganic chemistry, relevance to Alzheimer's disease, 228-245
- Aluminum chloride and lithium *tert*-butylamide reaction products, 201
- Aluminum cyclopentadienyl complexes
chemical structure, 37
synthesis, 32-33
- Aluminum β -diketiminate
molecular orbital energies, 6*t*-8
structural parameters, experimental and calculated, 4-5*t*
- Aluminum-enhanced iron-mediated oxidative stress, 242
- Aluminum-enhanced peptide-mediated oxidative stress, 241
- Aluminum ethyl polymerization, ethyl-to-ethene hydride transfer, 148-150
- Aluminum hydrolysis in aquatic systems and soil solutions, 247-252
- Aluminum hydrolysis-polymerization mechanisms, 250-252
- Aluminum in *N*-acetyl-L-aspartyl-L-glutamate modulation, 240
- Aluminum-induced amino acid racemization, 240-241
- Aluminum-induced cell death, 241-243*f*
- Aluminum-induced neurotoxicity, 279-280
- Aluminum interactions with DNA, 236-237

- Aluminum loading in humans, 231
- Aluminum, mono- and dinuclear olefin polymerization, 142-152
- Aluminum neurotoxicity
relevance to Alzheimer's disease, 238-242
speciation chemistry, 235-237
- Aluminum pentamethylcyclopentadienyl complex
structure, 18-22
synthesis, 17
- Aluminum polymerization in aquatic systems and soil solutions, 247-252
- Aluminum polynuclear hydroxyl species, 246-258
- Aluminum polynuclear species model, 250-252
- Aluminum role
anti-apoptotic and pro-apoptotic proteins expression, 239
metal homeostasis in human Alzheimer's brain, 233-234f
neurofibrillary tangle formation, 238-239
neuropeptide Y modulation, 239
- Aluminum sulfate as flocculation agent, 231
- Aluminum toxicity studies, 235-237
- Aluminum trifluoride, commercial uses, 261
- Aluminum trisamido complexes, reactions, 201-204
- Alzheimer's disease, aluminum bioinorganic chemistry relevance, 228-245
- Amide/azide-tetrazole isomer production in reaction mixture, 10-11
- Amino acid racemization, aluminum-induced 240-241
- Ammonium tetrafluoroaluminate, synthesis, 263-264
- Antiaromaticity effects on Lewis acidity in group 13 catalysts, 92-94
- Aqueous systems, polynuclear hydroxyl aluminum species, 246-258
- Aryl azide reaction with gallium β -diketiminato, 12-14
- Azides, reaction products with gallium β -diketiminato, 10-14
- B**
- Base injection methods, effect on flocculation and precipitation, polynuclear aluminum species, 254-255
- Benzaldehyde deoxygenation with diboron reagent, 78-79
- Benzonitrile, reaction as weak base, 92-93f
- Bidentate group 13 organometallics in ethylene polymerization, 98-100
- Bidentate metallocene-based Lewis acids, 104-117
- Bifunctional Lewis acid reactivity, diol-derived diboron reagents, 70-87
- 1,1'-Bifunctional metallocene-based Lewis acids, 106-108
- 1,2-Bifunctional metallocene-based Lewis acids, 108-113
- Bifunctional organoboranes in Ziegler-Natta catalysis, explosive decomposition, 91
- Biological activity, tetrafluoroaluminate complex, 266-268
- Biological carriers, aluminum, 231-232
- Bis(4-*tert*-butylcatecholato)-diboron in aldimine coupling, 72-74
- Bis(trimethylstannyl)ferrocene reaction products with boron trichloride, 109-110
- Bond lengths for M-N bonds in β -diketiminates, 5

Bonding molecular orbitals
 oblate tetragonal bipyramidal geometry, 218-220*f*
 octahedral geometry, 217-218*f*
 trigonal antiprismatic geometry, 218-220*f*

Boraamidinates
 dilithium alkyl/aryl, structure, 197*f*
 metal complexes, 197-200
 synthesis by lithiation of trisamidoboranes, 196

Boraamidinato ligand in dimerization inhibition, 198-199

Boraamidinato tellurium dichloride by metathetical reaction, 198

Boron carbide
 crystallization by bulk pyrolyses of polyhexenyldecaborane, 170-172
 nanocylinders synthesis, 176-178
 nanofibers synthesis, 174-176, 178
 precursors, single source, 169-174

Boron carbide/silicon-carbide precursors, single source, 169-174

Boron complexes, η^1 ring coordination geometry, 34

Boron cyclopentadienyl compounds, synthesis, 32-33

Boron pentamethylcyclopentadienyl complex, synthesis, 17-18

Boron-rich boron carbide from pyrolysis of decaborane-based precursor, 173

Boron, six-vertex polyhedra, molecular orbital energies, 213*t*

Boron-tin exchange
 1,2-dimetallated ferrocene synthesis, 109-113
 reaction mechanism, 111-112*f*

Brain cells with aluminum-13 polymer, 236

C

Cage alkylaluminumphosphonates with potentially ligating substituents, 185-188

Cage rearrangement in reactions of ${}^t\text{Bu}_3\text{Al}$ with methylphosphonic acid, 184-185

Capping principle in metallaboranes, 58-62

Cationic cyclopentadienylborane, molecular orbital diagram, 35*f*

Cell death events, aluminum role, 239, 241-243*f*

Ceramic conversion
 decaborane-based molecular precursor to boron-rich compositions, 172-174
 polyhexenyldecaborane polymer, 170

Chain transfer processes for mono- and dinuclear aluminum-ethyl species, 146-148

Chelated aluminum anions, 131-141

Chelation effects on Lewis acidity in group 13 catalysts, 92

Clay mineral type, effect on flocculation and precipitation, polynuclear aluminum species, 253-254

Cocatalytic activity
 coexistence ions, effect on flocculation and precipitation, polynuclear aluminum species, 254-255
 group 13 metalloles in ethylene polymerization, 100-101
 group 13 organometallics in ethylene polymerization, 98-100

Commercial uses
 aluminum trifluoride, 261
 tetrafluoroaluminates, 261

Computational methods in density functional theory, 210

Core-link ring model for aluminum species, 250-251*f*

Covalent boron-cyclopentadienyl ring bonding, 34

Cumulene, reaction with gallium β -diketiminato, 10-11

4-Cyanophenylphosphonic acid with ${}^t\text{Bu}_3\text{Al}$, reaction products, 186-187*f*

Cycloaddition reactions, pentamethylcyclopentadienyl complexes with monovalent group 13 elements, 26-28

Cyclopentadienyl boron complexes, synthesis, 32-33
See also Cyclopentadienylboranes

Cyclopentadienyl aluminum complexes, synthesis, 32-33

Cyclopentadienyl gallium complexes, 32-33, 38-39

Cyclopentadienyl metalloborane complexes
earlier transition element, 49-65
electron counting rules, 50-52
See also Metalloborane cyclopentadienyl complexes

Cyclopentadienyl thallium complexes, synthesis, 33

Cyclopentadienyl trivalent group 13 elements complexes
molecular structures, 33-40
precursors to III-V semiconductors, 42
reactivity, 40-43
synthesis, 32-33

Cyclopentadienylboranes
Diels-Alder dimerization, 41
diprotonation, 41-42
sigmatropic rearrangements, 34*f*
See also Cyclopentadienyl boron complexes, synthesis

D

Danger from explosive decomposition, bifunctional and fluoro-substituted organoboranes in Ziegler-Natta catalysis, 91

Danger to living organisms from aluminofluoride complexes, 271-282

Decaborane-based molecular precursor to boron-rich compositions, 172-174

Decamethylborocenium cation, structure, 35*f*

Deltahedra generation, diamond-square-diamond rearrangement, 58*f*-62

Density functional theory
computational methods, 210
distortions from octahedral symmetry in polyhedral clusters, group 13 elements, 208-225

Deoxygenation by boron reagents
affected by Lewis acidity of diborane compound, 76
main group element oxides, 75-79

Design, group 13 molecular and polymeric precursors to advanced ceramics, 168-180

DFT, *See* Density functional theory

Diamond-square-diamond conversion, regular octahedron into bicapped tetrahedron, 216*f*

Diamond-square-diamond rearrangement
for an icosahedron, 57*f*
in deltahedra generation, 58*f*-62

1,2-Diazines, selective receptor for, 124-126

Diborane reagents as two-electron reductants in stereoselective aldimine coupling, 71-75

- Diboration reaction, versatility, 71-72*f*
- 9,10-Dibromo-9,10-dihydro-9,10-diindanthracene
coordination chemistry, 124-127
polymer formation, 126-127
- Diborylated ferrocenes as bidentate metallocene-based Lewis acids, 106
- Diels-Alder dimerization in cyclopentadienylboranes, 41
- 9,10-Diindanthracenes in molecular recognition and polymer synthesis, 124-127
- Dilithium alkyl/aryl boraamidates, structures, 197*f*
- Dimeric trisamido derivatives reactions with organolithium compounds, 201-204
- 1,*n*-Dimetalloalkanes, conformational mobility effects on Lewis acid strength, 92
- Diol-derived diboron reagents, Lewis acid reactivity, 70-87
- Diprotonation, cyclopentadienylboranes, 41-42
- Distortions from octahedral symmetry in polyhedral clusters, group 13 elements, 208-225
- Divalent diol-derived diboron reagents, Lewis acidity, 79-84
- DNA, altered topology in Alzheimer's brain, 237
- Donor-acceptor complexes with pentamethylcyclopentadienyl complexes with monovalent group 13 elements as donors, 23-25
- Dsd, *See* Diamond-square-diamond
- E**
- Ecosystems, aluminofluoride complexes, 275, 278
- Electron counting rules, metallaboranes with M_2B_4 , MB_4 and M_2B_5 skeletons, 51*f*
- Electron density surfaces
aluminum β -diketiminato, 7*f*
gallium β -diketiminato, 7*f*
- Electron systems
10-skeletal, optimized calculated structures, 219, 221-222
12-skeletal, optimized calculated structures, 218-220
14-skeletal, optimized calculated structures, 215-218
- Elementoid cluster with respect to β -gallium, $Ga_{18}(Si^tBu_3)_8$, 159*f*
- Elementoid gallium clusters
synthesis and structure, 154-167
Wage-Mingos rules, inapplicability, 164-165
- Elimination reactions, cyclopentadienyl-aluminum bonds, 40-41
- Ethyl-to-ethene hydride transfer in aluminum ethyl polymerization, 148-150
- Ethylene polymerization with titanocene methyl chloride, 98-100
- Explosive decomposition, bifunctional and fluoro-substituted organoboranes in Ziegler-Natta catalysis, 91
- F**
- Ferrocene-based bifunctional Lewis acids, 106-107
- Flocculation and precipitation, polynuclear aluminum species, 252-255
- Fluoro-substituted organoboranes in Ziegler-Natta catalysis, explosive decomposition, 91

- Fluoroaluminate species, structures, 264-266
- Fluoroaluminates of organic base cations, preparation, 262-263
- Formation, polynuclear hydroxyl aluminum species, 246-258
- Functional difference between phosphate group and fluoroaluminate species, 273
- ## G
- Gallium chloride and lithium *tert*-butylamide reaction products, 201
- Gallium cluster compounds, synthesis and structure, 154-167
- Gallium complexes, η^1 ring coordination geometry, 38-39
- Gallium cyclopentadienyl compounds structure, 38-39 synthesis, 32-33
- Gallium β -diketiminate molecular orbital energies, 6*t*-8 planar ring structure with approximate C_2 symmetry axis, 4*f* reactivity, 8-14 structural parameters, experimental and calculated, 4-5*t*
- Gallium pentamethylcyclopentadienyl complex structure, 18-22 synthesis, 17-18
- Gallium trisamido complexes, reactions, 201-204
- Gallophosphate, molecular sieves, structure, 182*f*
- Gas phase structure, gallium pentamethylcyclopentadienyl complex, 19*f*
- Geometric structure, hypoelectronic metallaboranes, 53-55
- Gibbsite-fragment model, aluminum polymerization, 251*f*
- Glycolate ligand, chelate in aluminum coordination polymer 132*f*-133
- Group 13 bidentate organometallics, cocatalytic activity in ethylene polymerization with titanocene methyl chloride, 98-100
- Group 13 derivatives, Lewis acidity, 90-94
- Group 13 elements, density functional theory study, distortion from octahedral symmetry in polyhedral clusters, 208-225
- Group 13 Lewis acids, synthesis via metal-tin exchange reactions, 88-103
- Group 13 metalloles, cocatalytic activity in ethylene polymerization with titanocene dichloride, 100-101
- Group 13 molecular and polymeric precursors to advanced ceramics, design, synthesis and application, 168-180
- Group 13 molecular phosphates and phosphonates, 181-194
- Group 13 polyimido anions, 195-207
- ## H
- Haloboranes, Lewis acids, reactions, 32-34
- Hartree-Fock calculations Al-cyclopentadienyl ring bonding, 36 Ga-N bond investigation, 13-14
- Heterocyclic gallophosphates, isomerization to cis-trans mixtures, 183-184
- Heterolytic bond cleavage in pentamethylcyclopentadienyl complexes with monovalent group 13 elements, 22-23
- Hexameric ring model for aluminum species, 250-252

- 6-Hexenyl-decaborane monomer, synthesis, 170
- Homolytic bond cleavage in pentamethylcyclopentadienyl complexes with monovalent group 13 elements, 22-23
- Huckel aromaticity theory, applied to metallacyclopolyenes as Lewis acids, 92-93
- Human Alzheimer's brain, aluminum role in metal homeostatis, 233-234*f*
- Human health effects caused by synergistic action of aluminum and fluoride, 279-280
- Human intake
 dietary aluminum, 231
 major aluminum sources, 278
 major fluoride sources, 278
- Hybridization of atom attached directly to metal in enhanced Lewis acidity, 91
- Hydrolysis-polymerization mechanisms, aluminum, 250-252
- Hydrolysis reactions, aluminum, 235-236
- Hypercloso metallaboranes, filled cluster bonding orbitals, 55-56
- Hypoelectronic closed rhenaboranes, structure, 53*f*-54
- Hypoelectronic icosogen deltahedra flattening, study by density functional theory, results, 209-212
- Hypoelectronic metallaboranes analysis, 56-62
 molecular orbital model, 62-64
- I**
- Icosahedron, diamond-square-diamond rearrangement, 57*f*
- Imine coupling reaction, 72-75
- Indium complexes, η^1 ring coordination geometry, 40
- Indium cyclopentadienyl compounds, 32-33, 40
- Indium halides in transmetalation reactions, 120-123
- Indium Lewis acids, polyfunctional with *o*-phenylene backbones, 118-130
- Indium pentamethylcyclopentadienyl complex structure, 18-22
 synthesis, 17
- Indium, six-vertex polyhedra, molecular orbital energies, 214*t*
- Insertion reactions
 cyclopentadienyl-aluminum bonds, 41
 pentamethylcyclopentadienyl complexes with monovalent group 13 elements, 27-28
- Iron-mediated oxidative stress, aluminum-enhanced, 242
- Isocloso metallaboranes, geometric structure, 55-56
- Intermolecular rearrangements in molecular group 13 phosphonates, 183-185
- L**
- Laboratory investigations, aluminofluoride species effects, 273-274, 276*t*
- Large metalloid cluster anion in $[\text{Ga}_{84}\{\text{N}(\text{SiMe}_3)_2\}_{20}]^{4-} \cdot 2[\text{Li}(\text{THF})_4]^+ \cdot 2[\text{Li}_2\text{Br}(\text{THF})_6]^+ \cdot 2$ toluene, 163*f*-164
- Lewis acidity
 aluminum alkyls in olefin polymerization, 89
 group 13 derivatives, 90-94
See also Lewis acids

- Lewis acids
 ferrocene-based bifunctional, 106-107
 group 13, synthesis via metal-tin exchange reactions, 88-103
 haloboranes, reactions, 32-34
 metallocene-based bidentate, 104-117
 polyfunctional indium with *o*-phenylene backbones, 118-130
 reactivity, diol-derived diboron reagents, 70-87
See also Lewis acidity
- Ligand redistribution reactions in trivalent group 13 cyclopentadienyl complexes, 40
- Lithiation of trisamidoboranes forming boraamidinates, 196
- Lithium aluminum tetraamide complex, synthesis, 134
- Living organisms possibly endangered by aluminofluoride complexes, 271-282
- M**
- Main group element oxides, deoxygenation by boron reagents, 75-79
- Mechanisms, aluminum hydrolysis-polymerization models, 250-252
- Metal aluminum hydrides, reactions with primary amines, 204-205
- Metal-catalyzed deoxygenation reaction pathway with diboron reagent, 77-78*f*
- Metal homeostatis, aluminum role in human Alzheimer's brain, 233-234*f*
- Metal-tin exchange reactions, synthesis of group 13 Lewis acids, 88-103
- Metallaborane clusters containing earlier transition metal fragments, 49-67
 groups 6 and 7 metals, reactions, 52
- Metallaborane cyclopentadienyl complexes, 49-65
See also Cyclopentadienyl metallaborane complexes
- Metallaboranes containing rhenium, 53*f*-62
- Metallaboranes containing tungsten, 54*f*-62
- Metallaboranes with M₂B₄, MB₄ and M₂B₅ skeletons, electron counting rules, 51*f*
- Metallocene-based bidentate Lewis acids, 104-117
- Metallocene-based 1,1'-bifunctional Lewis acids, 106-108
- Metalloid gallium cluster in [Ga₁₂(C₁₃H₉)₁₀]²⁻·2[Li(THF)₄]⁺, 158*f*
- Metalloid gallium cluster in [Ga₁₉(CSiMe₃)₆][Li₂Br(THF₆)]⁺, 161-162*f*
- Metalloid gallium cluster in [Ga₈₄{N(SiMe₃)₂]₂₀]⁴⁻·2[Li(THF)₄]⁺·2[Li₂Br(THF)₆]⁺·2 toluene, 163*f*-164
- Metalloid gallium cluster in [Ga₆(SiPh₂Me)₈]²⁻·2[Li(THF)₄]⁺, 156-157
- Metalloid gallium cluster with composition, Ga₂₂R₈, 159-161
- Metastable gallium halide solution in gallium cluster compound preparation, 155-156
- 1-Methyl-2,3,4,5-tetraphenylaluminole, synthesis by tin-aluminum exchange reaction, 97-98
- Mineral/water interfaces, polynuclear aluminum species formation, 252
- Modulation, *N*-acetyl-L-aspartyl-L-glutamate by aluminum, 240

- Molecular group 13 phosphonates, intermolecular rearrangements, 183-185
- Molecular orbital calculation for pyridine adduct formation with diboron reagents, 80-84
- Molecular orbital description for pentamethylcyclopentadienyl monovalent group 13 element complexes, 21-22
- Molecular orbital diagram, cationic cyclopentadienylborane, 35*f*
- Molecular orbital energies
aluminum β -diketiminate, 6*t*-8
gallium β -diketiminate, 6*t*-8
- Molecular orbital energies calculated by density functional theory
boron cluster, B₆^{z+}, 213*t*
indium cluster, In₆^{z+}, 214*t*
thallium cluster, Tl₆^{z+}, 215*t*
- Molecular orbital model, hypoelectronic metallaboranes, 62-64
- Molecular phosphates and phosphonates, group 13, 181-194
- Molecular stairs and ladders, self assembly in polymer formation, 126-127
- Monocyclopentadienyl metal halides as source of transition metal metallaboranes, 50
- Monovalent group 13 elements, pentamethylcyclopentadienyl complexes, 16-30
- Morpholine *N*-oxide deoxygenation by boron reagent, 75-76
- N**
- N,N' ligands supporting aluminum anions, 134, 138-140
- N,N',O,O' ligands supporting aluminum anions, 135-140
- N,O ligands supporting aluminum anions, 134-135
- Nanocylinders synthesis, boron carbide, 174-179
- Nanofibers synthesis, boron carbide, 174-179
- Nanostructural element modifications, elementoid gallium clusters, 154-167
- Neurofibrillary tangle formation, aluminum role, 238-239
- Neuropeptide Y modulation by aluminum, 239
- Neurotoxicity, aluminum-induced, 279-280
- Neurotoxicity, aluminum, relevance to Alzheimer's disease, 238-242
- NFT formation
See Neurofibrillary tangle formation
- Nitrous oxide, reaction with gallium β -diketiminate yielding oxo bridged dimer, 8*f*-10
- Noyori's reagent, modified lithium aluminum hydride, 133-134
- O**
- O,O' ligands supporting aluminum anions, 132-134
- Oblate tetragonal bipyramidal geometry, bonding molecular orbitals, 218-220*f*
- Octahedral geometry, molecular bonding orbitals, 217-218*f*
- Octahedral symmetry, distortion in polyhedral clusters, 208-225
- Olefin polymerization
Lewis acidity of aluminum alkyls, 89
mono- and dinuclear at aluminum, 142-151
- Oligomerization at aluminum, 143-144

- Organic base cations,
fluoroaluminates, preparation, 262-263
- Organoaluminum analog syntheses by tin-aluminum exchange process, 95-96
- Organoaluminum cocatalysts with titanocene methyl chloride in ethylene polymerizations, 98-99
- Organoborane synthesis
thermal boron-boron interchange, 94-95*f*
tin-boron exchange, 94*f*
- Organolithium compounds, reactions with dimeric trisamido derivatives, 201-204
- Oxidative addition reactions, pentamethylcyclopentadienyl complexes with monovalent group 13 elements, 26-28
- Oxo bridged dimer, nitrous oxide with gallium β -diketimate reaction product, 8*f*-10
- P**
- Pentamethylcyclopentadienyl complexes with monovalent group 13 elements
reaction chemistry, 22-28
structure and bonding, 18-22
synthesis, 17-18
- Pentaphenylborole, antiaromatic nucleus, 92-93*f*
- pH, effect on flocculation and precipitation, polynuclear aluminum species, 253-254
- o*-Phenylene-indium complexes, synthesis, 120-123
- o*-Phenylene-mercury in transmetalation reactions, 120-122
- β -Phosphate, binding by tetrafluoroaluminate anion, 267*f*
- Phosphate group and fluoroaluminate species, functional difference, 273
- Phosphine ligands in diboration reaction, 71-72*f*
- Phosphoryl transfer transition state analog, aluminofluoride complex, 273-274
- Planar ring structure with approximate C_2 symmetry axis, gallium β -diketimate, 4*f*
- Polyfunctional indium Lewis acids with *o*-phenylene backbones, 118-130
- Polyhedral clusters, group 13 elements, density functional theory distortions from octahedral symmetry, 208-225
- Polyhexenyldecaborane boron carbide crystallization by bulk pyrolyses, 170-172
polyolefin polymer ceramic conversion, 170-171
polyolefin polymer synthesis, 170
- Polyimido anions, group 13 elements, 195-207
- Polymer formation by 9,10-dibromo-9,10-dihydro-9,10-diindaanthracene, 126-127
- Polymeric aluminum aqueous species, 248-250
- Polymerization at aluminum, 142-152
- Polynuclear aluminum species, flocculation and precipitation, 252-255
- Polynuclear hydroxyl aluminum species, formation and transformation, 246-258
- Potassium tetrafluoroaluminate as flux, 261
- Precipitation and flocculation, polynuclear aluminum species, 252-255
- Preparation, *See* Synthesis

Primary amines, reactions with metal aluminum hydrides, 204-205

Propagation barriers for mono- and dinuclear aluminum-ethyl species, 145-147*f*

Pyridine adduct formation with diboron dicatecholato reagent, 80-84

Pyridine *N*-oxide deoxygenation by boron reagent, 75-76

3-Pyridylphosphonic acid with ^tBu₃Al, reaction product, 188*f*

Pyrolysis in boron carbide crystallization decaborane-based precursor, 173 polyhexenyldecaborane, 170-172

Q

Quasi planar N₂GaNC array, preservation with steric congestion, 12-13*f*

R

Racemization, amino acid induced by aluminum, 240-241

Reaction chemistry, pentamethylcyclopentadienyl complexes with monovalent group 13 elements, 22-28

Reaction mechanism, boron-tin exchange, 111-112*f*

Reactivity, cyclopentadienyl complexes with trivalent group 13 elements, 40-43

Rhenaboranes, hypoelectronic closed, structure, 53*f*-54

Rhenium catalysis of sulfoxide deoxygenation, 76-78*f*

Rhenium hypoelectronic metallaboranes

dsd rearrangement, 56-62
molecular orbital model, 62-64

η^1 Ring coordination geometry boron complexes, 34
gallium complexes, 38-39
indium complexes, 40

S

Safety, bifunctional and fluoro-substituted organoboranes in Ziegler-Natta catalysis, 91

Salan ligands supporting aluminum anions, 135-138

Selective receptor for 1,2-diazines, 124-126

Self assembly of molecular stairs and ladders, polymer formation, 126-127

Semiconductors (III-V), cyclopentadienyl complexes with trivalent group 13 elements, as precursors, 42

Shell-structured metalloid gallium cluster in [Ga₁₉(CSiMe₃)₆]⁻ [Li₂,Br(THF)₆]⁺, 161-162*f*

Sigmatropic rearrangements, cyclopentadienylborane compounds, 34*f*

Soil systems, polynuclear hydroxyl aluminum species, 246-258

Speciation chemistry, aluminum, 235-237

1-Stannyl-2-borylferrocene, reactivity, 113

Steric effects, aryl substituent in reactions with aluminum β -diketiminato, 12-13

Steric hindrance effects on Lewis acidity in group 13 catalysts, 91

Stereoselective aldimine coupling, diborane reagents as two-electron reductants, 71-75

- Stereoselective imine coupling, transition state model, 75*f*
- Structural parameters, experimental and calculated
aluminum β -diketiminate, 4-5*t*
gallium β -diketiminate, 4-5*t*
- Structure, aluminum compounds
aluminum pentamethylcyclopentadienyl complex, 18-22
aluminum cyclopentadienyl complexes, 37
fluoroaluminate species, 264-266
- Structure, 4-cyanophenylphosphonic acid with ${}^t\text{Bu}_3\text{Al}$, reaction products, 186-187*f*
- Structure, cyclopentadienyl complexes with trivalent group 13 elements, 33-40
- Structure, decamethylborocenium cation, 35*f*
- Structure, dilithium alkyl/aryl boraamidates, 197*f*
- Structure, gallium compounds
distorted icosahedral with relatively short GaGa distances, in $\text{Ga}_{12}(\text{C}_{13}\text{H}_9)_{10}^{2+} \cdot 2[\text{Li}(\text{THF})_4]^+$, 158*f*
elementoid gallium clusters, 154-167
gallium cyclopentadienyl complexes, 38-39
gallium β -diketiminate with C_2 symmetry axis, 4*f*
gallium pentamethylcyclopentadienyl complex, 18-22
metalloid gallium cluster in $[\text{Ga}_{19}(\text{CSiMe}_3)_6][\text{Li}_2, \text{Br}(\text{THF}_6)]^+$, 161-162*f*
metalloid gallium cluster in $[\text{Ga}_{84}\{\text{N}(\text{SiMe}_3)_2\}_{20}]^{4+} \cdot 2[\text{Li}(\text{THF})_4]^+ \cdot 2[\text{Li}_2\text{Br}(\text{THF})_6]^+ \cdot 2$ toluene, 163*f*-164
metalloid gallium cluster with composition, Ga_{22}R_8 , 159-161
similar to β -gallium allotrope in $\text{Ga}_{18}(\text{Si}^t\text{Bu}_3)_8$, 159*f*
similar to β -gallium allotrope in $[\text{Ga}_6(\text{SiPh}_2\text{Me})_8]^{2+}$, 158*f*
- Structure, Group 13 molecular sieves, 182*f*
- Structure, indium
pentamethylcyclopentadienyl complex, 18-22
- Structure, metallaboranes with M_2B_4 , MB_4 and M_2B_5 skeletons, electron counting rules, 51*f*
- Structure, thallium
pentamethylcyclopentadienyl complex, 18-20
- Sulfoxide deoxygenation rate with diboron reagent, 76-77
- Sulfur, reaction with gallium β -diketiminate yielding sulfido bridged dimer, 8*f*-10
- Synergistic action of aluminum and fluoride, human health effects, 279-280
- Synthesis, aluminum compounds
aluminum pentamethylcyclopentadienyl complex, 17
ammonium tetrafluoroaluminate, 263-264
cyclopentadienyl compounds, 32-33
lithium aluminum tetraamide complex, 134
1-methyl-2,3,4,5-tetraphenylaluminole by tin-aluminum exchange reaction, 97-98
organoaluminum analogs by tin-aluminum exchange process, 95-96
tetrafluoroaluminate complexes, 262-264
tetrakisamido aluminates, 204-205
- Synthesis, boron compounds
boraamidates, by lithiation of trisamidoboranes, 196

- boron pentamethylcyclopentadienyl complex, 17-18
- cyclopentadienyl compounds, 32-33
- decaborane-based molecular precursor to boron-rich compositions, 172
- 1,2-dimetallated ferrocenes by boron-tin exchange, 109-113
- 6-hexenyl-decaborane monomer, 170
- nanofibers, boron carbide, 174-176, 178
- nanocylinders, boron carbide, 176-178
- organoboranes by thermal boron-boron interchange, 94-95*f*
- organoboranes by tin-boron exchange, 94*f*
- polyhexenyldecaborane, polyolefin polymer, 170
- Synthesis, gallium compounds
- cyclopentadienyl compounds, 32-33
 - elementoid gallium clusters, 154-167
 - gallium pentamethylcyclopentadienyl complex, 17-18
- Synthesis, group 13 Lewis acids, via metal-tin exchange reactions, 88-103
- Synthesis, group 13 molecular and polymeric precursors to advanced ceramics, 168-180
- Synthesis, indium compounds
- cyclopentadienyl compounds, 32-33
 - indium pentamethylcyclopentadienyl complex, 17
 - Lewis acids with tetrafluoronaphthalene backbones, 122-123
 - o*-phenylene-indium complexes, 120-123
- Synthesis, thallium compounds
- cyclopentadienyl compounds, 33
 - thallium pentamethylcyclopentadienyl complex, 17
- Synthesis, trivalent group 13 elements, cyclopentadienyl complexes, 32-33
- ## T
- Temperature, effect on flocculation and precipitation, polynuclear aluminum species, 254-255
- Tetrafluoroaluminate complex
- biological activity, 266-268
 - characterization, 264-266
 - synthesis, 262-264
- Tetrafluoroaluminates, commercial use, 261
- Tetrafluoronaphthalene backbones in indium Lewis acids, 122-123
- Tetrakisamido aluminates, synthesis, 204-205
- Tetrametric gallophosphonates, intermolecular exchange, 184
- Tetrazole-amide/azide isomer production in reaction mixture, 10-11
- Thallium cyclopentadienyl compounds, synthesis, 33
- Thallium pentamethylcyclopentadienyl complex
- structure, 18-20
 - synthesis, 17
- Thallium, six-vertex polyhedra, molecular orbital energies, 215*t*
- Thermal boron-boron interchange in organoborane synthesis, 94-95*f*
- Tin-aluminum exchange process in organoaluminum analog syntheses, 95-96
- Tin-aluminum exchange reaction in 1-methyl-2,3,4,5-tetraphenylaluminumole synthesis, 97-98
- Tin-boron exchange in organoborane synthesis, 94*f*

- Titanocene methyl chloride in ethylene polymerization with bidentate group 13 organometallics, 98-100
- Topology-preserving distortions involving descent of symmetry, 216*f*
- Toxicity studies, aluminum, 235-237
- Transition metal fragments in metallaborane clusters, 49-67
- Trigonal antiprismatic geometry, bonding molecular orbitals, 218-220*f*
- Trisamidoboranes in boraamidinates synthesis, 196
- Trivalent group 13 elements, cyclopentadienyl complexes molecular structures, 33-40 reactivity, 40-43 synthesis, 32-33
- Tungstaboranes, hypoelectronic closed, structure, 54*f*-55
- Tungsten containing hypoelectronic metallaboranes, 56-62
- Two-dimensional sheet of alkylaluminumphosphonate cage units with no structural rearrangement of precursor, 191-192
- Two-electron reductants in stereoselective aldimine coupling, 71-75
- U**
- Unsaturated molecules, reactions with gallium β -diketiminates, 8-14
- W**
- Wage-Mingos rules, inapplicability to elementoid gallium clusters, 164-165
- Wilkinson's catalyst, 76-77
- Z**
- Ziegler catalysts, Lewis acidity of aluminum alkyls, 89
- Ziegler-Natta catalysis, explosive decomposition, bifunctional and fluoro-substituted organoboranes, 91
- Ziegler-Natta polymerization, bidentate organoboron and organoaluminum species, 105
- Zigzag chain of alkylaluminumphosphonate cage units with structural rearrangement of precursor, 188-189*f*